Universidad de Oviedo

Departamento de Química Física y Analítica

Síntesis y Caracterización de Puntos Cuánticos de Carbono, Nanopartículas de ZnO y Magnéticas. Nuevas Aplicaciones Analíticas

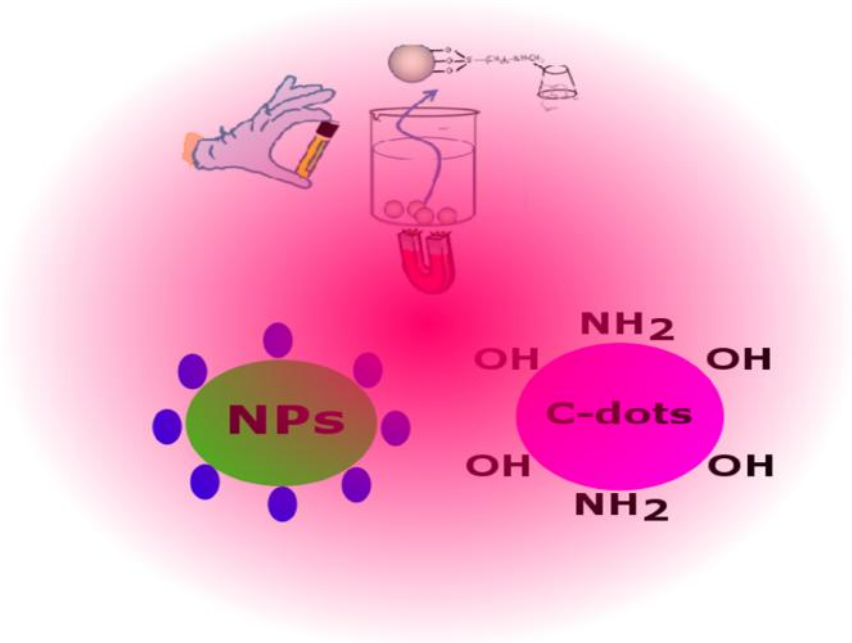

TESIS

Presentada Para Optar al Grado de Doctor

Gaber Hashem Gaber Ahmed

Oviedo, 2014

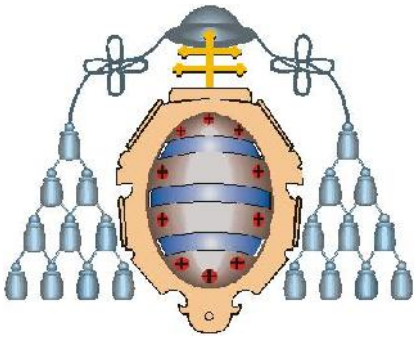

Universidad de Oviedo

Departamento de Química Física y Analítica

Síntesis y Caracterización de Puntos Cuánticos de Carbono, Nanopartículas de ZnO y Magnéticas. Nuevas Aplicaciones Analíticas

TESIS

Presentada Para Optar al Grado de Doctor

Gaber Hashem Gaber Ahmed

Oviedo, 2014

Acknowledgments

In the beginning I would like to thank everybody who directly or indirectly helped me in this thesis.

Then I would like to express my profound sense of reverence to my supervisor and promoter ***Prof. Dr. Marta Elena Diaz-Garcia***, for her constant guidance, support, motivation and untiring help during the course of my PhD. Her in-depth knowledge on a broad spectrum of different Nanotechnology and analytical chemistry topics has been extremely beneficial for me. She has given me enough freedom during my research, and she has always been nice to me. I will always remember her calm and relaxed nature. In fact without her there was no thesis, ¨Muchas gracias¨.

I would also like to acknowledge the kindness of ***Dr. Josefa Angela García Calzón*** & ***Dr. Rosana Badía Laíño*** and ***Dr Alfonso Fernandez*** for their attention and for their help.

For my colleagues during the period of my work, ***Jorge Espina, Natalia, Mohamed said, Marian,*** and ***Tere***.

I´d like to thank my mather-in-law (***W. Baghosh***) and my father-in-law (***Taha Shehata***) for their support and encouraging me all the time.

Also I am thankful to the ***Oviedo University*** and ***physical and analytical Chemistry department members*** to give me help to do this work.

This thesis wouldn´t be realized without the financial support from the EU (Erasmus Mendus MEDASTAR) and also I gratefully acknowledge financial support from the Science and Innovation Spanish Ministry (Projs # MICINN-09-CTQ2009-09595 and MAT2012-099)

To the soul of my parents

To my beloved children (Yousef and Rewayda)

To my dearest wife (E. Taha Shehata)

Acronyms

Abbrev.	Expression
NPs	Nanoparticles
QD	Quantum dot
FRET	Förster resonance energy transfer
BRET	Bioluminescence resonance energy transfer
CRET	Chemiluminescence resonance energy transfer
mNPs	Magnetic nanoparticles
CDs	Cyclodextrins
MIP	Molecularly imprinted polymer
SPE	Solid-phase extraction
C-dots	Carbon dots
MWCNT	Multiwalled carbon nanotube
QY	Quantum yield
MS	Mesoporous silica
TEOS	Tetraethoxysilane
PL	Photoluminescence
DFT	Density functional theory
ECL	Electrochemical luminescence
CL	Chemiluminescence
5-HIAA	5-Hydroxy-3-indole acetic acid
4-NP	4-Nitrophenol
TA	Tannic acid
CSF	Cerebrospinal fluid
SPME	Solid phase microextraction
DPE	1,2-Diphenylethylenediamine
CE	Capillary electrophoresis
CD-mNPs	β-cyclodextrin modified magnetic nanoparticles
APES	3-aminopropyltriethoxy silane
Ts-β-CD	Mono-6-deoxy-6-(*p*-tolylsulfonyl)-β-cyclodextrin
APES-mNPs	Silica modified magnetic nanoparticles
TsCl	*p*-toluenesulfonyl chloride
Citrate-mNPs	Citrate coated magnetic nanoparticles
EGTA	Ethyleneglycolbis-(2-aminoethylether)-N,N,N`,N`-tetra acetic acid
TRIS	Tris(hydroxymethyl)aminomethane
2-NP	2-Nitrophenol
2-CP	2-Chlorophenol
2-AP	2-Aminophenol
4-AP	4-Aminophenol
PEGA	Polyethyleneglycolbis(3-aminopropyl)
DPA	1,2-aminopropane
BrHBA	6-bromohexylboronic acid
PEGA-C-dots	Carbon dots prepared via Polyethyleneglycolbis(3-aminopropyl) precursor
DPA-C-dots	Carbon dots prepared via 1,2-aminopropane precursor
ZnO-R	Alkyl functionalized ZnO
ZnO-D	Decanoyl functionalized ZnO
ZnO-P	Palmitoyl functionalized ZnO
Ferron	8-hydroxy-7-iodo-5-quinolinesulfonic acid
FTIR	Fourier transform infrared spectroscopy
XRD	X-ray differaction
TEM	Transmission electron microscopy
HRTEM	High resolution transmission electron microscopy
NMR	Nuclear magnetic resonance
VSM	Vibrating sample magnetometer

Index

The article of chapter (2)

ESM of chapter (2)

Chapter (3): Highly fluorescent carbon dots as nanoprobes for sensitive and selective determination of 4-nitrophenol in surface waters

The article of chapter (3)

Chapter (6): Conclusions

List of Figures:

List of Tables:

Dissertation overview

It is no doubt that much focus nowadays is directed towards nanoparticles that are considered the most developing materials in all branches of real life. Their unique properties point out significant differences from bulk materials what give them such scientific interest. Advanced analytical methods focus on exploiting the potential of nanomaterials in quantification of analytes of environmental, toxicological, medical and food concern. In this dissertation, the physico-chemical evaluation of different nanoparticles with tailored surface chemistries was performed to develop new improved analytical methodologies for analytes of environmental, medical and food interest. Initially, the synthesis, optimization and characterization of magnetic nanoparticles grafted with β-cyclodextrin will be described in Chapter 2 along with their application for pre-concentration and determination of the cancer biomarker 5-hydroxy-3-indoleacetic acid in urine samples. Next, Chapter 3 will focus on the synthesis of fluorescent carbon nanodots, their characterization by different analytical techniques and their application to the analysis of the organic pollutant 4-nitrophenol in surface waters. The analytical sensing mechanism involving these carbon nanodots will be outlined. Chapter 4, will describe an easy one step synthesis of carbon nanodots by thermal carbonization of 6-bromohexylboronic acid using two different amine compounds and their characterization. These C-dots will exhibit analytical potential as sensing probes for tannic acid determination and the applicability of the method will be demonstrated by direct measurements of tannic acid in red and white wine samples. Also, a probable mechanism by which tannic acid quenched the carbon dots fluorescence will be proposed. Chapter 5 will present novel applications of metal oxide nanoparticles as additives to improve the rheological properties of lubricants. The synthesis and functionalization of ZnO nanoparticles will be described as well as their stability in organic media. Finally, Chapter 6 will present the conclusions and future directions of nanoparticles in analytical chemistry.

Significance and Objectives of the Work

The principle aims could be summarized in the following points:

1- Synthesis of magnetic nanoparticles grafted with β-cyclodextrin via layer by layer method.
2- Physico-chemical Characterization of the synthesized magnetic nanoparticles by the well-used analytical techniques; XRD, FTIR, TEM, and high-resolution TEM.
3- Applying the as-synthesized magnetic nanoparticles for preconcentration followed by quantification of the cancer biomarker 5-hydroxy-3-indoleacetic acid (5-HIAA) from urine samples.
4- Discussing and proving the main interaction between the β-cyclodextrin magnetic nanoparticles and 5-HIAA as well as adsorption kinetics and isotherms experimentally and theoretically.
5- Synthesis of different fluorescent carbon nanodots (C-dots) using the thermal carbonization method.
6- Characterization of the as-synthesized carbon dots by XRD, FTIR, NMR, and high-resolution TEM.
7- Application of the hydroxyl capped C-dots for analysis of the organic pollutant 4-nitrophenol (4-NP) in real surface waters.
8- Study the main interaction between the C-dots and 4-NP.
9- Application of the PEGA-C-dots for analysis of TA in wine samples.
10- Discussing the mechanism of PEGA-C-dos and TA interaction.
11- Synthesis of ZnO NPs and their alkyl functionalization
12- Characterization of the as-synthesized ZnO and ZnO-R
13- Applying the NPs either in improving rheological properties of lubricants or chemical sensing

This thesis comprises 3 main parts of reliable significance. In the 1st part, we have found that most articles focused on synthesis of mNPs with various surface reactivity such as natural or synthetic polymers (i.e. Chitosan, polyacrylic acid, poly-N-isopropylacrylamide etc.). However, very little work has been carried out in the preparation of organic-inorganic nanocomposite

materials through covalent bonding between mNPs and cyclodextrins (CDs) and their use as a tool for bioseparation/purification. The mixing of inclusion/complexation property of CDs and the superparamagnetic property of magnetite (Fe_3O_4) in one nanosystem is considered to be a promising tool for wide variety of applications such as bioseparation, drug delivery, molecular recognition, environmental pollution control etc. We have been successfully applying this nanosystem in solid phase extraction of the cancer biomarker 5-HIAA from urine samples.

The subsequent two parts study C-dots potential in analytical sensing. Although the origin of C-dots fluorescence spectra is not completely understood, but C-dots are in well developing since very few years and their potential have been approved to be promising besides they already exploited in various applications such as bioimaging and chemical sensing. However, the excellent exploiting of C-dots potential in analytical applications is still challenging for most analytes.

The new member of the nanocarbon family opened the door for much investigations and studies, according to this, we have found that no work has been done to study the interaction between C-dots and the well-known organic pollutant 4-NP. We could prepare a highly fluorescence quantum yield C-dots capped mainly by hydroxyl and carbonyl group. Moreover, analytical application of C-dots for 4-NP detection in real surface waters has been done successfully and a suggested interaction mechanism has been studied. In the same line, TA is an important natural compound found in most beverages like tea and wine, also it used in some industries and its analysis is of wide interest in analytical chemistry. Therefore, finding a facile, sensitive, and rapid method for TA analysis in wine is a challenge for analysts. Although the structure of the wine is very complex, due to the presence of a lot of chemical components. But herein we could find a novelty to apply successfully C-dots for TA determination in wine with a probable studied mechanism.

ZnO NPs is known to be a versatile material with multifunctional properties. As a result, alkyl functionalization of ZnO NPs may improve its properties by adding a hydrophobic organic chains on its surface. In chapter 5 we could synthesize successfully alkyl functionalized ZnO NPs. It exhibits a good optical properties, like room temperature fluorescence and phosphorescence. Its applications in improving the rheological properties of lubricants or chemical sensing are in progress.

Chapter 1

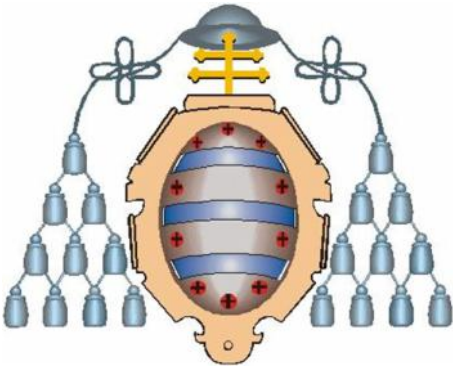

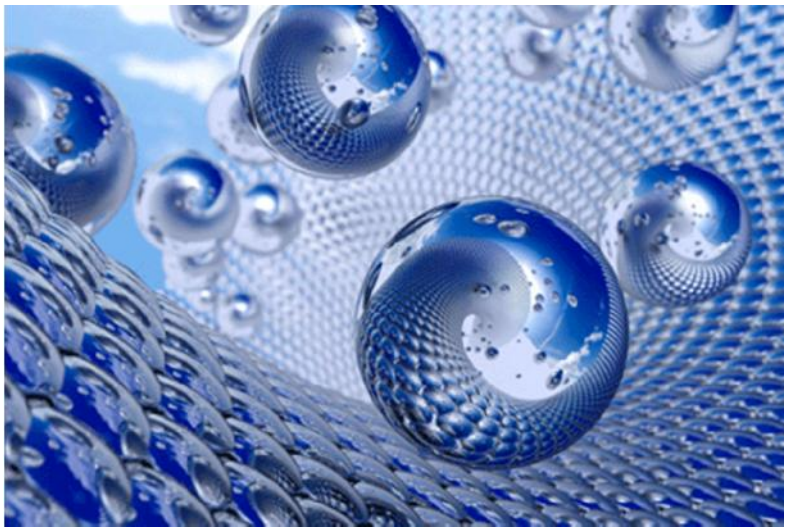

Introduction

I.1. Nanomaterials and Nanotechnology

No one can deny the great contribution of nanotechnology to the development of our modern life. As we down to the small world we define as the "nanoscale" the size regime between about 1-100 nm in one or more dimensions. Materials (and objects) in this scale have intermediate size between bulk materials and small molecules: nanomaterials (Figure 1) [1, 2]. Nanotechnology is the accepted term for the synthesis, characterization, and application of materials and/or devices with at least one characteristic dimension in the nanoscale [1].

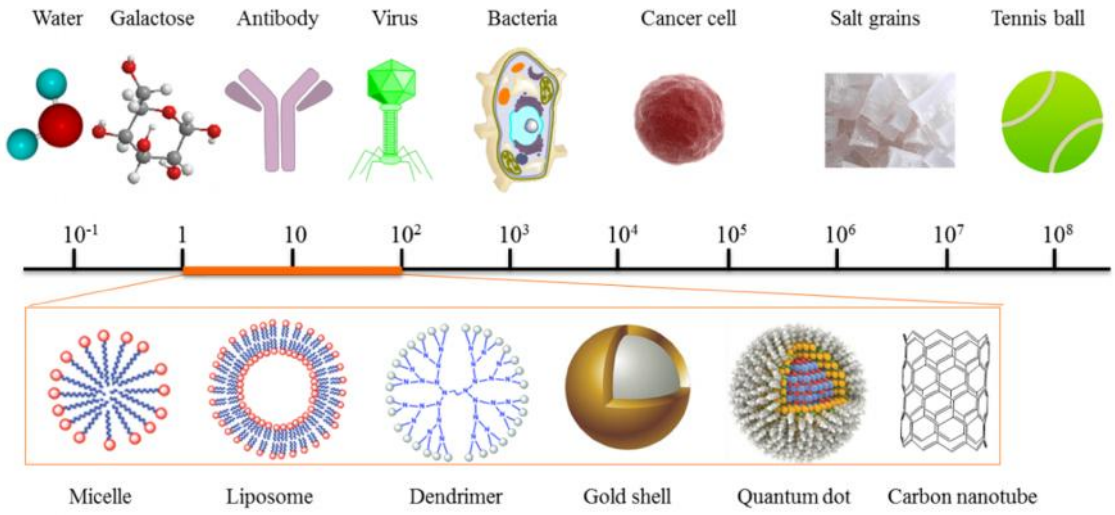

Figure 1: Comparison between bulk materials, independent atoms or molecules, and nanoparticles according to size.

Among these nanomaterials, nanoparticles (NPs) have received substantial attention as they exhibit unique physical and chemical properties relative to bulk samples of the same material. Nanoparticles are crystalline clusters of atoms (of a few hundred up to a few thousand) with sizes of a few nanometers. NPs have been used a long time ago. As early as the 4th century, artisans of the Roman Empire embedded colloidal gold and silver nanoparticles into glass to provide it with particular colors. A well-known surviving example of the technique is a ceremonial vessel, the Lycurgus Cup (Figure 2). The cup, which is now in the British Museum of London, changes its color

when lit from the front but blood-red when lit from behind. The technique was further employed during the middle ages to make stained glass windows for many Gothic European cathedrals. Those in the Cathedral of León (Spain) represent one of these unique masterpieces.

Figure 2. Lycurgus Cup displaying different color [3].

Recently, microscopy analysis [4] have demonstrated that the secret of a seventeenth century Damascus steel sword were carbon nanotubes, which provided the steel strength, durability, and ability to maintain a very sharp edge (Figure 3).

Although nanoparticles have been used a long time ago, it was not until powerful analytical techniques with capabilities to measure and to manipulate the matter at nano-scale that scientists discovered the nano-world and its potential in almost all the branches of science [5].

Unique attributes of nanoparticles and their rational integration herald a revolutionary age in many scientific disciplines such as physics, chemistry, biology, medicine, engineering and material science, provided their underlying nanoscale principles are well understood and used.

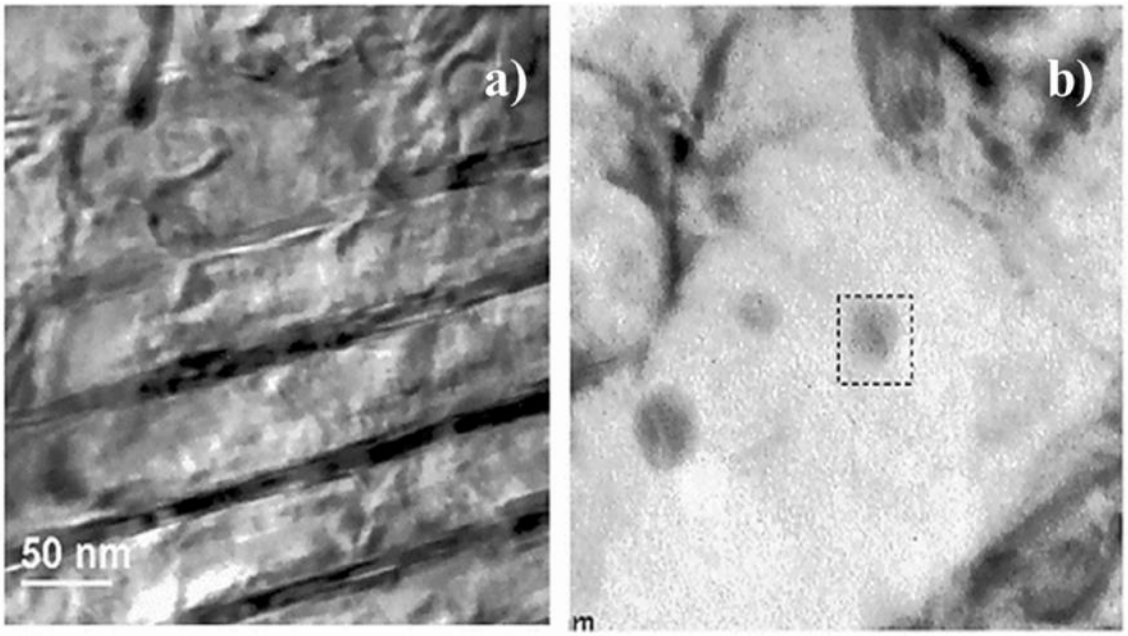

Figure 3: TEM image of cementite nanowires in a Damascus sabre. a) Dark stripes indicate wires of several hundred nanometers in length; b) View showing an almost circular cross section [6].

There are several ways to classify nanomaterials. One way focus on the nanoscale dimensions, according to which a 0-D material has no dimension with a length larger than 100 nm (e.g. an spherical nanoparticle), 1-D material has one dimension is larger than 100 nm (nanowires, nanotubes, nano-ribbons), 2-D material has two dimensions larger than 100 nm (thin films). 0-D, 1-D and 2-D nanomaterials may be embedded in a liquid or solid matrix or may be deposited onto a support, forming powders, fibers, multi-layer and polycrystalline materials [7]. In these materials, 0-D, 1-D and 2-D particles are closely packed together and belong to 3-D nanomaterials (see Figure 4). Nanoparticles can be synthesized not only from metallic materials (Au, Ag, Co) but also from metallic oxides (TiO_2, ZnO, Fe_3O_4), metallic semiconductors (CdS, CdTe, SZn) and rich carbon materials. Table 1 summarizes some of these nanoparticles with the materials used in each case [1].

Table 1: Different nanoparticles and the materials for their preparation

TYPE	APPROXIMATE SIZE	MATERIALS
Nanocrystals and clusters (quantum dots)	0.1-10 nm	Metals, semiconductors, carbon, magnetic materials
Other nanoparticles	1-100 nm	Ceramic oxides
Nanowires	1-100 nm	Metals, semiconductors, oxides, sulfides, nitrides
Nanotubes	1–100 nm	Carbon, layered metal chalcogenides
Nanoporous	Pore diam. 0.5–10 nm	Zeolites, phosphates etc
2-Dimensional arrays (of nano particles)	Several nm^2–mm^2	Metals, semiconductors, magnetic materials
Surfaces and thin films	Thickness 1–1000 nm	A variety of materials
3-Dimensional structures (superlattices)	Several nm in the three dimensions	Metals, semiconductors, magnetic materials

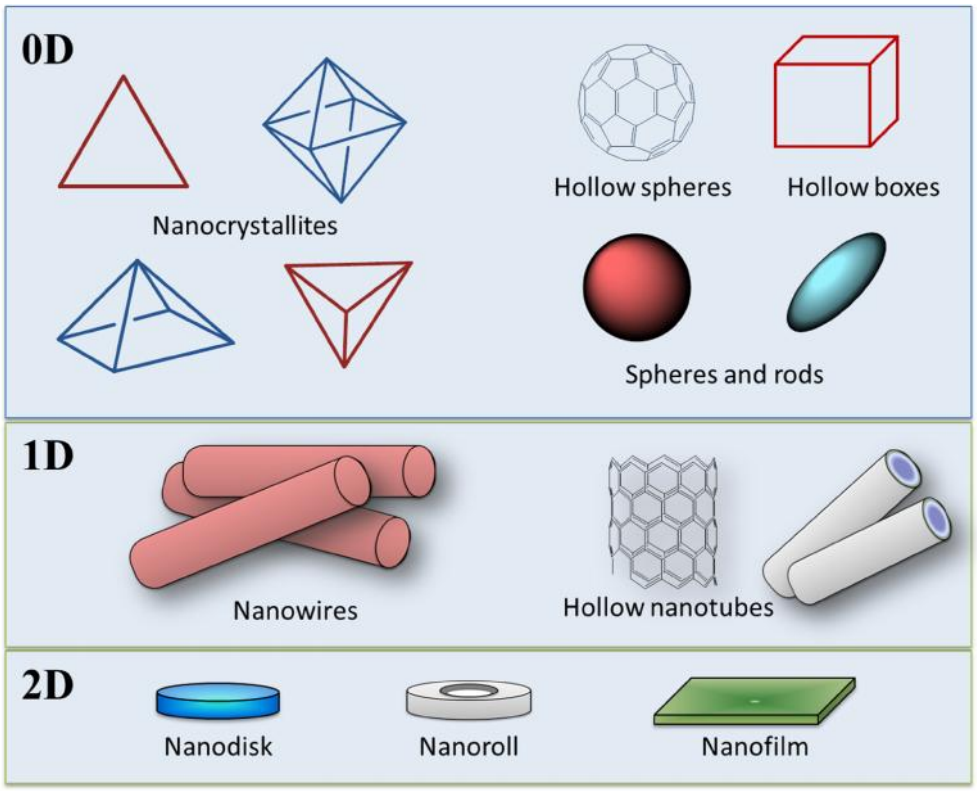

Figure 4: Schematic illustration of dimensionality in nanomaterials.

The unique properties exhibited by nanoparticles has been described taking into account some considerations. In decreasing the size of particles to 3D dimensions below a few tens of nanometers, the physical properties of the matter are significantly affected. These properties can be attributed to their extremely large surface area-to-volume ratio that provides them with a great number of active sites for binding or interaction with target molecules. In fact, the surface plays a key role in a nanoscale material. So, the optical properties of some nanoparticles are dictated by quantum confinement of electrons or other particles (excitons, holes, etc) in one or more dimensions. Due to their dual wave-particle nature, the behavior of electrons is sensitive to the dimensions of the solid in which they move. In bulk materials, electrons are not affected by the solid size (periodic boundary conditions), but if the size is reduced, electrons start to “feel” the boundaries in all three spatial coordinates: the system is “quantized” (in terms of wave-functions and energies) and hence it follows the rules of quantum mechanics instead of classical physics. So, while in bulk materials there will be a continuous distribution of states in all spatial directions, in nanoparticles the electrons can freely

move only along reduced dimensions. In the case of quantization in all directions, electrons possess discrete wavenumbers and the system is called a “quantum dot” (QD). The classical way to discriminate among the different quantized systems in terms of electronic states is the density of states, D(E), which represents the number of electronic states in a unitary interval of energy. In Figure 5 it is shown the well-known dependence of the density of states with the size of the material.

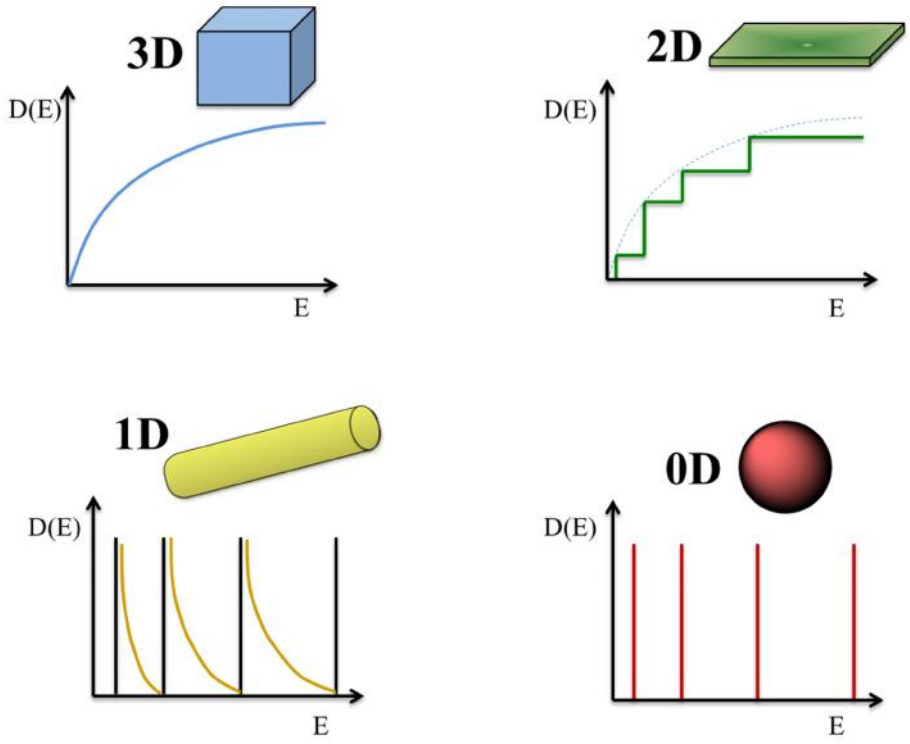

Figure 5: Electronic density of states for bulk 3D, a 2D quantum well, a 1D nanowire and 0D quantum dot.

The electronic states become progressively delocalized as the system size increases towards the bulk limit due to the increased overlapping of the electron wave functions. Nanoparticles lie in between the atomic (and molecular) limit with discrete density of electronic levels and the bulk material limit (with continuous bands) (Figure 6). As a consequence, optical properties of nanoparticles can be controlled by particle size and surface functionalization.

Nanoparticles can be incorporated into a solid matrix to obtain composites with different levels of enhanced physical properties, such as high elastic modulus, better thermal conduction,

enhancement of barrier properties, increased glass transition temperature, improved magnetic behavior and so on.

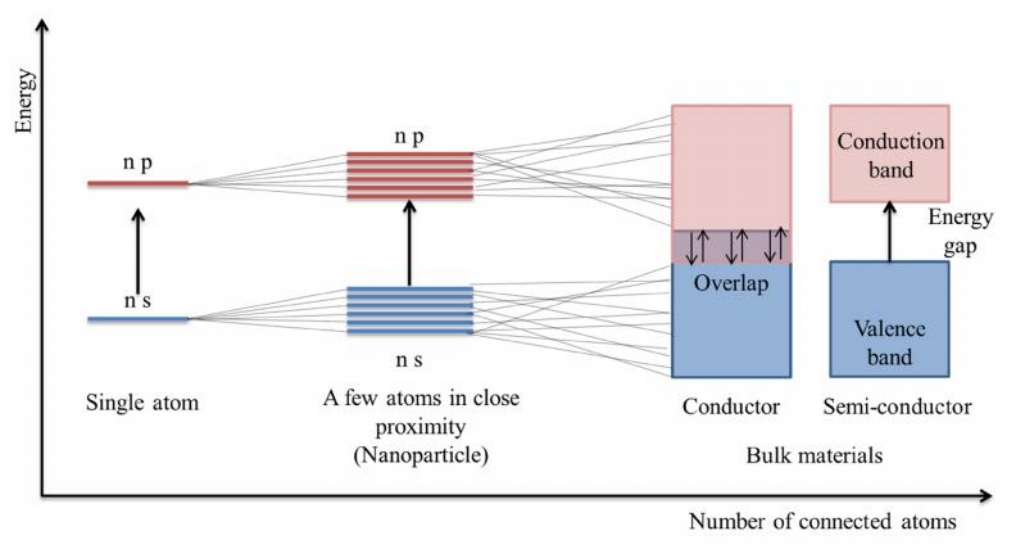

Figure 6: Electronic energy states of a nanoparticle in the bridge between discrete atoms (or molecules) and bulk materials.

I.2. Analytical and bioanalytical applications of NPs

An overview of the potential analytical and bioanalytical applications of nanoparticles is outlined in Figure 7.

In the following the characteristics of most used nanoparticles will be described, with special emphasis on magnetic nanoparticles and carbon dots, the ones investigated in this dissertation.

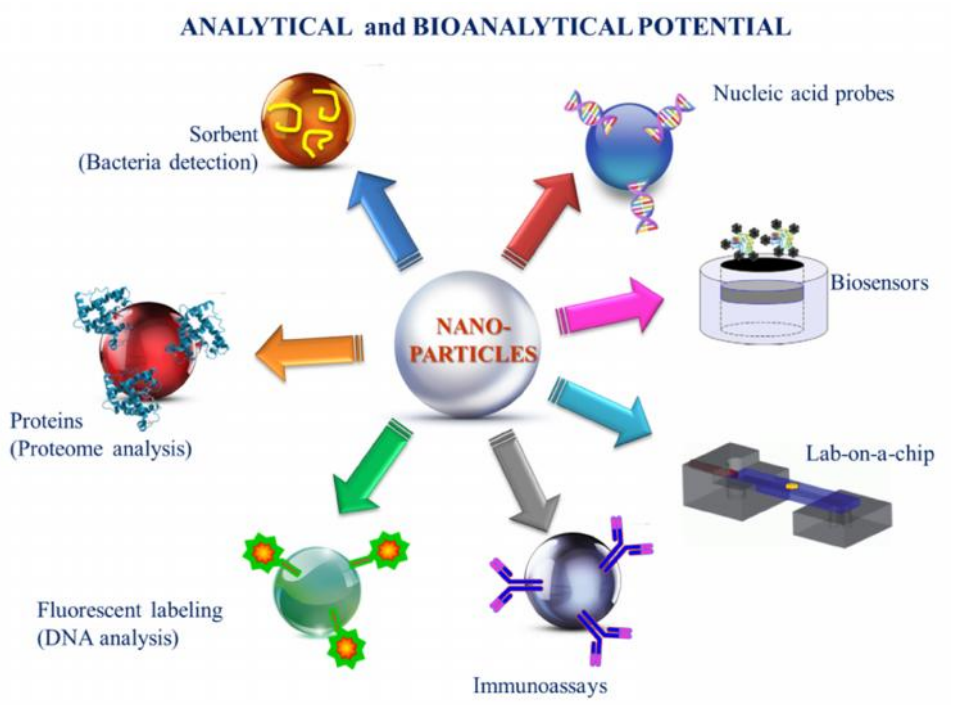

Figure 7: Analytical and bioanalytical potential of NPs.

I.2.1. Quantum dots

Semiconductor nanocrystals, composed of groups II-VI or III-V elements, often referred to as quantum dots (QDs), have been intensively investigated due to their particular luminescent properties. Usually QDs are binary systems composed of a core of semiconducting material enclosed within a shell of another semiconductor. When a photon of visible light hits such nanocrystals, some electrons of the valence are excited into higher energy states (conduction band), generating an electron-hole pair (exciton). This exciton can return to its ground state through recombination of the

constituent electron and hole, which may be accompanied by the conversion of the bandgap energy into an emitted photon. Since the energy of the bandgap dictates the photon's emission wavelength, it is possible to control the fluorescence wavelength by the size of the nanoparticle. As the bandgap energy is inversely proportional to the square of the size of the QD, the decrease of the QD size produces an exciton of higher energy (emission at shorter wavelengths).

Fluorescence is a powerful tool not only in analytical chemistry but also in biological research. However, commonly used chemical fluorophores have some drawbacks, which include photobleaching, polarity dependence of their luminescent properties, limited Stokes shift and low quantum yields. In comparison to organic dyes, QDs offer attractive properties for practical applications. The unique photo-physical and chemical properties of QDs could be summarized as follows [2]:

1- High fluorescence quantum yield and high photo-stability that can be exploited in situations where long-term monitoring of labeled substances is required.
2- Long fluorescence lifetimes (in the order of 10-40 ns) which may be advantageous in time-gated imaging.
3- Tunable luminescent properties by adjusting the particle size.
4- Fluorescence spectra with a narrow emission bands (usually 20-40 nm full width at half maximum intensity) exhibiting a large Stokes shift.
5- Broad absorbance band, unlike molecular fluorophores, that permits the photoexcitation of different sized QDs by a single wavelength.
6- The facile chemical coupling with other biomolecules via several synthetic methodologies to produce hybrid photo-composites renders the particle not only water-soluble but also allows its biocompatibilization and functionalization.

Most applications of QDs have been devoted to the biomedicine and life sciences [8]: labeling of biomolecules, drug delivery, intracellular and extracellular targeting, multiplexing, gene technology, in vivo and in vitro animal imaging, pathogen and toxin detection, tumour biology investigations [9-11]. However, QDs have also found some applications in Analytical Chemistry. QDs could be used as luminescent probes for (bio)chemical sensing or recognition. FRET (Förster Resonance Energy Transfer) and BRET (Bioluminescence Resonance Energy Transfer), along with charge transfer quenching and chemiluminescence resonance energy transfer (CRET) are the most

common strategies in biosensing applications using QDs as optical transducers [12]. Interesting applications of QDs have been reviewed by Chaniotakis et al. [13]. Also, applications in analytical proteomics for single molecule detection, microbial identification and detection and cancer diagnosis have been described [14].

I.2.2. Magnetic nanoparticles (mNPs)

Magnetic nanoparticles (mNPs) have attracted much attention in the past two decades due to their high specific surface area, low toxicity and strong magnetic responses [15–17]. They have been used as excellent materials in numerous applications in biomedicine and biology sciences such as magnetic resonance imaging, targeted drug delivery, rapid biological separation, biosensors, nuclear fuel separation, and magnetic hyperthermia therapy [18–24].

Several compounds such as nano zero-valent iron, Fe-Co, Co-γ-Fe_2O_3, γ-Fe_2O_3, and Fe_3O_4 have been used as mNPs in various applications [7, 15]. However, magnetite (Fe_3O_4) or its oxidized form maghemite (γ-Fe_2O_3), due to their super-paramagnetism, biocompatibility and low toxicity, have sparked an immense interest for analytical, engineering and biomedical applications [5, 7]. Table 2 shows a comparison between both magnetite and maghemite [5].

Table 2: Comparison between magnetite and maghemite.

FEATURE	MAGNETITE	MAGHEMITE
Content	Divalent and trivalent Fe (Fe^{2+} and Fe^{3+})	Trivalent Fe only (Fe^{3+})
IUPAC name and chemical formula	Iron (II,III) oxide, Fe_3O_4 or $FeO \cdot Fe_2O_3$	Iron (III) oxide, γ-Fe_2O_3
Color	Black or greyish black	Brown
Crystal structural formula	$[Fe^{3+}]_{Td}$ $[Fe^{3+},Fe^{2+}]_{Oh}$ $O^{2-}{}_4$, i.e there is a tetrahedral magnetic sublattice, containing Fe^{3+} ions, and an octahedral sublattice, containing Fe^{3+} and Fe^{2+} ions	Similar to magnetite, but with vacancies in octahedral sites due to oxidation of divalent iron ions
	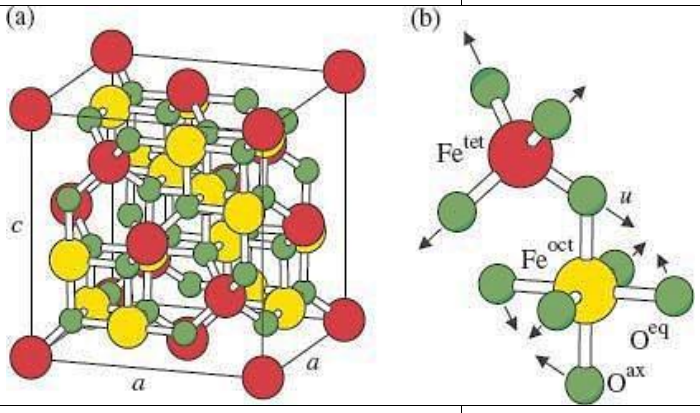	
Magnetization of bulk material at 25^0 C	90-92 emu/g	80 emu/g

I.2.2.1. Background about magnetic properties

According to their response to an externally applied magnetic field, materials can be classified into diamagnetic, paramagnetic, ferromagnetic, ferrimagnetic and antiferromagnetic. These magnetic responses differ greatly in strength. In the presence of an externally applied magnetic field, the atomic current loops created by the orbital motion of electrons (magnetic dipoles) respond to oppose the applied field. All materials display this type of weak repulsion to a magnetic field known as diamagnetism. This magnetic behavior is usually very weak and is observed in materials with filled electronic subshells (magnetic moments are paired and cancel each other). For paramagnetic materials the response is stronger than for diamagnetics: the magnetic dipoles become aligned in the

direction of the applied field and proportional to it. Ferromagnetic materials have net magnetic dipole moments in the absence of an external magnetic field. In antiferromagnetic and ferromagnetic materials, the atomic level magnetic dipole moments are similar to those of ferromagnetic materials; however, adjacent dipole moments exist that are no oriented in parallel and effectively cancel or reduce, respectively, the impact of neighboring magnetic dipoles within the material in the absence of an applied field. In Figure 8 an illustration of such situations is shown.

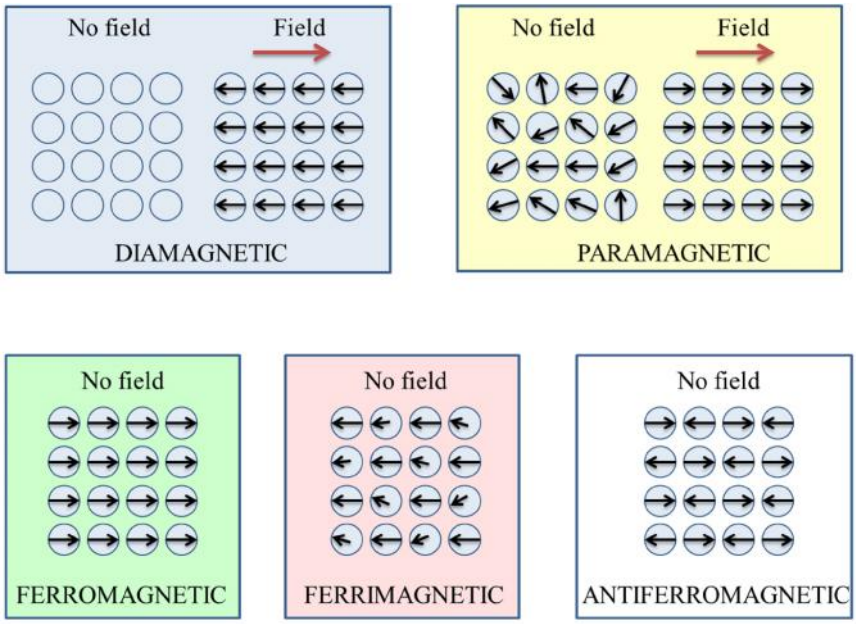

Figure 8: Magnetic dipoles and behavior in absence and presence of an applied magnetic field.

When a magnetic material is placed in a magnetic field of strength H, the individual atomic moments in the material contribute to its overall response, the magnetic induction B:

$$B = «_0(H+M)$$

where μ_0 is the permeability of the free space and M is the magnetization, a measure of the total magnetic dipole moments per unit volume of the material:

$$M = m/V$$

being *m* the magnetic moment on a volume *V* of the material. As all the materials are magnetic to some extent depending on their atomic structure and temperature, they can be classified in terms of their volumetric magnetic susceptibility, χ, defined as [25, 26]:

$$\chi = M/H$$

The parameter χ is known as the magnetic susceptibility of the material; it is a complicated function of several parameters (temperature, orientation, state of stress, applied field) but is often treated as a scalar. It is a measure of the effectiveness of an applied magnetic field for inducing a magnetic dipole in the material. As M and H have the same units (A m^{-1}), χ is dimensionless.
Another parameter that demonstrates the type of magnetic material is the permeability, μ, defined by the equation:

$$« = B/H$$

The permeability of a material measures how permeable the material is to the magnetic field. Another parameter to describe the magnetic properties of solids is the ratio of the permeability in a material to the permeability in a vacuum [25, 26]:

$$\mu_r = \frac{\mu}{\mu_o}$$

where μ_r is called the relative permeability (unitless) and μ_0 is the permeability of vacuum, a universal constant. The relative permeability is a measure of the degree to which the material can be magnetized or the ease with which a B field can be induced in the presence of an external H field. In Table 3 a brief distinction between diamagnetic, paramagnetic and ferromagnetic materials is given, taking into account some of the above described parameters [27].

Table 3: Comparison between diamagnetic, paramagnetic, and ferromagnetic materials

PROPERTY	DIAMAGNETIC	PARAMAGNETIC	FERROMAGNETIC
Magnetic moment and magnetization	Small negative	Small positive	Large positive
Permeability (μ)	$\mu < \mu_0$	$\mu > \mu_0$	$\mu >> \mu_0$
Relative permeability (μ_r)	$0 \leq \mu_r < 1$	$0 < \mu_r < 1+\varepsilon$	$\mu_r >> 1$
Magnetic susceptibility (χ)	$-1 < \chi < 0$	$0 < \chi < \varepsilon$	$\chi >> 1$

I.2.2.1.1. Magnetic domains

In most materials that are not magnetic, the magnetic moments of the atoms inside are all oriented in random directions that cancel each other. In ferromagnetic materials, the atoms form structures called domains, in which all the electrons have the same magnetic orientation. If there is no external magnetic field present, the domains are oriented randomly and no net magnetic field is observed. Magnetic domains exist in order to reduce the energy of the system. When an external magnetic field is applied, all or most of the domains are aligned in the same direction, thus becoming the material magnetized in that direction (Figure 9).

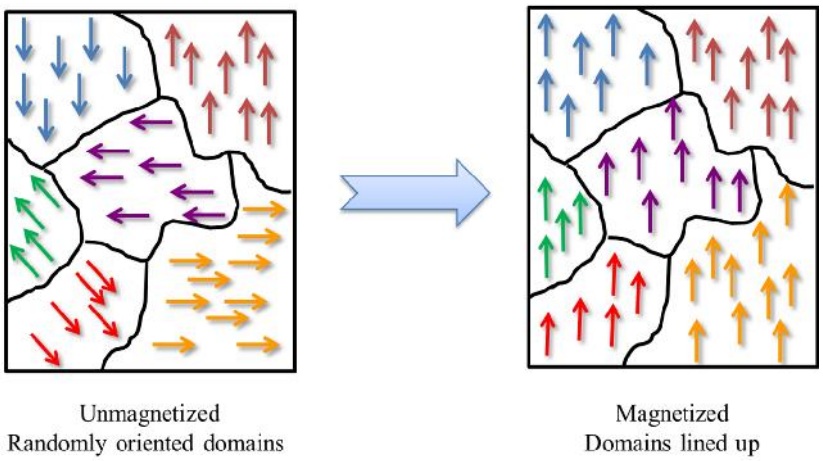

Figure 9: Ferromagnetic material under external magnetic field.

I.2.2.1.2. Hysteresis

In non-magnetized ferromagnetic or ferromagnetic materials, the collections of parallel spins in a domain are randomly oriented throughout the material and collectively self-cancel, thus resulting in a minimal to zero net magnetization (Figure 10 at M=0) If the external magnetic field is slowly increased in the positive direction, the magnetization (internal magnetic field of the material, B) rises rapidly until all of the domains are aligned with the external field, finally leveling off and becoming independent of H. This maximum value of B is the saturation magnetization M_s (represents the magnetization that results when all the magnetic dipoles in a solid are mutually aligned with the external field). If the external field is reduced (still positive), the aligned domains do not disalign easily, and the material does not retrace its original path. A hysteresis effect is produced in which the B field lags behind the applied H field. When H goes to zero, there is still an internal field that

remains. This field is called the “residual magnetization” or “remanence” and the material remains magnetized in the absence of an external H field. At this point, if the direction of H is reversed and its magnitude is increased, the internal field of the magnet, B, is forced to zero. The external field,- H_c, required to do this is called ”coercivity” or “coercive force”. Upon continuation of the applied field in the reverse direction, saturation is achieved in the opposite sense. A second reversal of the field to the initial saturation completes the symmetrical hysteresis loop and also yields both a negative remanence ($-B_r$) and a positive coercivity ($+H_c$) [25, 26, 28].

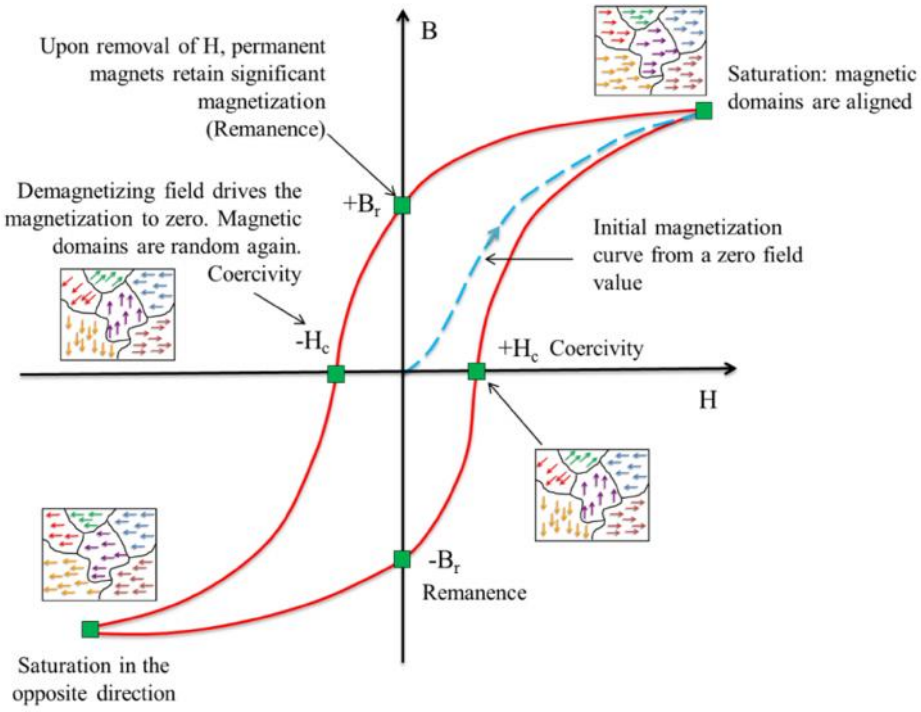

Figure 10: Typical magnetization curve for ferromagnetic materials.

I.2.2.1.3. Ferrimagnetism and antiferromagnetism

Some materials exhibit a permanent magnetization termed ferrimagnetism. Typical examples of ferromagnetic materials are cubic ferrites, being the mineral magnetite Fe_3O_4 the prototype. Materials, in which the alignment of the spin moments of neighboring atoms in exactly opposite directions, are termed antiferromagnetics. A material displaying such behavior is MnO as well as hematite and chromium [25, 26].

I.2.2.1.4. Superparamagnetism

It is a type of magnetism that appears when ferromagnetic or ferrimagnetic material particles with sizes as low as 10-20 nm [29]. This property is size-dependent. At such nanometric size, the nanoparticles do not exhibit multiple domains as it happens in bulk materials. Each particle turns into a single-domain structure and acts as a "single super spin" that exhibits high magnetic susceptibility. It means that on application of a magnetic field, these nanoparticles will provide a stronger and more rapid magnetic response in comparison with bulk materials, with negligible remanence and coercivity. Also, once the applied magnetic field is removed, the magnetic nanoparticles retain no residual magnetism at room temperature and hence they are easily dispersed (they have no tendency to agglomerate).

One assumption of the superparamagnetic theory is to consider that all the magnetic moments within the nanoparticle rotate coherently, i.e. to consider an effective uniaxial anisotropy K, which leads to an energy barrier which is proportional to KV, where V is the volume of the nanoparticle.

So, for a single domain particle with uniaxial anisotropy the energy barrier for coherent magnetization reversal is given as:

$$E = KV \sin^2\theta$$

where E is the energy barrier, K is the magnetic anisotropy of the nanoparticle, V the particle volume and θ is the angle between the magnetic moment and the easy axis of the particle. The magnetic moments in each nanoparticle will point to the same preferred direction known as the *easy axis*, a preferred crystallographic direction determined by the magnetocrystalline anisotropy (K) of the material [5]. The easy axis is given for a material and does not depend on the material shape.

The anisotropy energy barrier can be viewed as a simple potential well model as shown in Figure 11 [30]. In practice, there are can be many minima, each for different crystallographic directions. However, in thermal equilibrium the resulting magnetization of the nanoparticle will point to that direction that minimizes the total anisotropy energy (the easy axis).

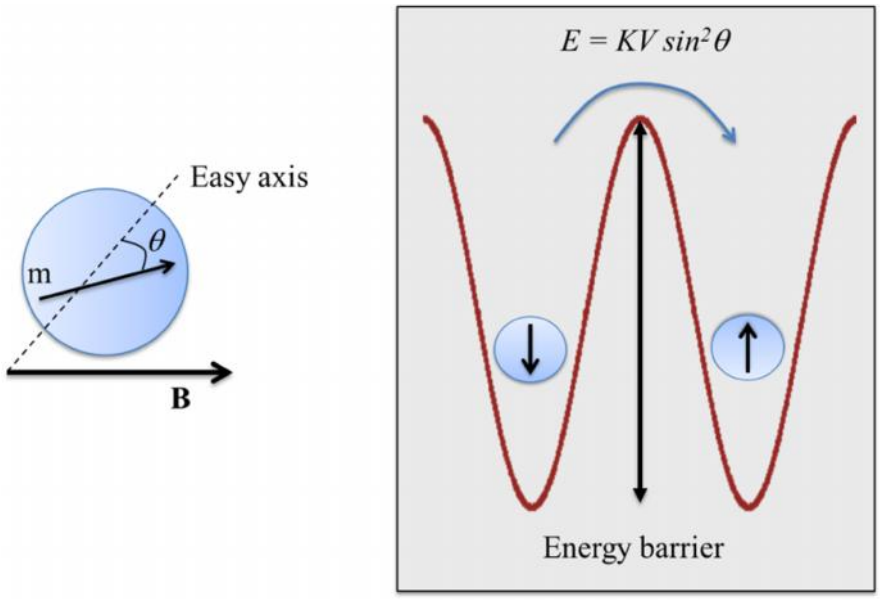

Figure 11: Dependence of magnetic energy from an angle of applied field relative to easy axis.

The energy barrier may be comparable to the thermal energy in such a way that the direction of the nanoparticles moment fluctuates and behaves like a paramagnetic material [**5**]. Notwithstanding, instead of a single magnetic moment per atom as in the case of a conventional paramagnetic material, each nanoparticle contains many spins magnetically coupled: the nanoparticle behaves as a "super-spin" with a relatively large moment per particle. The term superparamagnetism was coined to differentiate and describe such behavior [5].

A typical magnetization curve for uncoated superparamagnetic material is illustrated in figure 12. If the mNPs are coated by a layer of a different material, the magnetization would be decreased probably due to the existence of a magnetically dead layer on the particle's surface, the existence of canted spins, or the existence of a spin-glass-like behavior of the surface spins [28].

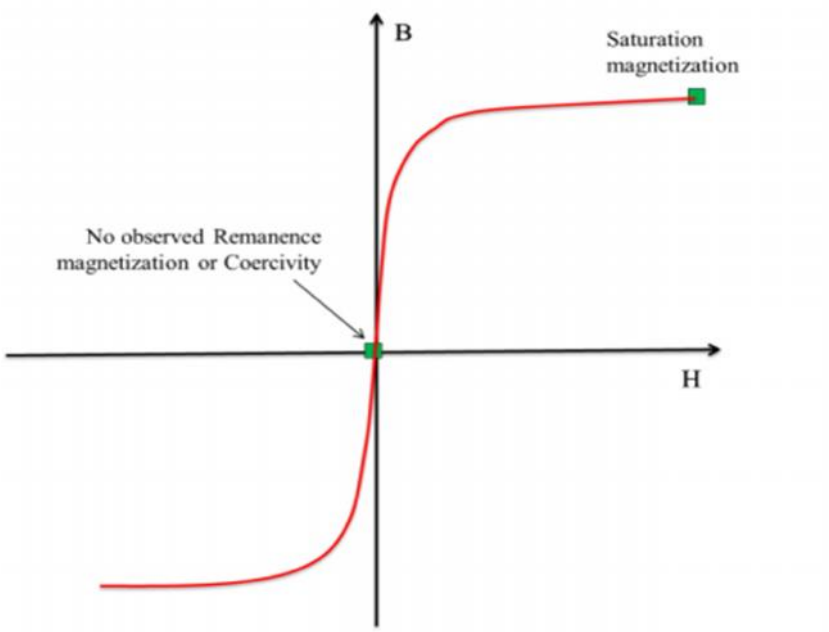

Figure 12: Typical magnetization curve for superparamagnetic materials.

Magnetite mNPs exhibit superparamagnetism: they are easily magnetized when exposed to an external magnetic field and become immediately demagnetized, without residual magnetism, when the field is removed [31, 32]. Therefore, they can be recovered easily from solution under the influence of an external magnetic field (magnetic separation).

I.2.2.2. Functionalization of mNPs

In the last decade, increased research with different types of iron oxides have been carried out in the field of mNPs, mostly including the Fe_3O_4 magnetite, α-Fe_2O_3 (hematite, weakly ferromagnetic or antiferromagnetic), γ-Fe_2O_3 (maghemite, ferrimagnetic), FeO (Würsite, antiferromagnetic), ε-Fe_2O_3 and β-Fe_2O_3. As magnetic iron oxide nanoparticles have a large surface to volume ratio and, consequently, high surface energies, they tend to aggregate in order to minimize the surface energies. Also, they have high chemical activity and become easily oxidized in air (particularly magnetite), resulting in a loss of magnetic properties and dispersibility [29].

Providing an adequate surface coating and effective protection to keep the stability of iron oxide mNPs are important aspects for further applications. The strategies of coating the surface of iron oxide mNPs with another layer can be divided mainly into two major groups: a) coating with

organic shell including surfactants and polymers and b) coating with inorganic components including silica, carbon, precious metals (such as Ag, Au) or oxides such as Y_2O_3 (Figure 13) [33]. The protecting shell not only stabilize the mNPs, but also permit further functionalization leading to multi-layer mNPs designed for various purposes (multifunctions).

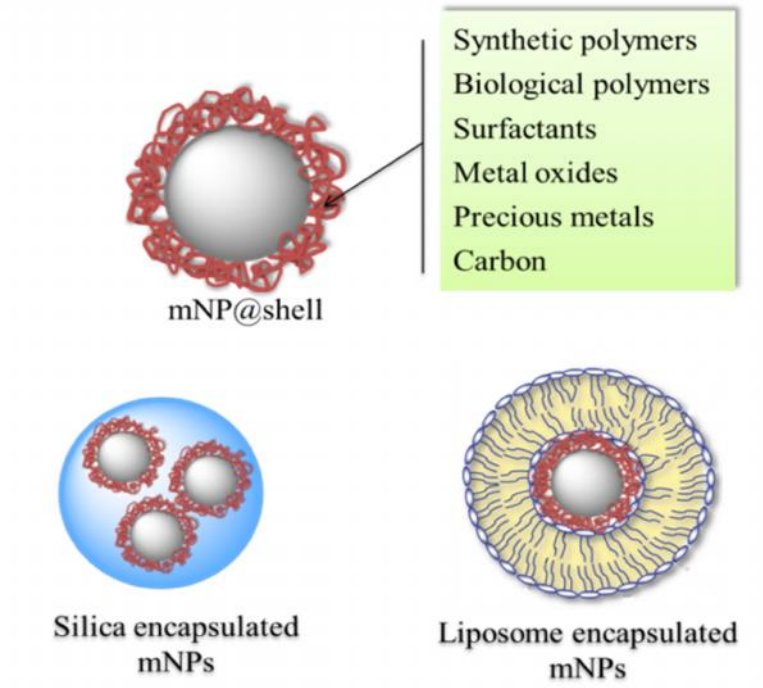

Figure 13: A representative strategy for functionalized mNPs.

Among the organic coatings, surfactants and polymers are used to passivate the surface of the iron oxide mNPs during or after the synthesis. If nanoparticles are coated during the synthesis, their growth can be limited. In general, electrostatic repulsion or steric repulsion are the driving forces to disperse nanoparticles, keeping them in a stable colloidal state. Surfactants and polymers can be chemically bound or physically adsorbed on the iron oxide mNPs, forming single or double layers which provide the steric repulsion forces to stabilize the nanoparticles by steric repulsion [34]. Among capping agents, oleic acid has been found to bind strongly to the surface of metal oxide nanoparticles, preventing them from being oxidized by air. Besides, the presence of double bond in oleic acid allows to form magnetic gels by polymerization and cross-linking [35].

Macromolecular chains of polymers can be irreversibly attached to the nanoparticle surface by chemisorption, offering potential to design purposive functional mNPs [36, 37]. Also, the polymerization can be initiated directly from the particle surface to provide it with a high number of attached polymer chains, using different polymerization routes [35]. Polymers act not only as stabilizers but also endow nanoparticles with biocompatibility. Among synthetic polymers polyethylene glycol, polyvinyl alcohol, polyacrylic acid and polymethylmethacrylate have been commonly used while alginate, cysteine, chitosan, polysaccharide-based coatings have been used to provide not only good solubility but also biocompatibility.

Another way to provide protection of iron mNPs is the use of metal oxide coatings. So, metal oxides with different nature of that of the core have been used as protective shell: TiO_2, ZrO_2, Al_2O_3 and SiO_2. Also, precious metals such as gold or platinum have been explored to increase the stability of magnetic nanoparticles. These coatings can be adequately modified with other synthetic and/or biological molecules for biological and medical applications [38, 39].

Due to the vast and widespread applications of mNPs, herein we will focus only on the functionalization of mNPs, according to the final layer in case of multi-layers, for (bio)analytical as well as biomedical applications as shown in Figure 14.

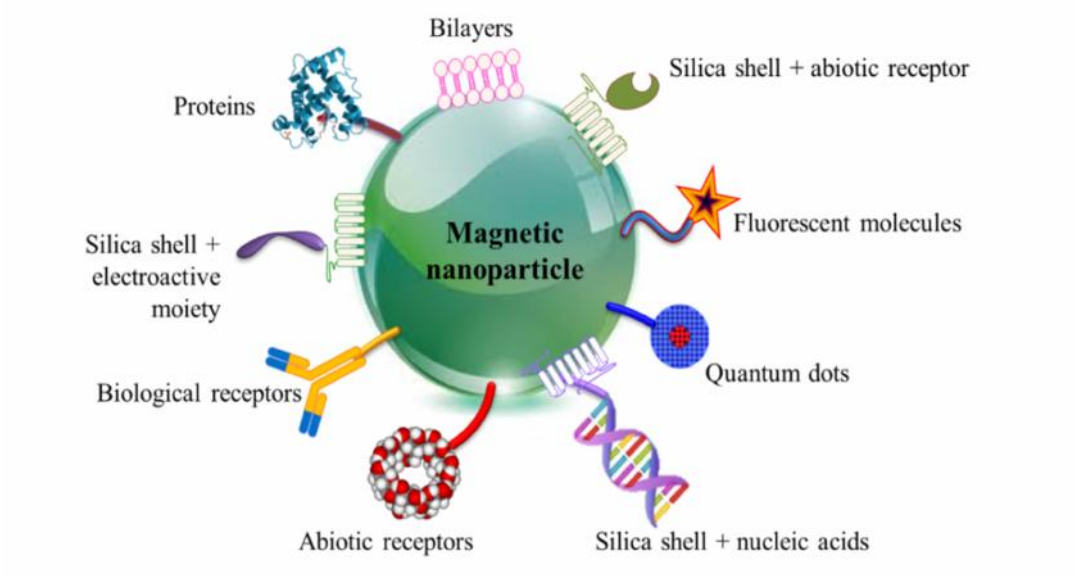

Figure 14: Multi-functional mNPs for (bio)analytical and medical applications.

I.2.2.2.1. mNPs functionalized with host–guest systems

Host–guest chemistry involves the design, synthesis and application of simple abiotic receptors that imitate the performance of naturally occurring molecules. A molecule (host) can bind another molecule (guest) forming a host-guest complex through non covalent interactions. Host-guest systems represent a powerful tool for those analytical systems based molecular recognition, such as sensors and separations. The development of host-guest chemistry started with the discovery of crown ethers [40] and the synthesis, afterwards, of different types of macrocyclic ligands (cryptands, calixarenes, cyclophanes, etc) [41]. It is important to point that to fit the definition of host-guest chemistry geometrical requirements are essential. Among these structures, cyclodextrins (natural cyclic oligosaccharides) have been the most widely used hosts in Analytical Chemistry [42]. Cyclodextrins (CDs) are cyclic oligomers consisting of six (α-CD), seven (β-CD), eight (γ-CD) or more of gucopyranose units linked by α-(1,4) bonds in a torus shaped structure. An overview of some of these cyclodextrins is provided in figure 15.

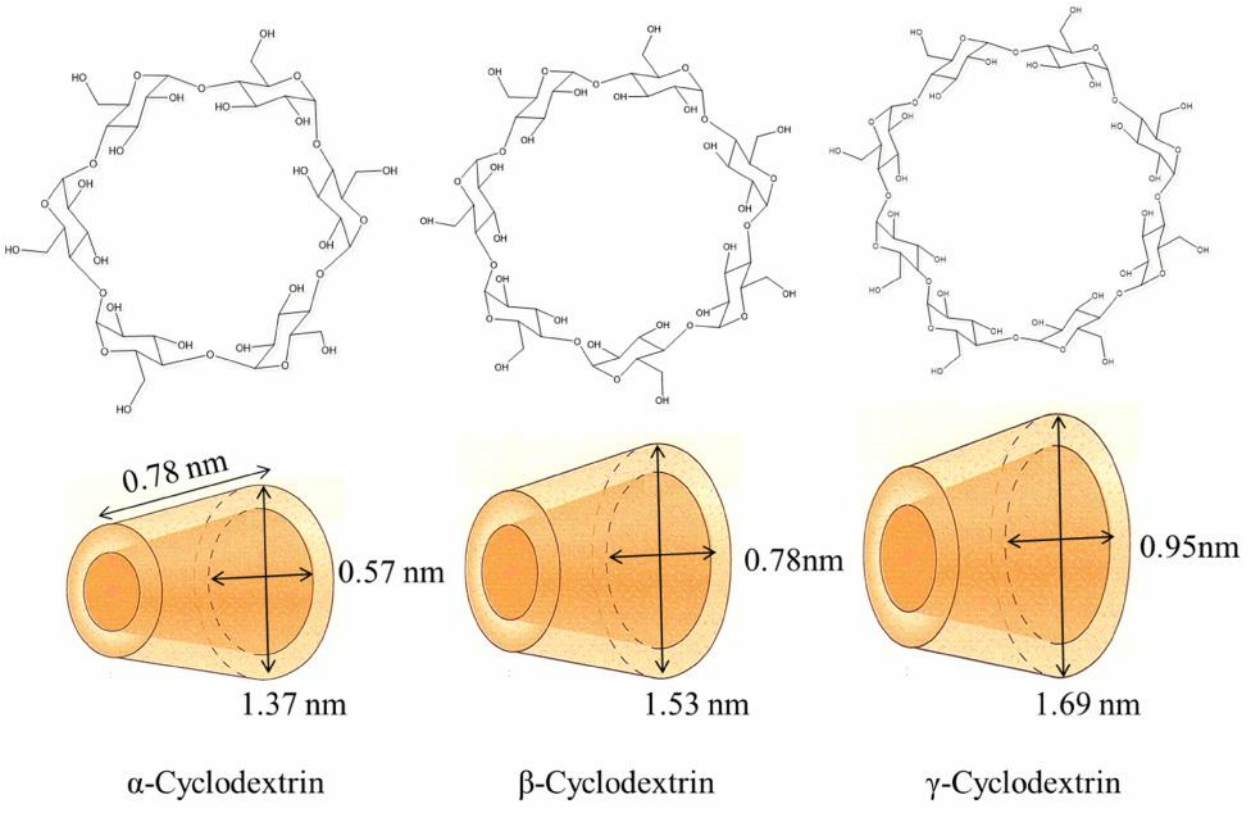

Figure 15: Structures and molecular dimensions of α, β and γ-Cyclodextrins.

Cyclodextrins (CDs) are a versatile group of host molecules which are known to form host-guest complexes with a wide range of organic molecules such as DNA, anticancer drugs, vitamins, and many other molecules [43].

The interior cavity of the CD, with a pronounced hydrophobic character, can accommodate different guest molecules in an aqueous environment. In contrast, the outer surface is hydrophilic due to the presence of hydroxyl groups. The major driving forces in the formation of the CDs inclusion complexes are believed to be hydrophobic and van der Waals interactions. Another important property of CDs is their easy derivatization, which provides them with specific properties and/or to bind them to different substrates (e.g. chromatographic stationary phases) [44].

Molecular recognition ability of β-CD has been exploited in different promising applications such as environment, protein refolding, catalysis, drug delivery and chemical sensing [43, 45-47]. Thus, combining β-CDs and mNPs in one nano-composite system via covalent bonding is considered to be promising and could be used in various applications. In recent reports, β-CDs have been bound to mNPs with different aims: a) for catalysis and adsorption [48, 49], b) for removal of drugs from biological fluids [50], c) for removal of metal ions and dyes [51, 52] and d) for delivery and stabilization of pharmaceuticals and drugs [53, 54].

I.2.2.2.2. mNPs functionalized with molecularly imprinted polymers

Molecular recognition using molecular imprinting is a technique to create template-shaped cavities in polymer matrices with the memory of the template molecules. In other words, molecularly imprinted materials are ready utilizing a template molecule and functional monomers that assemble around the template and in this way get cross-linked to one another. The functional monomers, which are self-assambled around the layout molecule by interaction between functional groups on both the template and monomers, are polymerized forming the molecularly imprinted polymer (MIP). At that point the template molecule can be removed from the lattice under specific conditions (solvent, pH), leaving behind a cavity complementary in size and shape to the template. The obtained cavity can accommodate selectively the specific template molecule [55].

MIPs were created for broad applications including solid-phase extraction (SPE), chromatography, enzymatic catalysis, and sensor technology, because of their high selectivity,

mechanical strength, resistance against acids, bases, organic solvents, and high pressures and temperatures, as well as the low cost and ease for preparation. Similarly, mNPs coated by MIPs have been prepared and applied. However, only a few works have been published describing the applications of these MIP functionalized mNPs [56].

In chromatography, Ping Qu et al [57] have been designed MIPs@mNPs as a stationary phase for rapid enantioseparation of ofloxacin enantiomers by capillary electrochromatography. More recently, S. Azodi-Deilami and co-workers [58] prepared magnetic molecularly imprinted polymer nanoparticles coupled with high performance liquid chromatography for solid-phase extraction of carvedilol in serum samples. In molecular recognition, mNPs functionalized by MIPs have been used for lysozyme and estrone recognition [59, 60].

I.2.3. Carbon nanodots

The carbon family, including fullerenes, carbon nano-tubes, nanodiamonds, carbon nanofibers, and graphene, are well developed, studied and exploited in various applications. C-dots, the newest member of the nanocarbon family with fascinating properties, are inspiring intensive research efforts especially in chemical sensing and bioimaging. C-dots have attracted interest in analytical science by using C-dots (a) passivated by a specific group or molecule directly via one-step simple synthesis, (b) functionalized after their preparation with various organic, polymeric, inorganic, or biological species or (c) (bio)conjugated via covalent bonding with another well-known nanoparticles such as TiO_2 to form nano-composites [61].

C-dots are carbon nanoparticles with diameters lower than 10 nm that exhibit several advantages such as simple synthesis, chemical inertness, low toxicity and environmental-friendly compared with semiconductor quantum dots. Due to their unique optical properties, such as broad excitation spectra, tunable emission wavelength and stable photoluminescence, considerable attention has been paid in recent years to C-dots to exploit their potential in many applications such as bioimaging, drug delivery and analytical sensing [62-65].

I.2.3.1. Synthetic routes of C-dots

Several methods are available for C-dots synthesis and they can be classified into chemical and physical methods. Also, synthesis of these nanoparticles can be classified into bottom-up and top-down methods. Top-down methods be chemical or physical (see Figure 16). Here, we will outline the C-dots synthesis by chemical methods and provide a brief insight into physical approaches.

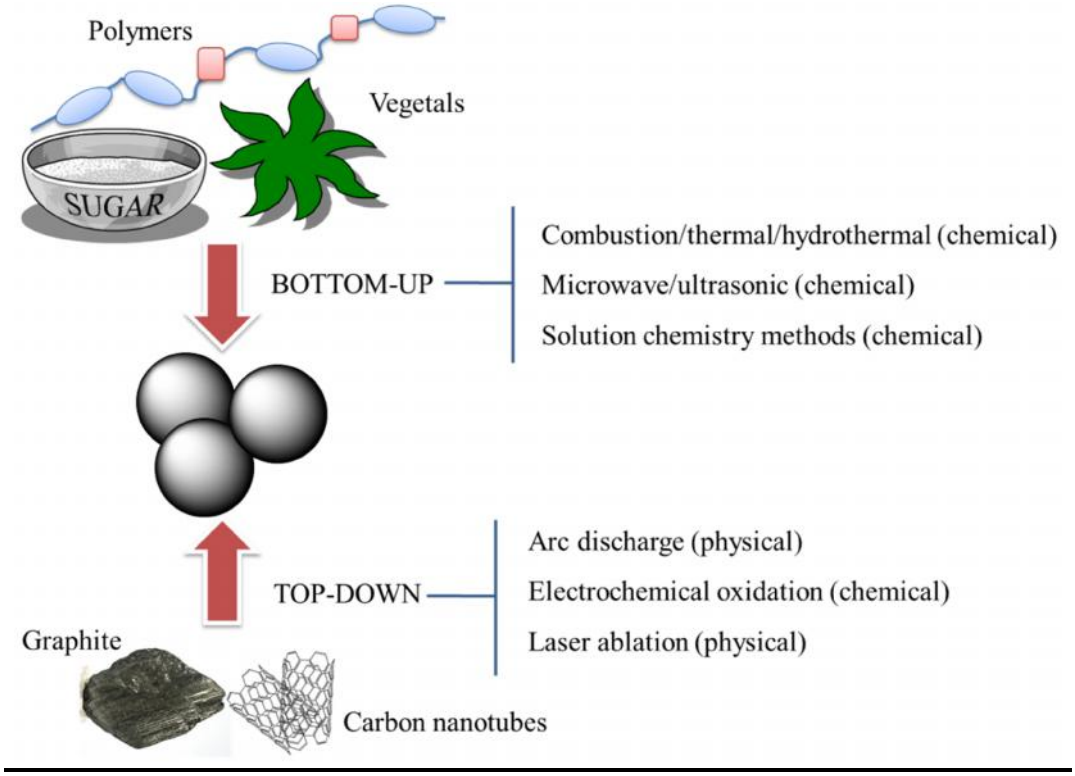

Figure 16: Schematic illustration of C-dots synthesis via top-down and bottom-up approaches.

I.2.3.1.1. Chemical methods

I.2.3.1.1.1. Electrochemical synthesis

Materials such as graphite or multiwalled carbon nanotubes (MWCNT) have been used as working electrodes for the electrochemical synthesis of carbon dots. In this approach, high redox

potentials are adopted, ranging from ±1.5 V to ±3V, an energy enough to either oxidize the C-C bonds or oxidize water to generate hydroxyl and oxygen radicals, which act as electrochemical "knives" in the oxidative cleavage reaction [66]. It is interesting to observe that the potential cycling may the supporting electrolyte (BF_4^- or TBA^+ ions) to intercalate into the carbon electrode, which can result in the exfoliation of the electrode and, consequently, in the production of C-dots. A typical example of this synthetic route is the preparation of 1-4 nm C-dots reported by Kang et al [67]. Using graphite rod as both anode and cathode in alkali medium (NaOH/EtOH), C-dots were synthesized with a current intensity of 10-200 mA cm^{-2}. Experiments demonstrated that an alkaline environment was a key factor in the synthesis: OH^- groups were essential for the formation of C-dots. In a later report [68], these researchers demonstrated the possibility of large-scale synthesis of high-quality C-dots using only pure water (no assistance of supporting electrolyte). The obtained C-dots exhibited high purity, high crystalline nature, excellent aqueous dispersibility, high photocatalytic activity and remarkable luminescence properties.

Recently, C-dots were synthesized electrochemically from other compounds than graphite. So, Chen et al [69] glycine under alkaline conditions through electro-oxidation, electro-polymerization, carbonization, and passivation. These C-dots exhibited excitation-wavelength-dependence and pH sensitive photoluminescence. On the other hand, Deng et al [70] developed a simple electrochemical method based on the direct electrochemical carbonization of low-molecular-weight alcohols which transited into carbon-containing particles under basic conditions. One of the advantages of C-dots produced by electrochemical oxidation is that they consist of 1–3 graphene layers due to strong intergraphene attraction [71].

I.2.3.1.1.2. Combustion/thermal/hydrothermal oxidation method

The combustion oxidation method was reported in 2007 by Mao et al [72]. In their study, candle soot was collected and refluxed with 5M HNO_3, an oxidative treatment that introduced OH and COOH groups in the C-dots surface. This approach resulted to be cheap, but particle sizes ranged from a few nanometers to bulky micrometer scale. A gel electrophoresis approach have to be used to resolve the mixture of nanoparticles. Nitric acid oxidation of other materials such as carbon soot [73], natural gas soot [74] or paraffin oil soot [75] have been also used for the preparation of C-dots.

The hydrothermal method is a facile approach for the preparation of C-dots that offer many advantages: environmentally friendly conditions, facile instruments and techniques, high carbon efficiency and many functional groups remaining on the nanoparticle surface. Usually, carbon precursors can be obtained from different biological sources (e.g. pomelo peel, orange juice, soy milk, etc) or from organic compounds such as carbohydrates (glucose, fructose), disaccharides (sugar), polysaccharides, cellulose, furfural, glutaraldehyde, dopamine and so on. The synthesis is usually assisted by the presence of another molecule (e.g. a polymer, an amine-terminated compound) in order to passivate the nanoparticles [76-78].

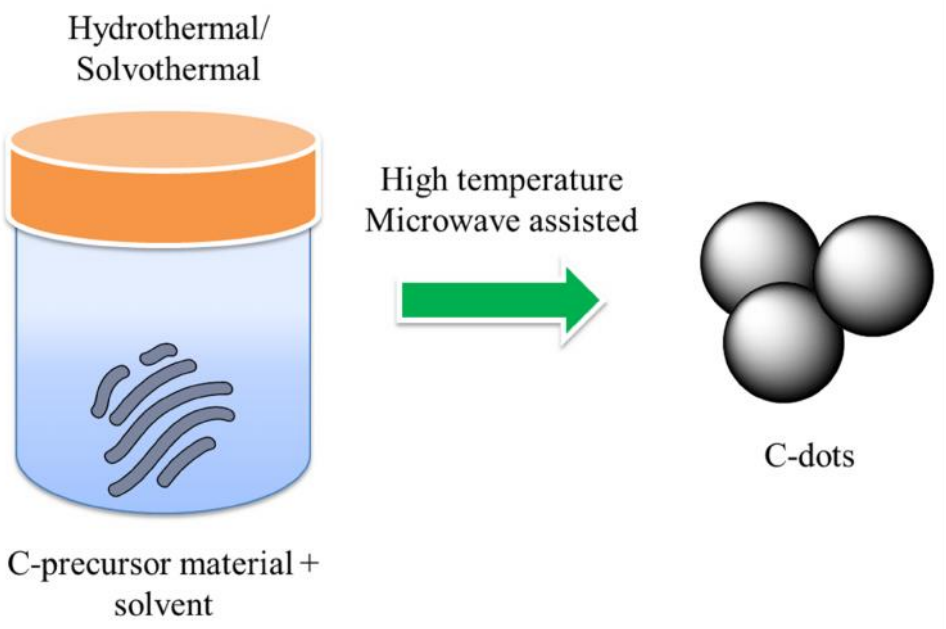

Figure 17: Simplified illustration of C-dots synthesis by thermal carbonization method.

Rui et al [79] reported the direct C-dots synthesis by a simple hydrothermal treatment using polyethylene glycol with different molar weight (400–6000 g mol^{-1}) as the sole carbon source was achieved. The synthesized C-dots with tunable diameters of 2–4 nm exhibited excitation-dependent photoluminescent behavior. Recently, multifunctional C-dots have been prepared from branched polyethyleneimine by oxidation with 1M ammonium persulfate and hydrothermal heating at 100-200ºC for 5-10 h [80]. The resulting C-dots were 3–4 nm in diameter, had graphitic structure with

lattice spacing of 0.30 nm and a quantum yield of 54.3%. Chen et al [81] reported the hydrothermal decomposition of folic acid at various reaction temperatures. The obtained C-dots at 260ºC, without assistance of any passivation agent, exhibited uniform size, strong fluorescence with a quantum yield of 68%. Highly blue luminescent C-dots with photo-luminescence quantum yields (QY) of 31.6%–40.6% were also prepared with a one-step pyrolytic route by using ethylenediamine-tetraacetic acid salts as a carbon source [82]. Many more articles are available by this method differing only in the carbon source as well as the passivation agent.

In recent years, doped C-dots have been the subject of interest due to their unusual properties and applications. In particular, C-dots doped with nitrogen groups (e.g. amino-groups) exhibit high luminescence QY as well as excitation-independent luminescence. Zhi et al [83] reported the hydrothermal synthesis of C-dots from ammonium citrate. The obtained nitrogen-doped C-dots emitted bright blue luminescence, had short fluorescence lifetime, pH-sensitivity and excellent stability at a high salt concentrations. Recently, Li et al [84] reported the hydrothermal synthesis of highly luminescent C-dots (QY = 44.7%) using citric acid. Urea was used not only as a carbon source but also provided surface amino-groups. The authors concluded that synthesis at low temperature (160ºC) resulted in fully surface-passivated C-dots that emitted independently on the excitation wavelength.

Other heteroatoms are currently being the subject of research for doping C-dots, among which sulphur [85] and phosphorus [86] have recently entered the arena of C-dots synthesis. This field is still in its infancy and further investigation is necessary.

I.2.3.1.1.3. Supported synthetic procedure

This method relies on using a mesoporous material (such as surfactant-modified silica) as the support to confine the reactants inside the pores and control the growth of the C-dots by blocking nanoparticle agglomeration during high-temperature treatment [87]. So, it is possible to obtain mono-disperse nanosized C-dots. Giannelis et al [88] used NaY zeolite as the solid host to support the carbogenic nanoparticles. The synthesis consisted of first ion exchanging NaY zeolite with 2,4-diaminophenol di-hydrochloride followed by thermal oxidation at 300ºC in air. This process resulted in C-dots residing mostly at the external surface of the zeolite matrix. Removal of the zeolite matrix

with hydrofluoric acid enabled imaging of the C-dots as near spherical with a size in the range 4-6 nm.

A facile approach using mesoporous silica (MS) spheres as nanoreactors in an impregnation method was reported by Zong et al [89]. First, MS spheres were prepared using N-hexadecylamine as the surfactant, tetraethoxysilane (TEOS) as the precursor and ammonia as a catalyst. Then, MS spheres were impregnated with a mixed solution of complex salts and citric acid. Subsequent calcination and removal of MS supports generated the nanosized hydrophilic C-dots. The resulting highly efficient photoluminescent C-dots were monodisperse, photostable and of low toxicity while showed excellent luminescence properties. The key performance characteristic of this method is the use of MS spheres as supports, which not only may limit the C-dots to a narrow size distribution in the pores of MS spheres, but also may hinder the agglomeration of the nanosized C-dots.

I.2.3.1.1.4. Microwave/ultrasonic synthesis

Although most reports deal with hydrothermal methods for the synthesis of C-dots, they also suffer from some drawbacks. For instance, the long-time of the procedure. Microwave-assisted synthesis combines the advantages of hydrothermal and those of microwave techniques. Microwave heating is more effective compared with conventional heat conduction methods, providing intensive and homogeneous energy, can be achieved at elevated temperature and shorten the reaction time. Microwave-assisted synthesis of C-dots has gained popularity due to the above mentioned advantages. The approach has been demonstrated to be an effective and alternative way of synthesizing C-dots from different starting materials and experimental conditions [90-97].

Ultrasonic chemical synthesis has also used for the synthesis of C-dots. Ultrasound can generate alternating expansive and compressive waves in liquids, leading to the formation of oscillating bubbles, which under the right conditions can violently collapse releasing the energy stored within them. These cavitational implosions are very localized and transient, with temperatures of ca. 5000K and pressures of about 1000 bar. These conditions can cause high-speed impinging liquid jets, deagglomeration, and strong hydrodynamic shear-forces [98]. Several works have been recently published in which ultrasounds are used both for synthesis and surface passivation of C-dots [99, 100].

I.2.3.1.2. Physical methods

We will describe some features of common physical methods for C-dots synthesis, including arc discharge, laser ablation, and plasma treatment. It is interesting to note that there is no fluorescence from the C-dots obtained by these methods and a passivation step is usually necessary to produce light emission.

I.2.3.1.2.1. Arc discharge method

Carbon dots were discovered serendipitously by Xu et al [101] while purification of SWCNTs obtained from arc-discharge soot. Treatment of an unexpected carbon nanomaterial with 3.3 N HNO_3 to introduce carboxyl functional groups improved the hydrophilicity of the material, which was then extracted with NaOH solution. The suspension was separated by gel electrophoresis and a fast moving band of highly fluorescent material composed of C-dots was separated from SWCNTs and short tubular carbons. In the arc discharge method two high purity graphite electrode, one acting as anode and the other as cathode, are involved in the arc discharge. The electrodes are in an inert gas chamber, are water cooled and separated a few millimeters. The electric arc discharge is ignited by a short contact between the electrodes, so that the carbon element contained in the cathode sublimes as result of the high discharge temperature.

I.2.3.1.2.2. Laser ablation/passivation method

C-dots can by synthesized by using high power laser extrusion of carbon targets (whether solid or in a liquid solution). Sun and co-workers produced C-dots via the laser ablation technique, by hot-pressing a mixture of graphite powder and cement in the presence of water vapor with argon as a carrier gas at 900°C and 75 kPa [102, 103]. In order to develop fluorescent C-dots, the authors passivated the surface of the C-dots attaching different diamine-terminated polymeric compounds. After refluxing in HNO_3 for up to 12 h, the acid-treated C-dots gave bright luminescence emission [104, 105]. Esteves da Silva et al [106] prepared C-dots by direct laser ablation of carbon targets immersed in water. After a three-step functionalization process with NH_2-polyethylene-glycol and N-acetyl-l-cysteine the C-dots become fluorescent. The fluorescence of these C-dots was found to be quenched by Hg(II) and Cu(II) ions. The quenching provoked by Hg(II) was used to develop an analytical approach to determine this metal ion. Later, these authors developed a fiber-optic based on these C-dot for the same purpose [107].

I.2.3.1.2.3. Plasma treatment

In 2009, Gokus et al. [108] reported the synthesis of C-dots from single-layer graphene flakes, using an oxygen/argon RF plasma. Oxygen plasma etching of graphite proceeded layer-by-layer. Confocal phololuminescence maps revealed bright pointlike luminescent features. More recently, Jing et al [109] described the synthesis of fluorescent C-dots from egg white and yolk by a low temperature plasma. Authors reported that the C-dots exhibited notable characteristics: 1) one-step generation in minutes from low-cost, natural, edible chicken eggs by plasma-induced pyrolysis; 2) good amphiphilicity with high solubility in a broad range of aqueous and organic solvents; 3) resistance to acids and bases; 4) versatile applications as fluorescent carbon inks for luminescent patterns [109].

I.2.3.2. Crystal structure of C-dots

The chemistry of carbon is particularly important to the stability and properties of many carbon-based nanostructures. A number of covalent carbon nanomaterials may exist in which the bonding nature is different: diamond-like (sp^1), graphite-like (sp^2), linear (sp) or mixed (sp^3/sp^2, sp^2/sp, sp^3/sp). In particular, the versatility in the s-p hybridization makes carbon a unique element leading to a diversity of structures. However, at the nanoscale that versatility is not the same. For example, graphite and some forms of amorphous carbon are semi-metallic with zero band-gaps but carbon nanoparticles in which quantum effects are important, large energy gaps may appear [110].

Hu et al [111] have reported that C-dots prepared by laser ablation/passivation exhibit a diamond-like structure, with the rings corresponding to the (111), (220), (311), (400) and (331) planes of diamond, whether or not the C-dots synthesized in water or in presence of a passivating ligand. On the other hand, sp^2 graphitic carbons have also been proposed for C-dots made from oxidizing candle soot, being the presence of sp^2 confirmed by ^{13}C NMR studies and that of C=C aromatic ring stretches by FTIR measurements [73]. Notwithstanding, amorphous carbon has also been detected in some studies [88]. In conclusion, C-dots consist of an amorphous to nanocrystalline core with predominantly sp^2 carbon while their surface is covered by carboxylic moieties in an extent that depend on the experimental conditions [63].

I.2.3.3. Optical properties of C-dots

I.2.3.3.1. Absorption

C-dot typically show strong optical absorption in the UV region, with a tail extending out into the visible range. For the UV-vis absorption spectrum a band located at 216 nm has been assigned to $\pi \rightarrow \pi^*$ transition of C=C and a band at 273 nm due to $n \rightarrow \pi^*$ of carbonyl groups [112]. In a recent report, Richards et al [113] have found in a study of C-dots produced by annealing nanodiamond powders at 1650ºC for 1h, that the UV-vis spectra of unoxidized C-dots showed a continuous absorption from 200 to 800 nm, indicative of no band gap, while oxidized C-dots (nitric acid treatment) showed a relatively sharp absorption peak at 230 nm. Authors argued that the shift from continuous to sharp absorption was due to the break of sp^2-bonded carbon conjugation which resulted in an increased band gap. Also, it was found that oxidized C-dots absorbed strongly at longer wavelengths due to the presence of lower energy states either from the C-dot cores or from oxygenated defect-related emissive traps on the particle surface [113]. Recently, it has been demonstrated that doping of heteroatoms like B, N or P in C-dots have pronounced effects on changing the absorption properties due to structural relaxations [114].

I.2.3.3. 2. Photoluminescence

Photoluminescence (PL) is one of the most fascinating features of C-dots from fundamentals to their applications. C-dots luminescence has been shown to be free of the blinking and bleaching, effects associated with conventional organic dyes and semiconductor quantum dots. This characteristic make C-dots attractive fluorescent labels.

Although most C-dots exhibit high intense emission in the blue-to-green spectral range, some have been reported to emit in the yellow [115] or even in the red region [116], depending on the synthetic route and the precursor used.

Different research groups have proposed possible PL mechanism such as surface-defects/traps and sp^2-carbon clusters embedded within carbon-core emission [105, 117]. Most of the reported C-dots exhibit emission and intensity excitation wavelength-dependence (see Figure 18) [118].

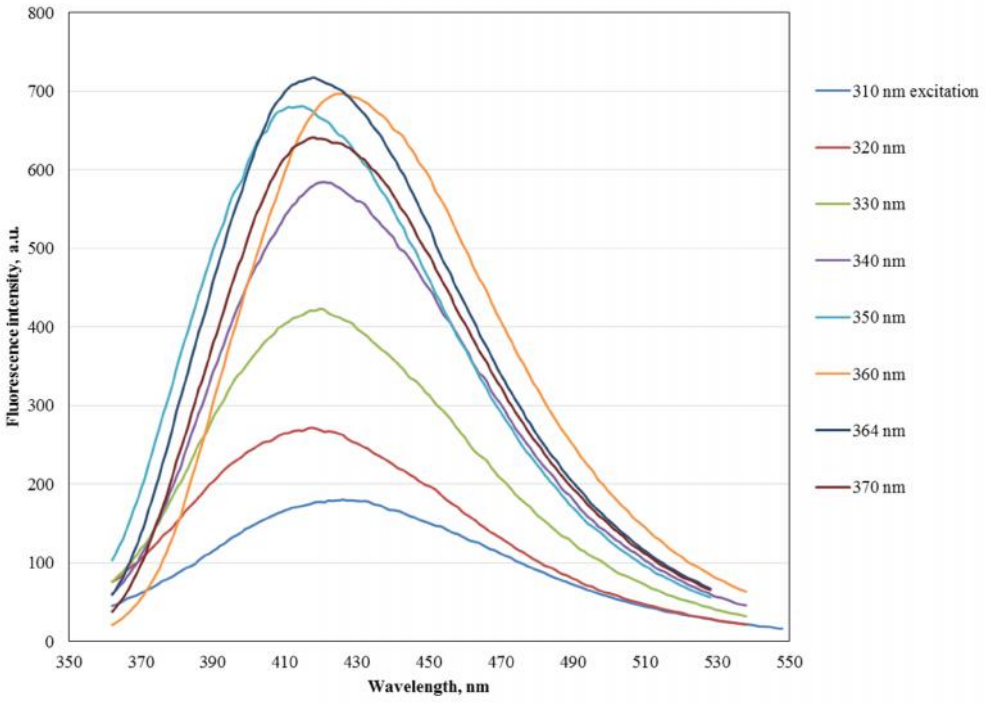

Figure 18: Excitation dependent-fluorescence of C-dots.

The explanation for this phenomenon is not totally understood. However, depending on the precursor used in the synthesis, excitation wavelength-independent PL can be observed. Recently, Dong et al [119] reported the synthesis of deep blue-emitting C-dots using citric acid and L-cysteine as precursor providing N and S as co-dopants. It was suggested that S dopants strongly suppress excitation-dependent PL, while N surface states favored a high yield of radiative recombination.

Up to date, one accepted theory for the excitation wavelength dependent emission relies on the fact that the prepared material is a mixture of nanoparticles of different sizes and nanoparticles containing different edge defects/emissive traps on the surface [63]. So, excitation wavelength-dependent emission was not observed in narrow size distribution C-dots [116] while the wavelength of the dominating emission peak was driven by the graphitic core size (good crystallinity is an essential requirement) [67], in other words, by its suitable quantum confinement similarly to traditional semiconductor quantum dots. DFT (density functional theory) calculations [120] have demonstrated the importance of the core size: an increase in the particle size and aromatic rings conjugation caused a decrease in the $\pi \rightarrow \pi^*$ transition bandgap. However, in a recent paper, Chizhik

et al [121] indicated that the C-dots emission originates not from their core but from a charge recombination on defect centers on the surface of the C-dots and that each C-dot contains only one single optically active emission center.

There are many physical and chemical factors that may modify the PL characteristics of C-dots. The first discussion about the origin of visible luminescence on graphitic carbon nanomaterials (short carbon nanotubes) was reported by Riggs et al. [122] which attributed it mainly to the presence of surface defect states, introduced by the chemical oxidation and functionalization. In different studies, it has been demonstrated that the surface functional groups, directly bound and conjugated to the graphitic core, may profoundly affect the C-dot PL characteristics. Surface groups such as -COOH, C-O, C=O, amino, P, B or S, can introduce trapping states with different energy level, changing the bandgap of the C-dots, shift the PL emission, enlarge the excitation wavelength or cause the emission dependent on the excitation wavelength [114, 123, 124].

The average value of radiative lifetime of the C-dots is in the range of 9-10 ns for all of the emission wavelengths, being difficult to distinguish the surface state emission from that associated with $n \rightarrow \pi^*$ transitions [125]. Besides, the quantum yield (QY) of C-dots may vary with the synthesis method and the surface passivation chemistry involved. So, raw C-dots may exhibit QYs between 4-10% while for those passivated with polymers or metal coated the QYs may increase to 45-50% [63]. The pH values and the ionic strength are also factors that affect the PL properties of C-dots: the emission wavelength peak and its intensity, the magnitude of the changes depending on the nature of the C-dots [63].

I.2.3.4. Photoinduced Electron Transfer and Redox Properties

The studies proved that C-dots can serve as an excellent electron donators and acceptors [119]. This behavior observed through their PL quenching in the toluene medium by the electron acceptor molecules 4-nitrotoluene and 2,4-dinitrotoluene, indicating the electron donor behavior of C-dots. On the other hand, C-dots also can act as electron acceptors by efficiently quenching the PL of electron donors such as N,N-diethylaniline [119].

I.2.3.5. Electrochemical Luminescence (ECL)

Electrochemiluminescence (ECL), a highly sensitive process in which reactive species are generated from stable precursors at the surface of an electrode, not only offer the advantages of CL but also has other interesting features, such as the use of simple equipment, an electrochemically triggered process with very low optical background and excellent temporal and spatial controllability, reasons for which this method has been employed in a number of fields. Zheng et al [126] reported for the first time the electrochemical formation of water soluble carbon nanocrystals (C-dots) from graphite rods. During their electrochemical synthesis, an ECL signal at 535 nm was observed without the addition of co-reactants. At the same time, ECL signal from C-dots was detected in the presence of 0.1 M $S_2O_8^{2-}$, as a co-reactant. This fact is relevant in chemical analysis as it suggests that C-dots offer potential for use in ECL without the addition of co-reactant, opening novel applications in biosensing and imaging. The ECL mechanism of C-dots has been explained as follows: when the potential is raised beyond a threshold value, the "loose shell" on the C-dots acts as a quantized double layer to produce radicals, reduced negatively charged ($R^{\cdot -}$) and oxidized positively charged ($R^{\cdot +}$) radical species. Then, the electron-transfer annihilation of the two oppositely charged radicals took place to form the excited state R*. Finally, the excited C-dots (R*) returned to the ground state via a radiative pathway by emitting a photon [126, 127].

ECL is characterized by surface-state transitions in nanoparticles (PL is more reminiscent of the core state) and is often significantly red shifted from the PL peaks by as much as hundreds of nanometers, due to defect states in the band gap [63, 126, 128]. If the nanoparticles are completely passivated, the ECL profile resembles the PL spectrum. Consequently, the observed ECL red-shift indicates that the emitting states are different and, in turn, the presence of surface traps with incomplete passivation.

In Figure 19 the ECL mechanism in C-dots is shown as a comparison with PL [127].

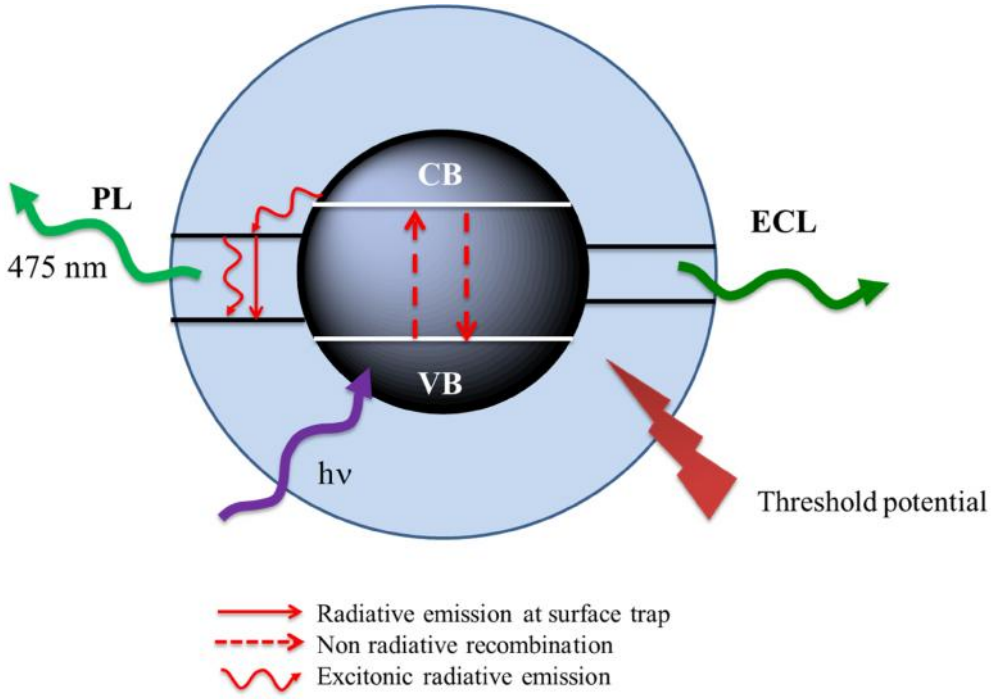

Figure 19: The ECL and PL mechanism for C-dots according to [127].

I.2.3.6. Multiple photon excitation

Another useful optical property of C-dots is the so-called up-conversion PL [104]. C-dots were reported to undergo multi-photon excitation with large two-photon absorption cross-section for laser excitation at 800—900 nm [104, 129]. Multiple photon excitation is observed when multiple low-energy photons arrive at the same time to a fluorophore and by interaction with it, provoke excitation of an electron that is normally excited by one higher energy photon (Figure 20) [64].

The two-photon absorption cross-section of C-dots at different excitation wavelengths was estimated by Gong et al [130]. The typical average value at 800 nm was 48,000 GM (Goeppert—Mayer unit, with 1GM = 10−50 cm^4s/photon), which is comparable or even better than that of organic molecules and high performance QDs (e.g. 47,000 GM for CdSe/ZnScore/shell QDs at 800 nm) [131].

The excitation at 800-900 nm (biological window) is particularly important for bioimaging applications, due to the deeper tissue penetration.

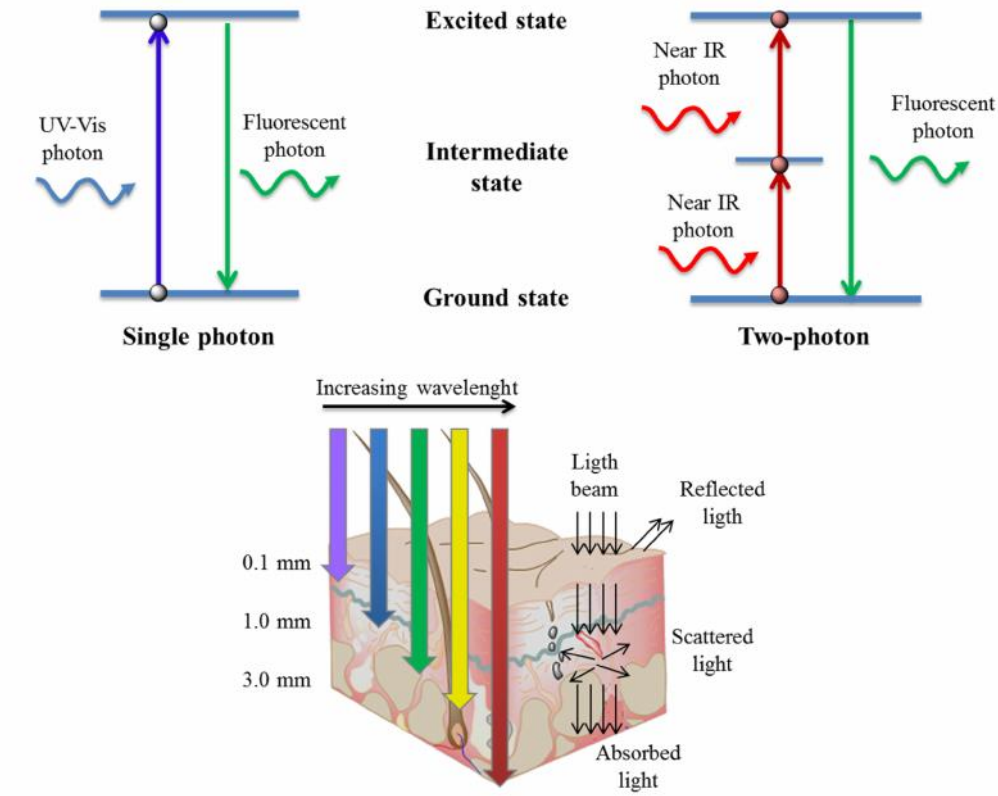

Figure 20: Electronic transitions by single photon or two photon excitation. Scheme of light penetration through tissue as a function to its wavelength.

I.2.3.7. Cytotoxicity of C-dots

The toxicity of nanoparticles is a current line of investigation, mainly due to the possibility of applying them for *in vivo* imaging and as advanced drug delivery systems. Carbon is not considered as an intrinsically toxic element; however, matter in the nanoscale may interact with living systems in different ways (see Figure 21). Consequently, many toxicity evaluations have been conducted in recent years, and the results highlight the very low toxicity of C-dots, thus representing a new class of non-heavy-metal containing optical probes with potential uses in bioimaging and analytical chemistry [63].

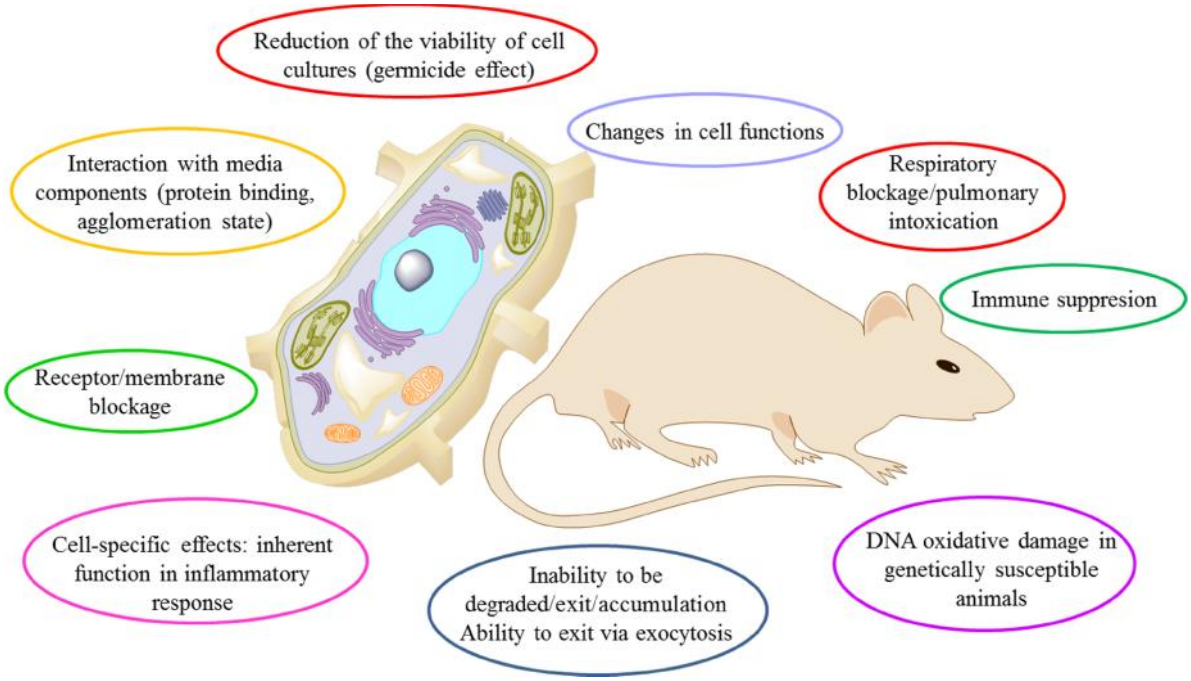

Figure 21: Potential toxicity of nanoparticles.

I.2.3.8. Analytical applications of C-dots

The above described properties of C-dots, the possibility of functionalization, their biocompatibility and their relative chemical inertness, make C-dots to offer a huge potential in different fields. Bioimaging and multimodal bioimaging of cells and tissues, sensor, photocalysts, optoelectronics, fluorescence quenching and electrochemiluminescent methods, are all arenas in which the exceptional characteristics of C-dots have been exploited. PL is the main driving force in all cases, while the surface groups or molecules determine the selectivity. Therefore, sensors or biosensors were developed based on C-dots for detecting several analytes, such as DNA, nitrite sensing, phosphate, iodide, glucose, α-fetoprotein or metal ions, in real matrices. The process depends mainly on the quenching or enhancing the fluorescence of C-dots. As the PL of C-dots is believed to arises from the radiative recombination of excitons, similarly to QDs, thus the fluorescence quenching process is probably due to facilitation of non-radiative electron/hole recombination through an effective electron transfer process. Another mechanism may be through a fluorescence resonance energy transfer process [62].

Some excellent recent reviews describe interesting applications in bioimaging biosensors, biomedicine delivery systems, dye sensitized solar cells, organic solar cells, supracapacitors, light emitting devices, photocatalysis and chemical sensors [62, 64, 65, 125, 132].

I.3. Analytes of interest

I.3.1. 5-hydroxyindoleacetic acid (5-HIAA)

5-hydroxyindolacetic acid (5-HIAA) is the major and final breakdown metabolite of serotonin in urine; it is also an important biomarker indicator in the diagnosis of carcinoid tumors. An increased urinary 5-HIAA level is found in patients with disseminated mid gut carcinoid tumors [133]. As the urinary 5-HIAA level has less biological variations than other markers (e.g. serotonin), it is useful in diagnosis and follow-up of patients with neuroendocrine tumors [134]. Figure 22 shows the possible humane parts in which gastrointestinal carcinoid tumors are formed.

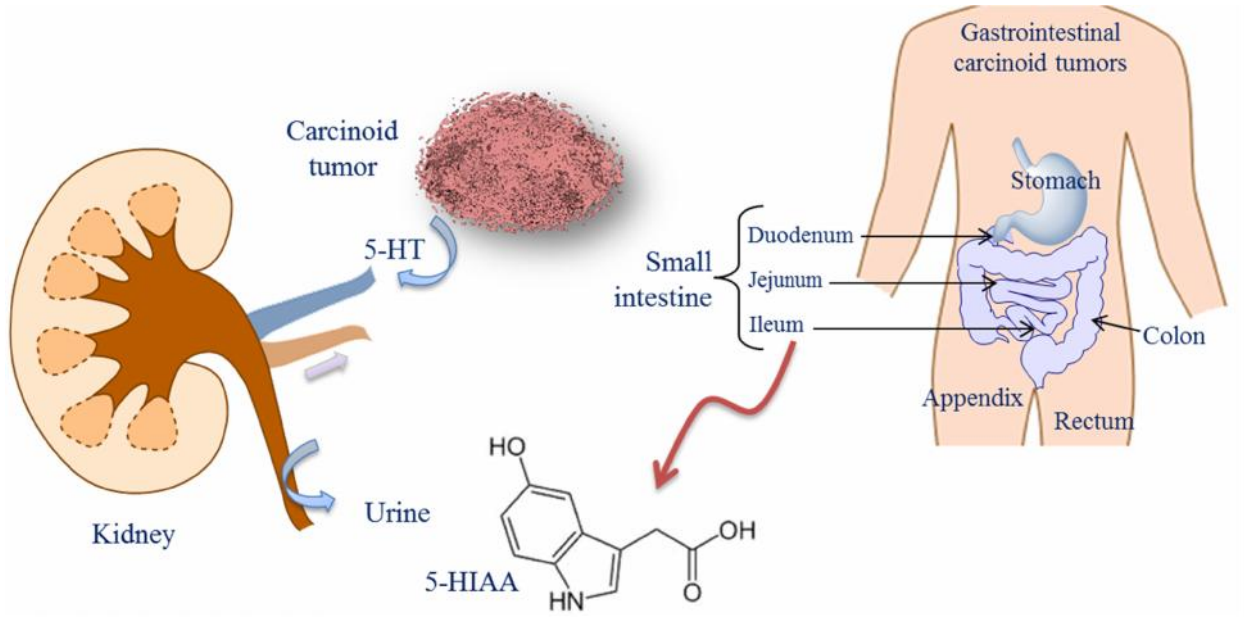

Figure 22: Parts of the body where gastrointestinal carcinoid tumors form.

Several methods have been reported for the quantification of 5-HIAA in human urine samples, such as HPLC, HPLC-MS and HPLC-fluorescence [135–137]. Most of these methods are

time-consuming, require solvent extractions and/or lack sensitivity. Thus, development of a simple, fast and accurate method to separate and detect 5-HIAA is essential for accurate biomedical analysis.

I.3.2. 4-nitrophenol

Nitrophenols are hazardous pollutants that are difficult to remove from groundwater and surface waters due to their solubility in water and their stability, particularly 4-nitrophenol (4 NP) and 2-nitrophenol (2 NP), which are both resonance stabilized. These nitrophenols enter the environment during manufacturing and processing as well as result of pesticides degradation (Figure 23) [138]. Most analytical methods described for 4-nitrophenol are based on its electrochemical properties [139, 140] and only a few papers have been published on the use of nanoparticles [141]. Due to their toxicity, carcinogenity and persistence in environment, simple, sensitive and reliable determination methods, based on sensitive luminescent nanomaterials, are currently deserving attention.

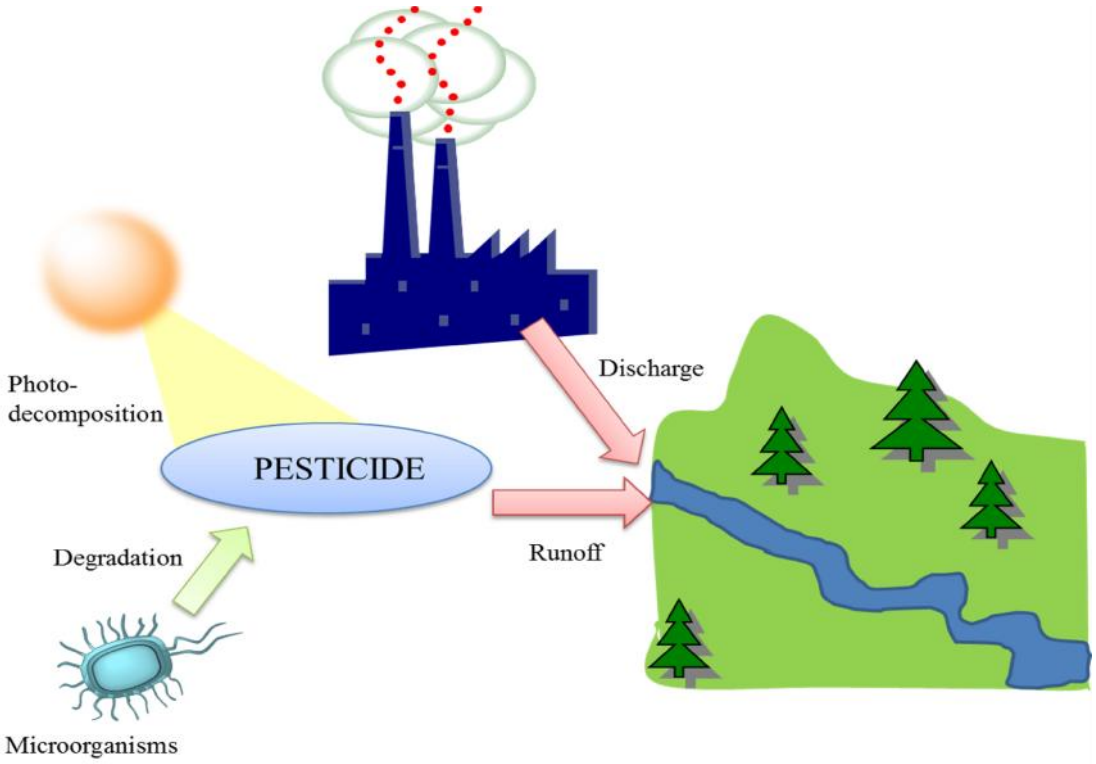

Figure 23: Most common ways for entering nitrophenols to the environment.

I.3.3.Tannic acid (TA)

Tannic acid (TA) is a natural hydrolyzable polyphenolic compound present in fruits and different kinds of vegetables and, along with other condensed polyphenols, can be found in several beverages including wine, beer, coffee, black tea and green tea. TA is composed of a polyol residue derived from D-glucose, which hydroxyl groups may be partially or fully substituted with galloyl units (gallotannins), see figure 24 [142]. It is used as a food additive (code number E-181) as clarifying agent, flavor adjunct and flavoring agent [143] as well as additive in medicinal products due to its astringent, diuretics and anti-inflammatory activities [144, 145]. Moreover, TA has also applications in the tannery industry to transform animal skins to leather and for re-tanning with Cr(III) to prevent leather putrefaction [146]. As an organic pollutant associated with the tanning industry, TA has been found to be toxic to aquatic microorganisms and may form metal complexes that alter the aquatic ecosystem [147, 148].

Due to its wide range of applications, analysis of tannic acid is of importance not only in food but also in the medical and environmental fields. Many analytical methods are based on the overall oxidation properties of polyphenols and, consequently, devoted to the determination of total phenolic content rather than specific determination of each component [149-153]. However, many efforts were attempted to measure TA in several kinds of food and beverage samples, as well as in industrial waters. So, a number of methods are available to quantitatively determine tannic acid content in waters, pharmaceuticals and foods, including spectrophotometry [154], electrochemical methods [155-157], luminescence [158-160] and chromatography [161, 162]. Each method has its advantages and drawbacks. For example, the determination of tannic acid in wines by the traditional spectrophotometric Folin-Ciocalteu method, based on the formation of a blue phosphotungstic phosphomolybdenum complex, is simple but lacks selectivity as many other compounds in wine interfere. Chromatographic methods allow the determination of tannic acid along other polyphenols but are time consuming and expensive. Electroanalytical methods with different types of electrodes were used for TA determination, but the presence of ascorbic acid limits the use of some of these methods, or laborious sample pretreatments are needed to remove ascorbic acid before analysis [156, 157]. These examples demonstrate that sensitive, selective and rapid TA detection is still a challenge.

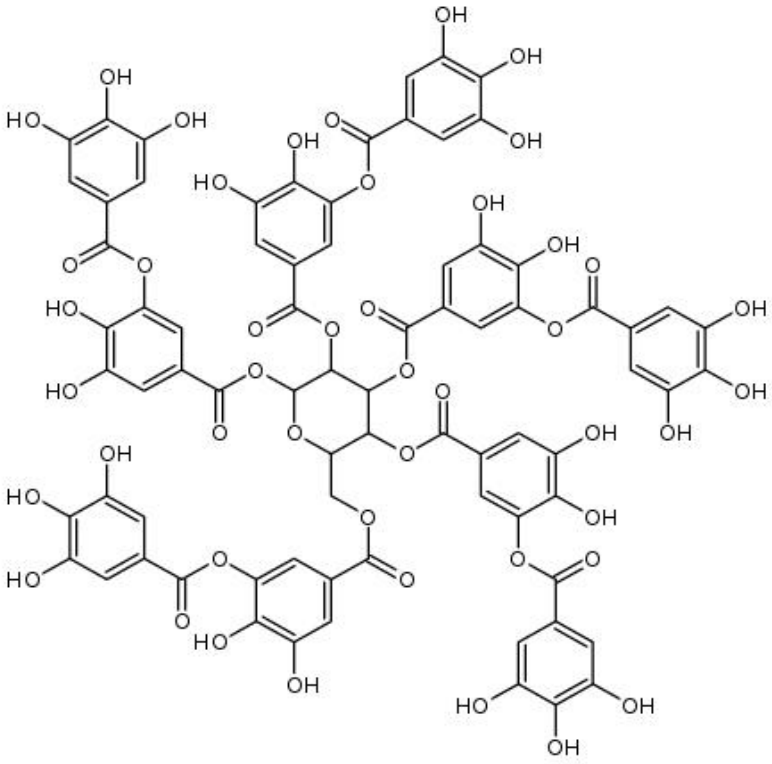

Figure 24: Chemical structure of TA.

References

[1] Rao CNR, Müller A, and Cheetham AK (2004) The Chemistry of Nanomaterials. WILEY-VCH Verlag GmbH & Co, Germany

[2] Günter S (2010) Nanoparticles:From Theory to Application; 2nd ed WILEY-VCH Verlag GmbH & Co, Germany

[3] Ulf L (2007) Optical metamaterials: Invisibility cup. Nature Photonics 1 : 207 - 208

[4] M Reibold, P Paufler, AA Levin, W Kochmann, N Patzke, and DC Meyer (2006) Materials-Carbon nanotubes in an ancient Damascus sabre. Nature 444 : 286–286

[5] Nguyen TKT (2010) Magnetic Nanoparticles From Fabrication to Clinical Applications. Taylor & Francis Group, LLC, Boca Raton

[6] Marianne R, Peter P, Aleksandr AL, Werner K, Nora P, and Dirk CM (2009) Discovery of Nanotubes in Ancient Damascus Steel. Physics and Engineering of New Materials. Springer Proceedings in Physics 127 : 305-310

[7] Sergey PG (2009) Magnetic Nanoparticles WILEY-VCH Verlag GmbH & Co, Germany.

[8] Gregor PCD (2010) Quantum dots-from synthesis to applications in biomedicine and life sciences. Sci Int J Mol 11 : 154-163.

[9] Ghaderi S, Ramesh B, and Seifalian AM (2011) Fluorescence nanoparticles "quantum dots" as drug deliverysystem and their toxicity: a review. J Drug Targ 19 : 475-86

[10] Lijia S, Yanfang G and Feng Y (2011) Semiconductor quantum dots for biomedical applications. Sensors 11 : 11736-11751

[11] SK Shukla (2014) Recent development in biomedical applications of quantum dots. Adv Mater Rev 1 : 2-12

[12] Michael H, Alan G and Serge C (2014) Nanomaterials for biosensing applications: a review. Front Chem 2 :1-12

[13] Manuela FF and Nikos C (2009) Semiconductor Quantum Dots in Chemical Sensors and Biosensors. Sensors 9 : 7266-7286

[14] Hui-Fen W, Judy G, Hani NA and Nazim H (2012) Quantum dot applications endowing novelty to analytical proteomics. Proteomics 12 : 2949-2961

[15] Gubin SP, Koksharov YA, Khomutov GB, Yurkov GY (2005) Magnetic nanoparticles: preparation, structure and properties. Russ Chem Rev 74:489

[16] Weddermann A, Ennen I, Regtmeier A, Albon C, Wolff A, Eckstädt K, Mill N, Peter MKH, Mattay J, Plattner C, Sewald N, Hütten A (2010) Review and outlook: from single nanoparticles to selfassembled monolayers and granular GMR sensors. Beilstein J Nanotechnol 1:75

[17] Tang SCN, Lo IMC (2013) Magnetic nanoparticles: essential factors for sustainable environmental applications. Water Res 47:2613

[18] Indira TK, Lakshmi PK (2010) Magnetic nanoparticles - a review. Int J Pharm Sci Nanotechnol 3:1035

[19] Chomoucka J, Drbohlavova J, Huska D, Adam V, Kizek R, Hubalek J (2010)Magnetic nanoparticles and targeted drug delivering. Pharm Res 62:144

[20] Sharma PK, Dutta RK, Pandey AC (2011) Advances in multifunctional magnetic nanoparticles. Adv Mater Lett 2:246

[21] Wadajkar AS, Menon JU, Kadapure T, Tran RT, Yang J, Nguyen KT (2013) Design and application of magnetic-based theranostic nanoparticle systems. Recent Patents Biomed Eng 6:47

[22] Laurent S, Forge D, Port M, Roch A, Robic C, Van der Elst L, Muller RN (2008) Magnetic iron oxide nanoparticles: synthesis, stabilization, vectorization, physicochemical characterizations, and biological applications. Chem Rev 108:2064

[23] Gao J, Gu H, Xu B (2009) Multifunctional magnetic nanoparticles: design, synthesis, and biomedical applications. Acc Chem Res 42: 1097

[24] Latham AH,WilliamsME (2008) Controlling transport and chemical functionality of magnetic nanoparticles. Acc Chem Res 41:411

[25] Coey JMD, Magnetism and Magnetic Materials (2010), Cambridge University Press, New York.

[26] Nicola AS, Magnetic Materials Fundamentals and Applications, 2nd ed. (2010), Cambridge University Press, New York.

[27] S Prakash (2007) Physics Vol I, VK (India) Enterprises. New Delhi : page 571

[28] An-Hui L, Salabas EL, and Ferdi S (2007) Magnetic Nanoparticles: Synthesis, Protection, Functionalization, and Application. Angew Chem Int Ed 46: 1222 – 1244

[29] Ioanna G and Franz K (2013) Microfluidic Biosensing Systems Using Magnetic Nanoparticles. Int J Mol Sci 14 : 18535-18556

[30] Steen M, Cathrine F and Mikkel FH (2010) Uniform excitations in magnetic nanoparticles. Beilstein J Nanotechnol 1 : 48–54

[31] Mørup S, Hansen MF, Frandsen C (2010) Magnetic interactions between nanoparticles. Beilstein J Nanotechnol 1:182

[32] Kolhatkar AG, Jamison AC, Litvinov D,Willson RC, Lee TR (2013) Tuning the magnetic properties of nanoparticles. Int J Mol Sci 14: 15977

[33] Wei W, Quanguo H, and Changzhong J (2008) Magnetic Iron Oxide Nanoparticles: Synthesis and Surface Functionalization Strategies. Nanoscale Res Lett 3:397–415

[34] Marcelo HS and Francisco AT (2001) New Electric Double-Layered Magnetic Fluids Based on Copper, Nickel, and Zinc Ferrite Nanostructures. J Phys Chem B 105 : 1168

[35] M Faraji, Y Yamini, and M Rezaee (2010) Magnetic nanoparticles: synthesis, stabilization, functionalization, characterization and applications. J Iran Chem Soc 7 : 1-37

[36] Berry CC, Curtis ASG (2003) Functionalisation of magnetic nanoparticles for applications in biomedicine. J Phys D Appl Phys 36:198

[37] Lu AH, Salabas EL, Schüth F (2007) Magnetic nanoparticles: synthesis, protection, functionalization and application. Angew ChemInt Edit 46:1222

[38] Jana C, Jana D, Dalibor H, Vojtech A, Rene K, and Jaromir H (2010) Magnetic nanoparticles and targeted drug delivering; Pharm.Res.; 62, 144-149,

[39] Sophie L and Morteza M (2011) Superparamagnetic iron oxide nanoparticles: promises for diagnosis and treatment of cancer. Int J Mol Epidemiol Genet 2 : 367-390

[40] Charles JP (1967) Cyclic polyethers and their complexes with metal salts. J Am Chem Soc 89 : 2495

[41] Jean ML (2007) From supramolecular chemistry towards constitutional dynamic chemistry and adaptive chemistry. Chem Soc Rev 36 : 151-160

[42] Lajos S and Julianna S (2013) Cyclodextrins in Analytical chemistry: host-guest type molecular recognition. Anal Chem 85 : 8024-8030

[43] Dodziuk H (ed) (2006) Cyclodextrins and their complexes. Chemistry, analytical methods, applications. Wiley-VCH, Winheim

[44] Douhal A (2006) Cyclodextrins materials photochemistry, photophysics and photobiology, 1st edn. Elsevier, Amsterdam

[45] Elbashir AA, Dsugi NF, Mohmed TO, Aboul-Enein HY (2013) Spectrofluorometric analytical applications of cyclodextrins. Luminescence. doi:10.1002/bio.2504

[46] Loftsson T, Duchêne D (2007) Cyclodextrins and their pharmaceutical applications. Int J Pharm 329:1

[47] Fakayode SO, Lowry M, Fletcher KA, Huang X, Powe AM,Warner IM (2007) Cyclodextrins host-guest chemistry in analytical and environmental chemistry. Curr Anal Chem 3:171

[48] Kang Y, Zhou L, Li X, Yuan J (2011) β-cyclodextrin-modified hybrid magnetic nanoparticles for catalysis and adsorption. J Mater Chem 21:3704

[49] Chalasani R, Vasudevan S (2013) Cyclodextrin-functionalized Fe_3O_4@TiO_2; reusable, magnetic nanoparticles for photocatalytic degradation of endocrine-disrupting chemicals in water supplies. ACS Nano 7:4093

[50] Cai K, Li J, Luo Z, Hu Y, Hou Y, Ding X (2011) β-cyclodextrin conjugatedmagnetic nanoparticles for diazepamremoval fromblood. Chem Commun 47:7719

[51] Badruddoza AZM, Tay ASH, Tan PY, Hidajat K, Uddin MS (2011) Carboxymethyl-β-cyclodextrin conjugated magnetic nanoparticles as nano-adsorbents for removal of copper ions: synthesis and adsorption studies. J Hazard Mater 185:1177

[52] Fan L, Zhang Y, Luo C, Lu F, Qiu H, Sun M (2012) Synthesis and characterization of magnetic β-cyclodextrin-chitosan nanoparticles as nano-adsorbents for removal of metyl blue. Int J Biol Macromol 50:444

[53] Du F, Meng H,Xu K, Xu Y, Luo P, LuoY, LuW,Huang J, Liu S,Yu J (2014) CPT loaded nanoparticles based on beta-cyclodextrin-grafted poly(ethylene glycol)/poly (L-glutamic acid) diblock copolymer and their inclusion complexes with CPT. Colloids Surf B Biointerfaces 113:230

[54] Sahua S, Mohapatra S (2013) Multifunctional magnetic fluorescent hybrid nanoparticles as carriers for the hydrophobic anticancer drug 5-fluorouracil. Dalton Trans 42:2224

[55] http://en.wikipedia.org/wiki/Molecularly_imprinted_polymer

[56] Alejandro SD, and Marta EDG (2010) Multifunctional nanoparticles: Analytical prospects. Analytica Chimica Acta 666 :1–22

[57] Ping Q, Jianping L, Lei Z, Ruizhuo O, and Huangxian J (2010) Molecularly imprinted magnetic nanoparticles as tunable stationary phase located in microfluidic channel for enantioseparation. J of Chrom A 1217 : 6115–6121

[58] Azodi DS, Abdouss M, Asadi E, Hassani NA, Sadeghi S, Farzaneh S, and Asadi S (2014) Magnetic molecularly imprinted polymer nanoparticles coupled with high performance liquid chromatography for solid-phase extraction of carvedilol in serum samples. J Appl Polym Sci 41209. doi: 10.1002/app.41209.

[59] Tao J, Hairong D, Qing D, Huan X, Jiwei N, Qiaolin H, Surong M, and Yikai Z (2010) Magnetic molecularly imprinted nanoparticles for recognition of lysozyme. Biosen and Bioelect 26 : 301–306

[60] Xin W, Lianyan W, Xiwen H, Yukui Z, and Langxing C (2009) A molecularly imprinted polymer-coated nanocomposite of magnetic nanoparticles for estrone recognition. Talanta 78 : 327–332

[61] Xuejiao Y, Jianjun L, Yingchun Y, Shengli Z, and Baoshan L (2014) Preparation and visible light photocatalytic activity of carbon quantum dots/TiO_2 nanosheet composites. Carbon 68 : 718–724

[62] Haitao L, Zhenhui K, Yang L and Shuit L (2012) Carbon nanodots: synthesis, properties and applications. J Mater Chem 22 : 24230

[63] Sheila NB and Gary AB (2010) Luminescent Carbon Nanodots: Emergent Nanolights. Angew Chem Int Ed 49 : 6726 – 6744

[64] Joaquim CGE, and Helena MRG (2011) Analytical and bioanalytical applications of carbon dots, Tren in Anal Chem 30: 1327

[65] Youfu W and Aiguo H (2014) Carbon quantum dots: synthesis, properties and Applications. DOI: 10.1039/c4tc00988f

[66] Jiong L, Jia-xiang Y, Junzhong W, Ailian L, Shuai W and Kian PL (2009) One-Pot Synthesis of Fluorescent Carbon Nanoribbons, Nanoparticles, and Graphene by the Exfoliation of Graphite in Ionic Liquids. ACS Nano 3 : 2367-2375

[67] Haitao L, Xiaodie H, Zhenhui K, Hui H, Yang L, Jinglin L, Suoyuan L, Chi HAT, Xiaobao Y and Shuit-Tong L (2010) Water-Soluble Fluorescent Carbon Quantum Dots and Photocatalyst Design. Angew Chem Int Ed 49 : 4430

[68] Hai M, Zheng M, Yang L, Keming P, Hang Y, Fang W and Zhenhui K (2012) Large scale electrochemical synthesis of high quality carbon nanodots and their photocatalytic property. Dalton Trans 41 : 9526

[69] Chen IW, W CW, Arun PP, and Huan TC (2014) Electrochemical synthesis of photoluminescent carbon nanodots from glycine for highly sensitive detection of hemoglobin. Green Chem 16 : 2509-2514

[70] Deng J, Lu Q, Mi N, Li H, Liu M, Xu M, Tan L, Xie Q, Zhang Y and Yao S (2014) Electrochemical Synthesis of Carbon Nanodots Directly from Alcohols. Chem Eur J 20 : 4993–4999. doi: 10.1002/chem.201304869.

[71] Wang J, Xin X and Lin Z (2011) Cu2ZnSnS4 nanocrystals and graphene quantum dots for photovoltaics. Nanoscale 3 : 3040

[72] Liu H, Ye T, and Mao C (2007) Fluorescent carbon nanoparticles derived from candle soot. Angew Chem Int Ed 46 : 6473

[73] SC Ray, Arindam S, Nikhil RJ and Rupa S (2009) Fluorescent Carbon Nanoparticles: Synthesis, Characterization, and Bioimaging Application. J Phys Chem C 113 : 18546–18551

[74] Lei T, Debraj G, Wei C, Sulolit P, Xijun C and Shaowei C (2009) Nanosized Carbon Particles From Natural Gas Soot Mater 21 : 2803

[75] Vinci JC and Colon LA (2012) Fractionation of carbon-based nanomaterials by anion-exchange HPLC. Anal Chem 84 : 1178

[76] Swagatika S, Birendra B, Tapas KM and Sasmita M (2012) Simple one-step synthesis of highly luminescent carbon dots from orange juice: application as excellent bio-imaging agents. Chem Commun 48 : 8835-8837

[77] Bibekananda D and Niranjan K (2013) A green and facile approach for the synthesis of water soluble fluorescent carbon dots from banana juice. RSC Adv 3 : 8286-8290

[78] Yin B, Deng J, Peng X, Long Q, Zhao J, Lu Q, Chen Q, Li H, Tang H, Zhang Y, and Yao S (2013) Green synthesis of carbon dots with down- and up-conversion fluorescent properties for sensitive detection of hypochlorite with a dual-readout assay. Analyst 138(21):6551-7

[79] Rui JF, Qiang S, Ling Z, Yan Z, and An HL (2014) Photoluminescent carbon dots directly derived from polyethylene glycol and their application for cellular imaging. Carbon 71 : 87–93

[80] Liming H, Yun S, Shengliang L, Xiaoli W, Kelei H, Lirong W, Xing L, and Yan W (2014) Multifunctional carbon dots with high quantum yield for imaging and gene delivery. Carbon 67 : 508–513

[81] Chen S, Yupeng S, Jing W and Yun L (2014) Facile route to highly photoluminescent carbon nanodots for ion detection, pH sensors and bioimaging. Nanoscale 6 : 9139-9147

[82] Dengyu P, Jingchun Z, Zhen L, Chao W, Xiumei Y and Minghong W (2010) Observation of pH-, solvent-, spin-, and excitation-dependent blue photoluminescence from carbon nanoparticles. Chem Commun 46 : 3681–3683

[83] Zhi Y, Minghan X, Yun L, Fengjiao H, Feng G, Yanjie S, Hao W and Yafei Z (2014) Nitrogen-doped, carbon-rich, highly photoluminescent carbon dots from ammonium citrate. Nanoscale 6 : 1890-1895. doi: 10.1039/C3NR05380F

[84] Xiaoming L, Shengli Z, Sergei AK, Yanli L and Haibo Z (2014) Engineering surface states of carbon dots to achieve controllable luminescence for solid-luminescent composites and sensitive Be^{2+} detection. Scientific Reports 4 : 4976, doi: 10.1038/srep04976

[85] Yaoping H, Jing Y, Jiangwei T, Li J, Jun-Sheng Y (2014) Waste frying oil as a precursor for one-step synthesis of sulfur doped carbon dots with pH sensitive photoluminescence. Carbon 77 : 775-782

[86] Zi-Qiang X, Li-Yun Y, Xiao-Yang F, Jian-Cheng J, Jie M, Wu P, Feng-Lei J, Qi X, and Yi L (2014) Low temperature synthesis of highly stable phosphate functionalized two color carbon nanodots and their application in cell imaging. Carbon 66 : 351-360

[87] Liu R, Wu D, Liu S, Koynov K, Knoll W, and Li Q (2009) An Aqueous Route to Multicolor Photoluminescent Carbon Dots Using Silica Spheres as Carriers. Angew Chem Int Ed 48 : 4598

[88] Athanasios BB, Andreas S, Demetrios A, Radek Z, Vasilios G and Emmanuel PG (2008) Photoluminescent Carbogenic Dots. Chem Mater 20 : 4539

[89] Jie Z, Yihua Z, Xiaoling Y, Jianhua S and Chunzhong L (2011) Synthesis of photoluminescent carbogenic dots using mesoporous silica spheres as nanoreactors. Chem Commun 47 : 764

[90] Xiaohui W, Konggang Q, Bailu X, Jinsong R and Xiaogang Q (2011) Microwave assisted one-step green synthesis of cell-permeable multicolor photoluminescent carbon dots without surface passivation reagents. J Mater Chem 21 : 2445-2450

[91] Yi L, Ning X, Ningqiang G, Hao W, Xin S, Wei G, and Ling Y (2014) One-step microwave-assisted polyol synthesis of green luminescent carbon dots as optical nanoprobes. Carbon 68 : 258–264

[92] Qinlong W, Huzhi Z, Yijuan L, Lingyan Z, Mei G, and Wenjun B (2011) Microwave–hydrothermal synthesis of fluorescent carbon dots from graphite oxide. Carbon 49 . 3134–3140

[93] Xinyun Z, Peng Z, Changjun L, Tao B, Wenchen L, Liming D and Wenguang L (2012) Highly luminescent carbon nanodots by microwave-assisted pyrolysis. Chem Commun 48 : 7955–7957

[94] Wang Q, Liu X, Zhang L, Lv Y (2012) Microwave-assisted synthesis of carbon nanodots through an eggshell membrane and their fluorescent application. Analyst 137(22):5392-7

[95] Nagaprasad P, B N P Kumar, Suraj K, Himani K, Mahitosh M and Amita P (2012) Synthesis of biocompatible multicolor luminescent carbon dots for bioimaging applications. Sci Technol Adv Mater 13 : 045008

[96] Hui Z, Xiaolei W, Yali L, Zhongjun W, Fan Y and Xiurong Y (2009) Microwave synthesis of fluorescent carbon nanoparticles with electrochemiluminescence properties. Chem Commun 34 : 5118

[97] Ningqiang G, Hao W, Shuai L, Yunlong D, Xiao'ai C, Ling Y, and Wei Gu (2014) Mocrowave-assisted polyol synthesis of gadolinium-doped green luminescent carbon dots as a bimodal nanoprobe. Langmuir 30 : 10933-10939

[98] Jin HB and Kenneth SS (2010) Applications of ultrasound to the synthesis of nanostructured materials. Adv Mater 22 : 1039-1059

[99] Zheng M, Hai M, Hui H, Yang L and Zhenhui K (2012) One-step ultrasonic synthesis of fluorescent N-doped carbon dots from glucose and their visible-light sensitive photocatalytic ability. New J Chem 36 : 861-864

[100] Shanaz J, Farrukh M, Shagufta N, Jianping L, and Shamsa K (2013) Oxidative synthesis of highly fluorescent boron/nitrogen co-doped carbon nanodots enabling detection of photosensitizer and carcinogenic dye. Anal Chem 85 : 10232-10239

[101] Xiaoyou X, Robert R, Yunlong G, Harry JP, Latha G, Kyle R, and Walter AS (2004) Electrophoretic Analysis and Purification of Fluorescent Single-Walled Carbon Nanotube Fragments. J Am Chem Soc. 126 : 12736

[102] Sheng TY, Li C, Pengju GL, Fushen L, Xin W, Haifang W, Mohammed JM, Yuanfang L, Gang Q and Ya PS (2009) Carbon Dots for Optical Imaging in Vivo. J Am Chem Soc 131 : 11308

[103] Wang X, Cao L, Lu F, Meziani MJ, Li H, Qi G, Zhou B, Harruff BA, Kermarrec F, Sun YP (2009) Photoinduced electron transfers with carbon dots. Chem Commun 3774.

[104] Li C, Xin W, Mohammed JM, Fushen L, Haifang W, Pengju GL, Yi L, Barbara AH, LM Veca, Davoy M, Su YX, and Ya PS (2007) Carbon Dots for Multiphoton Bioimaging. J Am Chem Soc 129 : 11318

[105] Ya PS, Bing Z, Yi L, Wei W, KAS Fernando, Pankaj P, Mohammed JM, Barbara AH, Xin W, Haifang W, Pengju GL, Hua Y, Muhammet EK, Bailin C, LM Veca, and Su YX (2006) Quantum-Sized Carbon Dots for Bright and Colorful Photoluminescence. J Am Chem Soc 128 : 7756

[106] Helena G, Pedro ASJ, JRA Fernandes, and Joaquim CGE (2010) Hg(II) sensing based on functionalized carbon dots obtained by direct laser ablation. Sensors and Actuators B: Chemical 145 : 702–707.

[107] Helena MRG, Abel JD, Frank D, Seamus PJH, Joaquim CGE (2012) Layer-by-layer immobilization of carbon dots fluorescent nanomaterials on single optical fiber. Anal Chim Acta 735 : 90– 95

[108] T Gokus, RR Nair, A Bonetti, M Böhmler, A Lombardo, KS Novoselov, AK Geim, AC Ferrari, A Hartschuh (2009) Making graphene luminescent by oxygen plasma treatment. ACS Nano 3 : 3963-3968

[109] Jing W, Cai W, and Su C (2012) Amphiphilic Egg-Derived Carbon Dots: Rapid Plasma Fabrication, Pyrolysis Process, and Multicolor Printing Patterns. Angew Chem Int Ed 51 : 9297 –9301

[110] Klaus S (2002) Handbook of thin films materials Ed by HS Nalwa. Volume 5: Nanomaterials and Magnetic thin films. Chapter 2. “The energy gap of clusters nanoparticles, and quantum dots” Academic Press

[111] Sheng-Liang H, Kai-Yang N, Jing S, Jing Y, Nai-Qin Z and Xi-Wen D (2009) One-step synthesis of fluorescent carbon nanoparticles by laser irradiation J Mater Chem 19 : 484–488

[112] Yongqiang D, Jingwei S, Congqiang C, Hao L, Ruixue W, Yuwu C , Xiaomei L, and Guonan C (2012) Blue luminescent graphene quantum dots and graphene oxide prepared by tuning the carbonization degree of citric acid. Carbon 50 : 4738–4743

[113] Somes KD, Yiyang L, Sinhea Y, Doo YK, and Christopher IR (2014) Single-particle fluorescence intensity fluctuations of carbon nanodots. Nano Lett 14 : 620-625

[114] Monoj KB, Bikash J, Santanu B, and Amitava P (2014) Photophysical Properties of Doped Carbon Dots (N, P, and B) and Their Influence on Electron/Hole Transfer in Carbon Dots−Nickel (II) Phthalocyanine Conjugates. J Phys Chem C 118 : 20034−20041

[115] Bhunia SK, Saha A, Maity AR, Ray SC, Jana NR (2013) Carbon nanoparticle-based fluorescent bioimaging probes, Sci Rep 3 :1473, doi: 10.1038/srep01473

[116] Weili W, Can X, Li W, Jiasi W, Jinsong R, and Xiaogang Q (2014) Non-Enzymatic-Browning-Reaction: A Versatile Route for Production of Nitrogen-Doped Carbon Dots with Tunable Multicolor Luminescent Display, Sci Rep 4 : 3564, doi: 10.1038/srep03564

[117] Yang X, Ming W, Yang L, Xi ZF, Xue BY, Xi WH and Yu KZ (2013) Nitrogen-Doped Carbon Dots: A Facile and General Preparation Method, Photoluminescence Investigation, and Imaging Applications Chem Eur J 19 : 2276–2283

[118] Gaber HGA, Rosana BL, Josefa AGC, Marta EDG (2014) Highly fluorescent carbon dots as nanoprobes for sensitive and selective determination of 4-nitrophenol in surface waters. Microchimi Acta, DOI: 10.1007/s00604-014-1302-x

[119] Yongqiang D, Hongchang P, Hong BY, Chunxian G, Jingwei S, Yuwu C, Chang ML and Ting Y (2013) Carbon-Based Dots Co-doped with Nitrogen and Sulfur for High Quantum Yield and Excitation-Independent Emission. Angew Chem Int Ed 52 : 7800-7804

[120] Goki E, Yun YL, Cecilia M, Hisato Y, Hsin AC, I-Sheng C, Chun WC and Manish C (2010) Blue Photoluminescence from Chemically Derived Graphene Oxide. Adv Mater 22 : 505-509

[121] Siddharth G, Anna MC, Narain K, Mariia OD, Ingo G, Henning S, Michael S, Kai B, Iwan ATS, Olaf S, Alexander PD, Jörg E, and Alexey IC (2014) Photoluminescence of Carbon Nanodots: Dipole Emission Centersand Electron−Phonon Coupling; Nano Lett 14 (10) : 5656–5661, doi: 10.1021/nl502372x

[122] Jason ER, Zhixin G, David LC, and Ya PS (2000) Strong luminescence of solubilized carbon nanotubes. J Am Chem Soc 122 : 5879

[123] Athanasios BB, Radek Z, Jan P, Aristides B, Marta K, and Emmanuel PG (2012) Luminescent Surface Quaternized Carbon Dots. Chem Mat 24 : 6-8

[124] Katerina H, Athanasios BB, Ondrej K, Karel B, Karolina MS, Marketa H, Jiri T, Klara S, Michal O, Emmanuel PG, and Radek Z (2014) Photoluminescence effects of graphitic core size and surface functional groups in carbon dots: COO^- induced red-shift emission. Carbon 70 : 279-286

[125] Katerina H, Yu Z, Yu W, Emmanuel PG, Radek Z, and Andrey LR (2014) Carbon dots-Emerging light emitters for bioimaging, cancer therapy and optoelectronics. Nano Today, DOI: 10.1016/j.nantod.2014.09.004

[126] Liyan Z, Yuwu C, Yongqing D, Jianpeng L and Binbin W (2009) Electrochemiluminescence of Water-Soluble Carbon Nanocrystals Released Electrochemically from Graphite. J Am Chem Soc 131 : 4564 – 4565

[127] Yang X, Ming W, Xi ZF, Xue BY, Xi WH and Yu KZ (2013) Reduced carbon dots versus oxidized carbon dots: photo- and electrochemiluminescence investigations for selected applications. Chem Eur J 19 : 6282-6288

[128] Noseung M, Zhifeng D, and Allen JB (2002) Electrogenerated Chemiluminescence of CdSe Nanocrystals. Nano Lett 2 : 1315.

[129] Pengju GL, Fan Y, Sheng TY, Sumit KS, Liju Y, Jessica JB, Yun L and Ya PS (2014) Carbon-based quantum dots for fluorescence imaging of cells and tissues. RSC Adv 4 : 10791-10807

[130] Qian L, Beidou G, Ziyu R, Baohong Z, and Jian RG (2013) Strong two-photon-induced fluorescence from photostable, biocompatible nitrogen-doped graphene quantum dots for cellular and deep-tissue imaging. Nano Lett 13 : 2436-2441

[131] Shih CP, Meng JY, Cheng CH, Chih WL, Cheng CH, Sheng HL, Yi MC and Pi TC (2006) The Empirical Correlation Between Size and Two-Photon Absorption Cross Section of CdSe and CdTe Quantum Dots. Small 2 : 1308−1313

[132] Changqin D, Anwei Z, and Yang T (2013) Functional Surface Engineering of C-Dots for Fluorescent Biosensing and in Vivo Bioimaging. Acc Chem Res 47 : 20

[133] Van der Horst SANA, Post WJ, Kema IP, Links TP, Willemse PHB, Wymenga ANM, de Vries EGE (2007) Persistent low urinary excretion of 5-HIAA is a marker for favourable survival during follow-up in patients with disseminated midgut carcinoid tumours. Eur J Cancer 43:2651

[134] Gedde DM, Thiis EE, Myklebust TA, Mordal KS, Vatn M, Bergestuen DS (2013) Comparison of 24-h and overnight samples of urinary 5-hydroxyindole acetic acid in patients with intestinal neuroendocrine tumors. Endocr Connect 2:50

[135] De JongWHA, Graham KS, De Vries EGE, and Kema IP (2008) Urinary 5-HIAA measurement using automated on-line solid-phase extraction-high performance liquid chromatography-tandem mass spectrometry. Ned Tijdschr Chem Labgeneesk 33:179

[136] Perry H and Keevil B (2008) Online extraction of 5-hydroxyindole acetic acid from urine for analysis by liquid chromatography-tandem mass spectrometry. Ann Clin Biochem 45:149

[137] Mulder EJ, Oosterloo-Duinkerken A, Anderson GM, De Vries EGE, Minderaa RB, Kema IP (2005) Automated on-line solid phase extraction coupled with HPLC for measurement of 5-hydroxyindole-3- acetic acid in urine. Clin Chem 51:1698

[138] Mononitrophenols. Concise International Chemical Assessment Document. (CICADs) (2000), World Health Organization, Geneva

[139] Xiaomeng X, Zhen L, Xin Z, Shuo D, Shuai X, and Changli Z (2011) β-Cyclodextrin functionalized mesoporous silica for electrochemical selective sensor: Simultaneous determination of nitrophenol isomers. Electrochimica Acta 58 : 142– 149

[140] Stelian L, Cecilia L, Mariana M, Nicolae T, and Paul CB (2009) Electrochemical sensors based on platinum electrodes modified with hybrid inorganic–organic coatings for determination of 4-nitrophenol and dopamine. Electrochimica Acta 54 : 1932–1938

[141] Anurag G, Bruce CK, Eugene E, Christina B, and Paul R (2012) Covalent functionalization of zinc oxide nanowires for high sensitivity p-nitrophenol detection in biological systems. Materials Science and Engineering B 177 : 1583– 1588

[142] Karamali K and Teunis vR (2001) Tannins: Classification and definition. Nat Prod Rep 18 : 641-649

[143] http://www.fao.org/food/food-safety-quality/scientific-advice/jecfa/jecfa-additives/en/

[144] Aelenei N, Popa MI, Novac O, Lisa G, Balaita L (2009) Tannic acid incorporation in chitosan-based nanoparticles and in vitro controlled release. J Mater Sci: Mater Med. DOI 10.1007/s10856-008-3675-z.

[145] Ren A, Zhang W, Thomas HG, Barish A, Berry S, Kiel JS, and Naren AP (2012) A Tannic Acid-based Medical Food, Cesinex® , Exhibits Broad-spectrum Antidiarrheal Properties: a Mechanistic and Clinical Study. Dig Dis Sci 57(1) : 99–108

[146] KJ Sreeram, and T Ramasami (2003) Sustaining tanning process through conservation, recovery and better utilization of chromium. Resources Conservation and Recycling 38 : 185-212

[147] NL Kruthika, GB Raju, and S Prabhakar (2014) Degradation of tannic acid using TiO_2 nanotubes as electrocatlyst. J of Nanoscience. http://dx.doi.org/10.1155/2014/481023

[148] King TC, Guojing Z, Edward SJ, Bill AS, and CI Wei (1995) Growth inhibition of selected aquatic bacteria by tannic acid and related compounds. J Aqu Animal Health 7 : 46-49

[149] Xavier C, Juan MG, Manuel G, Francisco C, Josefina C, Santiago M, Cecilia JJ, and Manel V (2012) Determination of total polyphenol index in wines employing a voltammetric electronic tongue. Analytica Chimica Acta 732 :172–179

[150] Tanya Y, Ivanka D, Konstantin B, Irina K (2006) Simultaneous determination of total polyphenols and caffeine contents of green tea by near-infrared reflectance spectroscopy. Microchemical Journal 83 : 42–47

[151] J González-Rodríguez, P Pérez-Juan, and MD Luque de Castro (2002) Method for the simultaneous determination of total polyphenol and anthocyan indexes in red wines using a flow injection approach. Talanta 56 : 53–59

[152] Marijan Š, Ivana N, and Lidija J (2011) Determination of polyphenols content and antioxidant activity of some red wines by differential pulse voltammetry, HPLC and spectrophotometric methods. Food Chemistry 124 : 1208–1216

[153] Bénédicte L, Isabelle K, Laurent P and Pierre LT (2013) Evolution of Analysis of Polyhenols from Grapes, Wines, and Extracts. Molecules 18 : 1076-1100

[154] Surya PG and Gopal G (2014) Quantitative analysis of tannic acid in crude drug and its ayurvedic formulation by UV spectrophotometry. Int J Pharmacogn & Phytochem Res 6 : 190-193

[155] Xu L, He N, Du J, Deng Y, Li Z, and Wang T (2009) A detailed investigation for determination of tannic acid by anodic stripping voltammetry using porous electrochemical sensor. Anal Chim Acta 634 : 49-53

[156] Dai LV, Bensu E, Libor Č, and Yusuf D (2013) Determination of Tannic Acid Using Silica Gel Modified Carbon Paste Electrode. Int J Electrochem Sci 8 : 9278 - 9286

[157] Huijun W, Qiaoli Z, Rui Y, Faqiong Z, Baizhao Z (2007) Electrochemistry and voltammetric determination of tannic acid on a single-wall carbon nanotube-coated glassy carbon electrode. Microchim Acta 159 : 109–115

[158] BGT Corominas, JV GarcıaMateo, LL Zamora, JM Calatayud (2002) Determination of tannic acid by direct chemiluminescence in a FIA assembly. Talanta 58 : 1243-1251

[159] Richie LCC, Chun HL, Chien YC, and Tzong JC (2005) Determination of tannin in green tea infusion by flow-injection analysis based on quenching the fluorescence of 3-aminophthalate. J Agric Food Chem 53 : 8443–8446. doi:10.1021/jf051077f.

[160] Yu GS, Hua C, Ying HL, Hua ZZ, and Xiang QL (2000) Flow injection analysis of tannic acid with inhibited electrochemiluminescent detection. Analytical Letters 33 : 2281-2291

[161] Zhu J, Ng J, and Filippich LJ (1992) Determination of tannic acid and its phenolic metabolites in biological fluids by high-performance liquid chromatography J Chromatogr 577(1) : 77-85

[162] SP Gupta, and G Garg (2014) Quantitative estimation of gallic acid and tannic acid in bhuvnesvara vati by RP-HPLC. Der Pharmacia Lettre 6 (2) : 31-36

Chapter 2

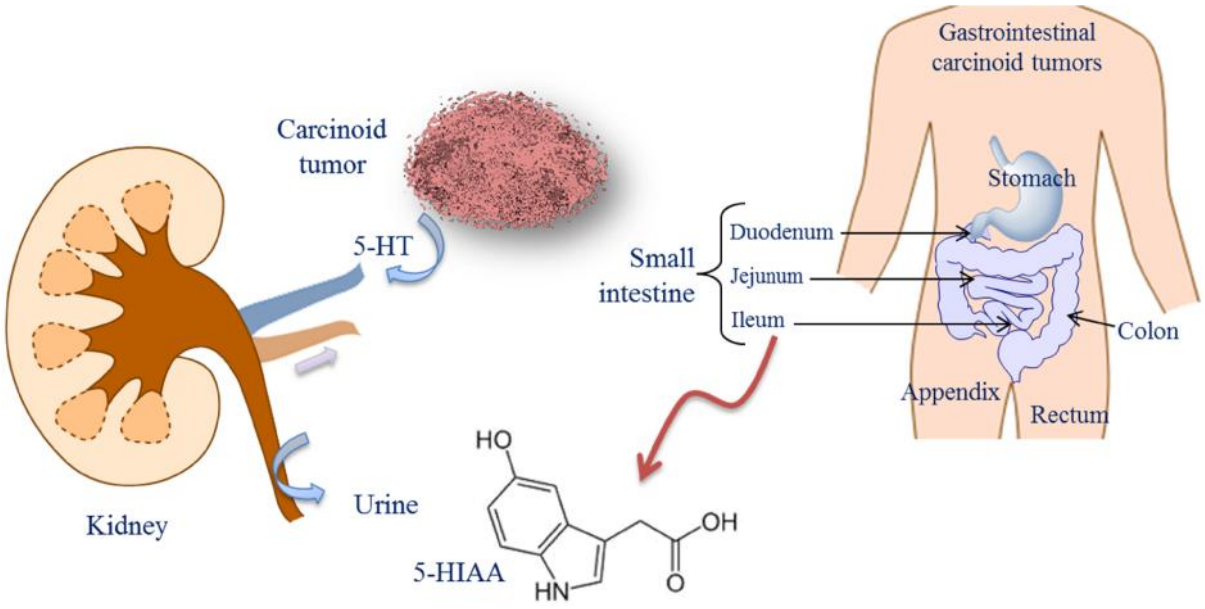

Magnetic nanoparticles grafted with β-cyclodextrin for solid-phase extraction of 5-hydroxy-3-indole acetic acid

II.1. Graphical Abstract

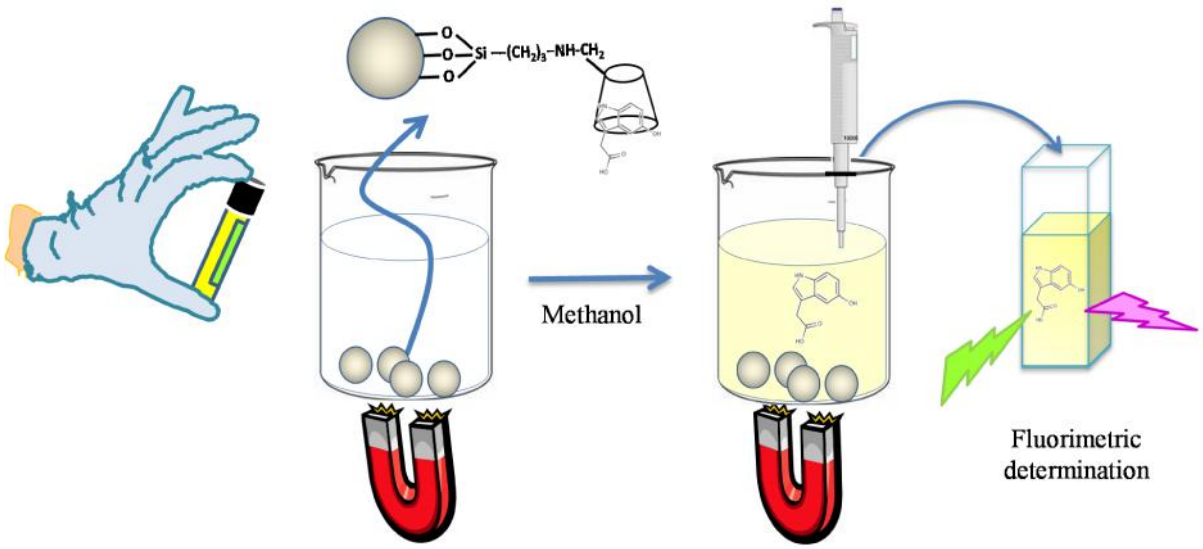

Cyclodextrin functional magnetic nanoparticles as sorbents for separation of 5-hydroxy-3-indole acetic acid and its fluorescence determination after released with methanol.

II.2. State of the art

Several factors could control the degree of the novelty and significance of the analytical method, for example, development of simple, facile, accurate, precise, fast, robust, reliable, etc. either for quantification or extraction of analytes of concern. This could be achieved by an enhancement of a present traditional instrumental method, like chromatography, or develop a new method depending on a superior synthesized material (which is used as a novel sensor) or could be done by both ways. Among all the frontiers materials, NPs are the star bright materials with interesting properties when compared with bulk materials. As a result, exploiting the potential of nanomaterials in analytical chemistry (advanced analytical methods) became predominant since very few decades. Nanomaterials opened the opportunity to analysts to develop excellent analytical methods for important analytes in different sample types. Therefore, and as the development of a reliable, sensitive, selective and robust method for molecular recognition of the cancer biomarker materials using biocompatible and nontoxic compounds is a major demand in biomedicine as well as analytical sciences, we began our work in this thesis.

In this line and aiming to extract and fluorimetrically detect the cancer biomarker 5-HIAA based on nanomaterials, we have found that most articles focused on synthesis of mNPs with various surface reactivities such as natural or synthetic polymers (i.e. Chitosan, polyacrylic acid, poly-N-isopropylacrylamide etc.). However, very little work has been carried out in the preparation of organic-inorganic nanocomposite materials through covalent bonding between mNPs and cyclodextrins (CDs) and their use as a tool for bioseparation/purification. Combining the inclusion/complexation property of CDs and the superparamagnetic property of magnetite (Fe_3O_4) in one nanosystem is considered to be a promising tool for wide variety of applications such as bioseparation, drug delivery, molecular recognition, environmental pollution control etc. In this work, we have successfully prepared β-CD covalently bonded to SiO_2-mNPs through layer by layer method. Physico-chemical characterization analysis, including XRD, FTIR, VSM, TEM, HRTEM, and fluorescence spectra, have been done to the synthesized nano-system and the structure has been confirmed. Both mNPs and β-CD properties have been exploited where the molecular complexation between β-CD and 5-HIAA is the main driving force for recognition

and extraction while the mNPs core allows their separation from the sample matrix. Also, the adsorption isotherms and kinetics of 5-HIAA by this nano-system were measured and studied.

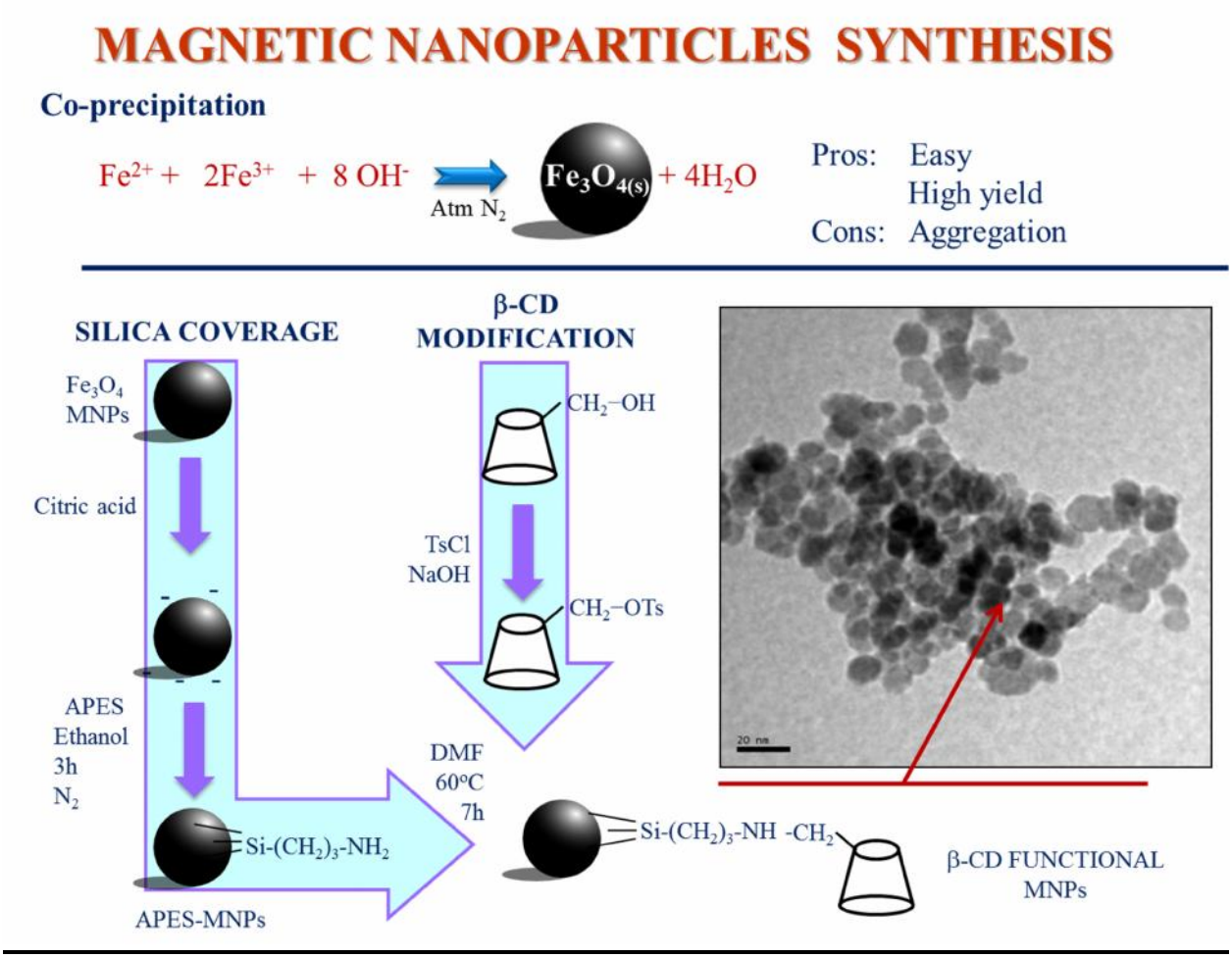

Figure 1. General steps for the synthesis and characterization of β-CD functional magnetic nanoparticles

II.3. Historical background

II.3.1. Medical aspects of 5-HIAA

5-HIAA is the final and stable metabolite of serotonin and biochemical confirmation of carcinoid syndrome includes elevated 24-h urine 5-HIAA excretion and raised plasma chromogranins. Notably quantification of 5-HIAA is useful in the diagnosis of carcinoid tumor as well as follow up serotonin levels in various humane organs. However, markedly elevated 24-h urine 5-HIAA excretion was observed due to 5-hydroxytryptophan self-medication. As a result an elevated 24-h urine 5-HIAA in patients with a low index of clinical suspicion for carcinoid disease should prompt specific enquiries about over-the-counter medication and herbal remedies to avoid undue patient anxiety and unnecessary investigation [1].

5-HIAA is created after oxidative deamination of serotonin and is the vital method for inactivation of the indole neurotransmitter. Other than oxidative deamination, deamination emulated by reduction to form 5-hydroxytryptophol, sulpho or glucuronide conjugation and N-acetylation represent minor pathways in serotonin metabolism. Given that the dominant part of serotonin in the body is created in the enterochromaffin cells of the gastrointestinal tract and that, to an extent of 80 % of the serotonin in entrance blood is cleared by the liver by means of the procedure of metabolism by monoamineoxidase A, it is not astonishing that there exist significant sources of 5-HIAA outside of the cerebrum [2].

Moreover, the hepatosplanchnic organs are the greatest contributor to the peripheral plasma pool, with the 5-HIAA flood into the hepatic vein being pretty nearly 10 times more prominent than that originating from the brain. Probably, the 5-HIAA overflow into the hepatic vein is inferred from the spontaneous release of serotonin and 5-HIAA from enterochromaftin cells of the digestive system into the circulation [2].

Serotonin and norepinephrine may be involved in the pathophysiology of anxiety and according to M. J. Garvey et al. [3] the severity of several anxiety symptoms was predicted by levels of 5-HIAA and vanillylmandelic acid. High serum concentrations of 5-HIAA and tryptophan showed a significant relation to low pain scores [4]. Moreover, 5-HIAA was strongly related to good quality of sleep [4].

Among never-hospitalized patients with unipolar depression, venlafaxine but not bupropion monotherapy diminished Cerebrospinal fluid 5-HIAA levels, while not, one or the other drug changed catecholamine metabolites [5]. The level of 5-HIAA in CSF (cerebrospinal fluid) is a biomarker in the prediction of early suicide in male high-risk suicide attempters [6]. In fact, those patients with low 5-HIAA content (below 15 ng mL^{-1}) attempted suicide a number of times significantly higher than those with a higher level and, besides, used violent media [7]. K. Nakayama [8] also found that site-specific diurnal changes in the 5-HIAA level occur in the medial prefrontal cortex (which is significantly involved in emotional responses) during the dark cycle. The finding suggested that these changes may serve as neurochemical indices for emotional states. On the other hand, serotonin level in serum and ascitic fluid, as well as 5-hydroxyindoleacetic acid in urine excretion depend on the grade of hepatic encephalopathy [9].

II.3.2. Extraction and Quantification of 5-HIAA

5-HIAA could be detected by different analytical techniques, however its quantification is based mainly on its extraction, particularly in complex matrices, like urine and human plasma (Figure 2)

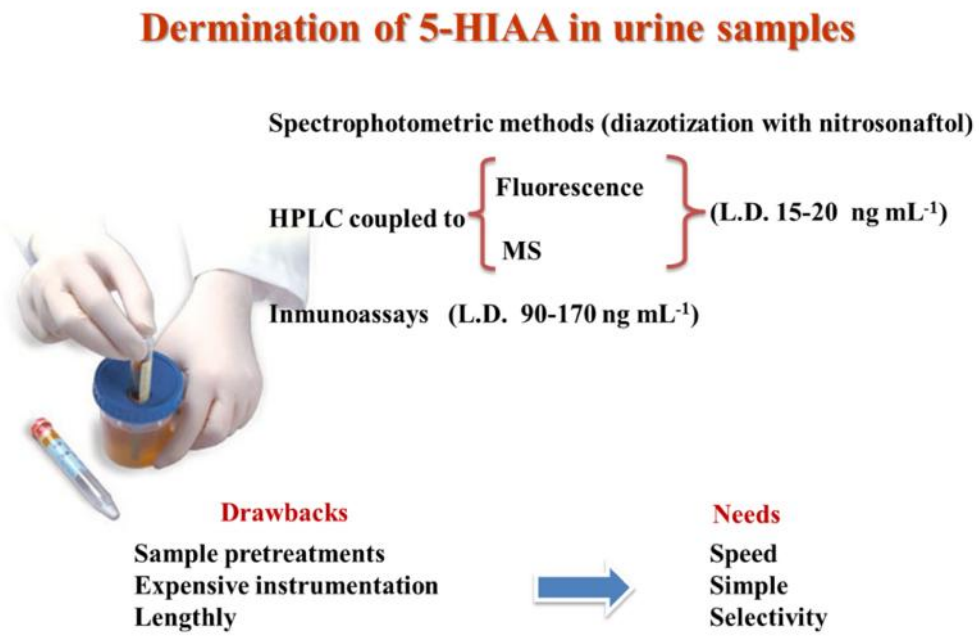

Figure 2. Common methods used for 5-HIAA determination in urine samples.

E. J. Mulder developed an automated on-line solid-phase extraction using Hysphere resin GP cartridge coupled with HPLC for measurement of 5-HIAA in urine obtaining recoveries in the range 87%-114% [10]. With the same technique de Jong et al. [11] have obtained recoveries ranging between 81%-98%. On the other hand Kestell et al. [12] reported on-line solid-phase extraction using C18 columns and cetyltrimethylammonium bromide as an organic modifier coupled with HPLC to efficiently separate 5-HIAA from possible interfering substances in human plasma, including a variety of pharmaceutical agents. Adequate precision, accuracy and sensitivity were achieved by electrochemical detection.

Citrate-capped gold nanoparticles (citrate-AuNPs) have been used for the selective extraction of indoleamines, including 5-HIAA, through van der Waals interactions between the indole ring and the citrate-AuNPs followed by their analysis by capillary electrophoresis/laser-induced native fluorescence. The extracted indoleamines could be liberated from the AuNPs surface by the addition of high concentrations of 2-mercaptoethanol, which bonded strongly to the AuNPs. Increasing the AuNPs concentration, incubation time, and sample volume significantly enhanced the sensitivity of this method to indoleamines [13].

Solid phase microextraction (SPME) of 5-HIAA combined with gas chromatography-triple quadrupole mass spectrometry was presented. In this method a preliminary derivatization with ethyl chloroformate/ethanol was used and the corresponding derivatives were then extracted by SPME in immersion mode. Polyacrylate fiber and ethyl chloroformate showed the best performance among the used SPME fibers [14].

Molecularly imprinted xero-gels prepared against 5-HIAA and serotonin, as the target molecules, using different alkoxy-silane precursors were used in molecular recognition of 5-HIAA followed by its fluorescence detection. The recognition ability of the imprinted xero-gel to 5-HIAA probably due to the hydrophobic interactions. Recoveries between 93% and 101% was obtained by this method [15]. Bracamonte et al. [16] determined 5-HIAA by direct fluorescence spectra in urine in presence of some cyclodextrins (CDs) media as recognition material. This method is based mainly on the supramolecular interaction between 5-HIAA and CDs.

HPLC–mass spectrometry method was used in the quantification of 5-HIAA in urine with no need to pre-treatment or derivatization but only dilution [17]. Similarly, Tohmola et al. [18] determined 5-HIAA in human serum by liquid chromatography tandem mass spectrometry method. A pre-column derivatization method for the quantitative determination of 5-HIAA using a fluorogenic reagent, 1,2-diphenylethylenediamine (DPE), followed by HPLC was proposed [19]. In this method the biogenic indole compounds were converted to their corresponding fluorescent derivatives with DPE in the presence of potassium hexacyanoferrate (III) at room temperature, and then the derivatives were separated by reversed-phase liquid chromatography with fluorescence detection. Xu et al. [20] reported a HPLC connected with chemically modified electrode for electrochemical detection of 5-HIAA.

Direct measurement of 5-HIAA in urine was achieved by capillary electrophoresis, with a neutral coated capillary and reversed polarity, optimized to process samples without pre-treatment [21]. More recently, a capillary electrophoresis (CE) with chemiluminescence (CL) detection method was developed for the quantification of 5-HIAA. In this method, CdTe quantum dot (QD) and horseradish peroxidase were used as enhancing reagents to co-catalyze the post-column CL reaction between luminol and hydrogen peroxide, achieving highly efficient CL emission [22].

References

[1] Magnus LPH, Kamala M, Ananth V and Rousseau G (2013) 'Sweet Dreams', 'Happy Days' and elevated 24-h urine 5-hydroxyindoleacetic acid excretion. Ann Clin Biochem 50 : 80–82, DOI: 10.1258/acb.2012.012041

[2] GW Lambert, DM Kaye, HS Cox, M Vaz, AG Turner, GL Jennings and MD Esler (1995) regional 5-hydroxyindoleacetic acid production in humans. Life Sciences 57 : 255-267

[3] Michael JG, Russell NJ, Catherine W, and Cindy L (1995) Relationship of generalized anxiety symptoms to urinary 5-hydroxyindoleacetic acid and vanillylmandelic acid. Psychiatry Research 57 : 1-5

[4] Marcus JS, Michael S, Hanns MB, Dieter EP, Brigitta B, and Manfred A (1999) Relationship of substance P, 5-hydroxyindole acetic acid and tryptophan in serum of fibromyalgia patients. Neuroscience Letters 259 : 196–198

[5] John TL, Terence AK, Aleksander AM, Mark AF, Dave L, and Robert MP (1999) Venlafaxine but Not Bupropion Decreases Cerebrospinal Fluid 5-Hydroxyindoleacetic Acid in Unipolar Depression. biol psychiatry 45 : 285–289

[6] Jussi J, Anna-Lena N, and Peter N (2007) The Relationship Between CSF HVA/5-HIAA Ratio and Suicide Intent in Suicide Attempters. Archives of Suicide Research 11 : 187-192

[7] Samuelsson M, Jokinen J, Nordström A-L, Nordström P (2006) CSF 5-HIAA, suicide intent and hopelessness in the prediction of early suicide in male high-risk suicide attempters Acta Psychiatr Scand 113 : 44

[8] Kazuhiko N (2002) Diurnal rhythm in extracellular levels of 5-hydroxyindoleacetic acid in the medial prefrontal cortex of freely moving rats: an in vivo microdialysis study. Prog in Neuro-Psychopharm & Biol Psychiatry 26 : 1383– 1388

[9] Chojnacki C, Walecka KE, Stepien A, Pawlowicz M, Wachowska KP, and Chojnacki J (2013) Serum and ascitic fluid serotonin levels and 5-hydroxyindoleacetic acid urine excretion in the liver of cirrhotic patients with encephalopathy. Advances in Medical Sciences,58(2) : 251-256, DOI: 10.2478/ams-2013-0010

[10] Mulder EJ, Oosterloo DA, Anderson GM, De Vries EGE, Minderaa RB, and Kema IP (2005) Automated on-line solid phase extraction coupled with HPLC for measurement of 5-hydroxyindole-3acetic acid in urine. Clin Chem 51:1698

[11] De Jong WHA, Graham KS, De Vries EGE, Kema IP (2008) Urinary 5-HIAA measurement using automated on-line solid-phase extraction-high performance liquid chromatography-tandem mass spectrometry. Ned Tijdschr Chem Labgeneesk 33:179

[12] Philip K, Liangli Z, Michael BJ, Michael RLS, Lisa KF, and Bruce CB (2001) Measurement of plasma 5-hydroxyindoleacetic acid as a possible clinical surrogate marker for the action of antivascular agents. Clinica Chimica Acta 314 : 159–166

[13] Mu-De L, Wei-Lung T, and Tian-Lu C, Ultrasensitive detection of indoleamines by combination of nanoparticle-based extraction with capillary electrophoresis/laser-induced native fluorescence (2009) Journal of Chromatography A 1216 : 6451–6458

[14] Marcello M, Attilio N, Giovanni S, and Antonio T (2013) A reliable and simple method for the assay of neuroendocrine tumor markers in human urine by solid-phase microextraction–gas chromatography-triple quadrupole mass spectrometry. Analytica Chimica Acta 759 : 66–73

[15] Alejandro DS, Rosana BL, and Marta EDG (2013) Cancer biomarker and neurotransmitters recognition by molecularly imprinted xero-gels. Sensors Actuators B Chem 184 : 48

[16] AG Bracamonte, and Alicia VV (2011) Spectrofluorimetric determination of serotonin and 5-hydroxyindoleacetic acid in urine with different cyclodextrin media. Talanta 83 : 1006–1013

[17] Luana L, Alfonso ML, Antonio S, Patrizia C, and Maurizio S (2008) HPLC–mass spectrometry method for quantitative detection of neuroendocrine tumor markers: Vanillylmandelic acid, homovanillic acid and 5-hydroxyindoleacetic acid. Clinica Chimica Acta 398 : 53–56

[18] Niina TO, Timo S, Helene M, Sakari J, Risto R, and Esa H (2014) Analytical and preanalytical validation of a new mass spectrometric serum 5-hydroxyindoleacetic acid assay as neuroendocrine tumor marker. Clinica Chimica Acta 428 : 38–43

[19] Masaaki K, Hiroko I, Hitoshi N, Myung KL, and Kazuko O (1998) Fluorescence derivatizing procedure for 5-hydroxytryptamine and 5hydroxyindoleacetic acid using 1,2-diphenylethylenediamine reagent and their sensitive liquid chromatographic determination. J of Chromatography B 720 : 25–31

[20] Haihong X, Wen Z, Dan W, Wei Z, and Litong J (2007) Simultaneous determination of 5-hydroxyindoleacetic acid and 5-hydroxytryptamine in urine samples from patients with acute appendicitis by liquid chromatography using poly(bromophenol blue) film modified electrode. Journal of Chromatography B 846 : 14–19

[21] A Garcia, M Heinanen, LM Jimenez, and C Barbas (2000) Direct measurement of homovanillic, vanillylmandelic and 5-hydroxyindoleacetic acids in urine by capillary electrophoresis. Journal of Chromatography A 871 : 341–350

[22] Liangliang Z, Yunsha Z, Junming H, and Shulin Z (2014) Simultaneous quantification of 5-hydroxyindoleacetic acid and 5-hydroxytryptamine by capillary electrophoresis with quantum dot and horseradish peroxidase enhanced chemiluminescence detection. Journal of Chromatography B 967 : 190–194

Microchim Acta (2014) 181:941–948
DOI 10.1007/s00604-014-1192-y

ORIGINAL PAPER

Magnetic nanoparticles grafted with β-cyclodextrin for solid-phase extraction of 5-hydroxy-3-indole acetic acid

Gaber Hashem Gaber Ahmed · Rosana Badía Laíño · Josefa Angela García Calzón · Marta Elena Díaz García

Received: 21 October 2013 / Accepted: 28 January 2014 / Published online: 13 February 2014

Abstract We describe the synthesis of ß-cyclodextrin modified magnetic nanoparticles (CD-mNPs) as a material for solid-phase extraction of the cancer biomarker 5-hydroxy-indole-3-acetic acid (5-HIAA) from urine. The CD-mNPs were characterized by TEM, FTIR, and XRD, and the kinetics and adsorption isotherms were studied. The strong interaction between the CD-mNPs and 5-HIAA is the main driving force for recognition and extraction, while the magnetic core of the NPs allows their separation from the sample matrix. Recovery of 5-HIAA from the adsorbent using an adequate solvent regenerated the adsorbent for further use. 5-HIAA was then quantified by fluorometry of its complex with ß-CD. The method works in the 1×10^{-7} to 1×10^{-5} mol L^{-1} (R^2 0.9982–0.9996) concentration range, and the limits of detection (3σ) and quantification (10 σ) of the method are 1.2×10^{-8} mol L^{-1} and 4.01×10^{-8} mol L^{-1} 5-HIAA, respectively. The recovery of 5-HIAA from urine samples spiked with 5-HIAA in three concentrations (1.4×10^{-6}, 4.50×10^{-6} and 1.0×10^{-5} mol L^{-1}) are within 63±3 %.

Keywords Carcinoma marker · Magnetic nanoparticles · β-cyclodextrin · Solid-phase extraction

Introduction

Magnetic nanoparticles (mNPs) have attracted much attention in the past two decades due to their high specific surface area, low toxicity and strong magnetic responses [1–3]. They have been used as excellent materials in numerous applications in biomedicine and biology sciences such as magnetic resonance imaging, targeted drug delivery, rapid biological separation, biosensors, nuclear fuel separation, and magnetic hyperthermia therapy [4–10].

mNPs exhibit superparamagnetism: they are easily magnetized when exposed to an external magnetic field and become immediately demagnetized, without residual magnetism, when the field is removed [11, 12]. Therefore, they can be recovered easily from solution under the influence of an external magnetic field (magnetic separation). However, colloidal instability and aggregation/agglomeration of the particles makes the surface modification of mNPs an important process as it may make mNPs biocompatible and fitted for further functionalization and applications [9].

In order to design purposive functional magnetic nanoparticles, many efforts have been made to modify the surface of mNPs with different organic and inorganic compounds, such as natural polymers like cyclodextrins (CDs), chitosan, dextran synthetic polymers like polyacrylic acid, poly(methyl methacrylate) and silica among others [13, 14]. Cyclodextrins (CDs) are a versatile group of host molecules which are known to form host-guest complexes with a wide range of organic molecules such as DNA, anticancer drugs, vitamins, and many other molecules [15]. CDs are naturally macrocyclic oligosaccharides, with 6-, 7-, or 8-D-glucose subunits linked by α-(1, 4) glycosidic bonds in a torus shaped structure.

Electronic supplementary material The online version of this article (doi:10.1007/s00604-014-1192-y) contains supplementary material, which is available to authorized users.

G. H. Gaber Ahmed · R. Badía Laíño · J. A. García Calzón · M. E. Díaz García (✉)
Department of Physical and Analytical Chemistry, Faculty of Chemistry, University of Oviedo, c/Julián Clavería, 8, Oviedo 33006, Spain
e-mail: medg@uniovi.es

M. E. Díaz García
e-mail: rbadia@uniovi.es

G. H. Gaber Ahmed
Chemistry Department, Faculty of Science, Damanhur University, Damanhur, Egypt

The interior cavity of the CD, with a pronounced hydrophobic character, can accommodate different guest molecules in an aqueous environment. In contrast, the outer surface is hydrophilic due to the presence of hydroxyl groups. The major driving forces in the formation of the CDs inclusion complexes are believed to be hydrophobic and van der Waals interactions. Another important property of CDs is their easy derivatization, which provides them with specific properties and/or to bind them to different substrates (e.g. chromatographic stationary phases) [16].

Molecular recognition ability of β-CD has been exploited in different promising applications such as environment, protein refolding, catalysis, drug delivery and chemical sensing [15, 17–19]. In recent reports, β-CDs have been bound to mNPs with different aims: a) for catalysis and adsorption [20, 21], b) for removal of drugs from biological fluids [22], c) for removal of metal ions and dyes [23, 24] and d) for delivery and stabilization of pharmaceuticals and drugs [25, 26].

5-hydroxyindolacetic acid (5-HIAA) is the major and final breakdown metabolite of serotonin in urine; it is also an important biomarker indicator in the diagnosis of carcinoid tumors. An increased urinary 5-HIAA level is found in patients with disseminated mid gut carcinoid tumors [27]. As the urinary 5-HIAA level has less biological variations than other markers (e.g. serotonin), it is useful in diagnosis and follow-up of patients with neuroendrocrine tumors [28]. Several methods have been reported for the quantification of 5-HIAA in human urine samples, such as HPLC, HPLC-MS and HPLC-fluorescence [29–31]. Most of these methods are time-consuming, require solvent extractions and/or lack sensitivity. Thus, development of a simple, fast and accurate method to separate and detect 5-HIAA is essential for accurate biomedical analysis.

Here we describe the synthesis of β-CD functional magnetic nanoparticles as solid phase extraction material for 5-HIAA determination in synthetic urine samples. The functional magnetic nanoparticles were characterized by different analytical techniques. The host-guest complex formed between 5-HIAA and the β-CD moiety served as the recognition/extraction driving force while the magnetic core of the nanoparticles allowed the separation from the urine matrix. Recovery of 5-HIAA from the adsorbent using methanol regenerated the adsorbent for further use (cost-effective). Reproducibility, selectivity and method validation have been investigated. In our knowledge, no work has been described in separation/molecular recognition of 5-HIAA by CD-mNPs.

Experimental

Chemicals and reagents

All the chemicals used were of analytical grade and used without further purification. The following materials are used in this study: Iron (II) chloride tetrahydrate, iron (III) chloride hexahydrate and ammonium hydroxide were obtained from Merck (www.merck.com), citric acid, 5-HIAA, β-cyclodextrin, p-toluenesulfonyl chloride, 3-aminopropyltriethoxysilane (APES), acetonitrile and 2-propanol were purchased from Sigma-Aldrich (www.sigmaaldrich.com), sodium hydroxide, hydrochloric acid, disodium hydrogen phosphate and acetone were achieved from Prolabo (www.prolabo.com).

Synthesis of bare magnetic nanoparticles and silica coated magnetic nanoparticles

Bare magnetite nanoparticles (bare mNPs) were synthesized by a chemical coprecipitation method (see Electronic Supplementary Material, ESM). Before coating mNPs with silica, the surface of mNPs was modified by negatively charged citrate groups in order to avoid aggregation/agglomeration due to attractive forces (van der Waals and magnetic dipole interactions) [32]. Briefly, 1 g of dry raw mNPs were dispersed in 200 mL 0.3 M citric acid by sonication for 1 h and then by mechanical stirring at 400 rpm for 12 h at room temperature. The resulting citric acid modified nanoparticles were isolated by magnetic decantation and thoroughly washed by milli-Q water. Finally, the nanoparticles were dried at 60 °C in vacuum for 2 h. In order to coat citrate-mNPs with APES (APES-mNPs), the procedure described by Badruddoza el al. [33] was followed with some modifications (see ESM for details).

Preparation of mono-6-deoxy-6(*p*-tolylsulfonyl) -β-cyclodextrin and its grafting on silica modified magnetic nanoparticles

Firstly, mono-6-deoxy-6(*p*-tolylsulfonyl)-β-cyclodextrin (Ts-β-CD) was synthesized according to R. C. Petter et al. [34] (see ESM) and its grafting on silica APES-mNPs (CD-mNPs) was performed adapting the method described by Badruddoza et al. [33]. In brief, 2 g of APES-mNPs were dispersed in 50 mL DMF at room temperature and then 10 mL DMF containing 0.25 g Ts-β-CD were added. The reaction was carried out under reflux, N_2 atmosphere and mechanical stirring at 60 °C for 7 h. Finally, the reaction was left to continue overnight at room temperature. The resulting functional nanoparticles were collected by magnetic filtration, thoroughly rinsed with DMF and acetone to remove any unreacted chemicals and dried in air. The whole synthesis steps are illustrated in Fig. 1.

Characterization of magnetic nanoparticles

The nanoparticles produced were characterized by transmission electron microscopy (TEM) using a MET JEOL 1011 transmission electron microscope operating at 100KV. All TEM specimens were prepared by dropping a diluted particle

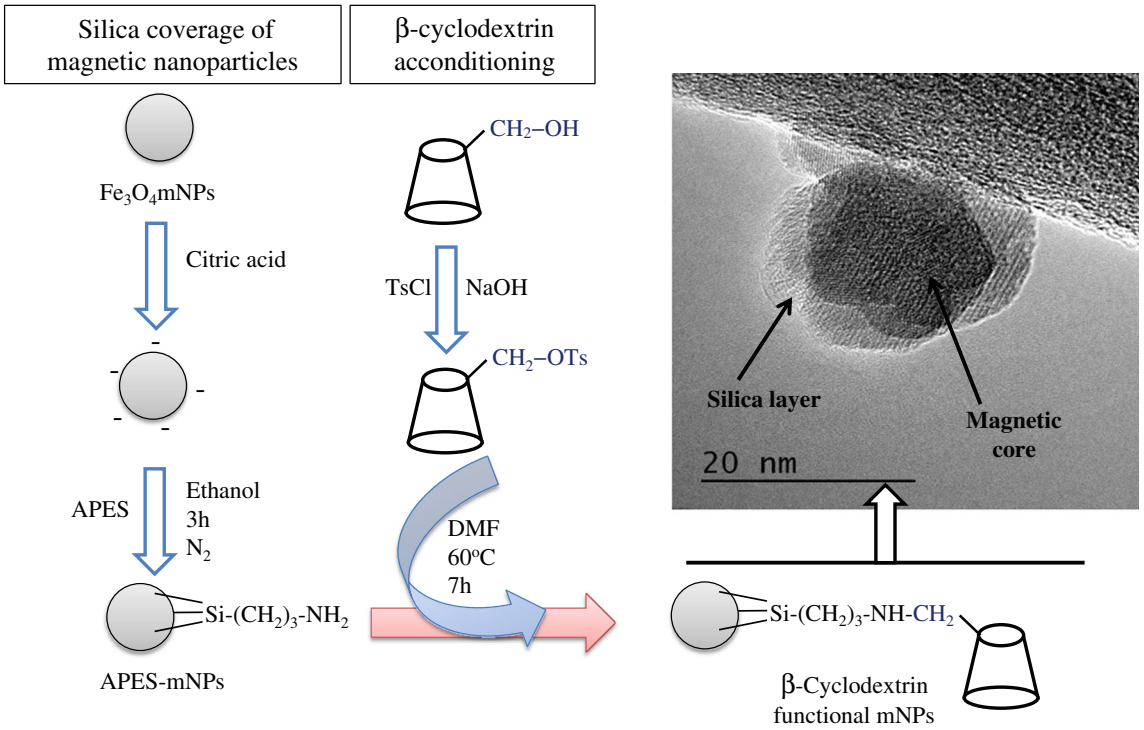

Fig. 1 Flow chart for the synthesis of CD-mNPs

suspension in ethanol on a copper grid and allowed to dry in air. HRTEM images were obtained using a JEOL JEM-2100F, 200 Kv. Powder X-ray diffraction studies were performed on a Bruker D8 Discover instrument with Cu Kα radiation. FTIR spectra were measured using a Varian 620-IR spectrophotometer in the region from 600 to 4,000 cm^1 on KBr pellets. Magnetization data was recorded using a vibrating sample magnetometer (MicrosenseEV9 VSM with PPMS-14T system) at room temperature with pressed pellets of prepared powdered samples with applied fields up to 20 kOe. Fluorescence measurements for analytical characterization were obtained with a spectrofluorometer of Edinburgh Instruments (model FLSP920), with 10 and 10 nm slits for excitation and emission, respectively. The excitation wavelength for 5-HIAA was set at 280 nm and the emission wavelength was set at 348 nm.

Adsorption of 5-HIAA by β-cyclodextrin grafted magnetic nanoparticles

Adsorption studies were performed by mixing a weighed amount (typically 25 mg) of CD-mNPs with 5 mL of 5-HIAA solutions of different concentration (5×10^{-7}–1×10^{-5} mol L^{-1}) adjusted at pH 6 (phosphate buffer 0.1 mol L^{-1}). The mixtures were equilibrated at room temperature by stirring at 300 rpm for 3 h. Then, CD-mNPs were separated by application of a magnetic field using a strong permanent magnet and the remaining solution was filtered through 0.45 μm nylon syringe filters. The uptake of the 5-HIAA (q_e, mg g^{-1}) was determined from the difference between the initial stock solution (C_0, mg L^{-1}) and the equilibrium 5-HIAA concentration (C_e, mg L^{-1}) in solution, using Eq. 1.

$$q_e = V\frac{C_0 - C_e}{M} \quad (1)$$

in which V is the volume of solution and M (mg) is the amount of CD-mNPs. The C_e value was obtained by fluorescence measurements using a Varian, Cary Eclipse spectrofluorometer, at 448 nm with excitation at 280 nm using a 1-cm path length quartz cell. A calibration curve of 5-HIAA in phosphate buffer (pH=6) was used for quantification of C_e after adsorption experiments.

Extraction of 5-HIAA from β-cyclodextrin grafted magnetic nanoparticles

Prior to desorption, the adsorption process was carried out. Specifically, 50 mg of CD-mNPs were contacted with 5 mL 5-HIAA (1×10^{-5} mol L^{-1}) at pH=6 and gently stirred for 3 h at room temperature. After reaching adsorption equilibrium, magnetic nanoparticles were separated by aid of magnet and the fluorescence of the clear solution was measured to determine the free 5-HIAA. Then, 5 mL of different organic solvents or their mixtures were added to the recovered magnetic nanoparticles and stirred for 1.5 h to ensure complete desorption of 5-HIAA. Again, nanoparticles were separated by magnet and the solution containing the released 5-HIAA

was analyzed for 5-HIAA concentration by fluorescence using a calibration graph prepared in the same solvent.

Solid phase extraction of 5-HIAA from synthetic urine samples

The 5-HIAA adsorption by CD-mNPs was performed in solutions mimicking the composition of human urine [35] and prepared as listed in Table S1 in ESM. The pH was found 5.33 and the specific gravity was 1.0058 g mL^{-1} at 25 °C. In a typical solid phase extraction experiments, 10 mL of synthetic urine sample was diluted to 50 mL by phosphate buffer (pH=6). 50 mg of CD-mNPs were added to 5 mL of this solution and stirred for 3 h to ensure adsorption equilibrium. The magnetic nanoparticles were then separated by magnet and 5 mL (x 2) methanol were added to them to release the 5-HIAA. As described in the previous section, 5-HIAA was fluorimetrically determined in the clear aliquot.

Results and discussion

Synthesis and FTIR characterization

The magnetic nanoparticles were prepared by the co-precipitation process under nitrogen atmosphere to avoid oxidation or phase transition (e.g. formation of maghemite, γ-Fe_2O_3). On the other hand, the tendency to agglomerate of mNPs prepared by this method was prevented by citrate surface modification. Synthesis of aminosilane-modified nanoparticles was achieved by reaction with APES which formed a silica shell covalently bound to the citrate modified mNPs and leaved the aminopropyl groups available for interacting with the tosyl group of Ts-β-CD. A low reaction temperature was used to avoid the side reaction between DMF and Ts-β-CD.

The FTIR spectra data of bare mNPs, citrate-mNPs, APES-mNPs and CD-mNPs in the range 600–4,000 cm^{-1} are shown in Fig. 2. The spectrum of bare mNPs (Fig. 2a) shows the characteristic absorption bands at 633 and 570 cm^{-1} attributed to the ν(Fe–O) deformations in the tetrahedral and the octahedral sites, respectively. The bare mNPs also show a broad band at 3,401 cm^{-1} due to surface –OH groups (stretching vibrations) while for nanoparticles modified with citric acid there are two characteristic bands: one at 1,406 cm^{-1} attributable to the asymmetric stretching of CO from –COOH group and other band at 1,621 cm^{-1} that may be assigned to the symmetric stretching of OH from COOH group (Fig. 2b). These results strongly suggest that citric acid was bonded to the magnetic nanoparticles. On the other hand, as shown in Fig. 2c for the APES coated nanoparticles, the peak at 2,931 cm^{-1} can be assigned to the stretching vibration of C–H bond of the propyl group and the band at 1,559 cm^{-1} to the bending mode of free NH_2. The absorption band of Fe-O-Si bonds (584 cm^{-1}) cannot be observed in the FTIR spectrum as it overlaps with the Fe-O vibration of magnetite nanoparticles. The band near 1,001 cm^{-1} is ascribed to the SiO–H bond and the bands at 1,387 and 1,077 cm^{-1} are the contribution of the stretching vibration of Si–O–Si bond. Figure 2e shows the spectrum of Ts-β-CD with characteristics peaks at 836, 1,021, and 1,152 cm^{-1}. The peak at 836 cm^{-1} is the contribution of the R-1,4-bond skeleton vibration of β-CD, while the other two peaks correspond to the anti-symmetric glycosidic ν_a (C–O–C) vibrations and coupled ν(C–C/C–O) stretch vibrations. Finally, in Fig. 2d, all the significant peaks for Ts-β-CD spectrum are present in the FTIR spectrum of CD-mNPs, with small shifting, indicating that Ts-β-CD was successfully immobilized on mNPs surface.

XRD analysis

The crystalline characterization of bare mNPs, citrate-mPs, APES-mNPs, and CD-mNPs was checked by observation of XRD patterns (Fig. 3). A series of seven characteristic peaks at 2θ=30.1°, 35.5°, 43.1°, 53.4°, 57°, 63.1°, and 74.9° related to the corresponding Miller indices (2 2 0), (3 1 1), (4 0 0), (4 2 2), (5 1 1), (4 4 0), and (5 3 3), respectively, are observed for all samples. These peaks are consistent with the standard pattern of iron oxide spinel cubic structure of magnetite and maghemite and match well with the JCPDS data [JCPDS cards #75-0033 (Fe_3O_4), # 39-1346 (γ-Fe_2O_3)]. These results demonstrate that surface functional groups did not modify the crystalline structure of magnetic nanoparticles. The characteristic diffraction peak of goethite (α-FeOOH) at 2θ=21.22° (1 1 0) and that of hematite (α-Fe_2O_3) at 2θ=33.15° (1 0 4) were not present in the studied samples demonstrating again that no phase changes were produced. The application of Debye-Scherrer's equation to the major peak intensities [36] revealed that the average size of crystallites was 6.3 nm.

VSM analysis

The magnetization characteristics of the magnetic particles under applied magnetic field were measured by vibration sample magnetometer (VSM). The VSM curves at 298 K for bare mNPs and CD-mNPs (Fig. S1 in ESM) resemble those of typical superparamagnetic behavior. Both curves present very narrow hysteresis loops and no remnant magnetization could be observed. The saturation magnetization values of bare mNPs and CD-mNPs are lower than that for bulk magnetite particles, 92 emu g^{-1} at 293 K [37], as expected when the size of the particles is decreased to a critical value [38]. The maximum magnetization values are 67.5 emu g^{-1} and 42 emu g^{-1}, respectively. The lower value for CD-mNPs can be attributed to the magnetically dead silica layer on the surface of the nanoparticles and, according to Ma et al. [39],

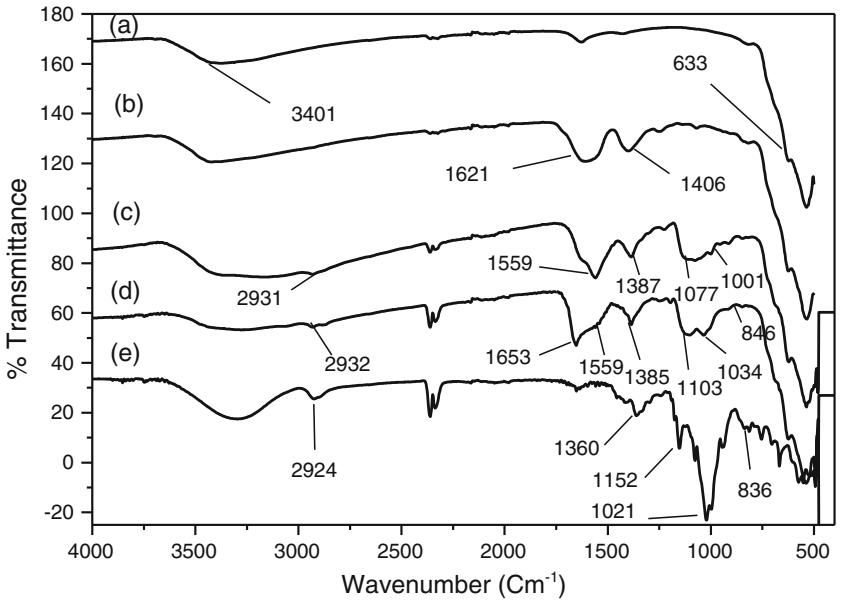

Fig. 2 FTIR spectra of **a** bare mNPs, **b** citrate-mNPs, **c** APES-mNPs, **d** CD-mNPs, and **e** Ts-β-CD

a saturation magnetization of 16.3 emu g^{-1} is enough for separation of magnetic nanoparticles using a conventional magnet. So, the synthesized CD-mNPs can be separated from solution using a simple laboratory magnet.

TEM and HRTEM analysis

In Fig. 1, a typical HRTEM image of CD-mNPs is included, in which the silica shell can be observed. The HRTEM elementary map of iron and silica clearly shows the boundary of iron nanoparticle regions coated by silica shell (Fig. S2a, ESM). The diameter of the CD-mNPs ranged around 11±2 nm as can be observed in the TEM image (Fig. S2b, ESM).

pH effect

The pH effect on adsorption of 5-HIAA was studied from pH 3 to pH 7 for 6.5×10^{-6} mol L^{-1} 5-HIAA with a fixed dose of CD-mNPs (5 mg mL^{-1}). Results showed that adsorption was favored by acidic conditions (pH 3-4, recovery ≥90 %). In this pH range, the carboxylic group of 5-HIIA (pK_a=4.75) [40] was not dissociated thus favoring the hydrophobic interaction within the –OH groups inside the cyclodextrin cavity. On the other hand, at these low pH values CD-mNPs slowly dissolved and the solution finally became yellow, thus limiting its reuse for 5-HIAA adsorption. In the pH range 5–7 an average recovery of ≥65 % was observed. In this pH range, the carboxylic group of 5-HIIA become deprotonated but

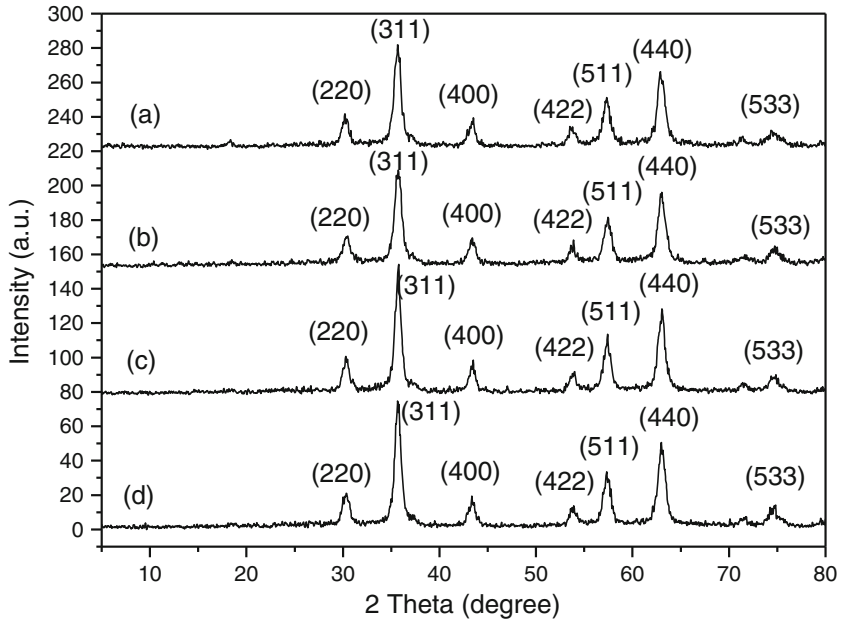

Fig. 3 XRD patterns of **a** bare mNPs, **b** citrate-mNPs, **c** APES-mNPs, and **d** CD-mNPs

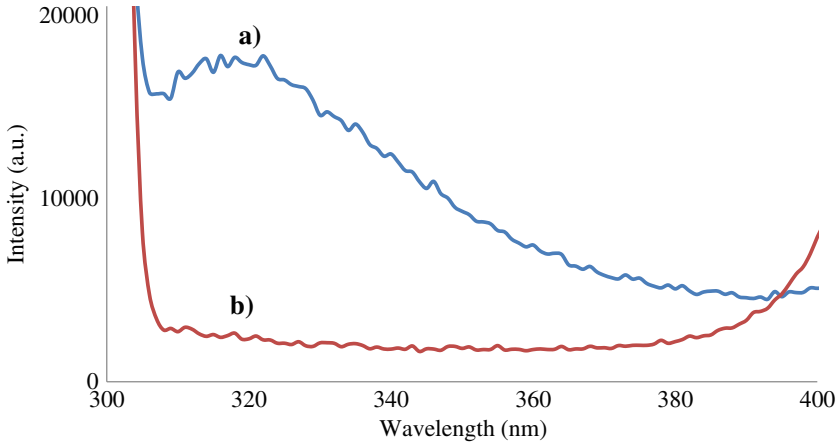

Fig. 4 **a** Fluorescence of solid CD-mNPs after adsorption of 5-HIAA study; **b** Fluorescence of CD-mNPs after desorption of 5-HIIA by methanol. 5-HIAA 1×10^{-4} M, pH=6, CD-mNPs 10 mg mL^{-1}. λ_{ex}=280

hydrogen bonds could still take place between the –OH groups inside the cyclodextrin cavity and groups (–OH and –NH) in the indol moiety of 5-HIAA. As no dissolution of CD-mNPs was observed in this pH range, a pH 6 was selected for further studies.

Adsorption kinetics

Experiments to assess the adsorption kinetics of the CD-mNPs were carried out with 5-HIAA in aqueous solution pH 6. The initial concentration of 5-HIAA was 1×10^{-5} mol L^{-1} and the amount of CD-mNPs used was 5 mg mL^{-1}. It can be seen from Fig. S3a (ESM) that adsorption of 5-HIAA by CD-mNPs increased instantly at initial stages and kept increasing gradually until equilibrium reached in approximately 20 min. These kinetic data showed that the process was rapid and uniform: a single and continuous curve that leads to saturation suggested monolayer coverage of 5-HIAA on the surface of the CD-mNPs. Two kinetic models, Lagergren [41] and Ho and McKay [42, 43] were applied to the experimental kinetic data in order to investigate the behavior of 5-HIAA on CD-mNPs. Results demonstrated that the Lagergren model was not adequate to fit the kinetic data for the initial concentrations studied; however, 5-HIAA adsorption by CD-mNPs followed the pseudo-second-order kinetics model, which assumes that chemisorption may be the rate-limiting step (Figure S3b, ESM). For 5-HIIA adsorption kinetic mechanisms, see ESM and Fig. S4.

Adsorption isotherms of 5-HIAA

The equilibrium adsorption of 5-HIAA by CD-mNPs at pH 6 and room temperature was analyzed by using Langmuir, Freundlich and Jovanovic isotherm equations (ESM, Table S2). Non-linear regression was performed with SigmaPlot software (Systat Software Inc.2012). The two parameter Freundlich isotherm provided the better fitting in terms of R^2 values (R^2=0.9993) and the Fisher parameter, resulting the binding capacity K_F=0.0309 and m=0.946 (see Table S2). According to the Freundlich model, these values seem to support that CD-mNPs exhibit a non-uniform distribution of adsorption affinities with a homogeneous surface (m → 1). Due to the short propyl-spacer between β-CD units and the silica coating it is expected that CD-mNPs have homogeneous surface due to presence of the macrocycles as the major functional groups on their surface. It is thus not surprising that the two-parameter isotherm models for homogeneous surfaces without lateral interactions, Langmuir and Jovanovic, also fit well the data.

Table 1 Figures of merits of comparable methods for extraction of 5-HIAA from urine samples

Solid phase extraction (SPE) method	Comments	Linear range, μmol L^{-1}	Limit of detection, μmol L^{-1}	Limit of quantification, μmol L^{-1}	C.V., %	Recovery, %	Biological sample	Reference
Hysphere resin GP cartridge	XLC-MS/MS[a]	0–1,200	0.1	0.13	9.5	81.5–98	Urine	29
Hysphere resin GP cartridge	On line SPE/HPLC Fluorescence detection	Up to 2,000	0.8	–	3.2–7.6	87.2–114	Urine	31
Molecularly imprinted sol–gel	Fluorescence detection	Up to 200	0.55	–	4.9–13	93–101	Urine	45
β-CD grafted magnetic nanoparticles	Fluorescence detection	0.1–10	0.012	0.04	1.58	63±3	Urine	This work

[a] Automated on-line solid-phase extraction-liquid chromatographic method with tandem mass spectrometry detection

Recovery of 5-HIAA from β-cyclodextrin grafted magnetic nanoparticles

Extraction of 5-HIAA from CD-mNPs with an appropriate solvent that ensured its quantitative recovery was performed using different solvents: HCl, H_2O, DMF, acetonitrile, ethanol, methanol and their mixtures. Among them, methanol was found to be most efficiently and eliminated the need to add co-solvents. The solid state fluorescence spectra of the CD-mNPs before and after removal of 5-HIAA with methanol were taken using a special support for solids. As can be seen from Fig. 4 the fluorescence band observed in the CD-mNPs after adsorption of 5-HIAA disappeared once the CD-mNPs were washed with methanol. It is worth mentioning that the fluorescence band of 5-HIAA was blue-shifted to λ=320 nm (excitation at λ=280 nm) respect to its value in solution as result of 5-HIAA immobilization onto the CD-mNPs. High recovery of 5-HIAA from CD-mNPs (97±4 %) were attained.

Analytical performance characteristics and β-cyclodextrin grafted magnetic nanoparticles solid phase extraction of 5-HIAA from synthetic urine samples

Under the specified optimum reaction conditions, the calibration curve for extraction of 5-HIAA by the synthesized CD-mNPs was constructed by analyzing a series of concentrations of the standard solutions of 5-HIAA. The regression equations for the results were derived using the least square method. The plots (n=9) were linear with very small intercept (0.0043–12.036) and good correlation coefficient (0.9982–0.9996) in the general concentration range 1×10^{-7}–1×10^{-5} mol L^{-1}. The limit of detection (3σ) and limit of quantitation (10σ) were found to be 1.2×10^{-8} and 4.01×10^{-8} mol L^{-1}, respectively. The normal physiological range for urinary 5-HIAA is 3–15 mg day^{-1} [44]. Considering a typical urine production per day of 1,500 mL, the reference range should be 1–5× 10^{-5} mol L^{-1}. Consequently, the present method fulfilled the requirements for sensitive determination of 5-HIAA.

The precision of the method was determined by replicate analysis of ten separate blank samples solutions. The relative standard deviation (RSD) was not more than 1.58 %. This good level of precision was suitable for control analysis of the investigated 5-HIAA. As synthetic urine sample has an important saline content and similar compounds that may interfere the analysis of 5-HIAA, such as serotonin, norepinephrine, and dopamine (see Table S1, ESM), it was used to study the effect of interferences on the analytical performance of the method. The applicability of CD-mNPs as a separation tool for 5-HIAA was investigated using the synthetic urine samples as model matrix. The recovery was evaluated for three different 5-HIAA concentrations: 1.39×10^{-6} mol L^{-1}, 4.50×10^{-6} mol L^{-1} and 1.0×10^{-5} mol L^{-1}, according to the procedure described in the "Experimental" section. The recovery was found to be 63±3 % regardless of the amount of analyte present and despite the presence of potentially interfering molecular species as well as anions and cations. On the other hand, reusability of the material was checked by using the same CD-mNPs for sorption/desorption of 5-HIAA for three times at the three concentrations above mentioned. The maximum change in the performance after repeated use was less than 3 %, independently of the 5-HIAA concentration. These results indicate that the repeated use of CD-mNPs for extraction of 5-HIAA from urine samples is feasible. The method compares favorably with those methods using conventional SPE cartridges or molecularly imprinted materials for analysis of 5-HIAA in urine samples [45], not only in sensitivity and selectivity but also considering simplicity, equipment, cost and speed (see Table 1).

Conclusions

In summary, we have successfully synthesized β-CD functionalized superparamagnetism magnetite nanoparticles through layer-by-layer method. The functional magnetic particles were characterized by TEM, FTIR, XRD and VSM. Results revealed that the β-CD modified magnetic particles were nanometer-sized with diameter range of around 11±2 nm. On the other hand, experimental data of equilibrium adsorption studies fitted well to Langmuir and Freundlich models while solid state fluorescence studies showed that 5-HIAA bound to coated nanoparticles could be removed simply by methanol washing. The procedure developed procedure for 5-HIAA extraction from synthetic urine samples offers several advantages. It is quick, inexpensive, robust, very sensitive and selective. Also, the method needs only a magnet and can be performed in any laboratory without the requirement of sophisticated instruments. The results suggest that CD-mNPs could be an effective alternative to other conventional adsorbents for the adsorption 5-HIAA from urine samples.

Acknowledgments Authors gratefully acknowledge financial support from the Science and Innovation Spanish Ministry (Projs # MICINN-09-CTQ2009-09595 and MAT2012-099). Also, G.H.Gaber Ahmed thanks an Erasmus Mundus Medastar grant.

References

1. Gubin SP, Koksharov YA, Khomutov GB, Yurkov GY (2005) Magnetic nanoparticles: preparation, structure and properties. Russ Chem Rev 74:489
2. Weddermann A, Ennen I, Regtmeier A, Albon C, Wolff A, Eckstädt K, Mill N, Peter MKH, Mattay J, Plattner C, Sewald N, Hütten A (2010) Review and outlook: from single nanoparticles to self-assembled monolayers and granular GMR sensors. Beilstein J Nanotechnol 1:75
3. Tang SCN, Lo IMC (2013) Magnetic nanoparticles: essential factors for sustainable environmental applications. Water Res 47:2613

4. Indira TK, Lakshmi PK (2010) Magnetic nanoparticles - a review. Int J Pharm Sci Nanotechnol 3:1035
5. Chomoucka J, Drbohlavova J, Huska D, Adam V, Kizek R, Hubalek J (2010) Magnetic nanoparticles and targeted drug delivering. Pharm Res 62:144
6. Sharma PK, Dutta RK, Pandey AC (2011) Advances in multifunctional magnetic nanoparticles. Adv Mater Lett 2:246
7. Wadajkar AS, Menon JU, Kadapure T, Tran RT, Yang J, Nguyen KT (2013) Design and application of magnetic-based theranostic nanoparticle systems. Recent Patents Biomed Eng 6:47
8. Laurent S, Forge D, Port M, Roch A, Robic C, Van der Elst L, Muller RN (2008) Magnetic iron oxide nanoparticles: synthesis, stabilization, vectorization, physicochemical characterizations, and biological applications. Chem Rev 108:2064
9. Gao J, Gu H, Xu B (2009) Multifunctional magnetic nanoparticles: design, synthesis, and biomedical applications. Acc Chem Res 42: 1097
10. Latham AH, Williams ME (2008) Controlling transport and chemical functionality of magnetic nanoparticles. Acc Chem Res 41:411
11. Mørup S, Hansen MF, Frandsen C (2010) Magnetic interactions between nanoparticles. Beilstein J Nanotechnol 1:182
12. Kolhatkar AG, Jamison AC, Litvinov D, Willson RC, Lee TR (2013) Tuning the magnetic properties of nanoparticles. Int J Mol Sci 14: 15977
13. Berry CC, Curtis ASG (2003) Functionalisation of magnetic nanoparticles for applications in biomedicine. J Phys D Appl Phys 36:198
14. Lu AH, Salabas EL, Schüth F (2007) Magnetic nanoparticles: synthesis, protection, functionalization and application. Angew Chem Int Edit 46:1222
15. Dodziuk H (ed) (2006) Cyclodextrins and their complexes. Chemistry, analytical methods, applications. Wiley-VCH, Winheim
16. Douhal A (2006) Cyclodextrins materials photochemistry, photophysics and photobiology, 1st edn. Elsevier, Amsterdam
17. Elbashir AA, Dsugi NF, Mohmed TO, Aboul-Enein HY (2013) Spectrofluorometric analytical applications of cyclodextrins. Luminescence. doi:10.1002/bio.2504
18. Loftsson T, Duchêne D (2007) Cyclodextrins and their pharmaceutical applications. Int J Pharm 329:1
19. Fakayode SO, Lowry M, Fletcher KA, Huang X, Powe AM, Warner IM (2007) Cyclodextrins host-guest chemistry in analytical and environmental chemistry. Curr Anal Chem 3:171
20. Kang Y, Zhou L, Li X, Yuan J (2011) β-cyclodextrin-modified hybrid magnetic nanoparticles for catalysis and adsorption. J Mater Chem 21:3704
21. Chalasani R, Vasudevan S (2013) Cyclodextrin-functionalized Fe_3O_4@TiO_2; reusable, magnetic nanoparticles for photocatalytic degradation of endocrine-disrupting chemicals in water supplies. ACS Nano 7:4093
22. Cai K, Li J, Luo Z, Hu Y, Hou Y, Ding X (2011) β-cyclodextrin conjugated magnetic nanoparticles for diazepam removal from blood. Chem Commun 47:7719
23. Badruddoza AZM, Tay ASH, Tan PY, Hidajat K, Uddin MS (2011) Carboxymethyl-β-cyclodextrin conjugated magnetic nanoparticles as nano-adsorbents for removal of copper ions: synthesis and adsorption studies. J Hazard Mater 185:1177
24. Fan L, Zhang Y, Luo C, Lu F, Qiu H, Sun M (2012) Synthesis and characterization of magnetic β-cyclodextrin-chitosan nanoparticles as nano-adsorbents for removal of metyl blue. Int J Biol Macromol 50:444
25. Du F, Meng H, Xu K, Xu Y, Luo P, Luo Y, Lu W, Huang J, Liu S, Yu J (2014) CPT loaded nanoparticles based on beta-cyclodextrin-grafted poly(ethylene glycol)/poly (L-glutamic acid) diblock copolymer and their inclusion complexes with CPT. Colloids Surf B Biointerfaces 113:230
26. Sahua S, Mohapatra S (2013) Multifunctional magnetic fluorescent hybrid nanoparticles as carriers for the hydrophobic anticancer drug 5-fluorouracil. Dalton Trans 42:2224
27. Van der Horst Schrivers ANA, Post WJ, Kema IP, Links TP, Willemse PHB, Wymenga ANM, de Vries EGE (2007) Persistent low urinary excretion of 5-HIAA is a marker for favourable survival during follow-up in patients with disseminated midgut carcinoid tumours. Eur J Cancer 43:2651
28. Gedde Dahl M, Thiis Evensen E, Myklebust Tjølsen A, Mordal KS, Vatn M, Bergestuen DS (2013) Comparison of 24-h and overnight samples of urinary 5-hydroxyindole acetic acid in patients with intestinal neuroendocrine tumors. Endocr Connect 2:50
29. De Jong WHA, Graham KS, De Vries EGE, Kema IP (2008) Urinary 5-HIAA measurement using automated on-line solid-phase extraction-high performance liquid chromatography-tandem mass spectrometry. Ned Tijdschr Chem Labgeneesk 33:179
30. Perry H, Keevil B (2008) Online extraction of 5-hydroxyindole acetic acid from urine for analysis by liquid chromatography-tandem mass spectrometry. Ann Clin Biochem 45:149
31. Mulder EJ, Oosterloo-Duinkerken A, Anderson GM, De Vries EGE, Minderaa RB, Kema IP (2005) Automated on-line solid phase extraction coupled with HPLC for measurement of 5-hydroxyindole-3-acetic acid in urine. Clin Chem 51:1698
32. Khosroshahi ME, Ghazanfari L (2010) Preparation and characterization of silica-coated iron-oxide bionanoparticles under N2 gas. Phys E 42:1824
33. Badruddoza AZM, Hidajat K, Uddin MS (2010) Synthesis and characterization of β-cyclodextrin-conjugated magnetic nanoparticles and their uses as solid-phase artificial chaperones in refolding of carbonic anhydrase bovine. J Colloid Interface Sci 346:337
34. Petter RC, Salek JS, Sikorski CT, Kumaravel G, Lin FT (1990) Cooperative binding by aggregated mono-6-(alky1amino)- β-cyclodextrins. J Am Chem Soc 112:3860
35. Chutipongtanate S, Thongboonkerd V (2010) Systematic comparisons of artificial urine formulas for in vitro cellular study. Anal Biochem 402:110
36. Qazi SJS, Rennie AR, Cockcroft JK, Vickers M (2009) Use of wide-angle X-ray diffraction to measure shape and size of dispersed colloidal particles. J Colloid Interface Sci 338:105
37. Cullity BD (1972) Introduction to magnetic materials. Addison Wesley, New York, p 525
38. Jun YW, Seo JW, Cheon J (2008) Nanoscaling laws of magnetic nanoparticles and their applicabilities in biomedical sciences. Acc Chem Res 41:179
39. Ma ZY, Guan YP, Liu HZ (2005) Synthesis and characterization of micron-sized monodisperse superparamagnetic polymer particles with amino groups. J Polym Sci Polym Chem 43:3433
40. Graffeo AP, Karger BL (1976) Analysis for indole compounds in urine by high-performance liquid chromatography with fluorometric detection. Clin Chem 22:184
41. Lagergren S (1898) About the theory of so-called adsorption of soluble substances. Kungliga Svenska Vetenskaps akademiens Handlingar 24:1
42. Ho YS, McKay G (1999) Pseudo-second order model for sorption processes. Process Biochem 34:451
43. Ho YS, McKay G (1998) A comparison of chemisorption kinetic models applied to pollutant removal on various sorbents. Trans Inst Chem Eng 76:332
44. Maroun J, Kocha W, Kvols L, Bjarnason G, Chen E, Germond C, Hanna S, Poitras P, Rayson D, Reid R, Rivera J, Roy A, Shah A, Sideris L, Siu L, Wong R (2006) Guidelines for the diagnosis and management of carcinoid tumours. Part 1: the gastrointestinal tract. A statement from a Canadian National Carcinoid Expert Group. Curr Oncol 13:67–76
45. Simón de Dios A, Badía Laíño R, Díaz García ME (2013) Cancer biomarker and neurotransmitters recognition by molecularly imprinted xero-gels. Sensors Actuators B Chem 184:48

Electronic Supplementary Material

Magnetic nanoparticles grafted with β-cyclodextrin for solid-phase extraction of 5-hydroxy-3-indole acetic acid

Gaber Hashem Gaber Ahmed[1,2], Rosana Badía Laíño[2], Josefa Angela García Calzón[2], Marta Elena Díaz García[2*]

[1]*Chemistry Department, Faculty of Science, Damanhur University, Damanhur, Egypt*
[2]*Department of Physical and Analytical Chemistry. Faculty of Chemistry*
University of Oviedo, c/Julián Clavería, 8. Oviedo, 33006, Spain

*Corresponding author, e-mails: rbadia@uniovi.es; medg@uniovi.es

Synthesis of bare magnetic nanoparticles

The chemical precipitation method for bare magnetic nanoparticles followed the reaction:

$$FeCl_2.4H_2O + 2FeCl_3.6H_2O + 8NH_4OH \rightarrow Fe_3O_4(s) + 8NH_4Cl + 20H_2O$$

Typically, in alkaline condition and maintaining the molar ratio between Fe^{3+} and Fe^{2+} as 2:1, 26 mmol L^{-1} of Fe^{3+} and 13 mmol L^{-1} of Fe^{2+} were dissolved in appropriate amount of milli-Q water under N_2 atmosphere with vigorous stirring and heating the solution to 80°C. After that 15 mL of aqueous NH_3 was added at once and the reaction continued for another 30 minutes at this temperature. A black precipitate was formed that was cooled to room temperature. The mNPs were recovered by aid of magnet (magnetic decantation) and washed well several times by milli-Q water to remove any unreacted chemicals.

Preparation of silica coated magnetic nanoparticles

3 g of citrate-mNPs were dispersed in 90 mL ethanol and 1 mL distilled water. The suspension was sonicated for 30 min after which the mixture was stirred for 40 min in a three-neck flask equipped with a reflux condenser. The system was then, flushed with N_2 and 10 mL of APES were slowly added without interrupting the stirring. The reaction continued for 3 h at the refluxing temperature. At the end, the resulting APES-mNPs were washed with milli-Q water and acetone and dried at air.

Synthesis of mono-6-deoxy-6(*p*-tolylsulfonyl)-β-cyclodextrin

In a typical procedure, 60 g of β-CD were dissolved in 500 mL H_2O by drop-wise addition over 6 min of a solution of NaOH (6.57 g dissolved in 20 mL H_2O). Then, 10.08 g *p*-toluene-sulfonyl chloride dissolved in 30 mL acetonitrile were added to the previous solution drop-wise over 8 min and a white precipitate was immediately formed. The reaction continued for 2 h with stirring at room temperature. The product was removed by suction filtration and the filtrate stored overnight at 4^{o}C. Finally, the formed precipitate was dried for 12 h under vacuum.

Table S1 Synthetic urine sample composition.

Main components	**mmol L^{-1}**	**Neurotransmitters and markers**	**mmol L^{-1}**
NaCl	241	Dopamine	8.43×10^{-4}
KCl	40	Serotonin	8.5×10^{-4}
$CaCl_2$	7.22	Norepinephrine	3.20×10^{-5}
$MgCl_2$	9.32	5-HIAA	2.75×10^{-2}
HCl	20		
NH_3	12		
Creatinine	15.55		
Urea	288		
Albumin	6×10^{-4}		

All the chemicals were of analytical grade from Sigma-Aldrich and used without further purification.

VSM analysis

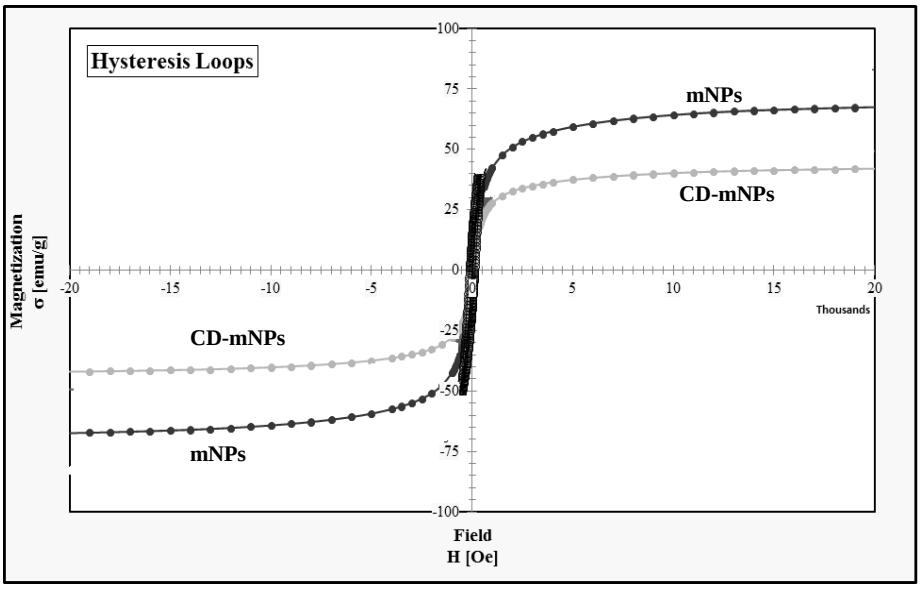

Fig. S1. Magnetization *vs*. magnetic field curves for bare MNPs and CD-mNPs obtained by VSM at 25ºC.

HRTEM and TEM analysis

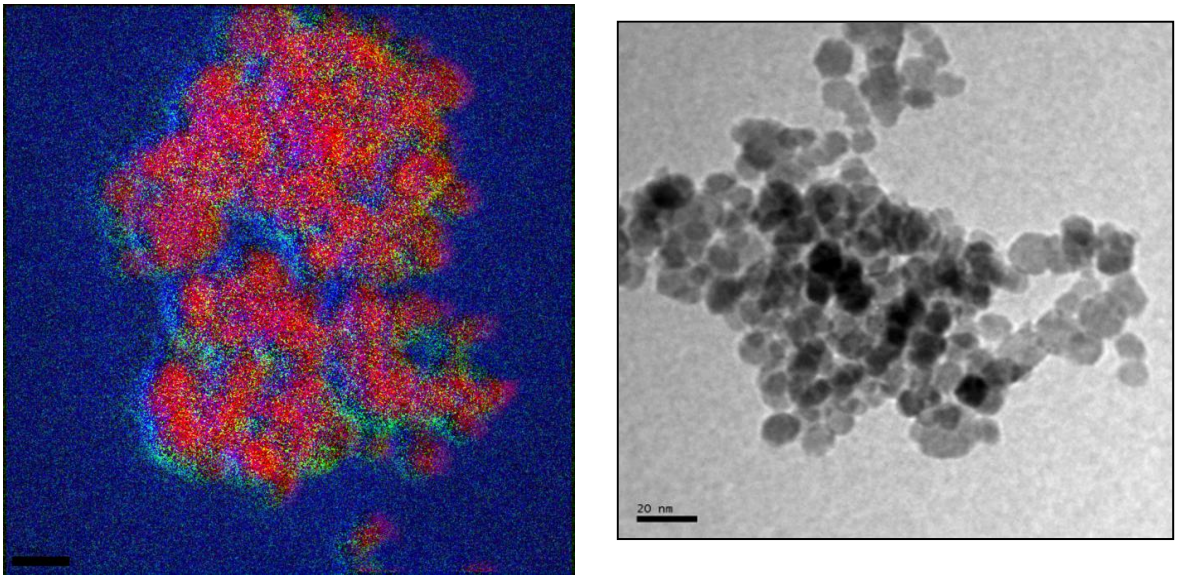

a **b**

Fig. S2 a. HRTEM elementary map of iron and silica of CD-mNPs, **b.** TEM image of CD-mNPs.

Adsorption kinetics

The model proposed by Lagergren can be represented in the following form [41]:

$$\ln(q_e - q_t) = \ln q_e - k_1 t$$

while the pseudo-second-order model proposed by Ho and McKay [42,43], can be expressed by the linear form:

$$\frac{t}{q_t} = \frac{1}{k_2 {q_e}^2} + \frac{1}{q_e} t$$

In these equations, q_e and q_t refer to the amount of 5-HIAA adsorbed (mg g^{-1}) at equilibrium and at any time, t (min), respectively. k_1 (min^{-1}) and k_2 (g $mg^{-1}min^{-1}$) are the equilibrium rate constant of pseudo-first-order and pseudo-second-order adsorption. The slope and intercept of the plot of $\log(q_e - q_t)$ versus t was used to determine the pseudo-first-order rate constant, k_1(results not shown). It was found that the correlation coefficient (R^2) was below 0.90. This result indicated that the Lagergren model was not adequate to fit the kinetic data for the initial concentrations studied.

In the case of the pseudo-second-order model, the slope and intercept of the plot of t/q_tversus t were used to calculate the second-order rate constant, k_2. The results (Figure S2b) demonstrated that the adsorption of 5-HIAA by followed the Ho and McKay equation, with a regression coefficient higher than 0.999 for the concentration range used in this work. The calculated amount of 5-HIAA adsorbed at equilibrium by CD- mNPs was 0.1101 mg g^{-1} and k_2 resulted to be 3.18 g $mg^{-1}min^{-1}$. On the basis of these results, it was suggested that 5-HIAA adsorption by CD-mNPs followed the pseudo-second-order kinetics model, which relies on the assumption that chemisorption may be the rate-limiting step. The 5-HIAA interacted with the β-CD host by forming an inclusion complex which maximized multipoint-interaction with the CD-mNPs surface: the organic moiety of 5-HIAA can be expected to fit into the hydrophobic cylindrical cavity of the β-CD while H-bonds may be formed between the carboxylic group of 5-HIAA and the external hydrophilic –OH groups of β-CD (Figure S3).

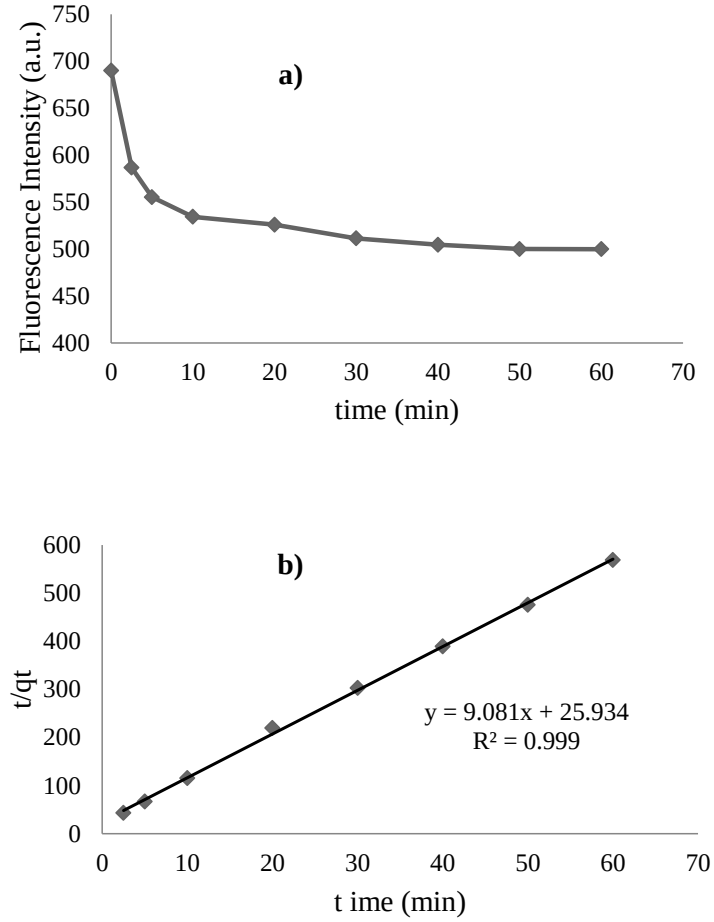

Fig. S3. a) Kinetic curve of 5-HIAA adsorption onto CD-mNPs at pH=6 and room temperature obtained by fluorescence measurements. λ_{ex} = 280 nm, λ_{em} = 348 nm; 5-HIAA 1x10^{-5} mol L^{-1}; CD- mNPs 5 mg mL^{-1}. b) Pseudo-second order sorption kinetics of 5-HIAA onto CD-mNPs, 5-HIAA 1x10^{-5} mol L^{-1}; CD-mNPs 5 mg mL^{-1}.

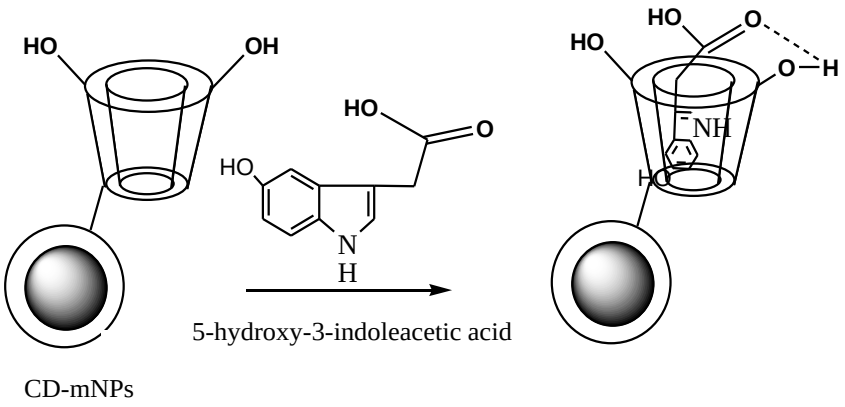

Fig. S4. Schematic representation of the reaction occurred between 5-HIAA and CD-mNPs.

Adsorption isotherms

Langmuir, Freundlich and Jovanovic isotherm equations were used to analyze equilibrium adsorption of 5-HIAA by CD-mNPs at pH 6 and room temperature. In these models q_e is the amount of 5-HIAA adsorbed on the CD-mNPs (mg g^{-1}) at equilibrium and C_e is the equilibrium 5-HIAA concentration in solution (mg L^{-1}). In the Langmuir model, q_m is the maximum capacity of adsorbent per unit weight of CD-mNPs (mg g^{-1}) while K_L is the Langmuir adsorption constant (L mg^{-1}). In the Freundlich isotherm equation K_F (mg^{1-m} g^{-1} L^m) is an empirical Freundlich parameter indicative of the relative adsorption capacity of the adsorbent and m is the heterogeneity factor. Finally, in the Jovanovic model K is the affinity constant and N_t is the binding site density.

TABLE 2S Fitting parameters obtained by non-linear regression for the different adsorption isotherms of 5-HIAA binding to CD-mNPs.

Model Isotherm	**Affinity constant K (L mg^{-1})**	**Binding site density, (mg g^{-1})**	**Binding capacity,**	**Heterogeneity parameter, m**	**Regression coefficient, R^2**	**Fisher test, F**
Langmuir $q_e = \frac{q_m K_L C_e}{1 + K_L C_e}$	43.18	1.08. 10^{-3}	0.0468	----------	0.9986	2215
Jovanovic $q_e = N_t(1-e^{-KC_e})$	82.78	7.25. 10^{-6}	0.0006	---------	0.9986	2204
Freundlich $q_e = K_F C_e^m$	----------	----------	0.0309	0.9461	0.9993	4207

Chapter 3

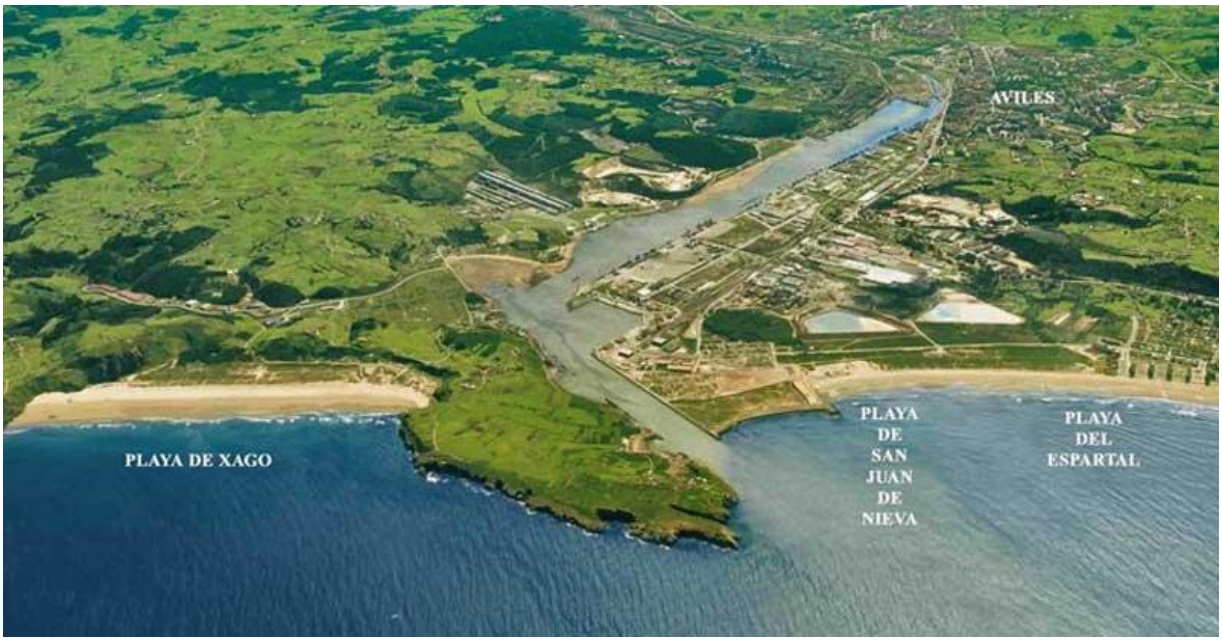

Highly fluorescent carbon dots as nanoprobes for sensitive and selective determination of 4-nitrophenol in surface waters

III.1. Graphical Abstract

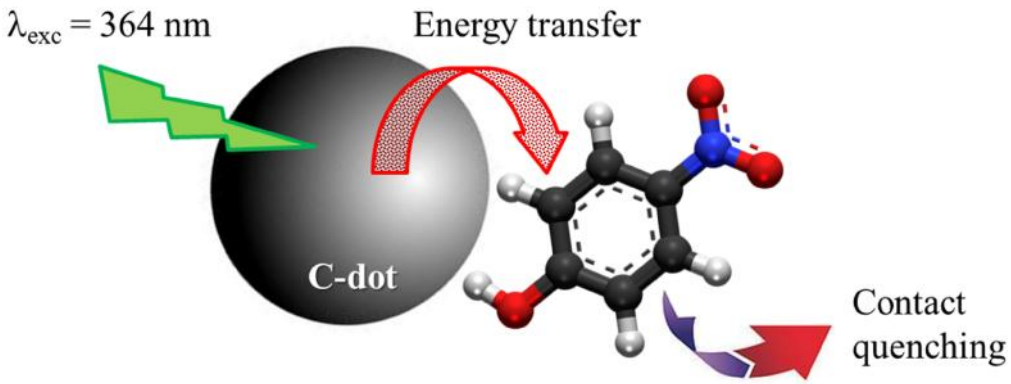

Contact quenching produced through the formation of a Meisenheimer complex with negative charge delocalized over the cyclohexadienine ring and the nitro group and positive charge distributed over an iminium group.

III.2. State of the art

C-dots acquire their novelty based on being benign chemical nanoparticles with fascinating optical properties, such as broad excitation spectra, tunable emission wavelength and stable photoluminescence. Besides that, other advantages characterize C-dots from other NPs, like simple synthesis, high solubility in water, chemical inertness, low toxicity and environmental-friendly. These advantages make C-dots more attractive than other competitive NPs, including their brothers from the nanocarbon family, such as fullerenes, carbon nanotubes, nanodiamonds, etc., or from semiconductor quantum dots.

As a result, C-dots inspired intensive studies since their discovery in 2004 until now. Moreover, they have been used in different applications, such as bioimaging, analytical sensing, drug delivery, etc. The important property of C-dots that gives them the preference for the semiconductor quantum dots in biomedical as well as (bio)analytical applications is their low toxicity.

In spite of their advantages, the exploiting of C-dots potential in analytical applications is not achieved completely. This opens opportunities for the researchers to study C-dots in different applications. In this line, we have found that no studies have been developed between C-dots and the organic pollutant 4-NP. Therefore, we synthesized highly fluorescent C-dots with a high fluorescence quantum yield as high as 28% and capped mainly by hydroxyl and carbonyl groups (figure 1). The novelty of the method is not only in the synthesis of a new highly fluorescent C-dots but also in their utilization for 4-NP determination in surface waters for the first time. A complete study was then accomplished after synthesis including complete physico-chemical characterization, analytical performance of the method, and a proposed interaction mechanism.

The physico-chemical characterization including XRD, FTIR, ^{1}HNMR, ^{13}CNMR, fluorescence spectra, and HRTEM techniques for the as-synthesized C-dots was explained in details within this chapter. Also, contact quenching through fluorescence resonance energy transfer was proposed as the main mechanism for the interaction between C-dots and 4-NP.

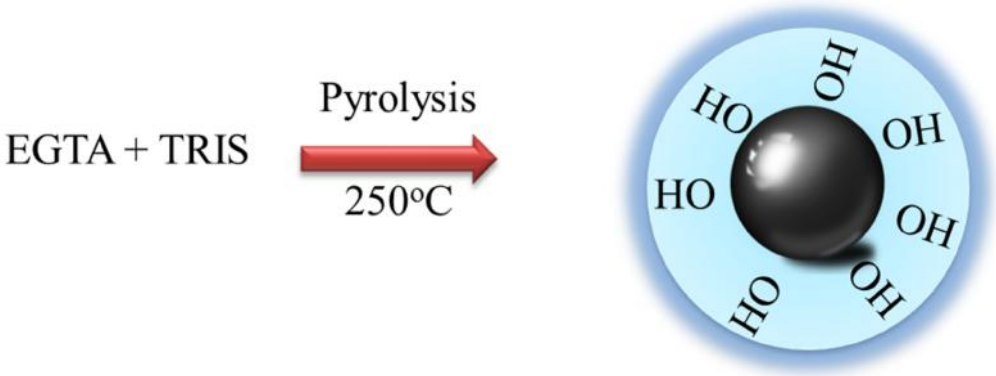

Figure 1: C-dots synthesis scheme

III.3. Historical background

III.3.1. Quantification of 4-NP

Nitroaromatic compounds are widely used in chemical industries, such as in the manufacturing of dyes, plasticizers, pesticides, fungicides, and explosives. As a result, highly hazardous compounds are released into the environment from these industrial activities. Among the leached compounds, 4-NP has higher solubility and stability in waters, stays longer time in water and surface soil without degradation and gets accumulated in deep soil indefinitely. The nitro group ($-NO_2$) in 4-NP is relatively more stable in biological systems and can cause several blood disorders, hormonal imbalance, central nervous system poisoning, kidney and liver damage and eye irritation [1]. As 4-NP is carcinogenic, mutagenic, and cyto- and embryonictoxic, it has been listed as priority pollutant by US Environmental Protection Agency (EPA) [2]. Therefore, simple, sensitive and reliable determination methods for 4-NP are required.

III.3.1.1. Electrochemical methods

4-NP is an electroactive species and thus many electrochemical methods are developed depending on its oxidation/reduction properties. Preparation of a new electrode with different materials is a common step followed by 4-NP electrosensing using various electrochemical techniques, such as cyclic voltammetry, differential pulse voltammetry, amperometry, etc. Table 1 review some of the electrochemical methods for 4-NP detection.

III.3.1.2. Chromatographic methods

Chromatographic methods are based mainly on separating the analyte from its matrix. However, they are known to be expensive and time consuming. Some HPLC methods are available for the quantification of 4-NP in different samples, differing among them in the type of column as well as the mobile phase [22-24].

On the other hand, some authors used on-line solid phase extraction coupled with HPLC for 4-NP determination. Fan et al. [25] used β-cyclodextrin bonded silica as the selective sorbent, while Zarejousheghani et al. [26] developed an in-tube molecularly imprinted polymer (using 4-NP as a target molecule)-solid phase microextraction device and the concentration of 4-NP was measured subsequently by HPLC-UV instrument. With a similar theory, Mehdinia et al. [27] fabricated mNPs fictionalized by a silica layer and finally grafted by molecularly imprinted polymer using 4-NP as a template. The method showed a very good selectivity towards 4-NP which quantified after extraction step by HPLC.

III.3.1.3. Miscellaneous Methods

A fluorescence flow immunoassay method based on the competition between a fluorescein labelled analyte derivative and the target compound for a limited amount of anti-4-nitrophenol antibody was proposed for 4-NP determination [28]. A flow-through optosensor based on diffuse reflectance spectroscopy and multivariate regression modelling was used for simultaneous determination of nitro-substituted phenols. On-line anion-exchange sorptive preconcentration and matrix removal with direct detection of sorbed species onto the sensing layer and chemometric deconvolution of overlapped spectra was achieved by the suggested optrode [29].

Fluorescent detection of 4-NP based on the fluorescence quenching of a Coumarin derivative was investigated [30]. A spectrophotometric determination of nitrophenols with a proposed orthogonal signal correction and partial least squares method to resolve ternary mixtures of nitrophenol isomers in synthetic and spike samples without prior separation has been studied [31]. Single-walled carbon nanohorn with exoteric structures and high surface area (SWCNH) was developed as new adsorbent for solid-phase extraction of 4-NP with large amount over a short time. After only 120 s extraction highly sensitive determination of 4-NP was achieved by linear sweep voltammetry [32]. High-quality ZnO nanowires covalently grafted with

1-pyrenebutyric acid fluorophore were used in photoluminescence measurements through fluorescence quenching of 1-pyrenebutyric acid by 4-NP [33]. Also, a microbial biosensor systems were developed for 4-NP determination [34, 35].

Table 1: Some electrochemical methods for 4-NP determination.

TYPE OF ELECTRODE	LINEAR CONC. RANGE (µM)	LOD (µM)	REFERENCE
β-Cyclodextrin functionalized mesoporous silica modified carbon paste	0.2 to1.6	0.05	3
hybrid inorganic–organic coatings based on Prussian blue, polyazulene, poly(3,4-ethylenedioxythiophene) and poly(3-[(E)-2-azulene-1yl)vinyl]thiophene) onto Pt substrate	30 to 90	8.23	4
cuprous oxide (Cu_2O) nanoparticles modified Pt rotating ring-disk	10 to 1000	0.1	5
Ordered mesoporous carbons modified glassy carbon electrode	2 to 90	0.1	6
reduced graphene oxide and molecularly imprinted polymer	0.01 to 100	0.005	7
Na-montmorillonite and anthraquione modified glassy carbon electrode	2.1 to 323	0.14	8
Lithium tetracyanoethylenide modified glassy carbon electrode	0.027 to 23.2	0.0075	9
Moleculary imprinted polymer- carbon paste	0.008 to 5	0.003	10
ZnO nanoparticles/multiwall carbon nanotubes - chitosan nanocomposite dripped onto an indium tin oxide electrode	0.01 to 200	0.001	11
boron-doped diamond film	0.4 to 20	0.02	12
mercury meniscus-modified silver solid amalgam electrode and liquid mercury free polished silver solid amalgam electrode	2 to 100	0.02	13
multi-wall carbon nanotubes Nafion-modified electrode	0.1 to 10	0.04	14
acetylene black paste electrode modified with a graphene-chitosan composite film	0.1 to 80	0.08	15
A poly(methylene blue)-modified glassy carbon electrode	0.015–0.25	0.009	16
apatite-modified carbon paste electrode	20 to 100	0.008	17
A graphene oxide film coated glassy carbon electrode	0.1 to 120	0.02	18
gold nanoparticles- 3-n-propyl-4-picoliniumsilsesquioxanechloride deposited onto a glassy carbon electrode	0.1 to1.5	0.046	19
polythiophene modified porous silicon	0.015 to 300	-	20
glassy carbon electrode modified with carbon nanotubes	2 to 4000	0.4	21

References:

[1] Kannan BN, and Natarajan S (2011) Heterogeneous catalytic reduction of anthropogenic pollutant, 4-nitrophenol by silver-bionanocomposite using Cylindrocladium floridanum. Bioresource Technology 102 : 10737–10740

[2] US Environmental Protection Agency, Nitrophenols, Ambient Water Quality Criteria. Criteria and Standards Division Office of Water Planning and Standards (1980), Washington, DC

[3] Xiaomeng X, Zhen L, Xin Z, Shuo D, Shuai X, and Changli Z (2011) β-Cyclodextrin functionalized mesoporous silica for electrochemical selective sensor: Simultaneous determination of nitrophenol isomers. Electrochimica Acta 58 : 142– 149

[4] Stelian L, Cecilia L, Mariana M, Nicolae T, and Paul CB (2009) Electrochemical sensors based on platinum electrodes modified with hybrid inorganic–organic coatings for determination of 4-nitrophenol and dopamine. Electrochimica Acta 54 : 1932–1938

[5] Yong-e G, Yuzhen Z, Fengyuan Z, Jinping W, Chunming W, Yongling D, and Weichun Y (2010) Investigation of photoelectrocatalytic activity of Cu2O nanoparticles for p-nitrophenol using rotating ring-disk electrode and application for electrocatalytic determination. Electrochimica Acta 56 : 953–958

[6] Tingting Z, Qiaolin L, Dapeng Y, Liang L, Lingxing Z, Cheng Z, Tie L, Mingdeng W, and Aihua L (2013) Simultaneous voltammetric determination of nitrophenol isomers at ordered mesoporous carbon modified electrode. Electrochimica Acta 106 : 127– 134

[7] Yanbo Z, Ying Z, Tianshu Z, and Guoyue S (2014) A novel composite of reduced graphene oxide and molecularly imprinted polymer for electrochemical sensing 4-nitrophenol. Electrochimica Acta 130 : 504–511

[8] Shengshui H, Cuiling X, Gaiping W, and Dafu C (2001)Voltammetric determination of 4-nitrophenol at a sodium montmorillonite-anthraquinone chemically modified glassy carbon electrode. Talanta 54 : 115-123

[9] Rita de Cássia SL, Flavio SD, Adriano BO, Johannes B, and Lauro TK (2004) Voltammetric determination of 4-nitrophenol at a lithium tetracyanoethylenide (LiTCNE) modified glassy carbon electrode. Talanta 64 : 935–942

[10] Taher A, Mohammad RG, Parviz N, Mashallah Z, and Ali Z (2009) A novel high selective and sensitive para-nitrophenol voltammetric sensor, based on a molecularly imprinted polymer–carbon paste electrode. Talanta 79 : 1197–1203

[11] Yu-fang H, Zhao-hui Z, Hua-bin Z, Li-juan L, and Shou-zhuo Y (2012) Sensitive and selective imprinted electrochemical sensor for p-nitrophenol based on ZnO nanoparticles/carbon nanotubes doped chitosan film. Thin Solid Films 520 5314–5321

[12] Jana M, Jiří B, and Karolina P (2011) Determination of Nitrophenols in Drinking and River Water by Differential Pulse Voltammetry at Boron-Doped Diamond Film Electrode. Electroanalysis, 23: 1236 – 1244

[13] Jan F, Lenka V, Ales D, Vlastimil V, Karel C, Karolina P, Bogdan Y, Tomas N, and Jiri B (2007) Voltammetric Determination of Nitrophenols at a Silver Solid Amalgam Electrode. Int J Electrochem Sci 2 : 226 – 234

[14] Wensheng H, Chunhai Y, and Shenghui Z (2003) Simultaneous determination of 2-nitrophenol and 4-nitrophenol based on the multi-wall carbon nanotubes Nafion-modified electrode. Anal Bioanal Chem 375 : 703–707

[15] Peihong D, Zhifeng X, and Junhua Li (2014) Simultaneous voltammetric determination of 2-nitrophenol and 4-nitrophenol based on an acetylene black paste electrode modified with a graphene-chitosan composite. Microchim Acta 181:1077–1084

[16] Krishnamoorthy G, Ranganathan S, Ramadoss M, Settu M, Sivakumar PK, Selvamani M and Vengidusamy N (2013) Nanomolar determination of 4-nitrophenol based on a poly(methylene blue)-modified glassy carbon electrode Analyst 138 : 5811

[17] MA El Mhammedi, M Achak, M Bakasse, and A Chtaini (2009) Electrochemical determination of para-nitrophenol at apatite-modified carbon paste electrode: Application in river water samples. J of Haz Mat 163 : 323–328

[18] Junhua L, Daizhi K, Yonglan F, Fuxing Z, Zhifeng X, Mengqin L (2012) A graphene oxide-based electrochemical sensor for sensitive determination of 4-nitrophenol. J of Haz Mat 201– 202 : 250– 259

[19] Paulo SS, Bianca CG, Hérica AM, and Almir S (2014) Gold nanoparticles hosted in a water-soluble silsesquioxane polymer applied as a catalytic material onto an electrochemical sensor for detection ofnitrophenolisomers. J of Haz Mat 273 : 70–77

[20] S Belhousse, N Belhaneche-Bensemra, K Lasmi, I Mezaache, T Sedrati, S Sam, FZ Tighilt, and N Gabouze (2014) Modified porous silicon for electrochemical sensor ofpara-nitrophenol. Materials Science and Engineering B 189 : 76–81

[21] Li-qiang L, Xue-lian Z, Ya-ping D, and Qing-sheng W (2008) Derivative voltammetric direct simultaneous determination of nitrophenol isomers at a carbon nanotube modified electrode. Sensors and Actuators B 135 : 61–65

[22] Kazimierz W, Katarzyna W, Edith MCU, and Jesus MR (2000) The determination of 3-nitrophenol and some other aromatic impurities in 4-nitrophenol by reversed phase HPLC with peak suppression diode array detection. J of Pharm and Biomed Anal 22 : 295-300

[23] Attila A, Emil F, and Pál P (2006) A simple and rapid ion-pair HPLC method for simultaneous quantitation of 4-nitrophenol and its glucuronide and sulfate conjugates. J. Biochem. Biophys. Methods 69 : 43–50

[24] Fawzy E, Kyle W, and Jane A (2006) Validation of a HPLC method for the determination of p-nitrophenol hydroxylase activity in rat hepatic microsomes. Journal of Chromatography B, 834 : 199–203

[25] Yi F, Yu-Qi F, and Shi-Lu D (2003) On-line selective solid-phase extraction of 4-nitrophenol with β-cyclodextrin bonded silica. Analytica Chimica Acta 484 : 145–153

[26] Mashaalah Z, Monika M, Helko B (2013) A new strategy for synthesis of an in-tube molecularly imprintedpolymer-solid phase microextraction device: Selective off-lineextraction of 4-nitrophenol as an example of priority pollutants fromenvironmental water samples. Analytica Chimica Acta 798 : 48– 55

[27] Ali M, Tohid BK, Ali J, Mohammad OAZ, and Ehsan Z (2013) Magnetic molecularly imprinted nanoparticles based on grafting polymerizationfor selective detection of 4-nitrophenol in aqueous samples. J of Chrom A 1283 : 82–88

[28] Catalin N, Anna O, Maria-Pilar M, Damià B, and Jenny E (2001) Competitive flow immunoassay with fluorescence detection for determination of 4-nitrophenol. Analytica Chimica Acta 426 : 185–195

[29] Matias M, Manuel M, José ME, Víctor C, Marcela AS, and José LFCL (2007)Flow-through solid-phase reflectometric method for simultaneous multiresidue determination of nitrophenol derivatives. analytica chimica acta 600 : 155–163

[30] Sheetal P, Melinda W, Theresa G, Janet G, James W, and Aleksandr S (2007) Fluorescence-based sensing of p-nitrophenol and p-nitrophenyl substituent organophosphates. Analytica Chimica Acta 596 : 9–15

[31] Ali N and Ateesa Y (2007) Spectrophotometric simultaneous determination of nitrophenol isomers by orthogonal signal correction and partial least squares Journal of Hazardous Materials 146 : 421–427

[32] Shuyun Z, Wenxin N, Haijuan L, Shuang H, and Guobao X (2009) Single-walled carbon nanohorn as new solid-phase extraction adsorbent for determination of 4-nitrophenol in water sample. Talanta 79 : 1441–1445

[33] Anurag G, Bruce CK, Eugene E, Christina B, and Paul R (2012) Covalent functionalization of zinc oxide nanowires for high sensitivity p-nitrophenol detection in biological systems. Materials Science and Engineering B 177 : 1583– 1588

[34] OI Guliy, OV Ignatov, OE Makarov, and VV Ignatov (2003) Determination of organophosphorus aromatic nitro insecticides and p-nitrophenol by microbial-cell respiratory activity. Biosensors and Bioelectronics 18 : 1005-1013

[35] RM Banik, Mayank, Rajiv P, and SN Upadhyay (2008) Microbial biosensor based on whole cell of Pseudomonas sp. For online measurement of p-Nitrophenol. Sensors and Actuators B 131 : 295–300

Microchim Acta
DOI 10.1007/s00604-014-1302-x

ORIGINAL PAPER

Highly fluorescent carbon dots as nanoprobes for sensitive and selective determination of 4-nitrophenol in surface waters

Gaber Hashem Gaber Ahmed · Rosana Badía Laíño · Josefa Angela García Calzón · Marta Elena Díaz García

Received: 3 March 2014 / Accepted: 23 May 2014

Abstract We report on the synthesis of carbon dots (C-dots) by thermal carbonization of a mixture of ethyleneglycol bis-(2-aminoethyl ether)-N,N,N',N'-tetraacetic acid (EGTA) and tris(hydroxymethyl)aminomethane (Tris). The resulting C-dots were characterized by X-ray diffraction, proton and carbon nuclear magnetic resonance, FTIR and fluorescence spectroscopy, and high-resolution TEM. The data reveal that the C-dots are mainly capped with hydroxy and carbonyl groups and are highly fluorescent with an emission peak that shifts from 427 to 438 nm if the excitation wavelength is increased from 310 to 360–370 nm. Fluorescence is quenched by 4-nitrophenol (4-NP), and this effect was exploited to design a simple and rapid protocol for the determination of 4-NP. The detection limit is 28 nM and the linear range extends from 0.1 to 50 μM. The method was successfully applied to the determination of 4-NP in spiked river and sea waters.

Keywords 4-nitrophenol · Carbon dots · Fluorescence · Water analysis

Electronic supplementary material The online version of this article (doi:10.1007/s00604-014-1302-x) contains supplementary material, which is available to authorized users.

G. H. G. Ahmed
Chemistry Department, Faculty of Science, Damanhur University, Damanhur, Egypt

R. B. Laíño · J. A. G. Calzón · M. E. D. García (✉)
Department of Physical and Analytical Chemistry, Faculty of Chemistry, University of Oviedo, c/Julián Clavería s/n, Oviedo 33006, Spain
e-mail: medg@uniovi.es

R. B. Laíño
e-mail: rbadia@uniovi.es

Introduction

C-dots are carbon nanoparticles with diameters lower than 10 nm that exhibit several advantages such as simple synthesis, chemical inertness, low toxicity and environmental-friendly compared with semiconductor quantum dots. Due to their unique optical properties, such as broad excitation spectra, tunable emission wavelength and stable photoluminescence, considerable attention has been paid in recent years to C-dots to exploit their potential in many applications such as bioimaging, drug delivery and analytical sensing. Some excellent reviews of synthesis, optical properties and applications of C-dots are available [1–5].

The origin of C-dots photoluminescence is not yet entirely understood, but it is supposed to arise from the radiative recombination of excitons, similarly to the process in semiconductor quantum dots. The fluorescence of C-dots has been found to be quenched by metal ions to different extents by facilitating non-radiative electron/hole recombination through an effective electron transfer process. Some research groups have used this phenomenon to detect different metal ions selectively [6–10]. Electron donor or electron acceptor molecules may also to effectively quench the C-dots fluorescence, thus indicating that the photoexcited C-dots are excellent electron acceptors and donors [3]. Until now, this property has been used for designing C-dots based analytical methods for detection of a few molecules. So, W.J. Bai et al. [11] have found that methylene blue quenched the fluorescence of C-dots, which acted as excellent electron donors. Addition of DNA removed the methylene blue from C-dots surface thus restoring the C-dots fluorescence. A sensitive method for DNA determination was thus reported by the authors. Other methods, based on the C-dots fluorescence quenching have been reported for hemoglobin [12], glucose and hydrogen peroxide [13], hemin [14] and dopamine [15].

Published online: 05 June 2014

Nitrophenols are hazardous pollutants that are difficult to remove from groundwater and surface waters due to their solubility in water and their stability, particularly 4-nitrophenol (4 NP) and 2-nitrophenol (2 NP), which are both resonance stabilized. These nitrophenols enter the environment during manufacturing and processing as well as result of pesticides degradation [16]. Due to their toxicity, carcinogenity and persistence in environment, simple, sensitive and reliable determination methods are required.

In our knowledge, only three studies have been reported for nitro-compounds detection using C-dots fluorescence quenching. Guo et al. [17] studied the intermolecular interactions between C-dots and nitroxide radicals in aqueous and aprotic media. The system was found to be sensitive not only to ascorbic acid at the μM level but also for the detection of antioxidants and carbon-centered radicals. On the other hand, Sun et al. [18] studied the C-dots quenching by the known electron acceptors 4-nitrotoluene and 2,4-nitrotoluene in toluene solution but they did not apply the process to the determination of the compounds. More recently, Wu et al. [19] have described a sensitive and selective method for detection of picric acid in water based on the fluorescence quenching of amine-capped C-dots.

In the present work, we have designed a sensitive and selective detection method based on fluorescent water soluble C-dots for 4 NP detection in aqueous solution. C-dots were prepared by thermal carbonization method using ETGA as the carbon source and Tris as the surface passivation agent (Scheme 1). The analytical potential of the method is demonstrated by directly detecting 4 NP in river and sea waters.

Experimental

Reagents

All the chemicals used were of analytical grade and used without further purification. The following materials are used in this study: Ethyleneglycol bis-(2-aminoethyl ether)-N,N,N',N'-tetraacetic acid (EGTA), phenol and 2-chlorophenol (2 CP) were purchased from Merck (www.merck.com), ethyleneglycol tris-(2-aminoethyl ether)-N,N,N',N'-tetraacetic acid, catechol, resorcinol, 2-aminophenol (2 AP), 4-aminophenol (4 AP) and a universal buffer solution consisting of disodium phosphate and citric acid for pH range 3–8 were achieved from Sigma-Aldrich (www.sigmaaldrich.com). Universal buffer solutions consisting of disodium phosphate and HCl or NaOH for pH range 8–11.5 and quinine dehydrate were obtained from Prolabo (www.vwr.com). Milli-Q water was used thoroughly.

Instrumentation

HRTEM (JEOL JEM-2100F, 200 KV) was used to determine the size and morphology of the synthesized C-dots. The structural and phase properties of grinded synthesized sample was obtained by powder XRD (Bruker D8 Discover) using a monochromatic X-ray beam from nickel-filtered Cu K_α radiation. A Varian 620-IR instrument was used to analyze FTIR spectra for the synthesized sample in the range 600 to 4,000 cm^{-1}. H^1NMR and C^{13}NMR (NAV400 with 9.0 T magnet shielded, 600 MHz) were used for structure analysis of the synthesized C-dots in D_2O solvent. Fluorescence spectra of the prepared C-dots and the subsequent experiments were measured using a Cary Eclipse Varian spectrofluorimeter.

C-dots synthesis

The C-dots were synthesized by a thermal carbonization method, according to the following procedure: 2 mmoL of EGTA were dissolved in about 30 mL of milli-Q water forming an acidic white suspension solution. To obtain completely soluble C-dots, 8 mmoL of solid Tris were added to the previous solution. It became clear and the pH neutral (=7). It was found that Tris:EGTA ratios lower than 4:1 lead to slightly soluble C-dots. The solution was then heated at 150 °C on a hot plate until near dryness at which a pale yellow gel was formed. 1 mL of water was then added and the previous procedure was repeated 5 times in about 30 min. The temperature was then increased to 180 °C. Temperatures lower than 200 °C should be used to avoid degradation of the reactants or the formed product. The heating continued until the pale yellow gel turned to reddish-orange, ensuring the formation of the C-dots. The gel that can be soften on heating was then dissolved in about 25 mL Milli-Q water, filtered through 0.45 μm nylon filter and the solution purified by dialysis through dialyzer tube (MWCO, 3.5 KDa) for 3 days. The pH 7 was found for the aqueous C-dots solution. The final solution was stored under 4 °C until use.

Analysis of real samples

Real water samples were collected from Arlos River and Cantabrian Sea (Salinas Beach, Castrillón, Spain). The samples were filtered through 0.45 μm nylon filters prior to analysis. The specific gravity for both river and sea water was measured and found to be 1.178 and 1.211 g mL^{-1}, respectively, while the pHs were 8.07 and 7.9, respectively. Samples were spiked with solution of 4 NP at 1, 2 and 4 μM levels after which 100 μL of C-dot solution were added and final dilution to 5 mL was made

Scheme 1 Schematic representation for C-dots synthesis

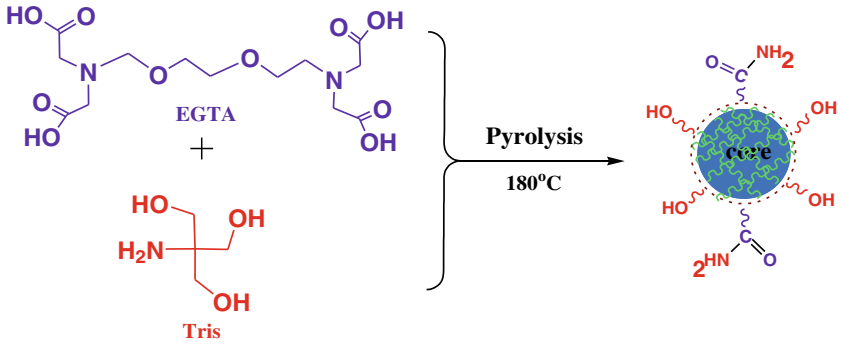

with universal buffer solution pH=8. The fluorescence was measured at 438 nm using λ_{ex} 364 nm and 4 NP quantified by running a calibration curve using standard solutions.

Fluorescence quantum yield measurement

The quantum yield of C-dots was estimated by a comparative method, according to established procedure [20], using quinine sulfate as standard. The method relied on the equations:

$$\Phi_c = \Phi_{st}\frac{F_c A_{st}}{F_{st} A_c}\frac{n_c^2}{n_{st}^2} \quad (1)$$

$$\Phi_c = \Phi_{st}\frac{G_c}{G_{st}}\frac{n_c^2}{n_{st}^2} \quad (2)$$

Here, Φ refers to the quantum yield, F to the calculated integrated fluorescence intensity, n to the refractive index of the solvent, A relative amount of light absorbed at the excitation wavelength (measured on a UV–Vis spectrophotometer, Perkin Elmer, Lambda 900), and G is the gradient of F vs A linear plot. The subscripts ***c*** and ***st*** denote C-dots and reference fluorophore, respectively. A quinine sulfate quantum yield of 0.54 at λ_{ex} = 350 nm dissolved in 0.1 M H_2SO_4 has been used as reference.

Results and discussion

Characterization of C-dots

Figure 1S (Electronic Supplementary Material, ESM) represents the XRD pattern of the C-dots produced by the one-step

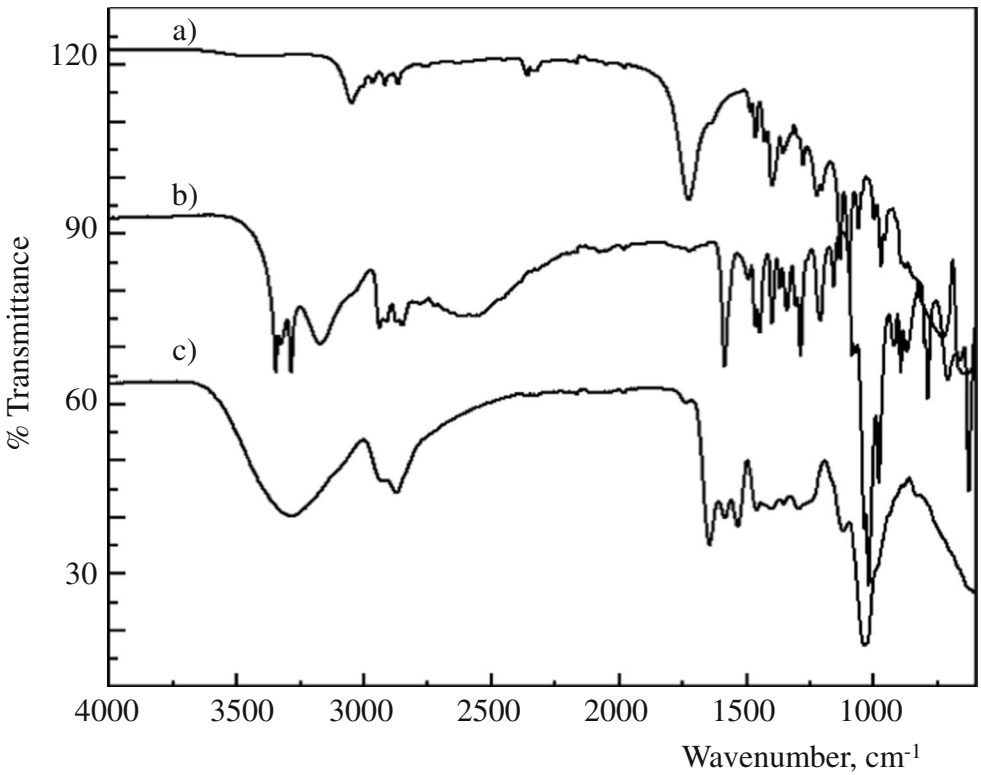

Fig. 1 FTIR spectra of C-dots and their precursors. **a** pure EGTA, **b** pure Tris, and **c** C-dots

thermal decomposition of EGTA/Tris, in which a sharp reflection band centered at 2θ=20.55° corresponds to [002] planes of a graphitic structure. The average thickness of interlayer spacing can be roughly estimated to be about 4.32 Å using the Bragg's equation. The crystallite stacking height L_c was calculated for the [002] band using Scherrer's equation $L_c = K\lambda/\beta \cos\theta$, where λ is the X-ray wavelength (1.542 Å), β is the broadening of the diffraction peak measured at half its maximum intensity (in radians), θ is the scattering angle and K is the Scherrer's constant, which accounts for the shape of the particle [21]. Having K=0.9 a L_c=3.85 Å was obtained. This interlayer spacing is slightly larger than that reported for graphite (3.34 Å), which may be indicative of poor crystallization and formation of turbostratic carbon structures [22]. Also, a weak peak at about 42.5° was observed which has been assigned to graphite planes [100] [23], indicating that the crystallites are graphite-like.

The functional groups of the C-dots were determined by FTIR analysis. In Fig. 1, the FTIR spectra of EGTA and Tris were included for comparison. The broad band between 3,000 and 3,454 cm^{-1} observed in the C-dots spectrum is assigned to –OH stretching, which indicated functional –OH groups or adsorbed water. On the other hand, the new stretching vibrations at 1,645 cm^{-1} and the strong peak at 1,537 cm^{-1} are attributed to amide C = O stretch and N-H vibrations, respectively. C-H stretching in the 2,800–2,930 cm^{-1} region and C-OH/C-O-C stretching in the region 1,050–1,120 cm^{-1} are also observed, typical of the ethylene glycol moiety. The asymmetrical and symmetrical carboxylate stretching in the 1,300–1,380 cm^{-1} region, present in the EGTA spectrum, as well as the 3,150 cm^{-1} vibration due to the $–NH_2$ group in Tris, could not be observed for the C-dots, thus indicating the formation of amide bonds.

In Fig. 2Sa (ESM) the HRTEM image reveals that the as-synthesized C-dots are mostly spherical and not crystal lattice is observable. STEM image (Fig. 2Sb, ESM) clearly showed the C-dots as white dots. The diameters of the C-dots were distributed in a narrow range, with an average value of 5± 2 nm. ^{13}C NMR spectra showed (Fig. 3Sa, ESM) signals in the range of 165 to 180 ppm corresponding to sp^2 carbons that can be ascribed to carboxylic/carbonyl carbons as well as signals in the range of 40 to 80 ppm corresponding to aliphatic sp^3 carbons [24]. In the ^1H-NMR spectra (Fig. 3Sb, ESM), the peaks at δ=3.1–3.4 and δ=2.6–2.9 ppm for the oxy ethylene and the $–CH_2$-COOH groups of EGTA, respectively, could be observed. Also, the peaks at δ=3.5–3.8 for the $–CH_2$-OH group of TRIS confirm the presence of free hydroxy groups while peaks at δ=4.1–4.3 ppm corresponding to the amide group confirms the information obtained by FTIR.

Fluorescence features of C-dots

The fluorescence spectra of C-dots in aqueous media at different excitation wavelengths are shown in Fig. 2. As seen, the maximum emission wavelength was dependent on the excitation wavelength and it was shifted from 425 to 438 nm ($\Delta\lambda_{em}$=13 nm) by changing the excitation wavelength from 310 to 370 nm ($\Delta\lambda_{ex}$=60 nm).

The full width at a half maximum at the different excitation wavelenghts resulted to be 93±5 nm, what confirmed a

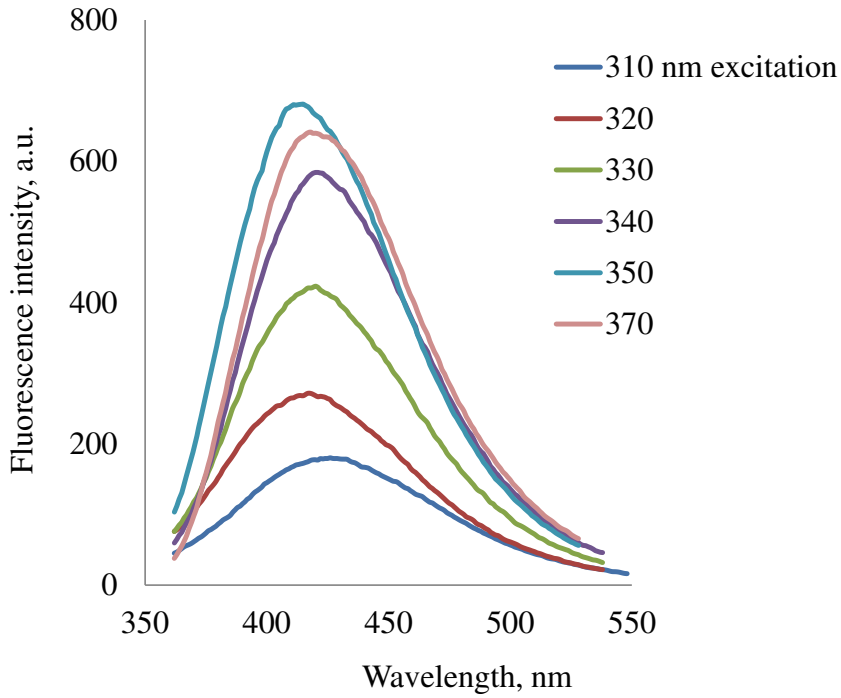

Fig. 2 Excitation dependent-fluorescence of C-dots

Table 1 The effect of some nitro compounds on the fluorescence of the as-synthesized C-dots at pH=8 and λ_{ex}=364 nm

Nitro compound	Fluorescence quenching %	RSD %
4-NP	31.37	0.2
2-NP	9.7	0.15
4-nitroaniline	23.9	0.2
Nitrobenzene	2.1	0.05
1-bromo-2,4-dinitrobenzene	−1.3	0.17
Bis(4-nitrophenyl) phosphate	2.9	0.3

The concentration of all nitro compounds is 10 μM

narrow size distribution of as-prepared C-dots. Consequently, the fluorescence dependence on the excitation wavelength cannot be ascribed to C-dots of different sizes. According to Tang et al. [25] the presence of different functional groups on the C-dots could be responsible for different emissive sites with different energy levels, thus explaining the excitation dependent emission phenomenon. In further experiments, excitation and emission wavelenghts of 364 and 438 nm, respectively, were used.

The maximum absorption band of the C-dots was found at 367 nm near to its excitation wavelength. The fluorescence quantum yield of the C-dots excited at 364 nm in milli-Q water was calculated to be 28 %, this value is considered high compared with other C-dots obtained by bottom up methods [26–28]. Two main reasons may account for the high value of the quantum yield; firstly, at the low temperature used during synthesis the surface passivation process of the C-dots could proceed adequately by formation of amide bonds (EGTA as precursor), as revealed by the FTIR analysis. It has been reported that N-passivation of C-dots creates a favorable energy trap to enhance their photoluminesce [29]. Secondly, the high number of hydroxy groups on the surface, provided by Tris and by transformation of carbonyl groups to hydroxy group during synthesis, may also increase the quantum yield [3].

C-dots were found to be stable over several days with fluorescence spectral profiles and intensities unchanged within the experimental error (see Figure 4S, ESM). This is an interesting property of C-dots as no photochemical reactions in the stock aqueous C-dot solutions seem to take place and provide them with potential for different applications such as chemical sensing or bioimaging.

Interaction of C-dots with nitrophenols

We could observe that addition of nitroaniline, 2- and 4 NP quenched the fluorescence of the C-dots (see Table 1). The other nitro compounds tested have negligible effect on the fluorescence of C-dots. In the following, we selected 4 NP as model compound of environmental interest as it has the highest toxicity, it is more water-soluble than the others and is the most important of the mononitrophenols in terms of quantities used and potential environmental contamination [30].

The quenching of C-dots fluorescence by 4 NP was rapid, sensitive and after 1 h reaction, the fluorescence intensity ramained stable. The pH played an important role in the sensing system for 4 NP, as both the fluorescence of C-dots solution in absence and in prescence of the 4 NP were pH dependent. According to the experimental results, fluorescence quenching was strongest in the pH range 8–10, but dropped drastically at pH values of 7 and 11 (Fig. 3).

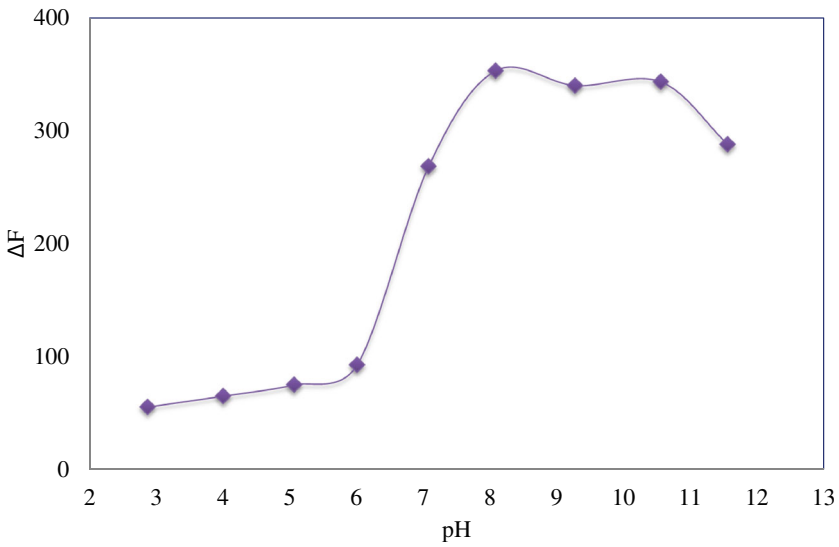

Fig. 3 pH effect on the fluorescence intensity of C-dots

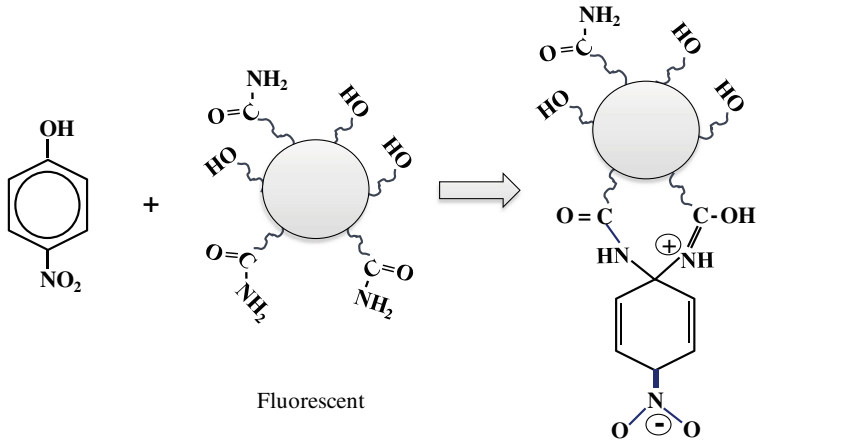

Meisenheimer non-fluorescent complex

Fig. 4 Possible quenching mechanism of C-dots in presence of 4-nitrophenol

Quenching mechanisms

Deprotonation of 4 NP takes place at pH>7 (pKa=7.15) (http://www.chemicalbook.com/ProductMSDSDetailCB7852550_EN.htm) and a possible mechanism for the C-dots quenching by 4-nitrophenolate could be due to an energy transfer process. The maximum absorption band of 4-nitrophenolate centered at 420 nm, overlapped the emission band of C-dots, thus giving rise to a resonant energy transfer process (contact quenching). As the 4-nitrophenolate does not exhibit fluorescence, only the C-dots fluorescence quenching was observed. This contact quenching may be produced through the formation of a zwitterionic spirocyclic Meisenheimer complex (Fig. 4) in which the negative charge may delocalized over the cyclohexadienine ring and the nitro group and the positive charge distributed over an iminium group [31].

Analytical figures

Under the optimum experimental conditions, the sensitivity, the linear response range, and the limit of detection of 4 NP by C-dot fluorescence quenching were determined. Calibration curve, obtained from a Stern-Volmer semilog plot, was linear within the range 0.1 to 50 μM 4 NP being the calibration equation $\log(F^0/F) = 0.0089C\ [\mu M]+0.0061$, ($R^2$=0.994), where F^0 and F account for the fluorescence intensities of C-dots in the absence and presence of 4 NP, respectively and C represents the concentration of 4 NP. A detection limit of 28 nM 4-NP was calculated, being the quantification one 0.3 μM 4-NP. The repeatability, expressed as standard relative deviation (n=8) was 0.1 % at the concentration level of 10 μM 4 NP. In our knowledge, no fluorescence methods for 4 NP based on the use of C-dots have been described to date, but from Table 2, it is apparent that the present method, exhibits high sensitivity and low detection limit when compared with some electrochemical methods based on the use of different nanomaterials as electron mediators.

These analytical performance characteristics offer potential for determination of trace amounts of 4-NP in real water samples. The potential influx of 4-NP into natural waters is the result of the degradation of pesticides such as methyl paraoxon, methyl parathion, nitrofen [25]. The effects of coexisting compounds on the C-dots fluorescence quenching detection of 10 μM 4 NP were investigated. Besides the already mentioned nitro compounds (Table 1) other major potential interference compounds chosen were 4-AP (pK_a= 9.3), 2-AP (pK_a=9.76), 2-CP (pK_a=8.49) and phenol (pK_a= 9.89). As can be seen from Fig. 5, these compounds have no significant effect on the fluorescence emission of C-dots (signal change <±5 %).

Table 2 Figures of merit of electrochemical methods for 4 NP determination based on the use of nanoparticles

Method	Linear dynamic range	LOD (nM)	Reference
Cyclic voltammetry	15 to 250 nM	90	[32]
Electrochemical reduction	10^{-7} to 1.2×10^{-4} M	20	[33]
Electrochemical oxidation	10^{-6} to 3×10^{-4} M	600	[34]
Hydrodynamic differential pulse voltammetry	10^{-5} to 10^{-3} M	100	[35]
Cyclic voltammetry	0.01 to 10 mg L^{-1}	287	[36]
Adsorptive stripping voltammetry	10^{-7} to 10^{-5} M	40	[37]
Fluorescence quenching of nano-carbon	0.1–50	28	This work

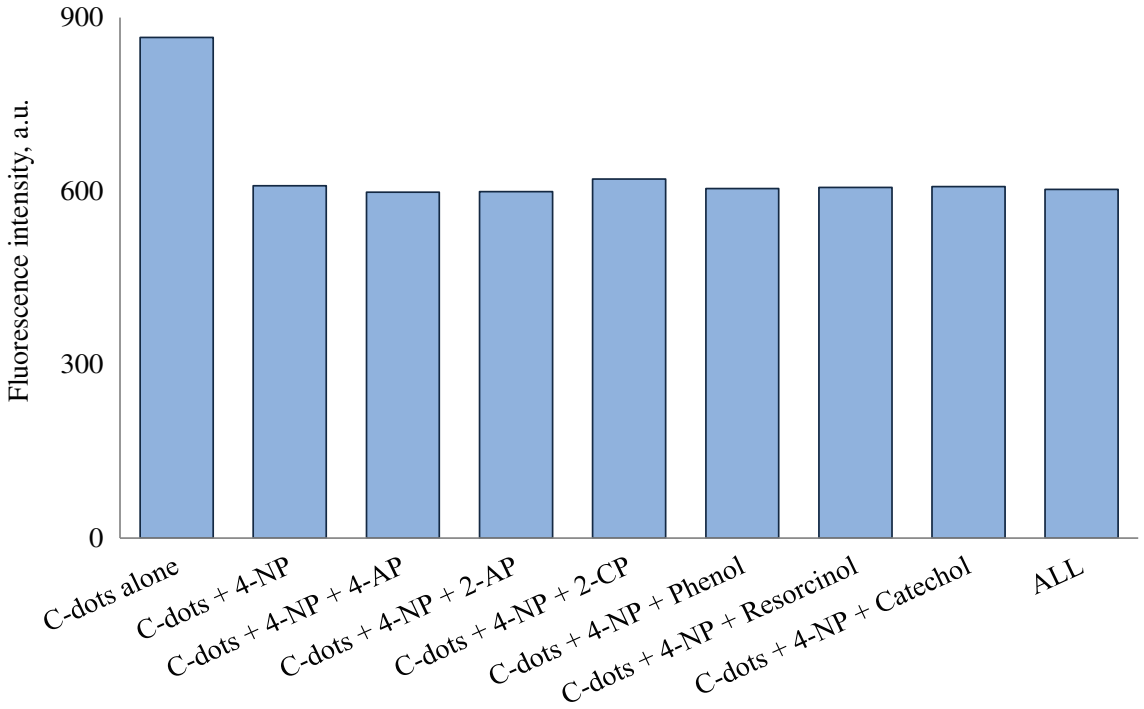

Fig. 5 Histogram of the fluorescence intensity of C-dots in the absence and presence of different phenols and nitrophenols. The concentration of all phenols used is 10 μM. All measurements were performed at pH 8

It has been reported that capped C-dots with oxygen-(hydroxy, carboxylic) or nitrogen (amine, amide) containing groups may be quenched by some metal ions or anions [38, 39]. The quenching has been attributed to the combination between the ions and the corresponding functional groups on the surface of the C-dots leading to their fluorescence quenching. In this line, we have also found that our C-dots were quenched by Fe^{3+} ions, which may represent an evidence for the presence of -OH/-COOH groups on their surface. However, at pH >6 Fe^{3+} hydrolyzed and precipitated as hydroxide so that it did not interfere with 4 NP determination at pH 8. Many other metal ions that may be found in real water samples (Fe^{2+}, Cu^{2+}, Hg^{2+}, Zn^{2+}, Al^{3+}, Pb^{2+}, Ca^{2+}, Na^{+}, K^{+}) had a marginal quenching effect, probably due to their lower trend to form complexes with the surface functional groups of C-dots. The effect of most anions, such as I^{-}, Br^{-}, Cl^{-}, PO_4^{3-} and SO_4^{2-} had no significant effect on the fluorescence emission of C-dots.

Real sample analysis

According to the procedure described in the "Experimental" section, river and sea waters were used to validate the method. It should be noted that no sample pre-treatments were applied. From the data in Table 3, it is obvious that satisfactory recoveries were achieved for the spiked samples and results demonstrated that the method offers potential for quantitative determination of 4 NP in waters.

Conclusions

In summary, we have synthesized a hydroxy capped C-dots as revealed by characterization analyses. They were found to be excellent fluorescence probes for 4 NP detection. 4 NP interaction with C-dots resulted in their fluorescence quenching,

Table 3 Results for the determination of 4 NP in spiked surface waters

Spiked concentration (μM)	River water			Sea water		
	Found concentration (μM)	Recovery %	RSD %	Found concentration (μM)	Recovery %	RSD %
1.00	1.09	109.0	0.1	0.91	91.0	0.3
2.00	1.93	96.5	0.1	2.04	102.0	0.2
4.00	4.20	105.0	0.2	4.16	104.0	0.2

probably via an energy transfer process. Development of an excellent fluorescence sensing system for 4 NP detection in aqueous media was set after optimizing the experimental conditions. The probes system of 4 NP based on C-dots fluorescence quenching showed analytical advantages such as rapid detection, considerable sensitivity, good selectivity, wide linear response range, and low cost. This method may be promising for 4 NP determinations in environmental samples

Acknowledgments Authors gratefully acknowledge financial support from the Science and Innovation Spanish Ministry (Proj # MAT2012-099). Also, G.H.Gaber Ahmed thanks an Erasmus Mundus Medastar grant.

References

1. Baker SN, Baker GA (2010) Luminescent carbon nanodots: emergent nanolights. Angew Chem Int Ed 49:6726
2. Esteves da Silva JCG, Gon alves HMR (2011) Analytical and bioanalytical applications of carbon dots. TrAC Trends Anal Chem 30:1327
3. Li H, Kang Z, Liu Y, Lee ST (2012) Carbon nanodots: synthesis, properties and applications. J Mater Chem 22:24230
4. Demchenko AP, Dekaliuk MO (2013) Novel fluorescent carbonic nanomaterials for sensing and imaging. Methods Appl Fluoresc 1: 042001
5. Yang Z, Li Z, Xu M, Ma Y, Zhang J, Su Y, Gao F, Wei H, Zhang L (2013) Controllable synthesis of fluorescent carbon dots and their detection application as nanoprobes. Nano Micro Lett 5:247
6. Liu LQ, Li YF, Zhan L, Liu Y, Huang CZ (2011) One-step synthesis of fluorescent hydroxy coated carbon dots wiyh hydrothermal reaction and its application to optical sensing of metal ions. Sci China Ser B Chem 54:1342
7. Zhou L, Lin YH, Huang ZZ, Ren JS, Qu XG (2012) Carbon nanodots as fluorescence probes for rapid, sensitive, and label-free detection of Hg^{2+} and biothiols in complex matrices. Chem Commun 48:1147
8. Zhu AW, Qu Q, Shao XL, Kong B, Tian Y (2012) Carbon-dot-based dual-emission nanohybrid produces a ratiometric fluorescent sensor for in vivo imaging of cellular copper ions. Angew Chem Int Ed 51: 7185
9. Dong YQ, Wang RX, Li H, Shao JW, Chi YW, Lin XM, Chen GN (2012) Polyamine-functionalized carbon quantum dots for chemical sensing. Carbon 50:2810
10. Lai T, Zheng E, Chen L, Wang X, Kong L, You C, Ruan Y, Weng X (2013) Hybrid carbon source for producing nitrogen-doped polymer nanodots: one-pot hydrothermal synthesis, fluorescence enhancement and highly selective detection of Fe(III). Nanoscale 5:8015
11. Bai WJ, Zheng HZ, Long YJ, Mao XJ, Gao M, Zhang L (2011) A carbon dots-based fluorescence turn-on method for DNA determination. Anal Sci 27:243
12. Wang CI, Wu WC, Periasamy AP, Chang HT (2014) Electrochemical synthesis of photoluminescent carbon nanodots from glycine for highly sensitive detection of hemoglobin. Green Chem. doi:10.1039/C3GC42325E
13. Wei J, Quiang L, Ren J, Ren X, Meng X, Tang F (2014) Fluorescence turn-off detection of hydrogen peroxide and glucose directly using carbon nanodots as probes. Anal Methods. doi:10.1039/C3AY41837E
14. Baruah U, Gogoi N, Majumdar G, Chowdhury D (2013) Capped fluorescent carbon dots for detection of hemin: role of number of –OH groups of capping agent in fluorescence quenching. Sci World J, Article ID 529159, 9 pages. doi:10.1155/2013/529159
15. Qu KG, Wang JS, Ren JS, Qu XG (2013) Carbon dots prepared by hydrothermal treatment of dopamine as an effective fluorescent sensing platform for the label-free detection. Chem Eur J 19:7243
16. Mononitrophenols. Concise International Chemical Assessment Document. (CICADs) (2000), World Health Organization, Geneva
17. Lin F, Pei D, He W, Huang Z, Huang Y, Guo X (2012) Electron transfer quenching by nitroxide radicals of the fluorescence of carbon dots. J Mater Chem 22:11801
18. Wang X, Cao L, Lu F, Meziani MJ, Li H, Qi G, Zhou B, Harruff BA, Kermarrec F, Sun YP (2009) Photoinduced electron transfers with carbon dots. Chem Commun 25:3774
19. Niu Q, Gao K, Lin Z, Wu W (2013) Amine-capped carbon dots as a nanosensor for sensitive and selective detection of picric acid in aqueous solution via electrostatic interaction. Anal Methods 5:6228
20. Lakowicz JR (1999) Principles of fluorescence spectroscopy, 2nd edn. Kluwer Academic/Plenum, New York
21. Smilgies DM (2009) Scherrer grain-size analysis adapted to grazing incidence scattering with area detectors. J Appl Crystallogr 42:1030
22. Short MA, Walker PL (1965) Measurement of interlayer spacing and crystal sizes in turbostatic carbons. Carbon 1:3
23. Sadezky A, Muckenhuber H, Grothe H, Niessner R, Pöschl U (2005) Raman microspectroscopy of soot and related carbonaceous materials: spectral analysis and structural information. Carbon 43:1731
24. AIST: RIO-DB. Spectral database for organic compounds, SDBS: http://riodb01.ibase.aist.go.jp/sdbs/cgi-bin/cre_index.cgi?lang=eng
25. Tang L, Ji R, Cao X, Lin J, Jiang H, Li X, Teng KS, Luk CM, Zeng S, Hao J, Lau SP (2012) Deep ultraviolet photoluminescence of water-soluble self-passivated graphene quantum dots. ACS Nano 6:5102
26. Liu XJ, Guo ML, Huang J, Yin XY (2013) Improved fluorescence of carbon dots prepared from bagasse under alkaline hydrothermal conditions. Bioresources 8:2537
27. De B, Karak N (2013) A green and facile approach for the synthesis of water soluble fluorescent carbon dots from banana juice. RSC Adv 3:8286
28. Mao LH, Tang WQ, Deng ZY, Liu SS, Wang CF, Chen S (2014) Facile access to white fluorescent carbon dots toward light emitting devices. Ind Eng Chem Res 53:6417
29. Qiao ZA, Wang Y, Gao Y, Li H, Dai T, Liu Y, Huo Q (2010) Chem Commun 46:8812
30. US Environmental Protection Agency, Nitrophenols, Ambient Water Quality Criteria. Criteria and Standards Division Office of Water Planning and Standards (1980), Washington, DC
31. Al-Kaysi RO, Creed D, Valente EJ (2004) Meisenheimer complex from picric acid and diisopropylcarbodiimide. J Chem Crystallogr 34:685
32. Giribabu K, Suresh R, Manigandan R, Munusamy S, Kumar SP, Muthamizh S, Narayanan V (2013) Nanomolar determination of 4-nitrophenol based on a poly(methylene blue)-modified glassy carbon electrode. Analyst 138:5811
33. Li J, Kuang D, Feng Y, Zhang F, Xu Z, Liu M (2012) A graphene oxide-based electrochemical sensor for sensitive determination of 4-nitrophenol. J Hazard Mater 201–202:250
34. Yin H, Zhou Y, Ai S, Liu X, Zhu L, Lu L (2010) Electrochemical oxidative determination of 4-nitrophenol based on a glassy carbon

electrode modified with a hydroxyapatite nanopowder. Microchim Acta 169:87
35. Gu Y, Zhang Y, Zhang F, Wei J, Wang C, Du Y, Ye W (2010) Electrochim Acta 56:953
36. Tapsoba I, Bourhis S, Feng T, Pontié M (2009) Sensitive and selective electrochemical analysis of methyl-parathion (MPT) and 4-nitrophenol (PNP) by a new type of p-NiTSPc/pPPD coated carbon fiber microelectrode (CFME). Electroanalysis 21:1167
37. Huang W, Yang C, Zhan S (2003) Simultaneous determination of 2-nitrophenol and 4-nitrophenol based on the multi-wall carbon nanotubes nafion-modified electrode. Anal Bioanal Chem 375:703
38. Du F, Zeng F, Ming Y, Wu S (2013) Carbon dots-based fluorescent probes for sensitive and selective detection of iodide. Microchim Acta 180:453
39. Yazid SNA, Chia SF, Pang SC, Ng SM (2013) Detection of Sn(II) ions via quenching of the fluorescence of carbon dots. Microchim Acta 180:137

Electronic Supporting Material

Highly fluorescent carbon dots as nanoprobes for sensitive and selective determination of 4-nitrophenol in surface waters

Gaber Hashem Gaber Ahmed

Chemistry Department, Faculty of Science, Damanhur University, Damanhur, Egypt

Rosana Badía Laíño, Josefa Angela García Calzón, Marta Elena Díaz García*

Department of Physical and Analytical Chemistry, Faculty of Chemistry

University of Oviedo, c/Julián Clavería s/n, Oviedo, 33006, Spain

*Corresponding author, e-mails: rbadia@uniovi.es; medg@uniovi.es

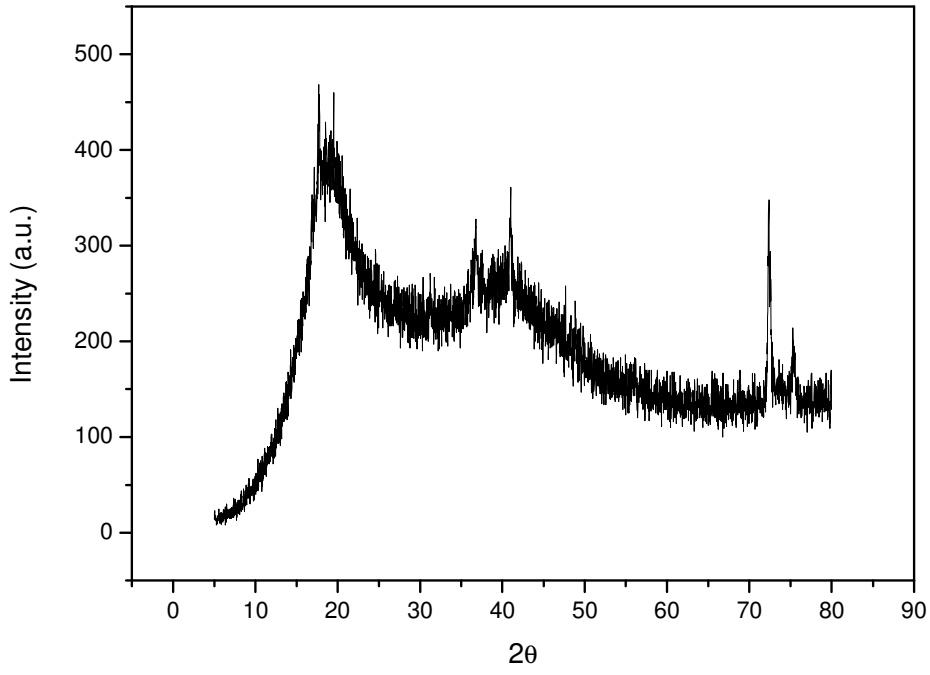

Figure 1S. XRD pattern of the synthesized C-dots

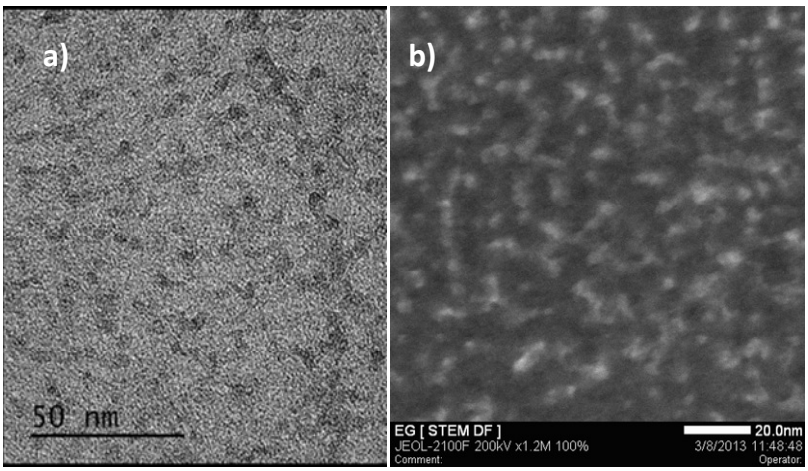

Figure 2S. a) HR-TEM image and b) STEM image for the C-dots

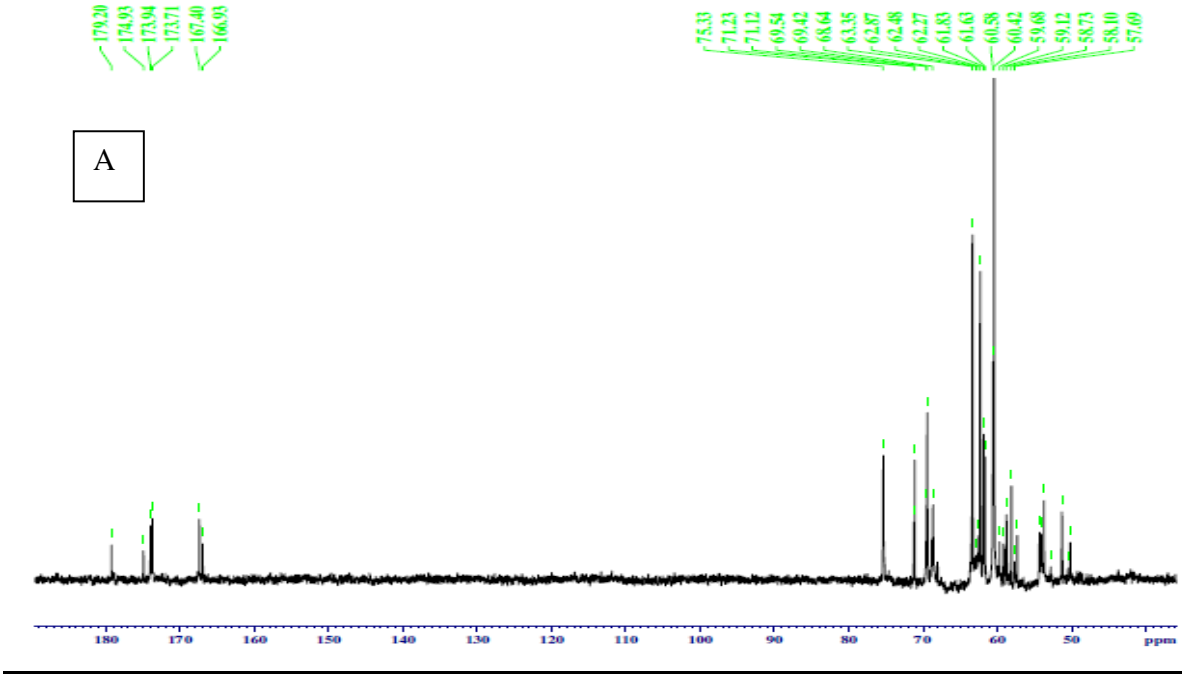

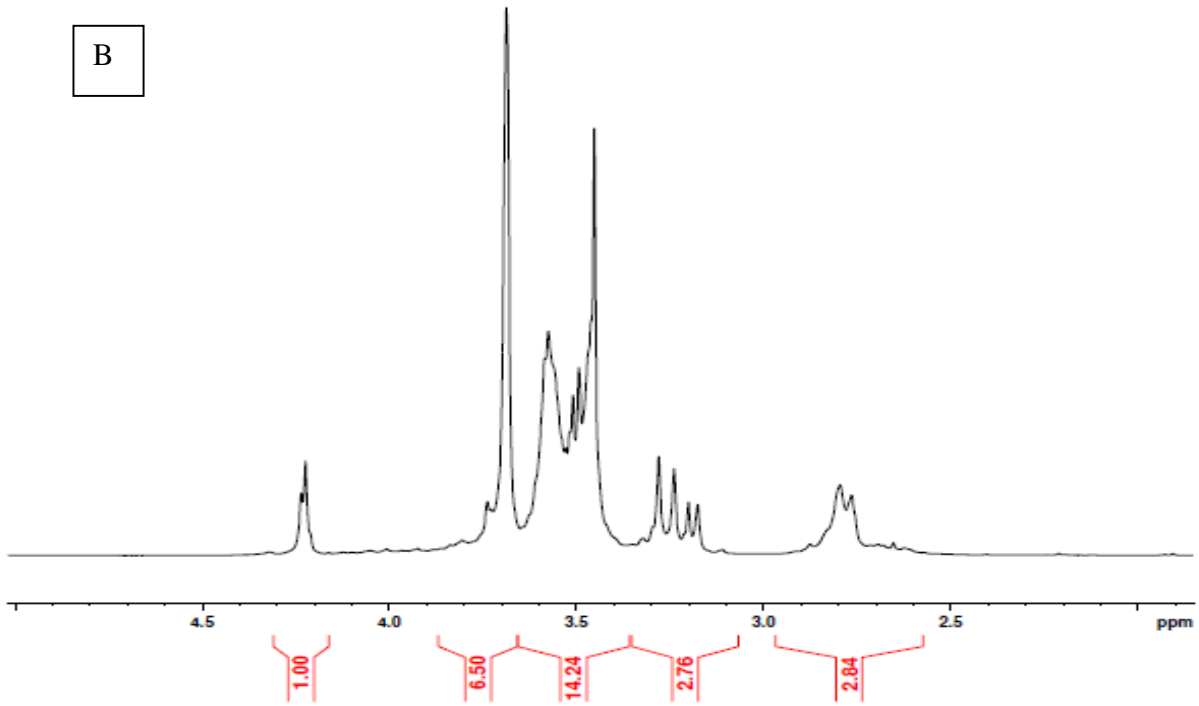

Figure 3S. a) C^{13}NMR spectra and b). H^{1}NMR spectra for the synthesized C-dots.

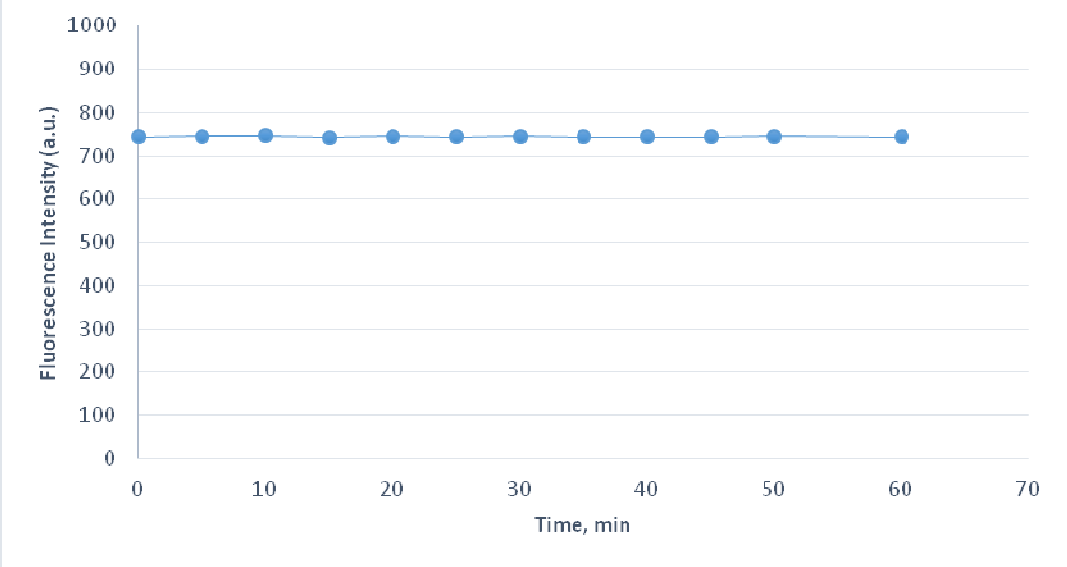

Figure 4S. Fluorescence intensity of C-dots as a function of time

Chapter 4

Fluorescent carbon nanodots for sensitive and selective detection of tannic acid in wines

IV.1. Graphical Abstract

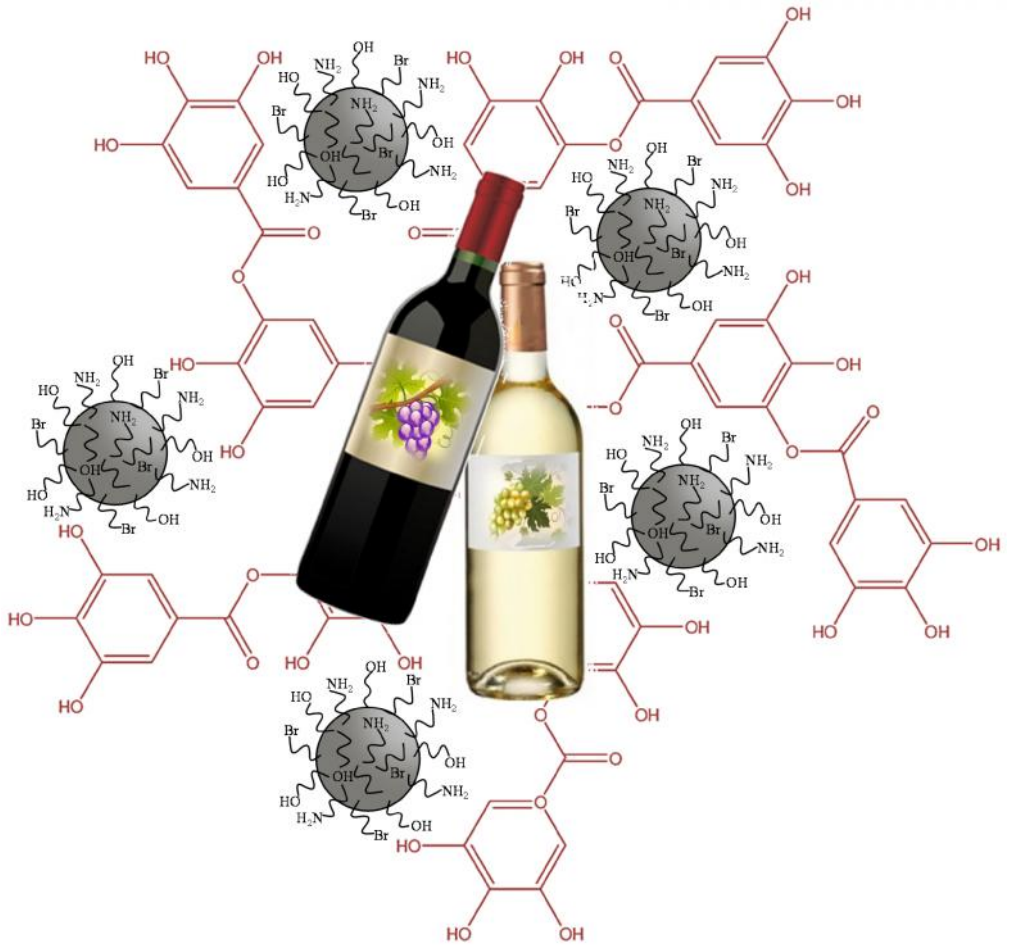

Tannic acid selectively quenched the fluorescence of carbon nanodots.

IV.2. State of the art

As indicated before, C-dots have fascinating optical properties offering a huge potential in analytical chemistry for developing new sensitive methods. Several factors could be changed, like the surface passivation, fluorescence quantum yield, and the targeted analyte. In this part we fabricated C-dots by thermal carbonization method and surface passivated fluorescent C-dots were obtained with a single reaction step. The as-synthesized C-dots showed sensitivity and selectivity towards TA (an important analyte in food science) in wine samples. Consequently, a simple, fast, robust, sensitive, and selective spectrofluorimetric method was developed and analytical application was achieved by the detection of TA in white and red wines for the first time by this approach.

FTIR, ^{1}HNMR, ^{13}CNMR, fluorescence spectra, and HRTEM techniques were utilized for the complete physico-chemical characterization of the prepared C-dots. Also, a mechanism that based on fluorescence resonance energy transfer process was suggested and explained as the main interaction mechanism between C-dots and TA.

IV.3. Historical background

IV.3.1. Quantification of TA

TA is an important analyte in nutrition chemistry as it is present naturally in most plants, fruits, and beverages, such as walnuts, tea, and wines. It is also used as a food additive as well as a component in various chemical industries, like leather manufacturing. Moreover, TA has healthy effects, for example, it was found to have a protective effect on the brain of the adult rats exposed to cadmium and lead [1]. Briefly, it is clear that development of a sensitive and selective method for TA determination is required in both food and analytical chemistry.

A flow injection analysis methods have been developed for the determination of tannic acid based on chemiluminescence [2-4]. Cui et al. [2] reported that tannic acid inhibit the chemiluminescence of the luminol-H_2O_2-Cu^{2+} system that used as the main basis of their method. Direct chemiluminescence is produced in a flow injection system when potassium permanganate merge with a solution mixture consisting of TA as analyte, quinine as sensitiser and perchloric acid [3]. Xie et al. [4] have found that TA enhanced the chemiluminescence of luminol-$K_3Fe(CN)_6$–OH^- system. On the other hand, an automatic reference flow injection analysis method based on the tannic acid reduction of phosphotungstic acid to form a blue compound was proposed [5]. In addition a novel fluorometric flow-injection analytical system was developed to determine TA depending on fluorescence quenching of 3-aminophthalate by tannin [6].

Electrochemical analysis of TA has been extensively utilized because of its oxidation reduction properties. Anodic stripping voltammetry using porous pseudo-carbon paste electrode for sensitive detection of TA was achieved [7, 8]. In like manner, silica gel modified carbon paste electrode was utilized for anodic stripping differential pulse voltammetry determination of TA [9]. Comparatively, an amperometric flow-injection assay was proposed for measuring the levels of tannin in tea. First, ferricyanide was used to pre-oxidize tannin for indirect quantification without electrode modification and then measured by a platinum electrode in an electrochemical flow cell [10]. In the nanomaterials arena, an indium tin oxide electrode modified with 4-amino-6-hydroxy-2-mercaptopyrimidine capped gold nanoparticles was prepared and used in the detection of TA by cyclic voltammetry [11].

Identically, other methods were developed for TA determination, for example, HPLC has been used to determine the hydrolysable tannins after a methanolysis step followed by oxidation with KIO_3 [12]. On the other hand, a solvent system of varying suitability was performed for thin layer chromatographic separation of simple phenolic compounds including TA [13]. Also, spectrophotometric determination of tannin was achieved in beverages based on the reduction of Cu(II) in the presence of 4,4'-dicarboxy-2,2'-biquinoline that yields a complex with maximum absorption at 558 nm [14]. Moreover, detection of TA in a batch system was performed using a fungus biosensor based on an oxygen electrode and *Aspergillus ustus* immobilized in poly(vinyl alcohol) [15].

References:

[1] Anna WM, (2013) Protective effect of tannic acid on the brain of adult rats exposed to cadmium and lead envr tox and pharm 36 : 9–18

[2] Hua C, Qiang L, Rong M, Huazhang Z, and Caixia H (1998) Flow injection analysis of tannic acid with inhibited chemiluminescent detection. Analytica Chimica Acta 362 : 151-155

[3] BGT Corominas, JVG Mateo, LL Zamora, and JM Calatayud (2002) Determination of tannic acid by direct chemiluminescence in a FIA assembly. Talanta 58 : 1243-1251

[4] Chenggen X, and Hua C (2003) Detection of tannic acid at trace level in industrial wastewaters using a highly sensitive chemiluminescence method. Water Research 37 : 233–237

[5] Liang W Online Determination of Trace Amounts of Tannic Acid in Colored Tannery Wastewaters by Automatic Reference Flow Injection Analysis. J of Aut Meth and Management in Chem, doi:10.1155/2010/920196

[6] Yueh-Tzu H, Po-Chung C, Richie LCC, and Tzong-Jih C (2010) Sequential determination of tannin and total amino acid contents in tea for taste assessment by a fluorescent flow-injection analytical system. Food Chemistry 118 : 876–881

[7] Lijian X, Nongyue H, Jingjing D, Yan D, Zhiyang L, and Ting W (2009) A detailed investigation for determination of tannic acid by anodic stripping voltammetry using porous electrochemical sensor. Analytica Chimica Acta 634 : 49–53

[8] Lijian Xu, Nongyue He, Jingjing Du, Yan Deng (2008) Determination of tannic acid by adsorptive anodic stripping voltammetry at porous pseudo-carbon paste electrode. Electrochemistry Communications 10 : 1657–1660

[9] Dai Long Vu, Bensu Ertek, Libor Cervenka, Yusuf Dilgin (2013) Determination of Tannic Acid Using Silica Gel Modified Carbon Paste Electrode. Int J Electrochem Sci 8 : 9278 – 9286

[10] Yueh-Tzu H, Po-Chung C, Richie LCC, Tzong-Jih C (2008) Determining the levels of tannin in tea by amperometry of ferricyanide pre-reaction with a sample in a flow-injection system. Sensors and Actuators B 130 : 135–140

[11] MA Raj, SB Revin, and SA John (2013) Synthesis, characterization and modification of functionalized pyrimidine stabilized gold nanoparticles on ITO electrode for the determination of tannic acid. Bioelectrochemistry 89 : 1–10

[12] Paul WH, Rebecca F, and Ann EH (2002) Determination of Hydrolyzable Tannins (Gallotannins and Ellagitannins) after Reaction with Potassium Iodate. J Agric Food Chem 50 : 1785-1790

[13] Om PS, Tej KB, and bhuhpinder S (1998) j of chrom A 822 : 167-171.

[14] Horacio DM, Patrícia D, Fábio RPR, and Nina C (2008) A multicommuted flow-system for spectrophotometric determination of tannin exploiting the Cu(I)/BCA complex formation. Microchem Journal 88 : 21–25

[15] Yi BZ, Meng LW, Shi QL, Zhi HL, Wu DZ, Yun Y, and Chang YW (1998) Microbial Sensor for Determination of Tannic Acid. Microchem Journal 60 : 201–209

Talanta 132 (2015) 252–257

Contents lists available at ScienceDirect

Talanta

journal homepage: www.elsevier.com/locate/talanta

Fluorescent carbon nanodots for sensitive and selective detection of tannic acid in wines

Gaber Hashem Gaber Ahmed [a,b], Rosana Badía Laíño [b], Josefa Angela García Calzón [b], Marta Elena Díaz García [b,*]

[a] Chemistry Department, Faculty of Science, Damanhur University, Damanhur, Egypt
[b] Department of Physical and Analytical Chemistry, Faculty of Chemistry, University of Oviedo, c/JuliánClavería, 8, Oviedo 33006, Spain

ARTICLE INFO

Article history:
Received 22 July 2014
Received in revised form
11 September 2014
Accepted 13 September 2014

Keywords:
Carbon nanodots
Tannic acid
Wines

ABSTRACT

Herein we describe an easy one step synthesis of carbon nanodots (C-dots) by thermal carbonization of 6-bromohexylboronic acid using two different amine compounds, polyethyleneglycol bis(3-aminopropyl (PEGA) and 1,2-aminopropane (DPA), at 180 °C in atmospheric oxygen. The as-synthesized C-dots were characterized by FTIR, HRTEM, NMR and fluorescence. The C-dots prepared using PEGA showed a strong emission at 440 nm with excitation at 362 nm. These C-dots exhibited analytical potential as sensing probes for tannic acid (TA) determination. pH effect, interferences, and analytical performance of the method were investigated. The method was found effective in the linear concentration range from 0.1 to 10 mg L^{-1} TA achieving a limit of detection equal 0.018 mg L^{-1} TA. The applicability of the method was demonstrated by direct measurements of TA in red and white wine samples. Validation of the method was achieved by spiking the wine samples with different standard TA concentrations obtaining recoveries in the range (90–112.5%). A probable mechanism by which TA quenched the C-dots fluorescence was proposed.

1. Introduction

Tannic acid (TA) is a natural hydrolysable polyphenol compound present in fruits and different kinds of vegetables and, along with other condensed polyphenols, can be found in several beverages including wine, beer, coffee, black tea and white tea. TA is composed of a polyol residue derived from D-glucose, which hydroxyl groups may be partially or fully substituted with galloyl units (gallotannins) [1]. It is used as a food additive (code number E-181) as clarifying agent, flavor adjunct and flavoring agent [2] as well as additive in medicinal products due to its astringent, diuretics and anti-inflammatory activities [3,4]. Moreover, TA has also applications in the tannery industry to transform animal skins to leather and for re-tanning with Cr(III) to prevent leather putrefaction [5]. As an organic pollutant associated with the tanning industry, TA has been found to be toxic to aquatic microorganisms and may form metal complexes that alter the aquatic ecosystem [6,7]. Due to its wide range of applications, analysis of tannic acid is of importance not only in food but also in the medical and environmental fields. Many analytical methods are based on the overall oxidation properties of polyphenols and, consequently, devoted to the determination of total phenolic content rather than specific determination of each component [8–12]. However, many efforts were attempted to measure TA in several kinds of food and beverage samples, as well as in industrial waters. So, a number of methods are available to quantitatively determine tannic acid content in waters, pharmaceuticals and foods, including spectrophotometry [13], electrochemical methods [14–16], luminescence [17–19] and chromatography [20,21]. Each method has its advantages and drawbacks. For example, the determination of tannic acid in wines by the traditional spectrophotometric Folin–Ciocalteu method, based on the formation of a blue phosphotungstic phosphomolybdenum complex, is simple but lacks selectivity as many other compounds in wine interfere. Chromatographic methods allow the determination of tannic acid along other polyphenols but are time consuming and expensive. Electroanalytical methods with different types of electrodes were used for TA determination, but the presence of ascorbic acid limits the use of some of these methods, or laborious sample pretreatments are needed to remove ascorbic acid before analysis [15,16]. These examples demonstrate that sensitive, selective and rapid TA detection is still a challenge.

Recent developments in analytical nanotechnology open the opportunity to develop new sensitive and selective methods for tannic acid determination. Carbon nano dots (C-dots) were found recently to be promising materials in analytical and bioanalytical

* Corresponding author.
E-mail addresses: rbadia@uniovi.es (R.B. Laíño), medg@uniovi.es (M.E.D. García).

http://dx.doi.org/10.1016/j.talanta.2014.09.028
0039-9140/

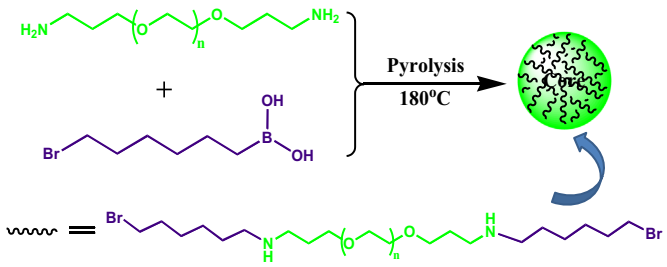

Scheme 1. Schematic representation of PEGA-C-dots synthesis .

applications, due to their unique optical properties, such as broad excitation spectra, tunable emission wavelength and stable photoluminescence [22]. Exploiting C-dots in analytical chemistry is relatively recent and most methods depend on the C-dots surface functional groups and/or their surface passivation effects. The number of analytical assays using C-dots has been increasing, but in the best of our knowledge, no work has been described for TA determination in real samples using carbon nanodots.

Herein we report a straightforward synthesis of passivated C-dots in one step via thermal carbonization method (Scheme 1), using two different amino precursors, polyethyleneglycol bis(3-aminopropyl) (PEGA) and 1,2-aminopropane (DPA). Those C-dots prepared with PEGA were found sensitive and selective fluorescent nanosensors for TA and were successfully applied to direct TA detection in real red and white wine without sample pretreatment. The synthesis reaction process as well as the mechanism for the selective sensing are also proposed.

2. Experimental

2.1. Materials

All the reagents used were highly pure analytical grade chemicals and used without further purification. The following reagents were used in this study: polyethylene glycol bis(3-aminopropyl) (PEGA), 6-bromohexylboronic acid (BrHBA), glucose, fructose, sucrose, gallic acid, citric acid, calcium chloride, and disodium hydrogen phosphate, all purchased from Sigma-Aldrich. Ascorbic acid, sodium fluoride, potassium chloride, and sodium sulfite were purchased from Merck. 1,2-diaminopropane, tartaric acid and caffeine were purchased from Fluka. NaOH, and HCl were purchased from Prolabo. TA was purchased from Hopkin & Williams chemicals (England).

2.2. Synthesis of C-dots

PEGA-C-dots and DAP-C-dots were synthesized by a thermal carbonization method, using PEGA and DAP, respectively. Typically, 1 mmol of PEGA was dissolved in about 25 mL of milli-Q water. To this solution, 0.25 mmol of BrHBA was added. The solution was then stirred and heated at 150 °C. The heating was continued until near dryness, after which 1 mL of milli-Q water was added. The process was repeated 5 times. Finally the temperature was raised to 180 °C. A yellow solution was formed and heating continued until obtaining a reddish-brown color solution to ensure the formation of the C-dots. The obtained PEGA-C-dots solution was then completed to 25 mL of milli-Q water filtered by nylon filters (0.45 μm) and purified through dialyzer tube (MWCO, 3.5 kDa) for 3 days. The purified solution was divided into two aliquots, the first one was dried completely for characterization analysis while the second was used for the analysis experiments of tannic acid. The pH of the aqueous PEGA-C-dots solution resulted to be 6.43. The same procedure was carried out to prepare DAP-C-dots using DAP instead of PEGA.

2.3. Spectrofluorimetric measurements

In a typical pH effect determination procedure, 100 μL of TA (so that the final concentration is 5 mg L^{-1}) were diluted by about 4 mL of universal buffer (in the range 3–11.5) and then 100 μL of C-dots solution was added. Finally, the solution was completed by the same buffer until a final volume of 5 mL. The fluorescence was measured immediately after the preparation in a 1-cm quartz cuvette 3 times at 440 nm with excitation at 362 nm and slit widths of excitation and emission as 20 and 10 nm, respectively. The average fluorescence data were calculated and presented as a graph. Similarly, for interference measurements, 100 μL of TA (final concentration is 5 mg L^{-1}) was mixed with the interference material (final concentration is 10 mg L^{-1}) and diluted by about 4 mL of universal buffer solution pH=9. Then, 100 μL of C-dots solution was added and finally the solution was completed to 5 mL using the same buffer solution. The subsequent fluorescence was measured as mentioned above with the same instrumental conditions.

2.4. Fluorescence quantum yield measurement

The fluorescence quantum yield was calculated through the well-established comparative method using quinine sulfate as a reference. The following equations were used in the quantum yield measurement:

$$\Phi_C = \Phi_{st}\frac{F_C}{F_{st}}\frac{A_{st}}{A_C}\frac{{n_C}^2}{{n_{st}}^2} \quad (1)$$

$$\Phi_C = \Phi_{st}\frac{G_C}{G_{st}}\frac{{n_C}^2}{{n_{st}}^2} \quad (2)$$

where ϕ is the quantum yield, F is the calculated integrated fluorescence intensity, n is the refractive index, A is the optical density (measured with a UV–Vis spectrophotometer, Perkin Elmer, Lambda 900), and G is the gradient of F vs A linear plot. The subscripts C and st refer to C-dots and the reference fluorophore, respectively. Quinine sulfate dissolved in 0.1 M H_2SO_4 (n=1.33) of quantum yield equal 0.54 at λ_{ex}=350 nm was used as a reference. C-dots were dissolved in milli-Q water (n=1.33).

2.5. Analysis of wine samples

The white wine sample (Soldepeñas, www.felixsolis.com) and red wine samples (Don Mendo, www.sanvelro.com) were used in the application experiment. The pHs of the wines were found 3.31 and 3.43, respectively. TA standards were prepared in 10% ethanol solution to avoid the effect of alcohol and sample pretreatment. Wine samples were diluted so that the alcoholic content was reduced to 10%. In a typical procedure, 100 μL of sample were spiked by 100 μL standard TA (0, 1, and 3 mg L^{-1}) followed by 4 mL buffer solution pH=9 (Na_2HPO_4 and NaOH and/or HCl) and 100 μL of the PEGA-C-dots solution. Finally, the solution was diluted to 5 mL by the same buffer. Fluorescence was measured at 440 nm with excitation at 362 nm. TA was quantified by running a calibration curve using standard solutions. All determinations were carried out in triplicate.

2.6. Instrumentation

HRTEM (JEOL JEM-2100F, 200 kV) was used to determine the size and morphology of the synthesized C-dots. A Varian 620-IR instrument was used to analyze FTIR spectra in the range 600 to 4000 cm^{-1}. ^{1}HNMR and ^{13}CNMR (NAV400 with 9.0 T magnet shielded, 600 MHz) were used for structural analysis of the synthesized C-dots in D_2O

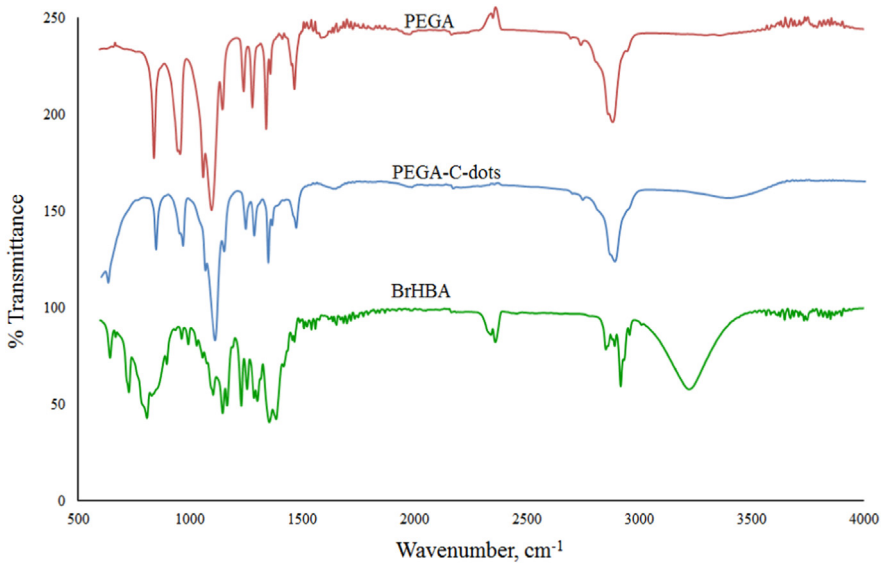

Fig. 1. FTIR spectra of PEGA-C-dots and their precursors.

solvent. Fluorescence spectra were measured using a Cary Eclipse Varian spectrofluorimeter.

3. Results and discussion

3.1. Synthesis and characterization of C-dots

The up-down strategy was used to synthesize C-dots via thermal carbonization method. It is well known that the reaction between the amine group and the alkyl halides proceeds easily and does not need extreme conditions. Higher temperatures than 180 °C were avoided in order to prevent product decomposition. According to the Scheme 1, it was expected that upon heating the long chain product formed between PEGA and BrHBA adhered to the C-dots surface. To confirm this reaction route, the same strategy of synthesis was performed using DAP, a small molecular weight amine, as precursor (Fig. S1).

3.2. FTIR analysis

Fig. 1 shows the spectra of the synthesized PEGA-C-dots and that of reaction precursors for comparison. Two characteristic peaks were identified in the synthesized PEGA-C-dots, the first at 1290 cm^{-1} ascribed to C–H wag (observed only in terminal alkyl halides) and a second at 650 cm^{-1} ascribed to C–Br stretching vibration. Similarly, the same two characteristic peaks were observed in DPA-C-dots (Fig. S2). The absence of characteristic peaks of B–O deformation at 500–550 cm^{-1}, B–O rocking at 725 cm^{-1}, B–OH deformation (at 1210 and 1305 cm^{-1}) and B–N stretching at 780 cm^{-1} in both types of C-dots suggested a pyrolytic deboronation mechanism according reaction route depicted in Scheme 1.

3.3. HRTEM and NMR analysis

The size and the morphology of the as-synthesized PEGA-C-dots and DPA-C-dots are spherical with size range 5 ± 3 nm as demonstrated by the HRTEM images (Fig. S3). Typical ^{13}C NMR spectra of PEGA-C-dots (Fig. S4) showed no signals in the range of 165 to 180 ppm corresponding to sp^2 carbons; however, signals in the range of 40 to 80 ppm revealed the presence of aliphatic sp^3 carbons [23]. On the other hand, ^{13}C NMR spectra of DAP-C-dots (Fig. S5) showed signals in the range of 165 to 170 ppm due to sp^2 carbons that could be ascribed to graphite carbons/planes and signals in the range of 40 to 80 ppm corresponding to aliphatic sp^3 carbons. The ^{1}HNMR spectra of PEGA-C-dots and DPA-C-dots are displayed in Figs. S6 and S7, respectively. Peaks in the range 3.4–3.5 ppm for RCH_2-Br and 0.5–5.0 ppm for R_2NH [23] for both types of C-dots confirmed the information obtained by FTIR.

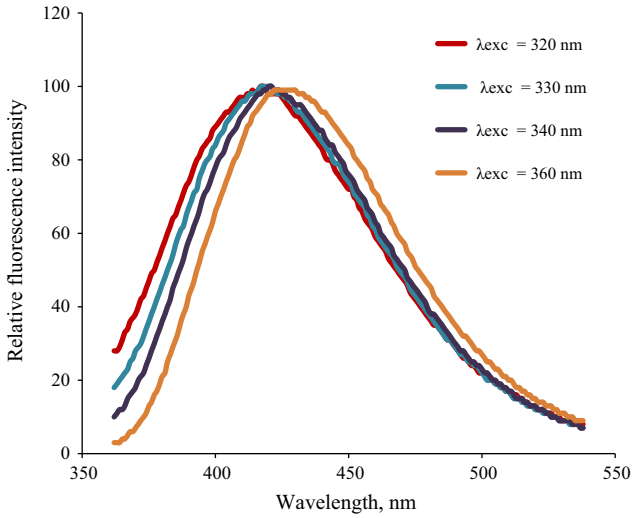

Fig. 2. PEGA-C-dots emission fluorescence as a function of excitation wavelength. (For interpretation of the references to color in this figure legend, the reader is referred to the web version of this article.)

3.4. Fluorescence features of the as-synthesized carbon nanodots

The fluorescence emission peak of PEGA-C-dots at pH 3 (0.2 M Na_2HPO_4/0.1 M citric acid) was blue shifted with the change of excitation wavelength (Fig. 2), a phenomenon frequently observed in C-dots which origin still remains unclear. Notwithstanding, it is frequently ascribed to different functional groups that create surface defects with the result of different energy levels [24]. In further experiments, excitation and emission wavelengths of 362 and 440 nm, respectively, were used. The full width at a half maximum at the different excitation wavelengths demonstrated a narrow size distribution of as-prepared PEGA-C-dots (90 ± 5 nm), thus confirming the absence of fluorescence color-dot size relationship.

On the other hand, the fluorescence quantum yield of the C-dots excited at 362 nm in milli-Q water was calculated to be 0.3%, a value similar to that found for other C-dots obtained from combustion soot of candles [25] or by using a plasma-induced method [26].

3.5. pH effect

The effect of pH is very important in this investigation, as the fluorescence of PEGA-C-dots in the absence and presence of TA is pH dependent. The influence of pH in the range 3–11.5 was investigated for TA interaction with PEGA-C-dots and results shown in Fig. 3. In the acidic pH range 3–6 a white precipitate was formed in presence of TA, particularly at concentrations of TA higher than 5 mg L^{-1}. Maximum quenching effect took place in basic media and a pH=9 was taken as the optimum value for further experimental measurements.

3.6. Analytical figures

Under the optimum experimental conditions, the sensitivity, the linear response range and the limit of detection of TA by PEGA-C-dots fluorescence quenching were determined. Calibration curve, obtained from a Stern–Volmer semilog plot, was linear within the range 0.1 to 10 mg L^{-1} TA being the calibration equation $\log(F^{\circ}/F)=0.0597\ C\ \{mg\ L^{-1}\}$, ($R^2=0.994$), where F° and F account for the fluorescence intensities of PEGA-C-dots in the absence and presence of TA, respectively and C represents the concentration of TA in mg L^{-1}. A detection limit of 0.018 mg L^{-1} TA was calculated (%RSD=0.2). As far as we know, no fluorescence methods for TA based on the use of C-dots have been described to date. From Table 1, it is apparent that the present method, exhibits high sensitivity and low detection limit when compared with some electrochemical and optical methods. Among them, that based on the TA oxidation by chitosan capped silver nanoparticles has been recently published for TA determination [27].

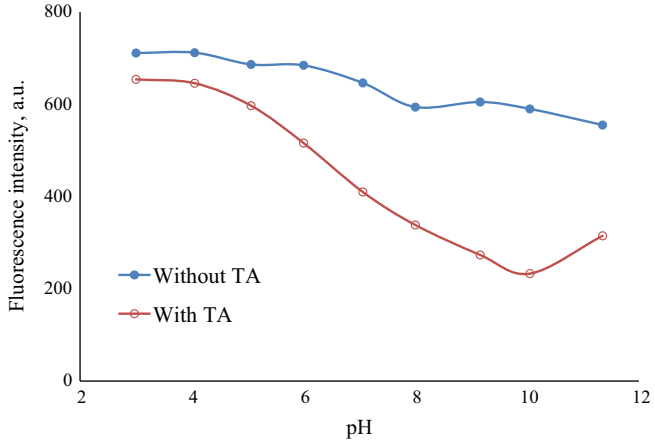

Fig. 3. pH influence on PEGA-C-dots fluorescence in absence and presence of TA (5 mg L^{-1}) at $\lambda_{ex}=362$ nm.

The effect of coexisting compounds on the PEGA-C-dots fluorescence quenching detection of 5 mg L^{-1} TA at pH 9 was investigated. The concentration of all compounds used was 10 mg L^{-1}. The tolerance limit was estimated with a ±5% relative error in fluoresence intensity. The major interference compounds chosen were ascorbic acid, sulfite, caffeine, Mg^{+2} and Ca^{+2} in addition to some abundant components in wine such as gallic acid, sucrose, glucose, fructose, tartaric acid and Na^{+}. It was found that these compounds have no significant effect on the fluorescence emission of PEGA-C-dots by TA. These analytical figures offer a high potential of sensitivity and selectivity for TA in wine samples with no need of sample treatment and it could be comparable to other analytical techniques used for TA determination in such samples.

3.7. Interaction of PEGA-C-dots with TA

The above experimental results showed that the fluorescence quenching observed on adding TA to a C-dots solution at pH=9 remained stable over a long time, indicating that a stable method could be optimized for TA. On the other hand, it was observed that gallic acid did not quench the PEGA-C-dots fluorescence. Carbon dots are known to be excellent electron acceptors and donors [28]; so, a possible mechanism for TA quenching may be attributed to an electron transfer process from the photo excited C-dots to the aromatic groups in TA. The PEGA-C-dots may be wrapped by the TA mimicking dendrimers, so allowing an effective non-radiative energy transfer process (Fig. 4).

On the contrary, in presence of gallic acid such interaction with PEGA-C-dots was not possible and fluorescence quenching did not take place.

3.8. Real sample analysis

Under the optimum experimental conditions described, TA determination in red and white wine samples was performed to validate the method. No sample pre-treatments were made but dilution with buffer. The fluorescence spectra of PEGA-C-dots without and with wine samples spiked by different concentrations (0, 1, and 3 mg L^{-1}) are illustrated in Fig. S8. Table 2 shows the results of TA obtained in wine samples after their dilution. Each result was the average of three samples. It is obvious that satisfactory recoveries were achieved for the spiked samples and results demonstrated that the method offers potential for quantitative determination of TA in wine samples.

4. Conclusions

In summary, we have been successfully synthesized passivated C-dots in an easy one step in which a deboronation process took

Table 1
Figures of merit of different analytical methods for tannic acid determination.

Method	Detection limit (μM)	Linear range (μM)	Samples	Ref.
Inhibition of luminol electrochemiluminescence	0.02	0.05 to 100	Chinese gall, hop pellet	[19]
Chemiluminescence/FIA	0.06	0.06 to 17	Pharmaceuticals, human urine, surface waters	[17]
Quenching of the 3-aminophthalate fluorescence	0.58	3 to 180	Tea beverages	[18]
Anodic stripping voltammetry	0.01	0.01 to 1	–	[14]
Colorimetric: oxidation by chitosan capped Ag nanoparticles	1	1–100	Water	[27]
Spectrophotometric	0.08	1 to 10	Ayurvedic formulation	[21]
Carbon dots fluorescence quenching	0.01	0.05 to 0.6	Wines	This method

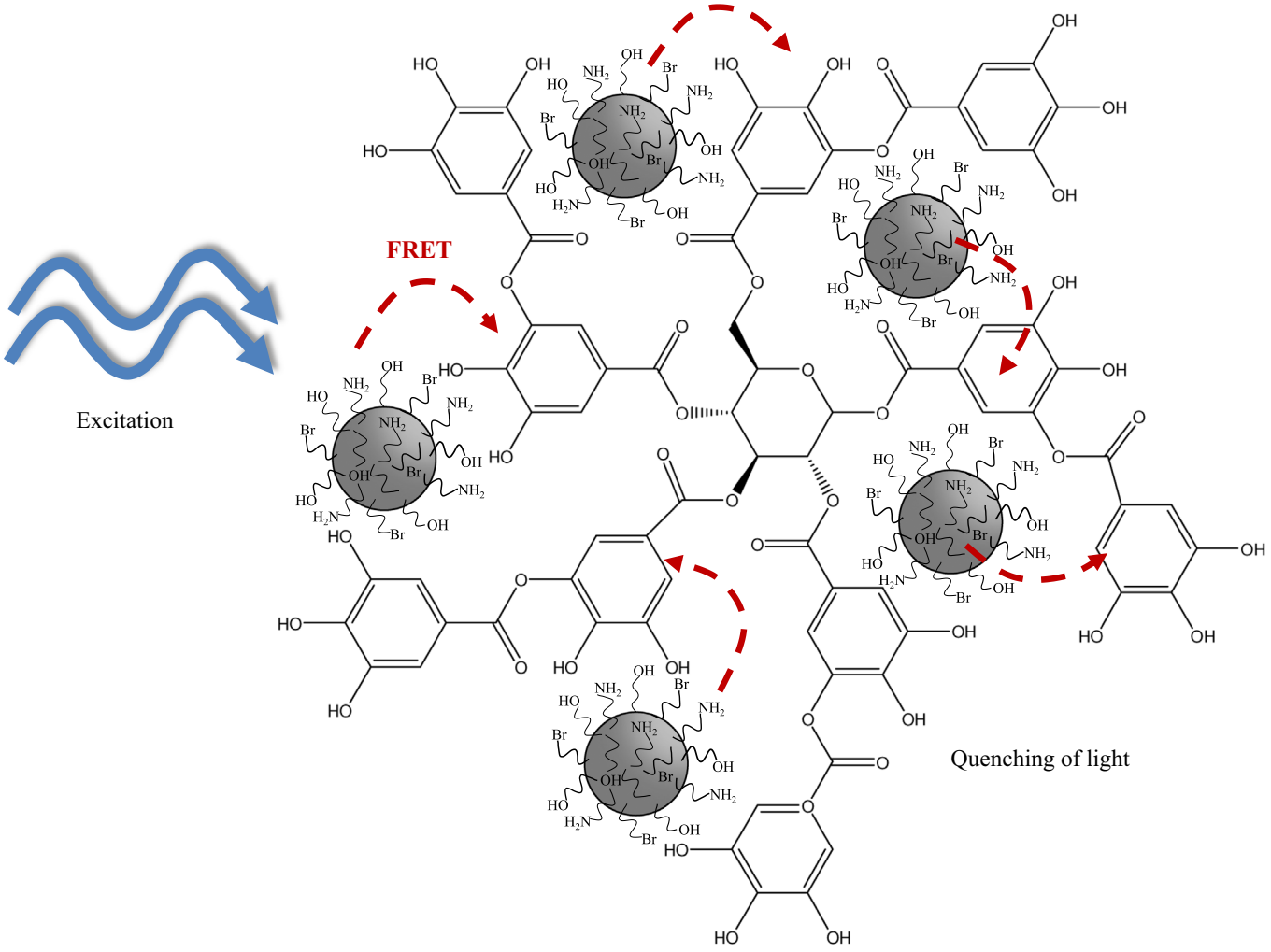

Fig. 4. PEGA-C-dots non-radiative energy transfer to tannic acid dendrimers under excitation wavelength λ_{ex}=362 nm, at pH=9.

Table 2
Results for TA determination in raw and spiked wines.

Spiked conc. (mg L^{-1})	Red wine			White wine		
	Found conc. (mg L^{-1})	% RSD	Recovery (%)	Found conc. (mg L^{-1})	% RSD	Recovery (%)
0	2.69	0.1	–	0.055	0.13	–
1	3.81	0.25	112.2	1.18	0.1	112.5
3	5.4	0.34	90.2	2.95	0.36	96.6

place. The as-synthesized PEGA-C-dots were found sensitive and selective towards TA, so that a promising fluorescence sensing system for TA detection in wines has been developed. The probe system of TA based on PEGA-C-dots fluorescence quenching showed analytical advantages such as rapid detection, high sensitivity and selectivity, wide linear response range, and low cost. A possible mechanism for TA sensing was attributed to a wrapping of the PEGA-C-dots by the TA mimicking dendrimers, so allowing an effective non-radiative energy transfer process.

Acknowledgments

Authors gratefully acknowledge financial support from the Science and Innovation Spanish Ministry (Projs # MICINN-09-CTQ2009-09595 and MAT2012-099). Also, G.H. Gaber Ahmed thanks an Erasmus Mundus Medastar grant.

Appendix A. Supporting information

Supplementary data associated with this article can be found in the online version at http://dx.doi.org/10.1016/j.talanta.2014.09.028.

References

[1] K. Khanbabaee, T. van Ree, Nat. Prod. Rep. 18 (2001) 641–649.
[2] ⟨http://www.fao.org/food/food-safety-quality/scientific-advice/jecfa/jecfa-additives/en/⟩.
[3] N. Aelenei, M.I. Popa, O. Novae, G. Lisa, L. Balaita, J. Mater. Sci.—Mater. Med. (2009), http://dx.doi.org/10.1007/s10856-008-3675-z.
[4] A. Ren, W. Zhang, H.G. Thomas, A. Barish, S. Berry, J.S. Kiel, A.P. Naren, Dig. Dis. Sci. 57 (1) (2012) 99–108.
[5] K.J. Sreeram, T. Ramasami, Resour. Conserv. Recycl. 38 (2003) 185–212.
[6] N.L. Kruthika, G.B. Raju, S. Prabhakar, J. Nanosci (2014), http://dx.doi.org/10.1155/2014/481023.
[7] K.T. Chung, G. Zhao, E. Stevens Jr., B.A. Simco, J. Aquat. Anim. Health 7 (1995) 46–49.

[8] X. Cetó, J.M. Gutiérrez, M. Gutiérrez, F. Céspedes, J. Capdevila, S. Mínguez, C. Jiménez-Jorquera, M. del Valle, Anal. Chim. Acta 732 (2012) 172–179.
[9] Q. Chen, J. Zhao, X. Huang, H. Zhang, M. Liu, Microchem. J. 83 (2006) 42–47.
[10] J. González-Rodríguez, P. Pérez-Juan, M.D. Luque de Castro, Talanta 56 (2002) 53–59.
[11] M. Šeruga, I. Novak, L. Jakobek, Food Chem. 124 (2011) 1208–1216.
[12] B. Lorrain, I. Ky, L. Pechamat, P. Teissedre, Molecules 18 (2013) 1076–1100.
[13] S.P. Gupta, G. Garg, Int. J. Pharmacogn. Phytochem. Res 6 (2014) 190–193.
[14] L. Xu, N. He, J. Du, Y. Deng, Z. Li, T. Wang, Anal. Chim. Acta 634 (2009) 49–53.
[15] D.L. Vu, B. Ertek, L. Červenka, Y. Dilgin, Int. J. Electrochem. Sci. 8 (2013) 9278–9286.
[16] H. Wan, Q. Zou, R. Yan, F. Zhao, B. Zeng, Microchim. Acta 159 (2007) 109–115.
[17] B. Gómez-Taylor Corominas, J.V. García Mateo, L. Lahuerta Zamora, J. Martínez Calatayud, Talanta 58 (2002) 1243–1251.
[18] R.L.C. Chen, C.H. Lin, C.Y. Chung, T.J. Cheng, J. Agric. Food Chem. 53 (2005) 8443–8446. http://dx.doi.org/10.1021/jf051077f.
[19] Y.G. Sun, H. Cui, Y.H. Li, H.Z. Zhao, X.Q. Lin, Anal. Lett. 33 (2000) 2281–2291.
[20] J. Zhu, J. Ng, L.J. Filippich, J. Chromatogr. 577 (1992) 77–85.
[21] S.P. Gupta, G Garg, Der Pharm. Lett. 6 (2014) 31–36.
[22] S.N. Baker, G.A. Baker, Angew. Chem. Int. Ed. 49 (2010) 6726–6744.
[23] ⟨http://www.rsc.org/learn-chemistry/wiki/Introduction_to_NMR_spectroscopy⟩.
[24] L. Tang, R. Ji, X. Cao, J. Lin, H. Jiang, X. Li, K.S. Teng, C.M. Luk, S. Zeng, J. Hao, S.P. Lau, ACS Nano 6 (2012) 5102–5110.
[25] H. Liu, T. Ye, C. Mao, Angew. Chem. Int. Ed. 46 (2007) 6473–6475.
[26] J. Wang, C.-F. Wang, S. Chen, Angew. Chem. Int. Ed. 51 (2012) 9297–9301.
[27] Z Chen, X. Zhang, H. Cao, Y. Huang, Analyst 138 (2013) 2343.
[28] Y.H. Wang, L. Bao, Z.H. Liu, D.W. Pang, Anal. Chem. 83 (2011) 8130–8137.

Electronic supplementary material

Fluorescent nano carbons for sensitive and selective detection of tannic acid in wines

Gaber Hashem Gaber Ahmed[1,2], Rosana Badía Laíño[2], Josefa Angela García Calzón[2], Marta Elena Díaz García[2*]

[1]Chemistry Department, Faculty of Science, Damanhur University, Damanhur, Egypt
[2]Department of Physical and Analytical Chemistry. Faculty of Chemistry
University of Oviedo, c/Julián Clavería, 8. Oviedo, 33006, Spain.

e-mails: rbadia@uniovi.es; medg@uniovi.es

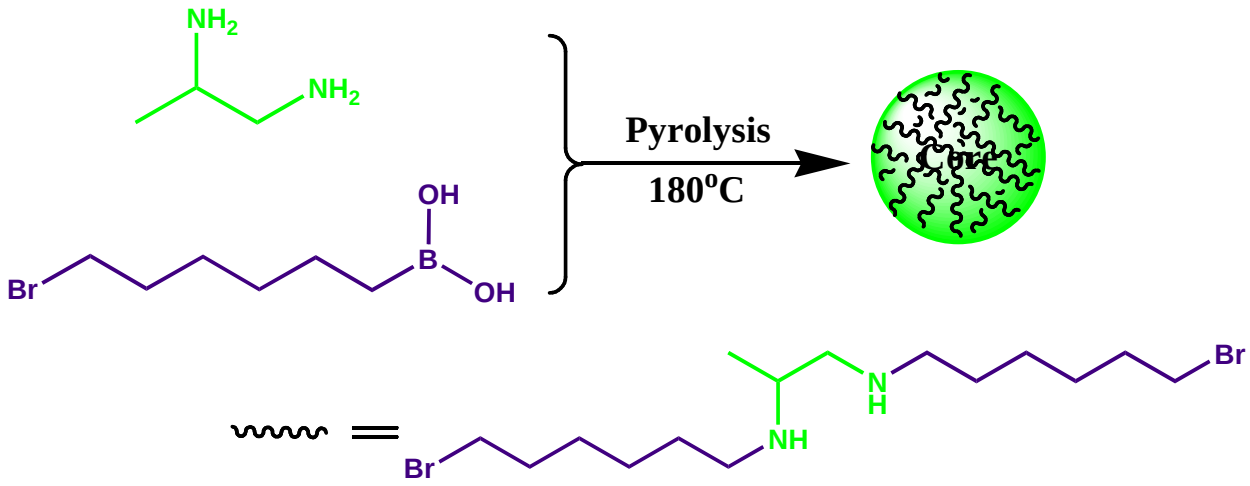

Figure S1: Schematic representation of DPA-C-dots synthesis.

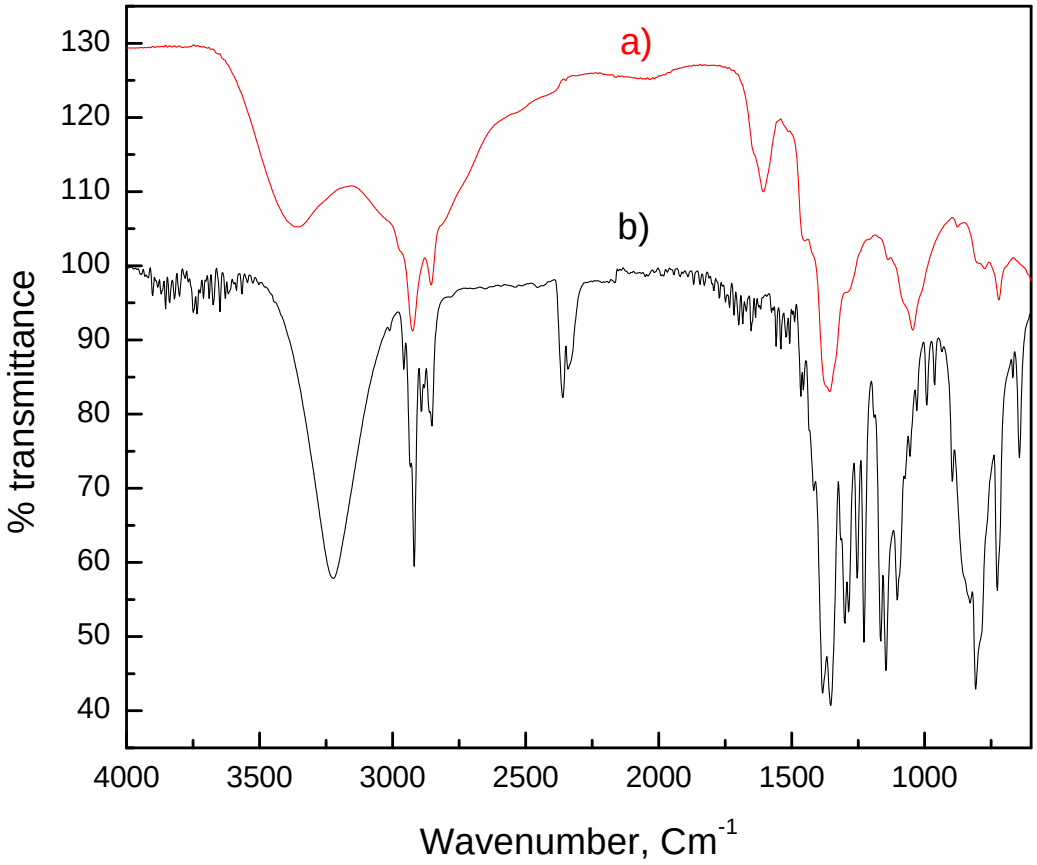

Figure S2: FTIR spectra of a) DPA-C-dots and b) 6-bromohexylboronic acid.

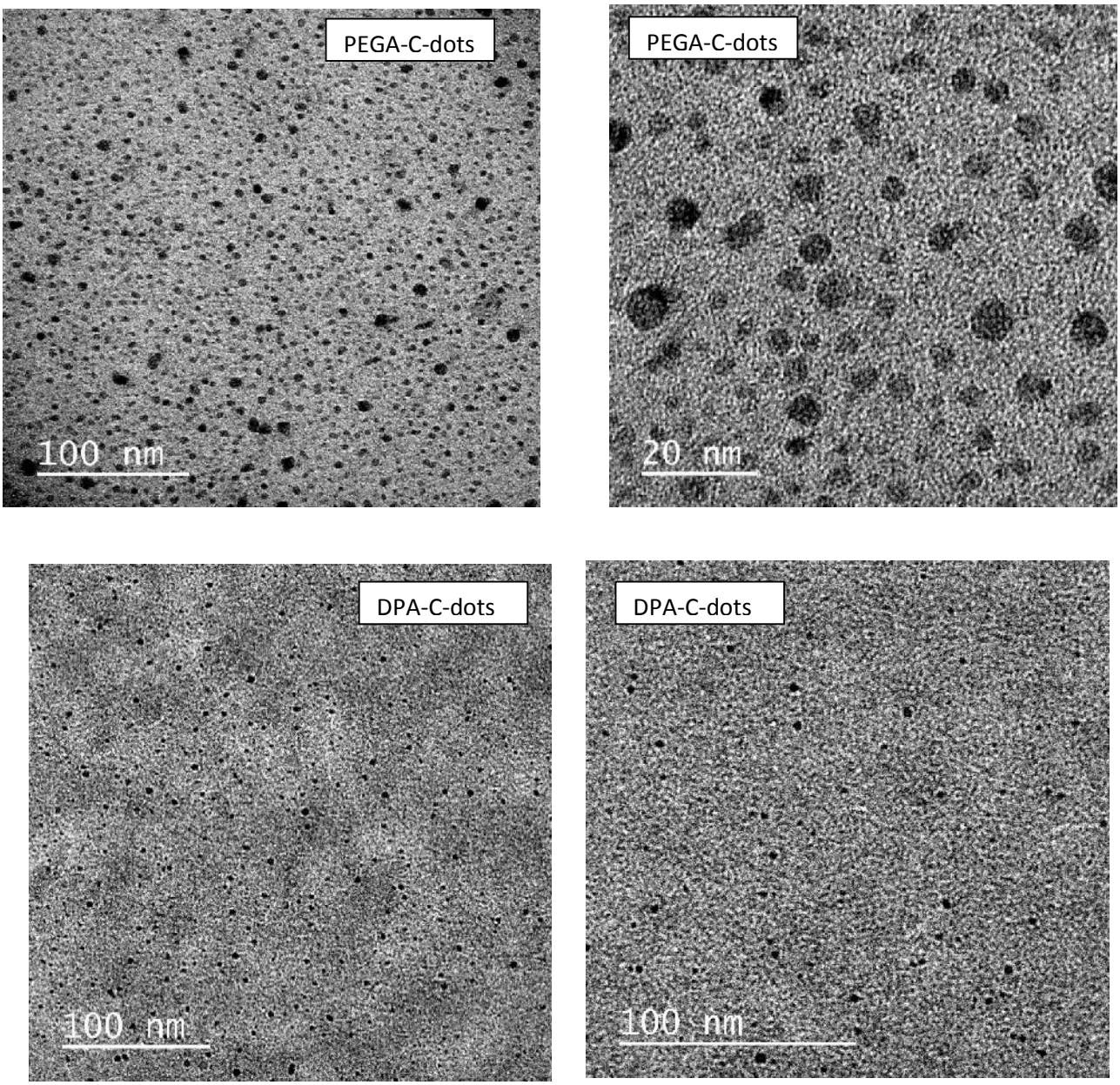

Figure S3. HR-TEM images of PEGA-C-dots and DPA-C-dots.

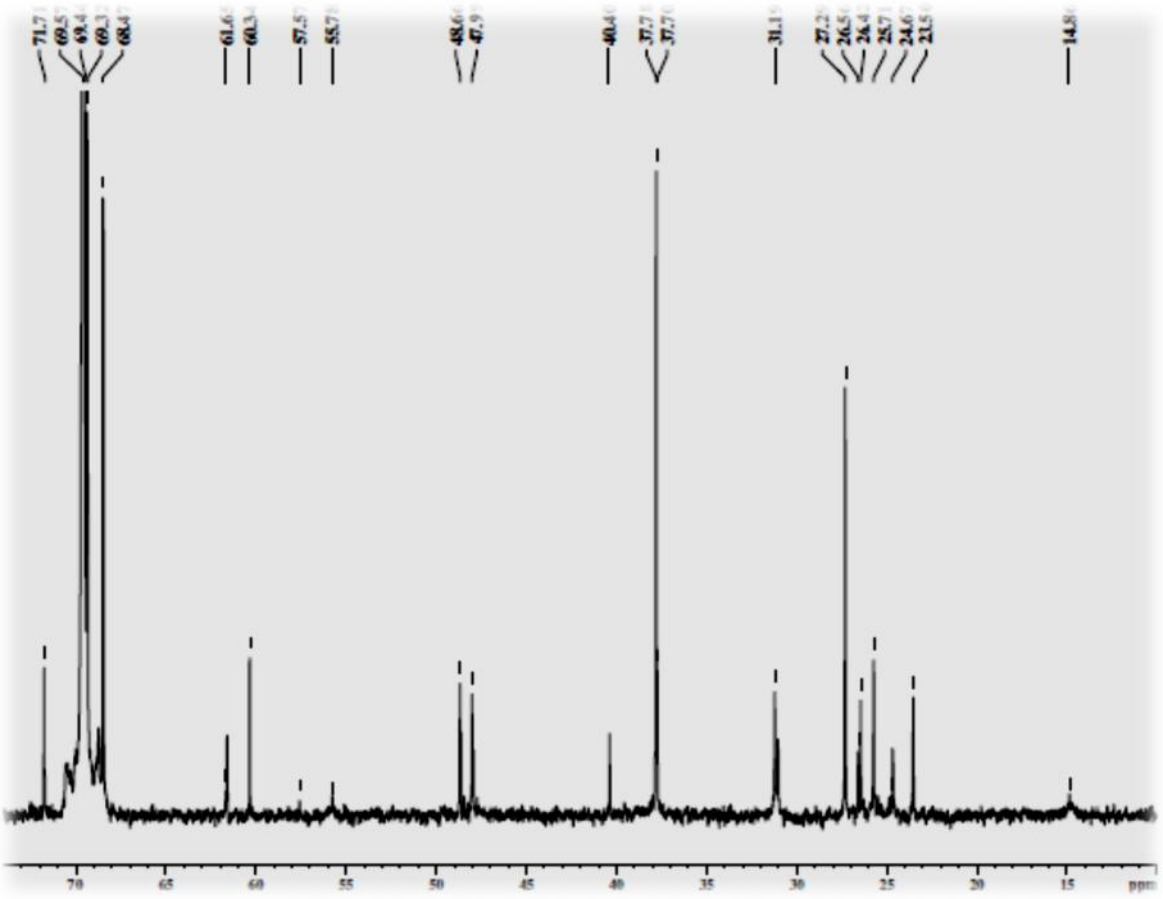

Figure S4: C13 NMR spectra of PEGA-C-dots

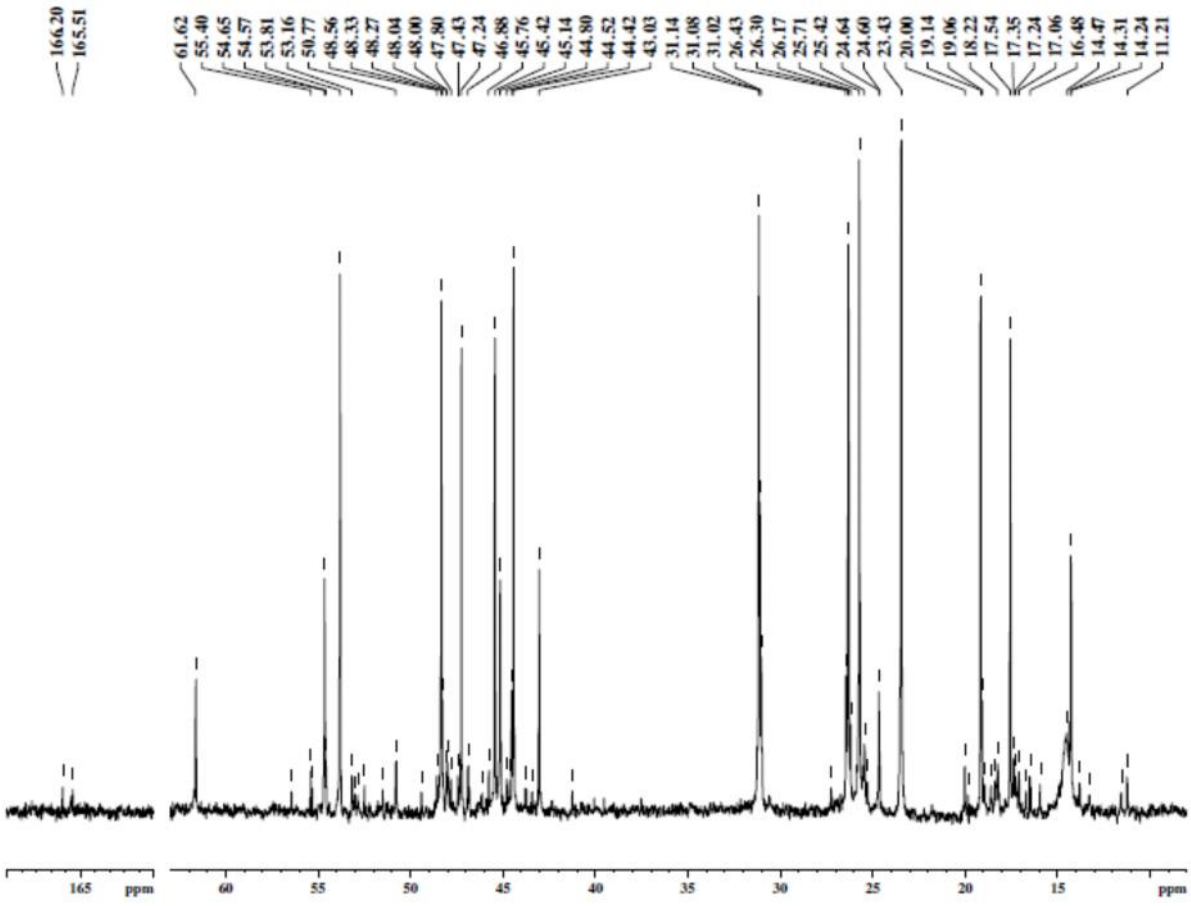

Figure S5: C13 NMR spectra of DPA-C-dots

Figure S6: 1HNMR spectra of PEGA-C-dots. Main peaks: δ = 0.63 (t), δ = 1.2-1.3 (m), δ = 1.45 (s), δ = 1.55 (t), δ = 1.85 (m), δ = 2.75-2.9 (m), δ = 3.5 (d), δ = 3.62 (s), and δ = 3.73 (s).

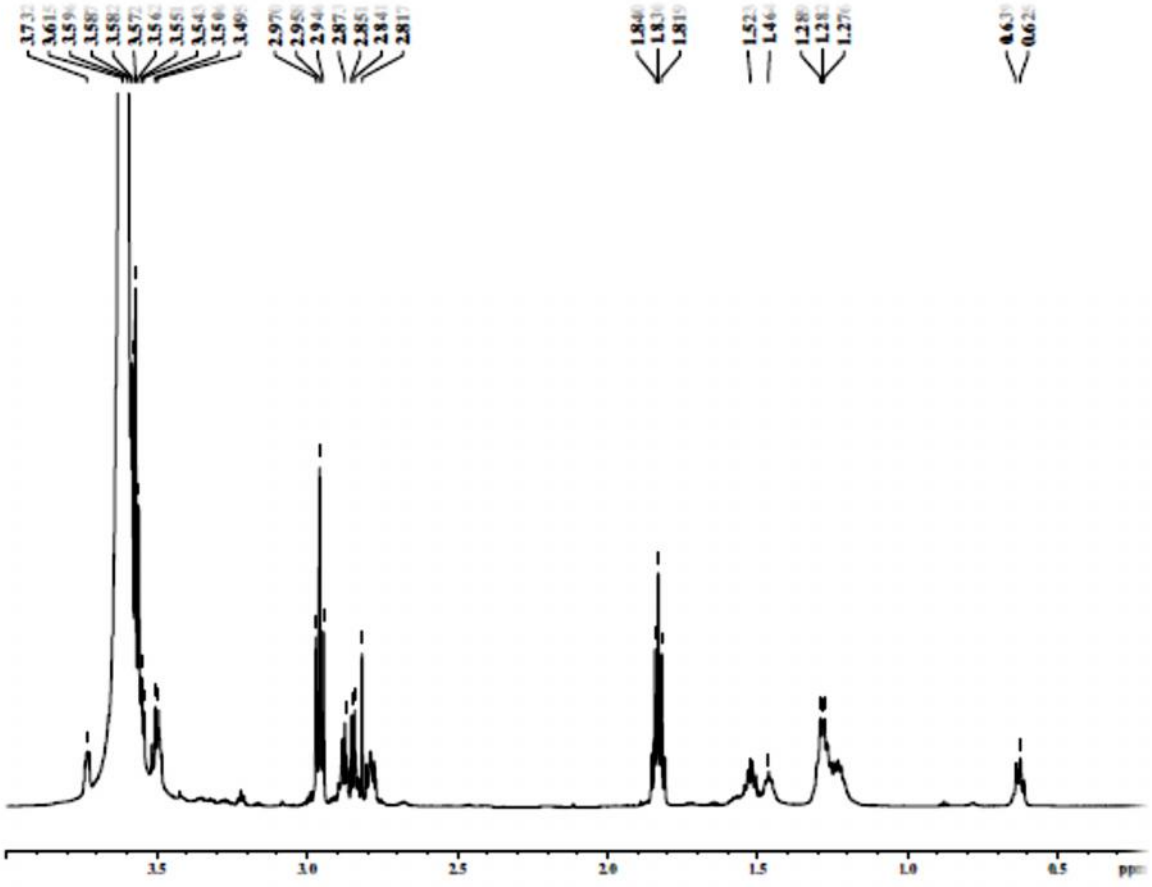

Figure S7: 1HNMR spectra of DPA-C-dots. Main peaks at δ = 0.15 (t, 3H), δ = 1.08 (m, 6H), δ = 1.21 (m, 6H), δ = 1.5 (m, 4H), δ = 2.1 (s, 2NH), δ = 2.67 (m, 4H), δ = 2.75 (m, 2H), δ = 3.12 (m, 1H), and δ = 3.5 (t, 4H).

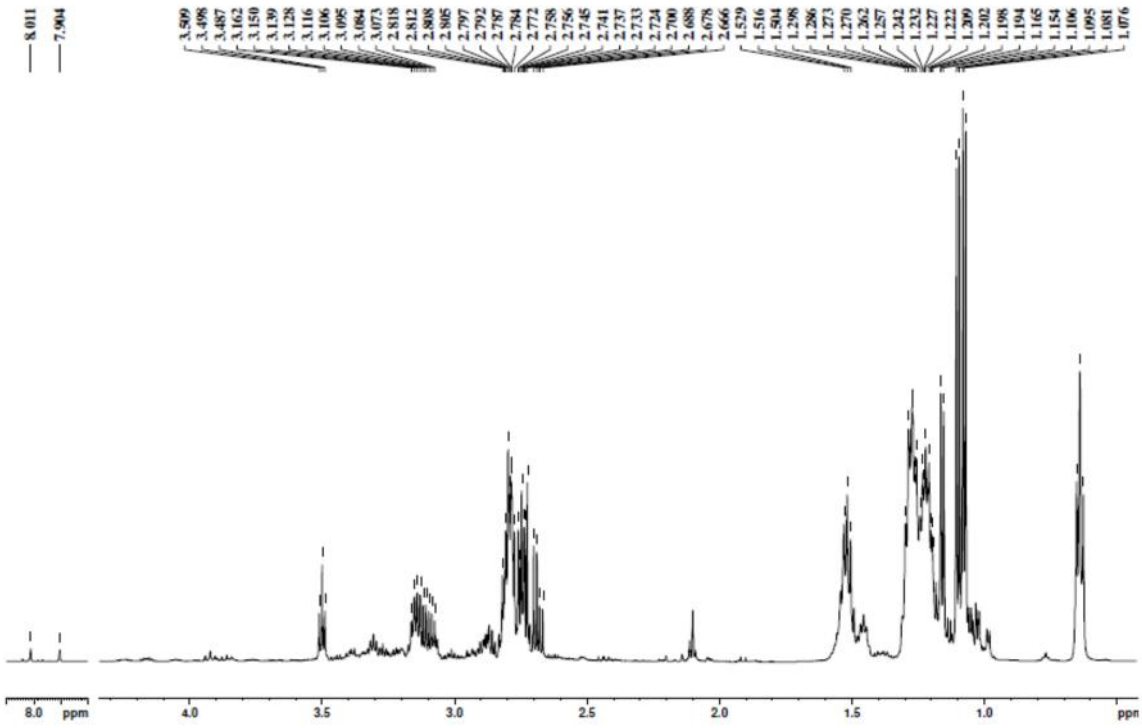

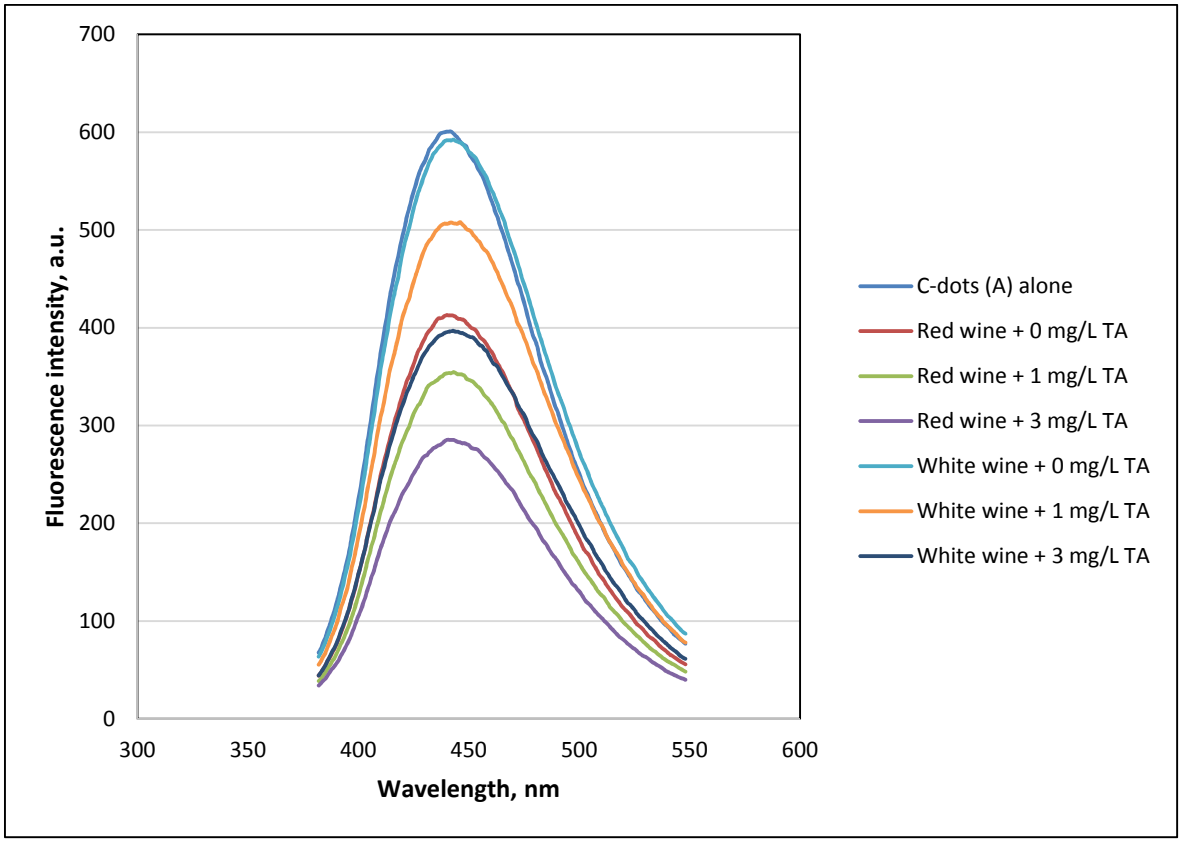

Figure S8: Fluorescence spectra of PEGA-C-dots in absence and presence of white wines spiked by different concentrations at pH=9, λ_{ex}=362 nm.

Chapter (5)

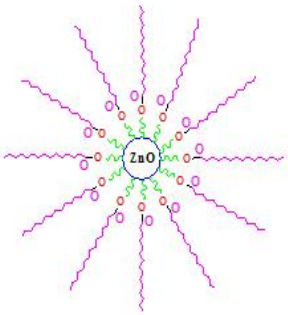

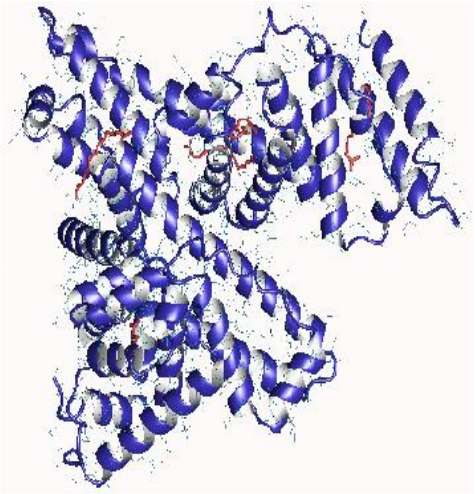

Alkyl functionalized ZnO Nanoparticles: Synthesis, Characterization and Optical Properties

Alkyl functionalized ZnO nanoparticles: Synthesis characterization and optical properties

V.1. Abstract

Synthesis of nano-ZnO and its functionalization by long organic chain via covalent bonding (ZnO-R) is described in this chapter for their further exploiting in analytical applications. XRD, FTIR, TEM, fluorescence of solid and liquid states, and phosphorescence characterization techniques were utilized for structural confirmation. XRD and TEM analyses reveal the formation of nano-ZnO and FTIR data confirm the successful functionalization with organic alkyl chains. Bare ZnO nanoparticles and ZnO-R exhibited fluorescence emission in both solid and dispersed liquid states. Also, the absorbance was determined and the band gap energy was calculated using the onset wavelength. The as-synthesized ZnO-R exhibit several advantages and can be used to improve the rheological properties of lubricants.

V.2. Introduction

Semiconductor nanoparticles (NPs) have gotten impressive considerations since few decades because of their basic arrangement, controllable size, morphological tunability, novel physical and chemical properties, simple functionalization, and more extensive applications such as solar cells, electroluminescent devices, electrochromic windows and chemical sensors [1, 2]. The metal oxides utilized within these applications are obliged to have high surface area in addition to great electrical, electrochemical and structural properties.

Among them, ZnO is a versatile material with multifunctional properties that has a wide band gap (3.3 eV) with a substantial exciton binding energy of 60 meV at room temperature [2], has high chemical stability, high electrochemical coupling coefficient, broad range of radiation absorption and high photostability [3]. It has been utilized within gas sensors, optoelectronics, photovoltaics applications, photocatalytic oxidation, sun-based cells and analytical sensing. Also, it has been included in different industries like, rubber, pharmaceutical, cosmetics, textile, electronics and electrotechnology, and other industries [1, 3]. Moreover, differing qualities of novel nanostructures of ZnO have been effectively integrated through numerous synthetic routes, for example, nanowires, nanobelts, and nanotetrapods [1].

One of the characteristic features of ZnO is its easy surface functionalization that is an important process for adapting the NPs in specific purposes. Several attempts have been made for surface modification of ZnO using different organic templates like organic acids and polymers. Different polymer-functionalized ZnO were synthesized, characterized and used in different applications. Li et al. [4, 5] have been prepared ZnO NPs modified by side-chain thiol functional poly(3-thiophenehexanethiol) and applied them for hybrid bulk heterojunction solar cells directly or after blending with poly(3-hexylthiophene). Novel bio-nanocomposites consist of poly(ester-amide) and ZnO NPs functionalized by γ-methacryloxypropyltrimethoxysilane were prepared and used as polymer matrix [6]. Geng and co-workers [7] functionalized ZnO nanorods surface with poly(1-methoxy-4-(2-ethylhexyloxy)-p- phenylenevinylene) that were directly applied for the preparation of active layer in hybrids photovoltaic devices. Grafting the thermal responsive poly(N-isopropylacrylamide) material onto ZnO NPs via surface-initiated

atom transfer radical polymerization was fabricated and exploited as a thermally responsive drug delivery system [8].

On the other hand, organic acids and other molecules were assembled on the surface of ZnO NPs or nanotetrapods. Lenz and co-workers [9] have been functionalized ZnO NPs with four different organic acids, three aromatic (benzoic, nicotinic, and trans-cinnamic acid) and one nonaromatic (formic acid). However, they didn´t apply their work, instead the characterization and theoretical quantum-chemical study have been reported. A significant enhancing of NPs solubility in nonpolar solvents, such as chloroform and toluene, has been achieved after oleyl chains were assembled on the surfaces of the ZnO nanotetrapods. The surface functionalization strategies have been extended to electroactive and photoactive molecules such as protoporphyrin and C60 on the ZnO nanotetrapods [1]. Other organic molecules such as β-cyclodextrin and organic chains composed of hydrophilic amide and urethane linkages were also attached to the surface of ZnO NPs for different applications [10, 11].

Nanoparticles are today potential lubricant additives as the offer major advantages compared to organic molecules currently used as lubricant additives, for example: their nanometre size allows them to enter the contact area easily, are often efficient at ambient temperature and no induction period is necessary to obtain interesting tribological properties [12]. Several types of nanoparticles have been used as lubricant additives: nested nanoparticles (fullerenes, onions and nanotubes) made on metal dichalcogenides or carbon, reverse overbased micelles, metallic nanoparticles and boron-based nanolubricants. The good or poor quality of lubricating oils depends on the performance of additives in lubricating oils. Nanoparticles in oil based lubricants tend to form agglomerates due to their high surface energy. Distribution of the nanoparticles in oil based nanofluids and nano lubricants plays a vital role in dictating many important constitutive properties.

In the present study we focused on the synthesis and characterization of ZnO NPs and their functionalization by long alkyl chain via covalent bonding with the aim to use them as both lubricant additive and sensing material. For the sensing material, 8-hydroxyquinoline-based compounds were used during the derivatization process. Scheme 1 shows the functionalization process with a long-chain fatty acyl halide. The structural analysis of the as-synthesized NPs were performed using XRD analysis, the surface groups and the correct functionalization using

FTIR analysis, the size and surface morphology using TEM analysis, and the optical properties using fluorescence and spectrophotometric analyses. The characterization data reveal that the synthesized materials are ZnO in the nano-scale with correct long chain organic acid surface functionalization via covalent bonding. Also, the NPs exhibited characteristic optical properties suggesting that they could be used effectively in different applications. Dispersibility studies are also outlined.

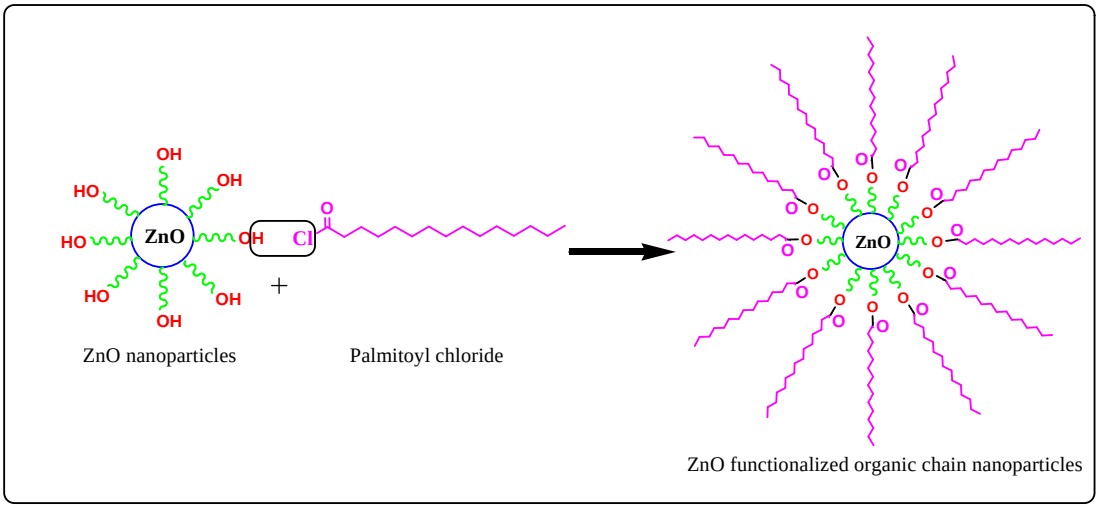

Scheme 1: Schematic representation for the functionalization of ZnO nanoparticles with a long-chain fatty acid.

V.3. Experimental

V.3.1. Materials

Highly pure reagents with high analytical grades were used in this study without further purifications. The following chemicals were used in this investigation: $Zn(Ac)_2$ purchased from Montplet & Esteban S.A. (Barcelona, http://www.montplet.es/), $ZnCl_2$, ethanol, and $NaHCO_3$ were purchased from (Merck), KOH, 8-Hydroxy-7-iodo-5-quinolinesufonic acid (Ferron), 8-hydroxy-5-quinolinesufonic acid, decanoyl chloride, palmitoyl, methylene chloride, and triethylamine were purchased from (Sigma-Aldrich), NaOH, hexane and isopropanol were purchased from (Prolabo, www.vwr.com), DMPA was purchased from (Merck) and methanol was purchased from (J.T.Baker).

V.3.2. Synthesis of bare ZnO and ZnO-ferron

Different approaches were examined in order to obtain better ZnO nanoparticles by sol-gel synthesis method. As reference material, purchased ZnO NPs were also used. $Zn(AC)_2$ as well as $ZnCl_2$ were used as precursors, and different alkali solutions were tested, such as NaOH, KOH, and $NaHCO_3$ in different solvents media like ethanol, methanol, and isopropanol. Accordingly nano-ZnO was prepared using the following methods:

Method (A): 1 mmoL of $Zn(Ac)_2$ was dissolved in 100 mL of ethanol and sonicated for 10 min, the temperature was raised to 70°C. Separately 3 mmoL of NaOH was dissolved in 50 mL ethanol by sonication and slowly added dropwise after heating to the previous solution with vigorous stirring at the same temperature. A milky solution appeared that was stirred at 70ºC for 4 h and then for 24 h at 25°C. A white precipitate was then filtered through nylon filter paper (0.45 µm) using NPs filtration system. Subsequently, ZnO NPs were washed well by ethanol, Millipore water and acetone, respectively.

Method (B): The same procedure of method (A) but dissolving both $Zn(Ac)_2$ and NaOH in 50% ethanolic aqueous solution.

Method (C): In this method, hydrothermal preparation of ZnO NPs was used. In a typical procedure, 0.11 g $Zn(Ac)_2$ were dissolved in 25 mL hot ethanol and then 25 mL ethanol containing 0.06 g NaOH was added to this solution. 30 mL of the mixture was transferred to a 30

mL-Teflon autoclave and sealed well. The autoclave was then putted in the heater at 80°C for 6 h. After the reaction the same filtration and rinsing steps as those in method (A) were followed.

Method (D): 1 mmoL of $Zn(Ac)_2$ were dissolved in ethanol at 70°C following by dropwise addition of $NaHCO_3$ solution (0.84 g dissolved in 50 mL H_2O) with vigorous stirring. The stirring was continued at this temperature for 4 h and then at 25°C for 24 h. The same filtration and rinsing steps as those in method (A) were followed.

Method (E): The same of method (C) but using $Zn(Ac)_2$ dissolved in ethanol and $NaHCO_3$ dissolved in water.

Method (F): The same of method (D) but using $ZnCl_2$ as a precursor.

Method (G): The same of method (E) but using $ZnCl_2$ as precoursor.

Method (H): The same of method (A) but we used KOH instead of NaOH.

Method (I): In this method, 1 mmoL of $Zn(Ac)_2$ was dissolved in about 150 mL methanol using a powerful sonicator. Separately, 3 mmoL of KOH were dissolved in 100 mL isopropanol by sonication. The solution of KOH was added drop by drop to $Zn(Ac)_2$ solution with vigorous stirring at 40°C. Temperature was gradually increased until 70°C during the addition step. First a white precipitate began to form, which then disappeared, probably due to the excess of either Zn^{2+} or OH^- ions in the solution. The solution stirring went on at this temperature for 2 h. ZnO NPs were obtained immediately by adding milli-Q water slowly to this solution with stirring at room temperature. The same filtration and rinsing steps as those in method (A) were followed.

With the same protocols of the previous steps and methods, ZnO NPs were synthesized in presence of 0.05 mmoL of Ferron or 8-hydroxy-5-quinolinesufonic acid, in order to introduce luminescent chelating groups into the ZnO NPs.

V.3.3. Functionalization of ZnO NPs using different acyl chloride derivatives

The reaction was carried out between 1 equivalent of ZnO (or ZnO modified with Ferron and 8-hydroxy-5-quinolinesufonic acid), the same equivalent of the acyl chloride (decanoyl chloride or palmitoyl chloride), and 1.5 equivalent of triethylamine in methylene chloride as solvent. A few amount of DMAP was used as a catalyst. Typically, 1 g ZnO (12.3 mmoL) was putted in 2-neck glass tube and evacuated for 10 min. All the subsequent steps were carried out carefully away of oxygen and always flushed by N_2 through all steps. 50 mL of methylene chloride was then mixed with the ZnO nanoparticles, after that 3.8 mL of palmitoyl chloride (12.3 mmoL) were added while the solution is stirred. 2.56 mL of triethylamine (18.44 mmoL) were then added to the reaction mixture slowly followed by adding a few amount of the catalyst. The reaction temperature was raised to 40°C in an oil path and continued for 24 h at this temperature. After turning off the reaction, the ZnO functionalized by the alkyl chain were filtered through nylon filter papers (0.45) in a special filtration system for nanoparticles. After that, the nanoparticles were washed very well by enough amounts of methylene chloride, Millipore water, ethanol, and heptane, respectively. The powder nanoparticles were ready to be used after drying in the oven at 50°C followed by grinding.

V.3.4. Instrumentation

The as-synthesized nanoparticles were characterized by transmission electron microscopy (TEM) using a MET JEOL 1011 transmission electron microscope operating at 100KV. All TEM specimens were prepared by dropping a diluted particle suspension on a copper grid and allowed to dry in air. Powder X-ray diffraction studies were performed on a Bruker D8 Discover instrument with Cu Kα radiation. FTIR spectra were measured using a Varian 620-IR spectrophotometer in the region from 600 cm^{-1} to 4000 cm^{-1} on KBr pellets. Fluorescence measurements for analytical characterization were obtained with a spectrofluorimeter of Edinburgh Instruments (model FLSP920), with 10 and 10 nm slits for excitation and emission, respectively. The excitation wavelength for bare ZnO, ZnO-Ferron (and ZnO-8-hydroxy-5-quinolinesufonic acid) and ZnO-R was set at 390 nm, 350 nm, and 360 nm, respectively. The fluorescence or photoluminescence spectra of dispersed nanoparticles in solution were measured with Varian, Cary Eclipse spectrofluorimeter in a 1-cm quartz. Spectrophotometric analysis were

performed with (UV–Vis spectrophotometer, Perkin Elmer, lambda 900) in a 1-cm quartz cuvette.

V.4. Results and discussion

V.4.1. Characterization analyses

V.4.1.1. XRD analysis

The nanocrystalline structure of bare ZnO and ZnO-Ferron was checked using XRD patterns (Fig.1, 2, and 3). A series of seven characteristic peaks at 2θ=31.8º, 34.5º, 36.36º, 47.32º, 56.7º, 62.8º, and 68.1º as well as at 2θ=66.3º and 69º related to the corresponding Miller indices (1 0 0), (0 0 2), (1 0 1), (1 0 2), (1 1 0), (1 0 3), and (1 1 2), as well as (2 0 0), and (2 0 1), respectively, were observed for all samples. These diffraction peaks are consistent well with the standard pattern of the hexagonal ZnO wurtzite structure (JCPDS no. 36–1451). Other peaks corresponding to impurities were absent meaning a highly pure samples were obtained. On the other hand, no phase change was observed for ZnO in the presence of Ferron (Figure 3). The average crystallite size could be calculated by Debye-Scherrer's equation (1), where λ is the X-ray wavelength, β the peak width of half-maximum, θ is the Bragg diffraction angle and K is a constant equal to 0.94.

$$D = \frac{K\,\lambda}{B\cos\theta}$$

From these spectra, it was clear that neither the reagent used to get the basic media nor the Zn precursor salt have influence on the lattice parameters of the ZnO nanoparticles. The same could be said for the synthesis heating procedure (conventional heating or hydrothermal) and the stirring method (conventional vs sonication). However, the XRD spectrum of particles obtained by method B showed a narrowing of the diffraction profiles with respect to the remaining materials. The broadening of XRD peaks has been attributed to a decrease in the particle size [13]. The presence of Ferron or 8-hydroxyquinoleine 5 sulfonic acid did not modify broadening of the peaks as compared with the materials prepared in their absence. In Table 1 the calculated

crystallite size using data from the more intense peak at 36.36º for all the ZnO NPs, are summarized. In the following, the ZnO NPs prepared according method (I) were used, due to their small size, less aggregation and good crystallinity.

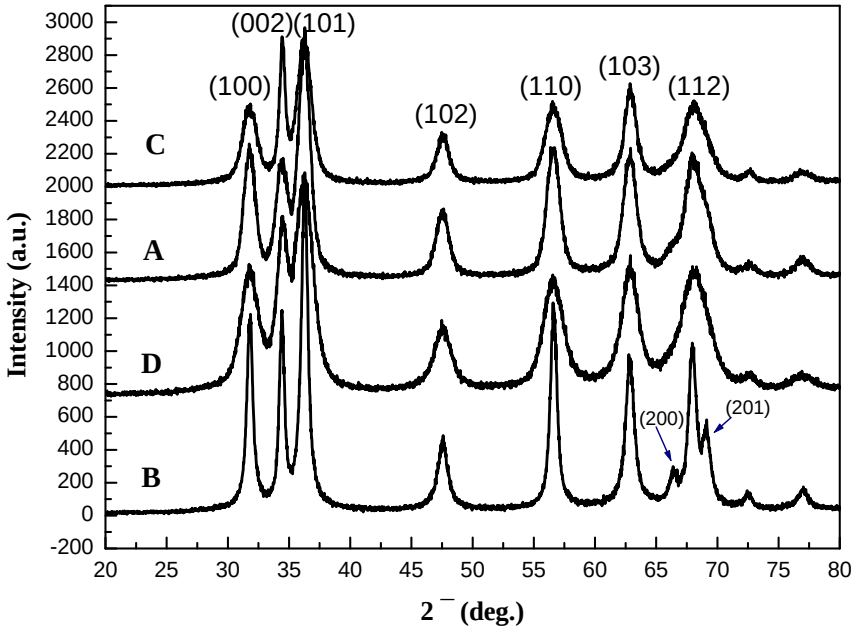

Figure 1: XRD patterns of bare ZnO NPs prepared by methods C, A, D, and B, respectively.

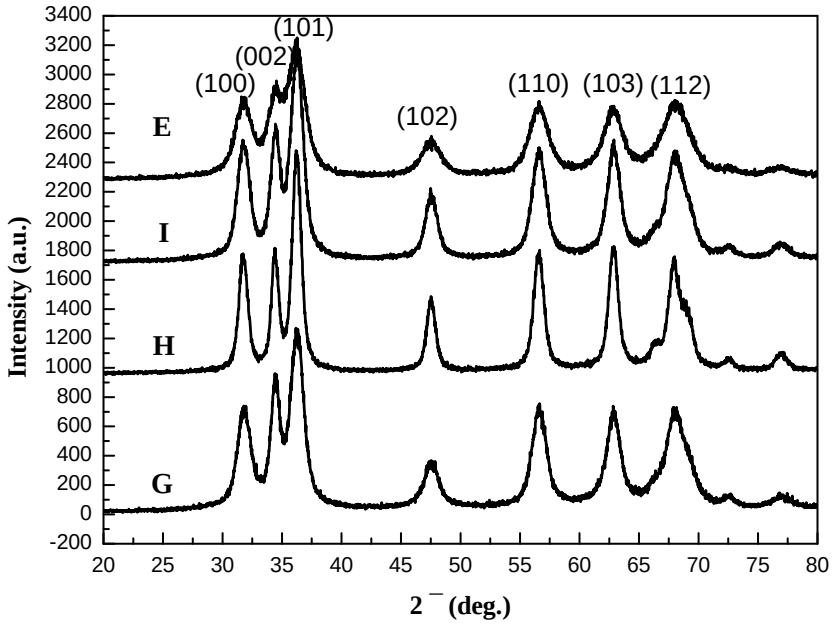

Figure 2: XRD patterns of bare ZnO NPs prepared by methods E, I, H, and G, respectively.

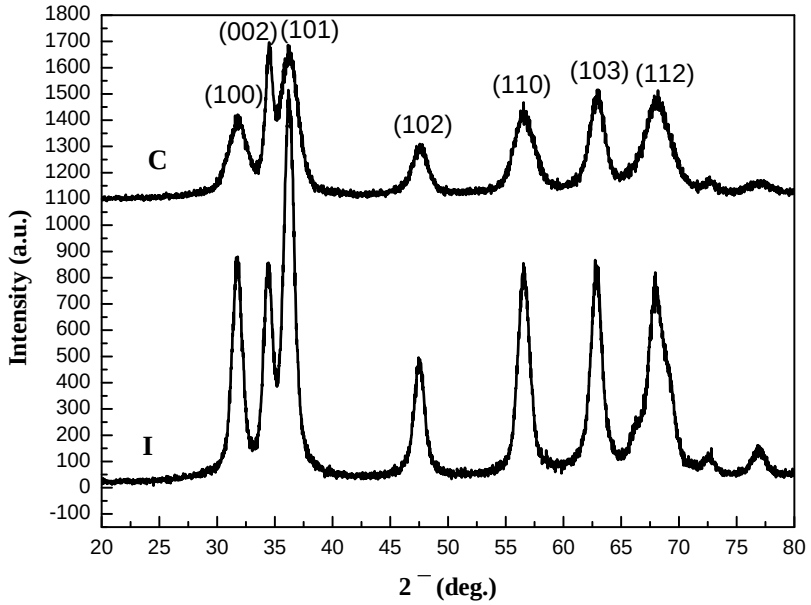

Figure 3: XRD patterns of ZnO NPs in prepared by methods C, and I, respectively in presence of Ferron.

Table 1: Calculated Crystallite size for the synthesized ZnO NPs using Debye–Scherrer formula

METHOD	CRYSTALLITE SIZE (nm)
A	13.13
B	24.18
C	11.28
D	7.58
E	6.74
G	11.99
H	16.74
I	12.49
C + Ferron	10.43
I + Ferron	14.37

V.4.1.2. FTIR analysis

The FTIR spectra of bare ZnO prepared by most methods are shown in Figure 4. The presence of peaks around 1444 and 1540 cm^{-1} corresponded to water molecules. The broad band between 3170 and 3650 cm^{-1} was ascribed to hydroxyl group stretching. In Figure 5, the FTIR spectra for ZnO-decanoyl NPs (ZnO-D) prepared according to method (I) is shown. In ZnO-D, adsorbed Ferron is the used material for decanoyl functionalization. We could observe a peak at 1560 cm^{-1} which was assigned to C=O, while peaks at 2845 and 2930 cm^{-1} were ascribed to the aliphatic organic chain stretching. The fine structure between 625 cm^{-1} and 1000 cm^{-1} was assigned to the presence of Ferron molecules. In Figure 6, FTIR spectra for ZnO-P NPs prepared according to the same method exhibited similar FTIR pattern to that of ZnO-D NPs.

These results suggested that ZnO NPs were effectively functionalized with the alkyl chains and demonstrated the presence of Ferron molecules in the material.

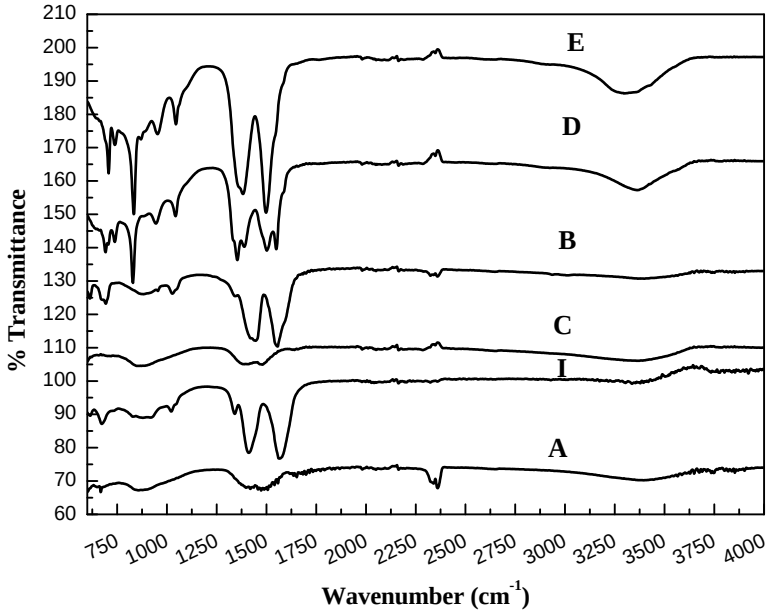

Figure 4: FTIR analysis of bare ZnO NPs prepared by methods E, D, B, C, I, and A, respectively.

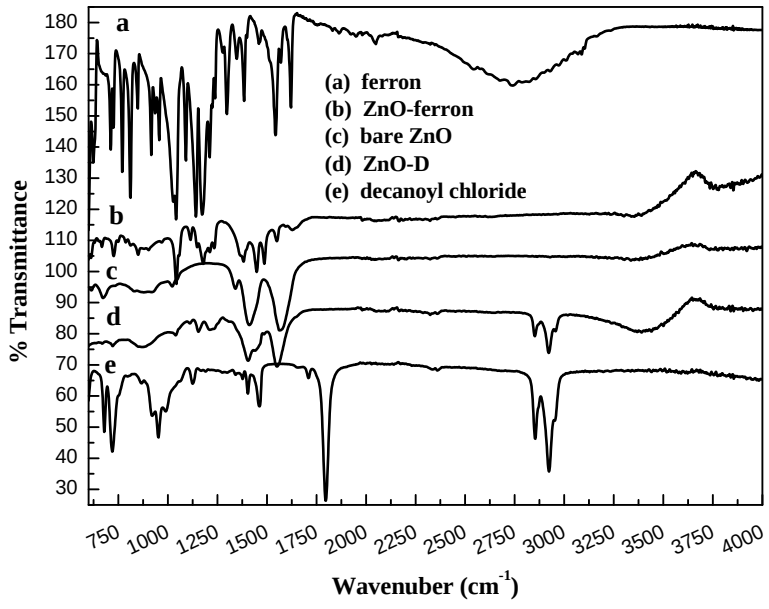

Figure 5: FTIR spectra of bare ZnO, ZnO-Ferron, and ZnO-D. In addition, Ferron and decanoyl chloride for comparison.

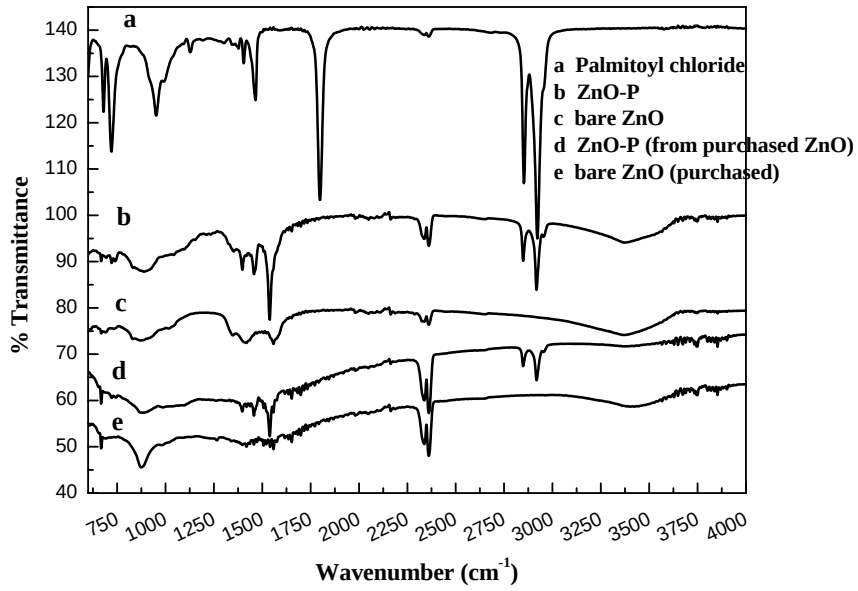

Figure 6: FTIR analysis of bare ZnO and ZnO-P, in addition to palmitoyl chloride for comparison.

V.4.1.3. TEM analysis

The size and the surface morphology of the synthesized ZnO NPs by the different synthetic routes were determined using TEM analysis (Figures 7 and 8). ZnO of size less than 20 nm was obtained by all methods. Agglomerates or aggregates are present in most cases, probably due to the absence of surface protection. In solvothermal/hydrothermal synthesis of ZnO by method (E) we could observe the formation of nanowires besides the NPs. TEM images of ZnO prepared in the presence of Ferron or 8-Hydroxy-5-quinolinesufonic acid are shown in Figure 9. No significant difference could be observed comparing with bare ZnO NPs.

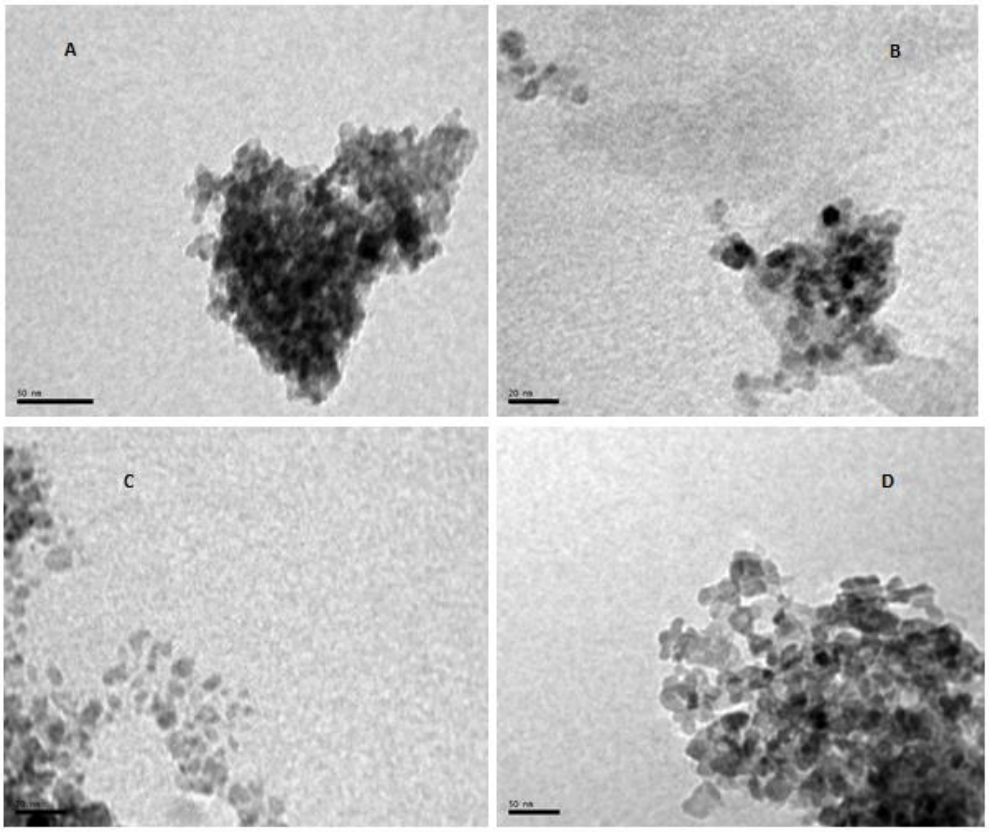

Figure 7: TEM images of ZnO prepared by methods A, B, C, and D.

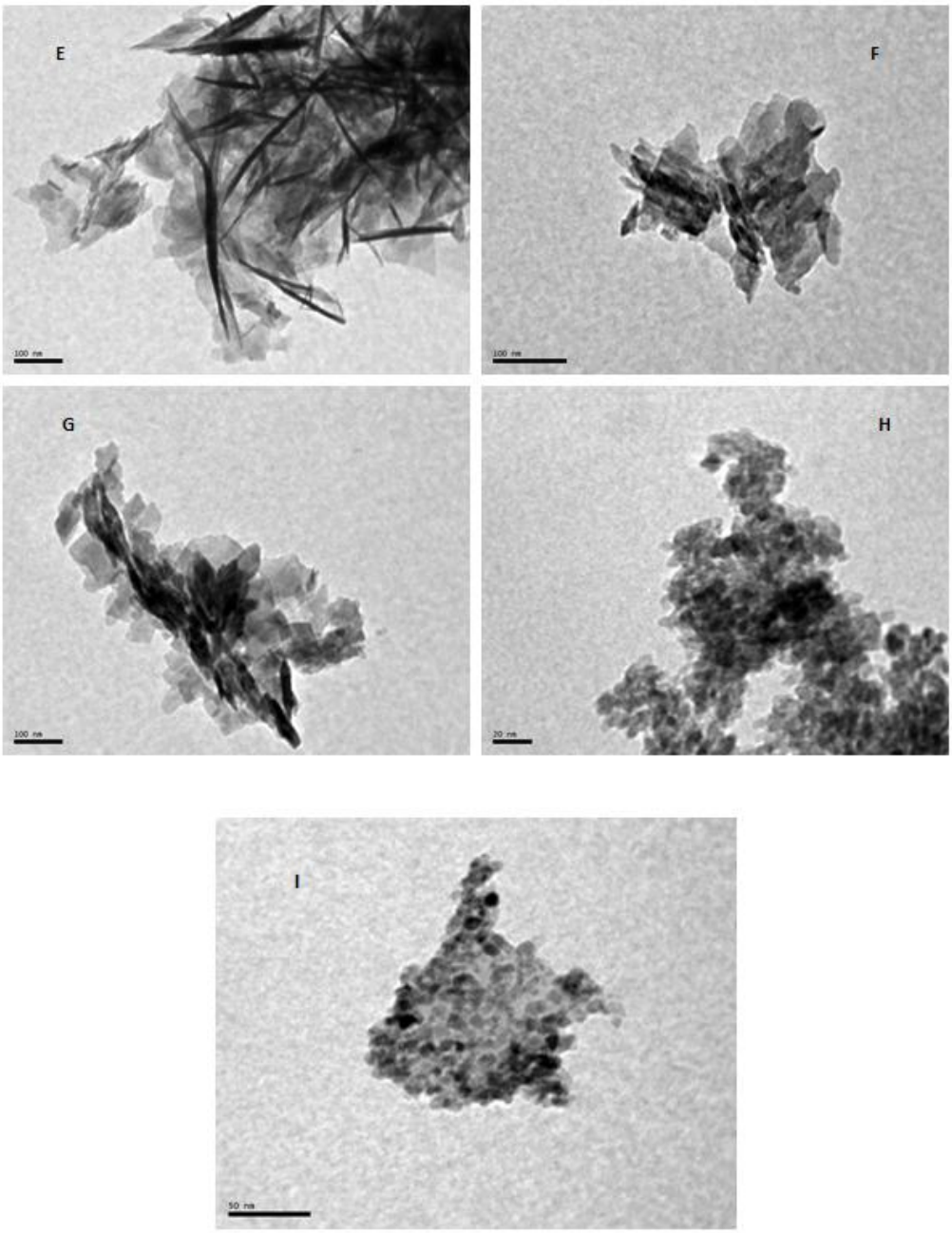

Figure 8: TEM images of bare ZnO NPs prepared by methods E, F, G, H, and I.

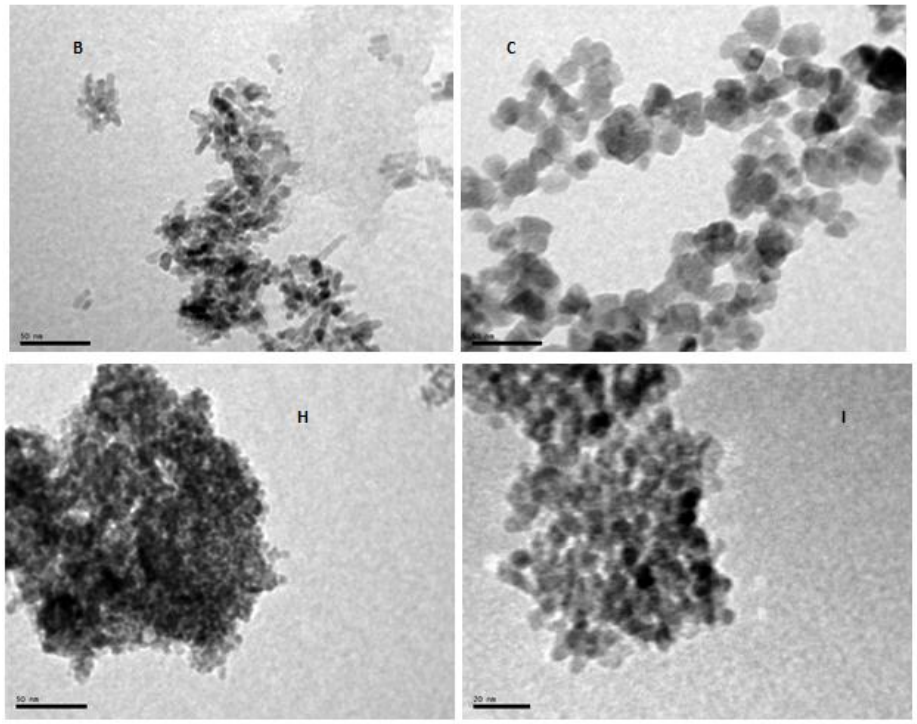

Figure 9: TEM images of ZnO NPs prepared in presence of 8-Hydroxy-5-quinolinesufonic acid (B, C, and H) or Ferron (I).

V.4.2. Optical properties

V.4.2.1. Fluorescence and phosphorescence spectra

The room temperature phosphorescence and the fluorescence in both solid state and dispersed in water were investigated for the as-synthesized NPs (Figures 10, 11 and 12). Bare ZnO NPs were found to be fluorescent and kept its fluorescence even after alkyl chain functionalization. The intensity decreased due to the presence of the long chain organic layer on the ZnO surface, which quenched the fluorescence. This could be a confirmation for the correct surface functionalization of ZnO by the organic chain in agreement with FTIR analysis.

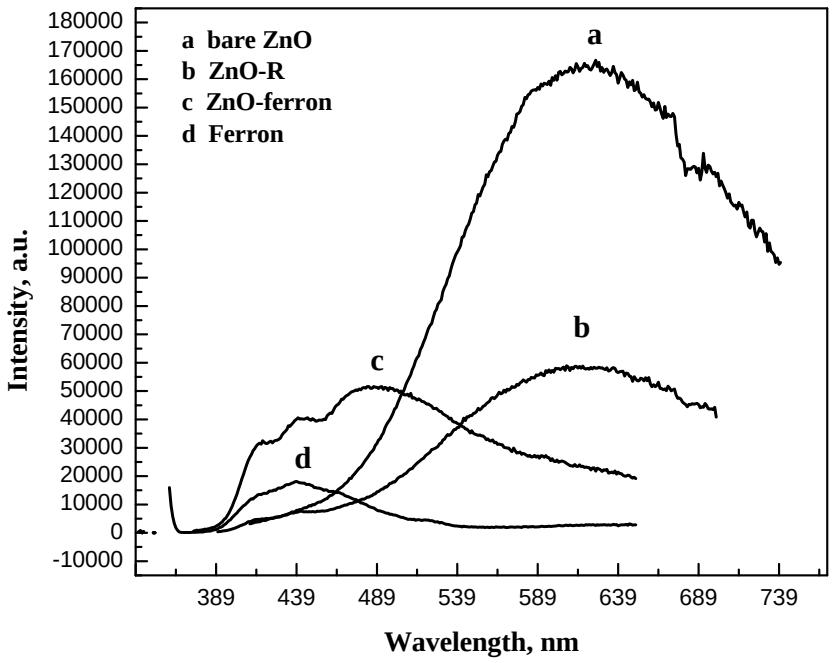

Figure 10: Solid fluorescence spectra of bare ZnO, ZnO-Ferron, Ferron, and ZnO-D. The slit width of excitation and emission are 10/10 nm, respectively. λ_{ex}= 390 nm for bare ZnO, λ_{ex}= 360 nm for ZnO-D, λ_{ex}= 350 nm for ZnO-Ferron, and λ_{ex}= 350 nm for Ferron. ZnO NPs were prepared according to method (I).

As can be seen, ZnO-Ferron exhibited a lower fluorescence intensity and a maximum emission blue-shifting when compared with raw ZnO nanoparticles. The presence of Ferron molecules inside or over the nanoparticles were deleterious for the fluorescence properties of ZnO nanoparticles. A plausible explanation for this behavior may be due to an energy transfer process from the ZnO nanoparticles to the Ferron molecules, so decreasing the ZnO fluorescence.

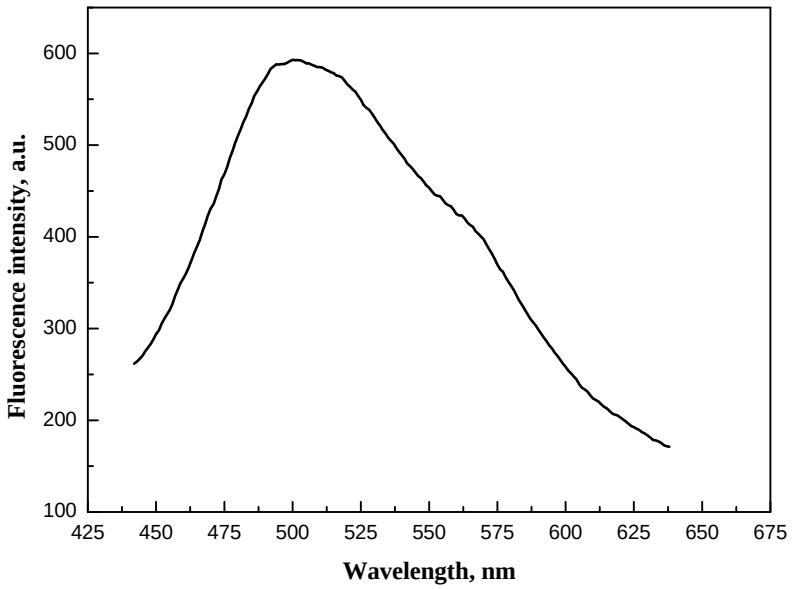

Figure 11: Fluorescence spectra of ZnO-D dispersed in water. The slit width of excitation and emission are 20/20 nm, respectively. λ_{ex}= 360 nm for ZnO-D.

On the other hand, when ZnO-D was dispersed in water, a large blue shift of the fluorescence emission maximum was also observed ($\Delta\lambda$= 140 nm). This fact may be attributable to a change of the nanoenvironment polarity around the ZnO nanoparticle surface or to a decrease in the nanoparticle size as result of hydrophobic repulsions between the oily ZnO-D surface and water molecules (see Figure 12).

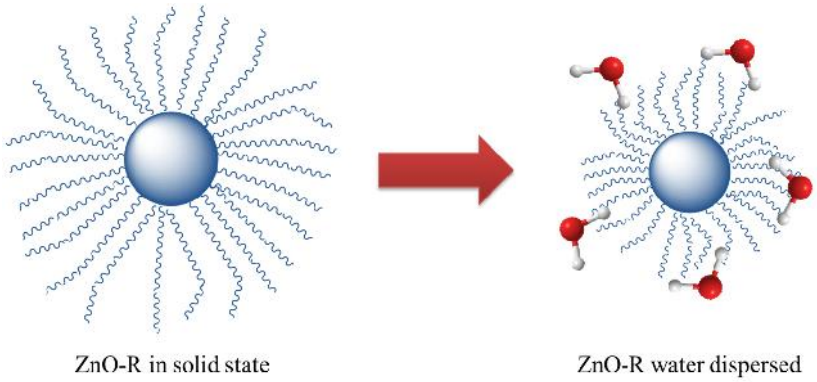

Figure 12. Changes in the nanoenvironment of ZnO-D nanoparticles

Also, ZnO-D exhibited room temperature phosphorescence in solid state as shown in Figure 13. The presence of oxygen slightly quenched the phosphorescence. This means that ZnO-D nanoparticles may act as photosensitizers producing singlet oxygen [14].

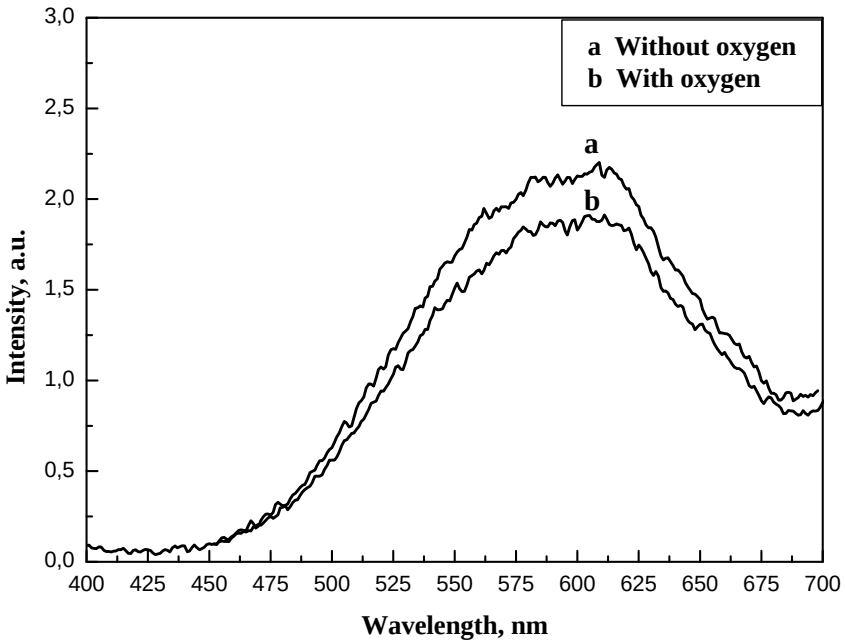

Figure 13: Phosphorescence spectra of ZnO-D dispersed in water. Decay time 0.04 s, no. of flashes is 1, delay time 0.1 ms, gate time 2 ms. The slit width of excitation and emission are 20/20 nm respectively. λ_{ex}= 360 nm.

V.4.2.2. Spectrophotometric analysis and calculation of band gap energy

The absorbance spectra of ZnO NPs prepared by method (I) before and after functionalization by the two different organic chains (palmitoyl and decanoyl) are shown in Figure 14. The bandgap energy, E_g, was calculated to be 3.33 eV using equation (2):

$$E_g = \frac{h*C}{\lambda} \qquad (2)$$

where E_g is the band gap energy in joules, h is plank´s constant and equal 6.63×10^{-34} joules s, and λ is the onset wavelength in meter (where the absorbance is minimum) and determined from

the graphical drawing of the spectrophotometric analysis, E_g is transferred into eV using the conversion factor (1 eV= 1.6×10^{-19} joules). This value is very near to the standard value which equal 3.37 eV [3]. As it can be seen, the surface modification of ZnO NPs did not affect the maximum λ_{max} and hence the band gap energy (E_g). These data reveal that the optical properties as well as electrical properties, characteristic features of ZnO NPs, not changed after the surface functionalization by the organic chain; therefore, these nanoparticles could be used by nearly the same efficiency of ZnO NPs in analytical applications.

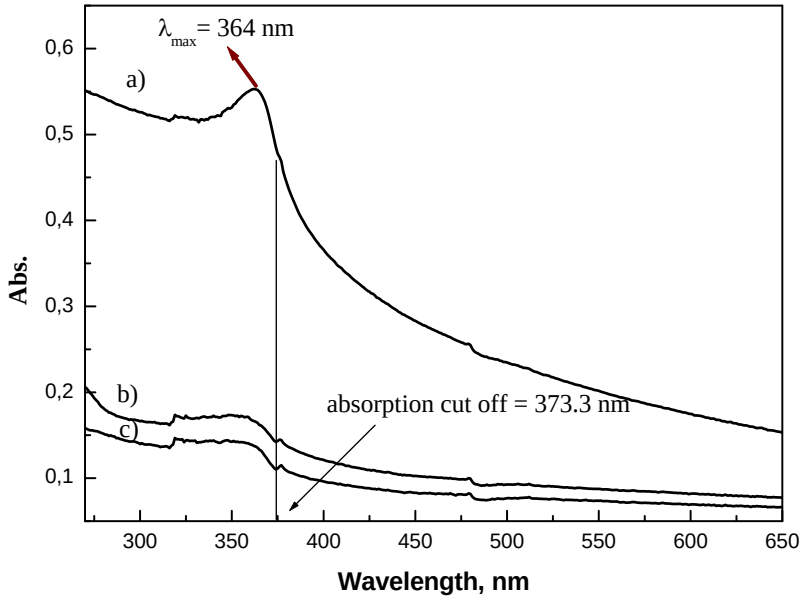

Figure 14: Absorbance of dispersed a) bare ZnO, b) ZnO-D and c) ZnO-P NPs in aqueous medium (0.005 %).

We assayed also synchronous fluorescence as a method to evaluate the band gap of the ZnO nanoparticles using spectrofluorimeter of (Edinburgh Instruments, model FLSP920). Reflectance measurements were obtained from synchronous fluorescence spectra measured at $\Delta\lambda=0$. Samples were dried well and measurements were made in solid state. Synchronous fluorescence spectra of raw ZnO, ZnO-D and ZnO-P NPs are shown in Figure 15. For the all the nanoparticles, a gradual change in the reflectance was seen in the wavelength corresponding to the band gap energy: light with lower energy photons (long wavelength) was reflected and light with higher energy photons (short wavelength) was absorbed. The photon energy at which the

transition between absorbing and non-absorbing behavior took place (absorption edge) corresponded to the band gap energy. Excellent straight line fits were observed in a narrow photon energy range. Intercepts on the wavelength axis and converting wavelength (nm) into energy (eV) band gap values of 3.369 eV, 3.306 eV and 3.402 eV were obtained for ZnO, ZnO-D and ZnO-P, respectively. These data suggested that functionalization of ZnO NPs with long alkyl chains did not change their electronic transition modes.

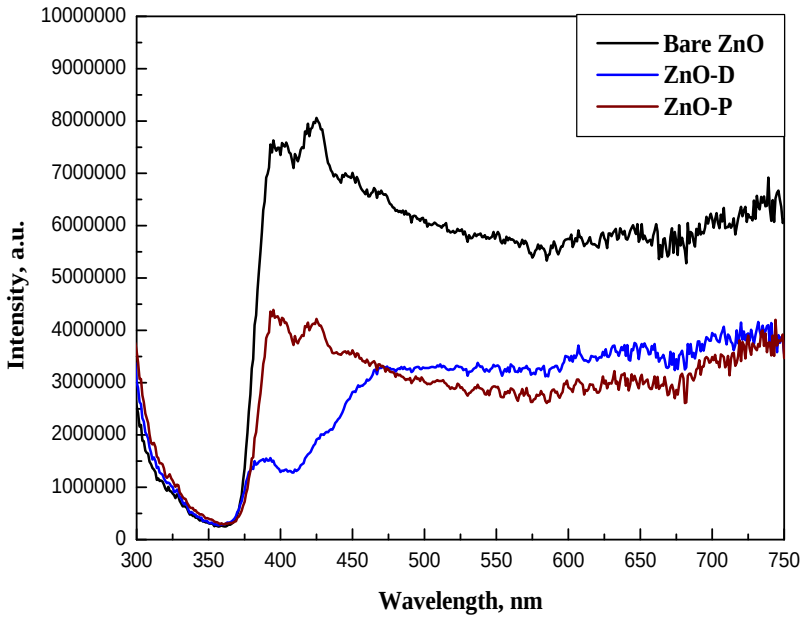

Figure 15: Synchronous fluorescence spectra of ZnO, ZnO-P and ZnO-D NPs.

V.4.3. Preliminary experiments on dispersibility of the synthesized NPs

In order NPs to be exploited in improving the rheological properties of lubricants, their stability, when dispersed in the lubricant oil, is obliged. As a result, we have tested the stability of ZnO-D NPs in lubricant oil at different times using different concentrations of NPs (Figures 16, 17, and 18). Dispersion of the solid was performed by sonication during 5 min. It was obvious that the as-synthesized ZnO-D NPs were stable after 3h of dispersion even for the higher concentration assayed. Also, it was found stable after 16 h (image not shown). These results indicate that the synthesized NPs may be utilized in improving the rheological properties of lubricants. Moreover, the stability of ZnO-D in hexane and water was also investigated (Figures

19 and 20, respectively). The NPs dispersions resulted to be stable for shorter times than in the case of the lubricant oil. These results suggested that ZnO-D NPs, could be useful for chemical sensing especially in aqueous media. In Figure 21, dispersions of ZnO-D NPs in water and hexane, after standing for 3h, are shown. Both dispersions appear cloudy, but the part highlighted by a circle in hexane bottle indicated that the velocity of ZnO-D NPs sedimentation in hexane was higher than that in water. This could be clearer in Figure 22 that shows the increased of ZnO-D NPs sedimentation in hexane with time.

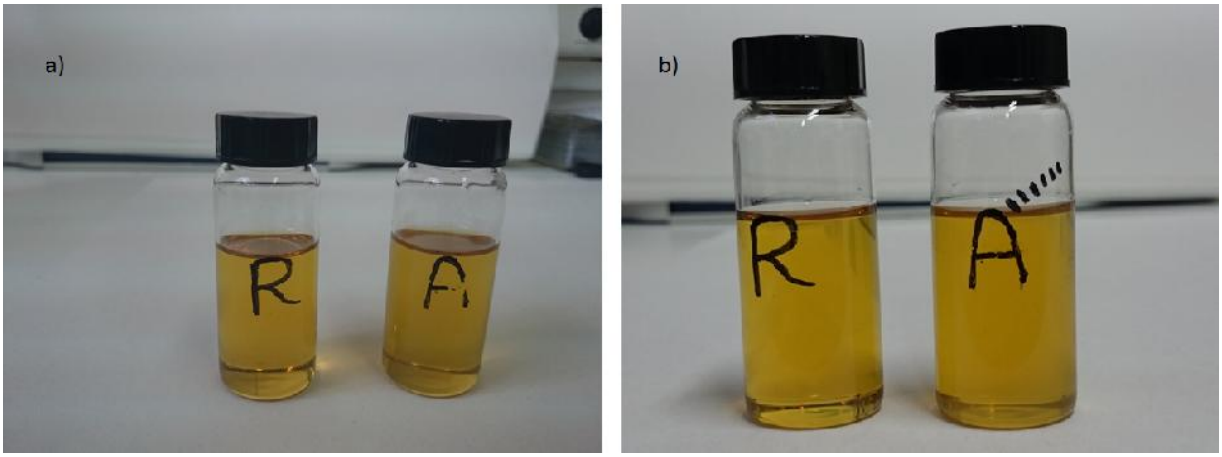

Figure 16: Images of ZnO-D NPs (0.01%) dispersed in lubricant oil a) immediately after dispersion b) after 3h of dispersion. R stands for pure lubricant oil and A for ZnO-D NPs dispersed in oil.

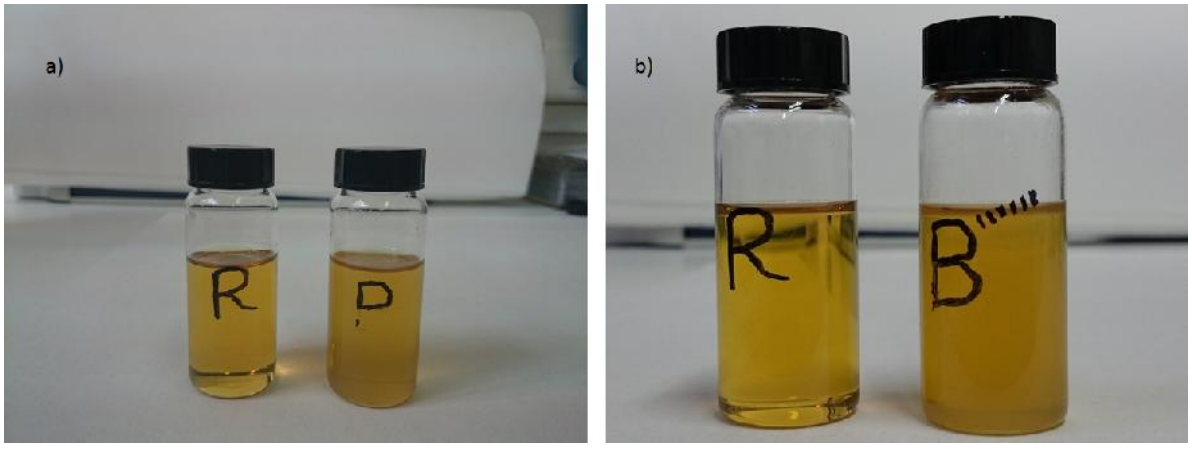

Figure 17: Images of ZnO-D NPs (0.025%) dispersed in lubricant oil a) immediately after dispersion b) after 3h of dispersion. R stands for pure lubricant oil and A for ZnO-D NPs dispersed in oil.

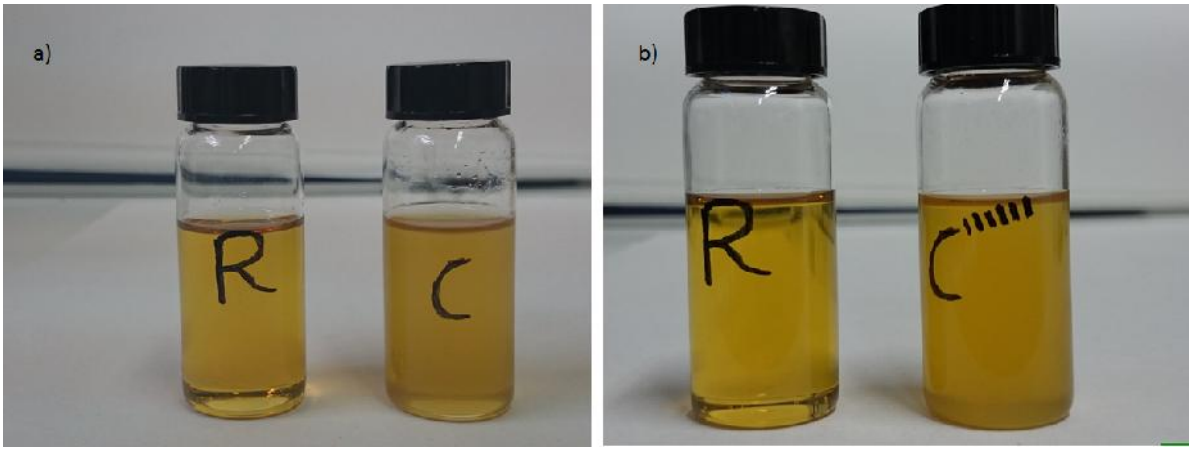

Figure 18: Images of ZnO-D NPs (0.05%) dispersed in lubricant oil a) immediately after dispersion b) after 3h of dispersion. R stands for pure lubricant oil and A for ZnO-D NPs dispersed in oil.

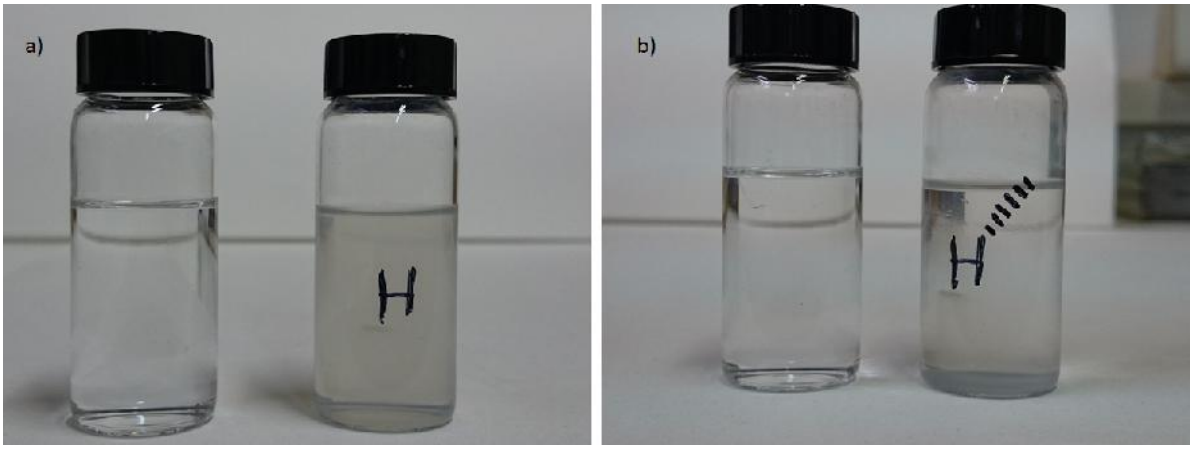

Figure 19: Images of ZnO-D NPs (0.025%) dispersed in hexane a) immediately after dispersion b) after 3h of dispersion. The left bottle of pure hexane and H stands for ZnO-D NPs dispersed in hexane.

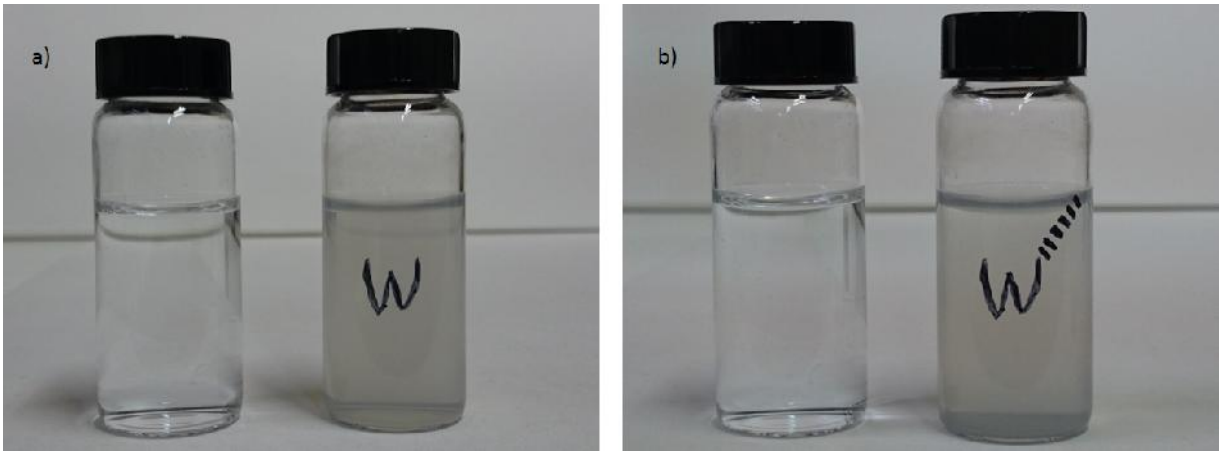

Figure 20: Images of ZnO-D NPs (0.025%) dispersed in water a) immediately after dispersion b) after 3h of dispersion. The left bottle of pure water and W stands for ZnO-D NPs dispersed in water.

Figure 21: Comparison between ZnO-D (0.025%) dispersion in water (left bottle) and in hexane (right bottle).

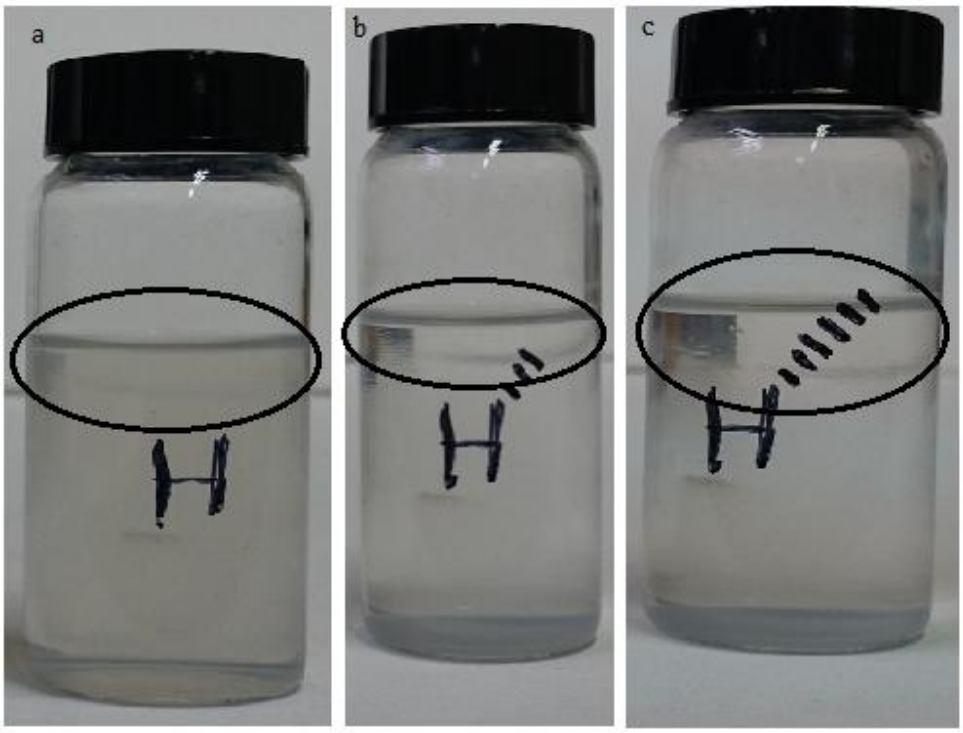

Figure 22: Dispersed ZnO-D (0.025%) in hexane after a) t=0 min. b) t=90 min. and c) t=180 min.

V.5. Conclusions

Herein we synthesized ZnO NPs by sol-gel method using different approaches. All the prepared materials are ZnO in the nanoscale as revealed by characterization analysis. ZnO NPs were functionalized correctly by different long chain organic acids (ZnO-R) via covalent bonding as indicated by FTIR analysis. The as-synthesized ZnO-R exhibit characteristic optical properties. They are fluorescent in solid state and when dispersed in solvents including water. Also, phosphorescence spectra was obtained by ZnO-R dispersed in water. The maximum absorption was observed at 364 nm by spectrophotometric analysis, and the band gap energy calculated to be 3.33 eV that is very close to the standard value for ZnO. The as-synthesized ZnO-R exhibit several advantages such as good dispersibility in lubricant oil and might be used to improve the rheological properties of lubricants, as well as good dispersibility in water, what may offer advantages for chemical sensing. Further work to develop these will be the aims of future work.

References

[1] Dongfang L, Wei W, Yongfu Q, Shihe Y, Si X, Qu-Quan W, Lu D, and Jiannong W (2008) Surface Functionalization of ZnO Nanotetrapods with Photoactive and Electroactive Organic Monolayers. Langmuir 24 : 5052-5059

[2] ZLS Seow, ASW Wong, V Thavasi, R Jose, S Ramakrishna and GW Ho (2009) Controlled synthesis and application of ZnO nanoparticles, nanorods and nanospheres in dye-sensitized solar cells. Nanotechnology 20 : 045604

[3] Agnieszka KR and Teofil J (2014) Zinc Oxide-From Synthesis to Application: A Review. Materials 7 : 2833-2881, doi:10.3390/ma7042833

[4] Fan L, Yanhui D, and Yiwang C (2012) Hybrid bulk heterojunction solar cells based on poly(3-hexylthiophene) and ZnO nanoparticles modified by side-chain functional polythiophenes. Thin Solid Films 526 : 120–126

[5] Fan, Yanhui D, Yiwang C, Lie C, Jie Z, and Peishan W (2012) Direct application of P3HT-DOPO@ZnO nanocomposites in hybrid bulk heterojunction solar cells via grafting P3HT onto ZnO nanoparticles. Solar Energy Materials & Solar Cells 97 : 64–70

[6] Amir A, Shadpour M, and Sedigheh B (2011) Preparation, characterization and surface morphology of novel optically active poly(ester-amide)/functionalized ZnO bionanocomposites via ultrasonication assisted process. Applied Surface Science 257 : 6725–6733

[7] Hongwei G, Ying G, Ruixiang P, Shikui H, and Mingtai W (2010) A facile route for preparation of conjugated polymer functionalized inorganic semiconductors and direct application in hybrid photovoltaic devices. Solar Energy Materials & Solar Cells 94 : 1293–1299

[8] Jian L, Licheng T, Weihua Z, Junchao W, and Zhiping P (2014) A novel thermal and pH responsive drug delivery system based on ZnO@PNIPAM hybrid nanoparticles. Materials Science & Engineering C, doi:10.1016/j.msec.2014.09.031

[9] Annika L, Linnéa S, Fredrik S, Arvid L, Per OH, Kajsa U, Lars O, and Per-Olov K (2009) ZnO Nanoparticles Functionalized with Organic Acids: An Experimental and Quantum-Chemical Study. J. Phys. Chem. C 113 : 17332–17341

[10] Amir A, Shadpour M, and Sedigheh B (2014) Tailored functionalization of ZnO nanoparticle via reactivecyclodextrin and its bionanocomposite synthesis. Carbohydrate Polymers 103 : 32– 37

[11] Moriyuki S, Hajime H, Shigekazu M, Yasuhisa F, Shunsuke S, Takeshi U, and Morihiko N (2010) Preparation, characterization and properties of novel covalently surfacefunctionalized zinc oxide nanoparticles. Applied Surface Science 256 : 4497‑4501

[12] Jean MM and Nobuo O (2008) Nanolubricants 2nd ed. John Wiley&Sons Ltd, UK.

[13] Klaus DS (2011) Handbook of Nanophysics. Nanoparticles and Quantum dots. CRC Press. Taylor&Francis Group. Boca Raton, Florida.

[14] S Wang, R Gao, F Zhou, and M Selke (2004) Nanomaterials and singlet oxygen photosensitizers: potential applications in photodynamic therapy. J Mat Chem 14 : 487-493

Chapter (6)

Conclusions

Conclusions

β-CD functionalized superparamagnetic nanoparticles

1. β-CD functionalized superparamagnetic magnetite nanoparticles (11±2 nm) through layer-by-layer method were successfully synthetized and characterized by different analytical tools.
2. β-CD functional magnetic nanoparticles were used as effective solid phase extraction material for 5- HIAA determination in synthetic urine samples
3. The procedure developed procedure for 5-HIAA extraction from synthetic urine samples offers several advantages: quick, inexpensive, robust, very sensitive and selective.
4. The method needs only a magnet and can be performed in any laboratory without the requirement of sophisticated instruments.

Highly fluorescent carbon dots for determination of 4-nitrophenol in surface waters

1. Highly fluorescent C-dots were prepared by thermal carbonization
2. C-dots fluorescence was selectively quenched by 4-nitrophenol
3. C-dots acted as sensitive and selective nanoprobes for 4-nitrophenol determination
4. No interference from common species present river and sea waters was observed
5. 4-nitrophenol analysis in surface waters was performed with no need of sample pre-treatment

Fluorescent carbon nanodots for tannic acid determination in wines

1. Fluorescent C-dots were prepared by thermal carbonization
2. C-dots fluorescence was selectively quenched by tannic acid
3. C-dots acted as sensitive and selective nanoprobes for tannic acid determination
4. No interference from common species present in wines was observed
5. Tannic acid analysis in wines was performed with no need of sample pre-treatment

Alkyl functionalized ZnO NPs synthesis and optical properties

6. Alkyl functionalized ZnO NPs were synthesized and characterized
7. The as-synthesized NPs exhibit characteristic optical properties
8. A very good dispersibility of the synthesized ZnO-R in lubricant oil was observed indicating the possibility of their utilization for improving the rheological properties of oils
9. The obtained good dispersibility of NPs in water suggests their utilization in chemical sensing

Conclusiones

Nanopartículas magnéticas funcionalizadas con β-CD

1. Se sintetizaron con éxito nanopartículas de magnetita superparamagneticas (11±2 nm) funcionalizadas con β-CD por el método capa a capa y se caracterizaron utilizando diferentes técnicas analíticas
2. Las nanoapartículas magnéticas funcionalizadas con β-CD se utilizaron como un material efectivo para la extracción en fase sólida de %-HIAA y su determinación en muestras sintéticas de orina.
3. El procedimiento desarrollado para la extracción de 5-HIAA de muestras sintéticas de orina ofrece varias ventajas: rapidez, economía, robustez, elevada sensibilidad y selectividad.
4. En el método se precisa únicamente un imán y puede ser desarrollado en cualquier laboratorio sin necesidad de utilizar instrumentos sofisticados.

Puntos cuánticos de carbono altamente fluorescentes para la determinación de 4-nitrofenol en aguas superficiales.

1. Se sintetizaron puntos cuánticos de carbono (C-dots) altamente fluorescente mediante carbonización térmica.
2. Los C-dots fluorescentes se desactivaron selectivamente en presencia de 4-nitrofeno
3. Los C-dots se utilizaron como nanosensores sensibles y selectivos para la determinación de 4-nitrofenol
4. No se observaron interferencias debidas a especies comúnmente presentes en aguas de rio y agua de mar.
5. El análisis de 4-nitrofenol en aguas superficiales se llevó a cabo sin necesidad de un pretratamiento de la muestra.

Puntos cuánticos de carbono fluorescente para la determinación de ácido tánico en vinos.

1. Se sintetizaron puntos cuánticos de carbono por carbonización térmica
2. La fluorescencia de los C-dots así preparados se desactiva selectivamente en presencia de ácido tánico.

3. Los C-dots se utilizaron como nanosensores sensibles y selectivos para la determinación de ácido tánico
4. No se observaron interferencias debidas a otras sustancias comunes en vinos.
5. El análisis de ácido tánico en vinos se llevó a cabo sin necesidad de pretratamiento de las muestras.

Nanopartículas de ZnO alquil-funcionalizadas: síntesis y propiedades ópticas.

1. Se sintetizaron nanopartículas de ZnO alquil-funcionalizadas y se caracterizaron
2. Las nanopartículas así sintetizadas mostraron propiedades ópticas características.
3. Se observó una buena dispersibilidad de las nanopartículas funcionalizadas en aceites lubricantes, lo que augura la posibilidad de su utilización para la mejora de las propiedades reológicas de los aceites.
4. También se observó buena dispersibilidad en agua, lo que ofrece potencial para su empleo como sensores químicos.

Future work

In chapter (5) we used different approaches to synthesize ZnO NPs by sol-gel method in order to obtain the smallest and least aggregated NPs that would be exhibit the best properties for their use as lubricant additives and as a sensing material. After the different synthetic methods assayed, we could functionalize ZnO by two different long chain organic acids (ZnO-R) via covalent bonding. In this way, the NPs are covered by a hydrophobic shell that provides them with the ability to be dispersed in hydrophobic lubricants (oils). The optical properties of ZnO-R were determined and found to be fluorescent in solid state and aqueous liquid dispersed state. Also, it exhibit a weak phosphorescence and has a wide band gap energy as indicated from the spectrophotometric analysis.

Based on the excellent dispersion of the prepared NPs in oil and its fluorescence in dispersed aqueous media, they could be exploited in several ways. One of the ways to exploit the NPs is the improving of the rheological properties of lubricants. Also, it may be used to detect some metal ions in edible oil based on their good dispersion. On the other hand, according to their fluorescence, they may be used to detect some long chain water soluble proteins, such as albumin, through the interaction between the long hydrophobic chains in the NPs with albumin.

Conferences

Some of the work within the thesis has been participated in the following conferences:

1- Gaber H.G. Ahmed, Rosana B. Laiñao, Josefa A. Calzon, and Marta E.D. Garcia, Magnetic nanoparticles decorated with β-cyclodextrin for cáncer biomarker recognition, XXXIV meeting of the Spanish royal society of chemistry, 15-18 November 2013, Samtander, Spain.

2- Diaz-Garcia, M:E:, Badia Laiñao, R., Garcia Calzon, J:A:, Escudero Francos, M.A., Diaz faes Lopez, T., Espina Casado, J., Fernandez Gonzalez, A., Gaber Ahmed, G:H: Functional and luminescent nanoparticles: synthesis and applications. IX Symposium: Chemical research in the border región, 20-22 November 2013, Tijuana, Baja California, Mexico.